

THESIS FOR THE DEGREE OF DOCTOR OF PHILOSOPHY

Systems Biology of Yeast Lipid Metabolism

PRAMOTE CHUMNANPUEN



Systems and Synthetic Biology
Department of Chemical and Biological Engineering
CHALMERS UNIVERSITY OF TECHNOLOGY
Göteborg, Sweden 2012

Systems Biology of Yeast Lipid Metabolism

PRAMOTE CHUMNANPUEN

© PRAMOTE CHUMNANPUEN, 2012.

ISBN 978-91-7385-661-4

Doktorsavhandlingar vid Chalmers tekniska högskola
Ny serie nr 3342
ISSN 0346-718X

Systems and Synthetic Biology
Department of Chemical and Biological Engineering
Chalmers University of Technology
SE-412 96 Göteborg
Sweden
Telephone + 46 (0)31-772 1000

Cover:

Multi-level regulation of yeast lipid metabolism
By Pramote Chumnanpuen

Printed by Chalmers Reproservice

Göteborg, Sweden 2012

PREFACE

This PhD thesis serves as a partial fulfillment of the Doctoral degree at Chalmers University of Technology, Sweden. My PhD project can be divided into two parts. The first part is mainly focus on the influence(s) of different components affecting lipid metabolism by using integrative analysis. Through combined measurements of the transcriptome, metabolome, and lipidome it was possible to obtain a large dataset that could be used to identify the effect of *INO*-level and also establish correlations and co-influences between the different components such as Snf1-inositol/choline, and Snf1-TORC1. The second part is the development of high throughput method for yeast lipid analysis containing i) lipid monitoring at single-cell level using CARS microscopy, ii) total lipid extraction using microwave-assisted and a modified closed-vessel system, iii) lipid classes separation and quantification using HPLC-CAD, and iv) fatty acid methyl ester (FAME) derivatization using microwave-assisted method. Part of this work was financed by Chalmers Foundation, the Knut and Alice Wallenberg Foundation and the Swedish Research Council (Vetenskapsrådet). We also acknowledge funding from the EU-funded project UNICELLSYS.

Pramote Chumnanpuen

March 2012

Systems Biology of Yeast Lipid Metabolism

PRAMOTE CHUMNANPUEN

Systems and Synthetic Biology
Department of Chemical and Biological Engineering
Chalmers University of Technology

ABSTRACT

Lipid metabolism plays an important role in the development of many different life-style related diseases, such as type 2 diabetes and atherosclerosis, and understanding the molecular mechanisms behind regulation of lipid biosynthesis and degradation may lead to development of new therapies. In this project we undertook a global study of lipid metabolism in the eukaryotic model organism *Saccharomyces cerevisiae*. The objective of this project is to quantify how the fluxes in lipid metabolism of eukaryotic cells are controlled by different component of the regulatory network. Using systems biology approaches there was established a global regulatory model for lipid metabolism, and it was quantified how the fluxes toward different lipid components are regulated. Using different mutants that carry deletion in genes encoding key transcriptional factors and protein kinases involved in lipid regulation, the fluxes towards the different lipid components was perturbed. The wild-type yeast strain CEN.PK113-7D and the yeast mutants *opi1Δ*, *snf1Δ*, *tor1Δ*, *ino2Δ*, *ino4Δ*, and *ino2Δino4Δ* were grown in chemostat cultures at carbon or nitrogen-limited conditions and also high or low inositol-choline (IC) condition at a dilution rate of 0.1 h-1. At steady state conditions samples were withdrawn for analysis of the transcriptome, the metabolome and the lipidome. There was also developed 3 high-throughput methods for lipid quantification, i) for storage lipid monitoring at single-cell level using CARS microscopy, ii) for lipid classes analysis based on microwave-assisted extraction, HPLC-CAD, and iii) for fatty acids species analysis based on microwave-assisted derivatization. Through combined measurements of the transcriptome, the metabolome, the lipidome and the fluxome it was possible to obtain a large dataset that could be used to identify correlations between the different components such as the co-influences of Snf1-IC effects, *INO*-level, and Snf1-TORC1 effects on yeast lipid metabolism.

Keywords: Yeast lipid metabolism, Integrated analysis, Inositol-choline, Snf1, TORC1, Ino2, Ino4, Opi1, high throughput techniques, Transcriptome, Lipidome.

LIST OF PUBLICATIONS

This thesis is based on the work described in the following publications, referred to as **Paper I-VI** in the text:

- I. **Chumnanpuen, P.**, J. Zhang, I. Nookaew, J. Nielsen. 2012. Integrated analysis of the transcriptome-lipid profiling reveals the co-influences of inositol-choline and Snf1 in controlling lipid biosynthesis in yeast. Under revision in *Molecular Genetics and Genomics*.
- II. **Chumnanpuen, P.**, I. Nookaew, J. Nielsen. 2012. Integrated analysis, transcriptome-lipidome, reveals the effects of *INO2* and *INO4* level on lipid metabolism in yeast. Submitted for publication.
- III. Zhang, J., S. Vaga, **P. Chumnanpuen**, R. Kumar, G. N. Vemuri, R. Aebersold, and J. Nielsen. 2011. Mapping the interaction of Snf1 with TORC1 in *Saccharomyces cerevisiae*. *Molecular Systems Biology* **7**.
- IV. **Chumnanpuen, P.**, C. Brackmann, S. K. Nandy, S. Chatzipapadopoulos, J. Nielsen, and A. Enejder. 2011. Lipid biosynthesis monitored at the single-cell level in *Saccharomyces cerevisiae*. *Biotechnology Journal*: n/a-n/a. DOI: 10.1002/biot.201000386
- V. **Chumnanpuen, P.***, S. Khoomrung*, I. Nookaew, J. Nielsen. 2012. Rapid quantification of yeast lipid using microwave-assisted total lipid extraction and HPLC-CAD. Submitted for publication.
- VI. Khoomrung, S.*, **P. Chumnanpuen***, S. Jansa-ard, I. Nookaew, J. Nielsen. 2012. Fast and accurate preparation fatty acid methyl esters by microwave-assisted derivatization in yeast *Saccharomyces cerevisiae*. Under minor revision in *Applied Microbiology and Biotechnology*.

Other contributions:

- VII. Canelas, A. B.* , N. Harrison, A*. Fazio, J*. Zhang, J*. P. Pitkanen, J. van den Brink, B. M. Bakker, L. Bogner, J. Bouwman, J. I. Castrillo, A. Cankorur, **P. Chumnanpuen**, P. Daran-Lapujade, D. Dikicioglu, K. van Eunen, J. C. Ewald, J. J. Heijnen, B. Kirdar, I. Mattila, F. I. Mensonides, A. Niebel, M. Penttila, J. T. Pronk, M. Reuss, L. Salusjarvi, U. Sauer, D. Sherman, M. Siemann-Herzberg, H. Westerhoff, J. de Winde, D. Petranovic, S. G. Oliver, C. T. Workman, N. Zamboni, and J. Nielsen. 2010. Integrated multilaboratory systems biology reveals differences in protein metabolism between two reference yeast strains. *Nat Commun* **1**: 145.

(*) Authors contributed equally

CONTRIBUTION SUMMARY

A summary of the contributions of Pramote Chumnanpuen to each of the publications listed in the section **List of Publications** is provided below:

- I. I performed all the data acquisition and data analysis and wrote the manuscript.
- II. I conducted all the experiments, analyzed the data and prepared the manuscript.
- III. I performed the fatty acids quantification and assisted in manuscript preparation.
- IV. I carried out the fermentation, extracted and measured TAG, analyzed the data, and prepared the manuscript.
- V. I performed all the data acquisition and data analysis and wrote the manuscript.
- VI. I assisted in the sample preparation, method development, data analysis and prepared the manuscript.

ABBREVIATION AND SYMBOLS

AcCoA:	Acetyl coenzyme A
AceAcCoA:	acetoacetyl coenzyme A
AdoMet:	S-adenosyl- <i>L</i> -methionine
AdoHcy:	S-adenosyl- <i>L</i> -homocysteine
AHCY:	S-adenosyl- <i>L</i> -homocysteine hydrolase in mammals
CARS:	Coherent Anti Roman Scattering
CBS:	Cystathionine β -synthase
CDP-DAG:	Cytidine diphosphate-diacylglycerol
DAG:	Diacylglycerides
ES:	Ergosterol
Etn:	Ethanolamine
FA:	Fatty acid or fatty acyl-CoA
fl:	femtoliter
HIC:	High inositol-choline
HGLN:	High Glucose, Low Nitrogen
IC:	Inositol-choline
ICRE:	inositol/choline-responsive element
LIC:	Low inositol-choline
LGHN:	Low Glucose, High Nitrogen
gDW:	Gram dry weight
G-3-P:	Glycerol 3-phosphate
Glc-6-P:	Glucose 6-phosphate
Hcy:	Homocysteine
MalCoA:	Malonyl-CoA
NEFAs:	Non-esterified fatty acids
OPO:	Optical Parametric Oscillator
PA:	Phosphatidic acid
pA:	picoampere
PC:	Phosphatidylcholine
PE:	Phosphatidylethanolamine
PI:	Phosphatidylinositol
PL:	Phospholipids
PL-PUFA:	Phospholipids containing poly-unsaturated fatty acids.
PS:	Phosphatidylserine
Pyr:	Pyruvate
SE:	Sterylester
ST:	Strain factor
TAG:	Triacylglycerides
TF:	Transcription factor
CAD:	Charged aerosol detector
UAS _{INO} :	Inositol-sensitive upstream activating sequence
UPR:	Unfolded protein response

Nomenclatures

Standard nomenclature for *S. cerevisiae* is used for designating genes, proteins and gene deletions: *SNF1*, Snf1, and *snf1* Δ , respectively, for the catalytic subunit of Snf1 protein kinase complex as an example.

TABLE OF CONTENTS

PREFACE.....	iii
ABSTRACT.....	iv
LIST OF PUBLICATIONS	v
ABBREVIATION AND SYMBOLS	vii
Chapter 1 Introduction.....	1
1.1Lipids of Yeasts	1
1.1.1 Fatty acids.....	4
1.1.2 Phospholipids.....	5
1.1.2 Sterol.....	6
1.1.3 Storage lipids.....	8
1.2Systems Biology of the Regulation in Yeast Lipid Metabolism	8
1.2.1 Regulation by protein phosphorylation.....	9
1.2.2 Transcriptional level	11
1.2.3 Enzyme activity level	14
1.3Yeast <i>Saccharomyces cerevisiae</i> as a model system for lipid metabolism	16
1.4Challenging of lipid quantification.....	17
1.4.1 At single-cell level using CARS microscopy.....	18
1.4.2 At population level.....	19
Chapter 2 Results and Discussions	25
2.1 Integrated analysis reveals that regulation of lipid metabolism occurs at multiple levels.....	25
2.1.1 Co-influence of Snf1 and IC effects on yeast lipid metabolism	25
2.1.2 The effects of <i>INO</i> -level on yeast lipid metabolism	30
2.1.3 Linkage between lipid and amino acid (protein) biosynthesis.....	35
2.2 High through-put techniques for lipid quantification.....	42
2.2.1 At single cell level using CARS microscope	42
2.2.2 At population level.....	44
Chapter 3 Conclusions and Perspectives.....	53
Acknowledgements.....	55

Paper I

Paper II

Paper III

Paper IV

Paper V

Paper VI

Chapter 1 Introduction

1.1 Lipids of Yeasts

The total cell lipid of are so diverse among various yeast strains, and there is much interest in use of oleaginous yeasts such as *Yarrowia lipolytica* as lipid cell factories as they have the capability to accumulate lipids at levels corresponding to more than 36% of their biomass (Beopoulos et al. 2009). On the contrary *Saccharomyces cerevisiae* accumulates only minor amounts of lipids, estimated to less than 15% of its biomass considered as a medium lipid producing strain (Rattray et al. 1975).

Table 1.1 Total cell lipid of various strains of yeasts (Rattray et al. 1975). Cell cultivation under different conditions; lipid extraction generally involved the treatment of freeze-dried cells with chloroform/methanol system.

Lipid (%DCW)	Strain
Low (<5%)	<i>Candida albicans</i> <i>C. lipolytica</i> <i>C. utilis</i> <i>Lipomyces starkeyi</i> <i>Rhodotorula glutinis</i> <i>Saccharomyces fragilis</i>
Medium (5 to 15%)	<i>Blastomyces dermatitidis</i> <i>C. lipolytica</i> <i>C. scottii</i> <i>C. tropicalis</i> <i>Debaromyces hansenii</i> <i>Endomycopsis vernalis</i> <i>Hanseniasporo valbyensis</i> <i>Hansenula anomala</i> <i>Histoplasma capsulatum</i> <i>L. starkeyi</i> <i>Mucor rouxii</i> <i>Pullularia pullulans</i> <i>R. glutinis</i> <i>R. graminis</i> <i>S. carlsbergensis</i> <i>S. cerevisiae</i>
High (> 15%)	<i>B. dermatitidis</i> <i>Candida 107</i> <i>Cryptococcus terriculus</i> <i>E. vernalis</i> <i>H. capsulatum</i> <i>H. duboisii</i> <i>L. lipofer</i> <i>L. starkeyi</i> <i>R. glutinis</i> <i>R. gracilis</i> <i>R. graminis</i> <i>S. cerevisiae</i> <i>Trigonopsis variabilis</i> <i>Yarrowia lipolytica</i>

In yeast cells, lipids and, for the most part, the enzymes responsible for their biosynthesis, remodeling and turn over are differentially localized among membrane compartments (Zinser et al. 1991; Schneiter et al. 1999; Tuller et al. 1999; Kumar et al. 2002; Huh et al. 2003; Natter et al. 2005). Recently, genome-wide approaches to protein localization have been undertaken in yeast adding greatly to our understanding

of the cellular localization of proteins involved in lipid metabolism (Kumar et al. 2002; Huh et al. 2003). Using green fluorescent protein (GFP), 493 candidate proteins known or predicted to function in lipid metabolism as well as the proteins that regulate or have interaction with lipid metabolism were localized (Natter et al. 2005). The compartments that have been known to be specialized in lipid metabolism are ER, lipid droplets, and peroxisomes. About 65% were found as non-cytosolic and they mainly appeared to be associated with the endoplasmic reticulum (ER) and located in other membrane compartments such as mitochondria, peroxisome, lipid droplets, and vesicles. Only a few proteins were found in Golgi, vacuoles, and nuclear envelope, or inside the nucleus. However, many of these proteins displayed a complex pattern, indicating more than one location (Table 1.2). The numbers in parentheses represent the number of proteins localized in that compartment.

Yeast cell membranes are composed of three main components: phospholipids, sterols, and intramembrane proteins (Nurminen et al. 1970; Rattray et al. 1975; Natter et al. 2005). Lipid is an important group of macromolecules in yeast cells, not only being the components of cell membrane, but also involved in signal transduction. Lipids are also known as the energy storage molecules and important structural components of all eukaryotic cell membranes.

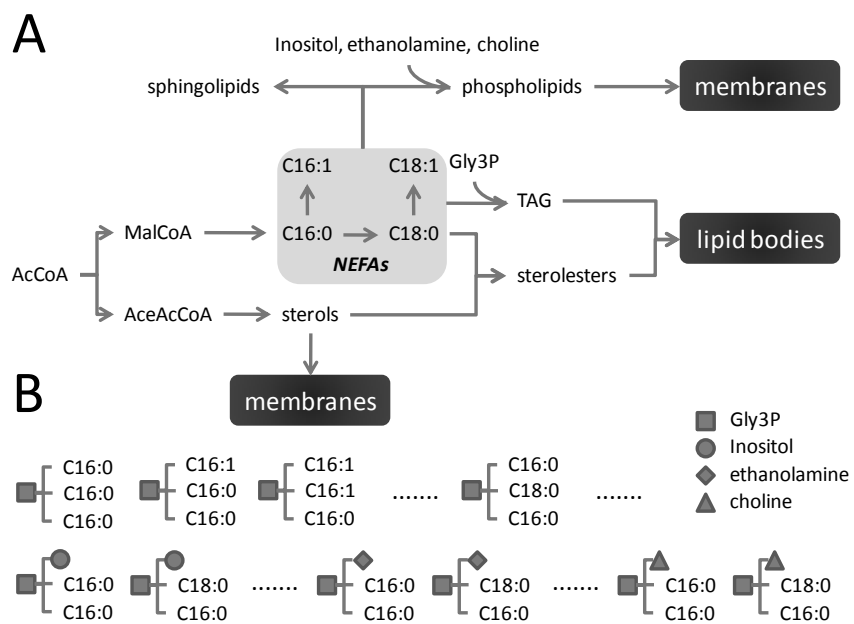


Figure 1.1 Overview of lipid metabolism. (A) The main pathways in lipid biosynthesis and illustration of how different lipid species are incorporated into the biomass as either lipid bodies or membranes. (B) Illustration of the large number of different lipid species that may be present in lipid bodies and membranes. The first row indicates TAGs and the second row indicates three key phospholipids (besides the three shown there are also phosphatidylserine and phosphatidylglycerol species) (Nielsen 2009).

Table 1.2 Lipid proteome adopted from (Natter et al. 2005). *Subcellular distribution of the lipid proteome.* Proteins localized in more than one compartment are listed in each relevant compartment and are marked with an asterisk.

Compartments	Lipid proteins
Endoplasmic reticulum (92)	ALG9, AQY1, ARE1, ARE2, AUR1, AYR1*, BOS1*, CHO1, CHO2, COX10*, CSG2*, CSR1*, CYB5, DGA1*, DPL1, DPP1*, EHT1*, ELO1, EPT1*, ERG1*, ERG2*, ERG24*, ERG25*, ERG26, ERG27*, ERG3*, ERG4, ERG5, ERG6*, ERG7*, ERG9*, EUG1*, FAA1*, FAA4*, FAT1*, FEN1, FEN2, FPS1, GAA1*, GOG5, GPI11, GPI2, GPI8, GSF2, GUP1, HMG1*, INP54*, IRE1, LCB2, LPP1*, MEC1, NCP1, NCR1, OLE1, OPI3*, PAU7*, PHO86, PIK1*, PIS1*, PLB1*, PLB2*, PTC2*, RVS161*, SAC1*, SCS7*, SEC14*, SEC22*, SLA1*, SLC1*, SPC1, STE14, SUR2, SUR4, TIP1, TSC10*, YBR204C*, YDC1*, YDL015C*, YDL193W*, YDR018C*, YIL011W, YIM1*, YJU3*, YKL174C*, YKR003W*, YLR343W, YOL132W*, YOR059C*, LCB1, YJU3*, NVJ1, YDL015C*
Lipid droplets (23)	AYR1*, DGA1*, EHT1*, ERG1*, ERG6*, ERG7*, FAA4*, FAT1*, PDR16*, SLC1*, TGL1, TGL3, YBR042C, YBR204C*, YDL193W*, YDR018C*, YIM1*, YJU3*, YKR046C, YKR089C, YOR059C*, YOR081C
Peroxisomes (17)	ACS1, DCI1*, FAA2*, MDH3*, PEX10, PEX11, PEX13, PEX14, PEX17*, PEX19*, PEX2*, PEX3, PEX4, PEX5*, POT1, POX1, SPS19*
Plasma membrane (14)	ALR1*, ERG13*, FAA1*, FAA3, GIT1*, PDR16*, PDR17*, SNQ2, TSC10*, VHT1*, YJL145W*, YLL012W, YMR210W*, YOR009W*
Mitochondria (27)	AAD10, ACP1, AGP2, BIO2, CEM1*, COQ1, COX10*, COX4, CPT1, CRC1, CYB2, ECM1, ERG13*, GUT1, HEM1, PGS1, PPT2*, PSD1, RAM1*, RVS167, SCS3, TES1, TGL2, YAP1, YBR159W*, YDR531W, YPR140W
Vacuole, membrane (7)	ALR1*, AST2*, DPP1*, PIB1, PIB2, VPH1, YBR161W*
Vacuole, lumen (5)	GIT1*, PKA3*, SUR1*, YIL005W, YOR009W*
Nucleus, lumen (56)	ACS2, ADA2*, ALD2, ARD1*, BDF1, BET2*, BET4, CDC43*, DCI1*, ERG10, ERG13*, FMS1*, GCN5, GDS1, HAP2, HAP5, HDA1, HHF1, HHT1, HHT2, HTA3*, IML3*, INO4*, MRS6*, MUQ1*, NAT1, NDD1*, PGD1*, PIP2*, PKA3*, QRI2, RAD61, RAM2*, REX3, RFA2*, RFA3*, ROX1, RPD3*, RTT105, SCM3, SEC21, SKN7, SPO12, THI3, TOR2*, TUP1*, YCR072C*, YGL144C*, YGR198W*, YHR046C*, YJR107W*, YKL091C, YLR323C, YMR192W, YNL086W*, YOL054W
Nucleus, nucleolus (5)	ADA2*, HTA3*, IML3*, RER2*, YCR072C*
Nucleus, envelope (6)	ADR1, NDD1*, NUP53, OPI1, PCT1, YPC1*
Vesicles (55)	APG7*, APL2*, AQY2, AST2*, BET1, BOS1*, CDC48*, CSG2*, DPP1*, ERG2*, ERG20, ERG24*, ERG25*, ERG3*, ERG9*, EUG1*, FAA1*, GAA1*, GIT1*, GTS1, HES1*, HFA1*, HMG1*, INP54*, KES1*, LPP1*, OPI3*, PAU7*, PDR5*, PIS1*, PKA3*, PLB1*, PLB2*, PLB3*, PPT2*, PTC2*, RER2*, SCS7*, SEC22*, SUR1*, TSC10*, VHT1*, VPS4*, YBR108W*, YBR161W*, YDC1*, YDL015C*, YGR198W*, YJL072C, YKL174C*, YKR003W*, YKT6, YOL132W*, YOR009W*, YPC1*
Golgi (7)	BET3*, EPT1*, GDA1, PIK1*, PIS1*, SAC1*, SEC14*
Cytoskeleton (7)	SAC6*, SLA1*, SRV2*, YGR136W, YSC84*, YDR532C*, ZTA1*
Others (8)	SEC2*, VPS24, CEM1*, GCD7, HNM1, STT4, TOR1, YDR541C*
Cytoplasm (177)	AAD6, AAH1, ACB1, ACF2, ACH1, ALD6, APG1, APG12, APG13, APG16, APG7*, APG9, APL2*, ARD1*, AST1, AST2*, AUT7, BET2*, BET3*, BIO4, BMH1, BMH2, BOI2, BPL1, BTS1, CAR2, CDC43*, CDC48*, CSR1*, DAK1, DCI1*, DEP1, DJP1, DOA1, ECII, EKI1, ERG8, FAA2*, FAB1, FAS2, FAT2, FMS1*, FPR1, FRQ1, GCR1, HAP3, HCS1, HES1*, HFA1*, HPR1, IDI1, IDP3, INO1, INO4*, INP51, IPT1, ISC1, JNM1, KES1*, LAS17, LCB4, LCB5, MAD2, MDH3*, MRS6*, MSS4, MUQ1*, MVD1, MYO2, NMT1, OYE2, OYE3, PDI1, PDR17*, PDR5*, PDX3, PEX17*, PEX19*, PEX2*, PEX5*, PGD1*, PHO84, PIP2*, PKC1, PLB3*, PLC1, PRM1, PRT1, PSD2, PTP1, RAM1*, RAM2*, RER2*, RFA2*, RFA3*, RIO2, RPD3*, RSP5, RTT101, RVS161*, SAC6*, SAH1, SEC14*, SEC2*, SEC24, SEC3, SEC59, SEC9, SFB2, SHE2, SHM2, SIN3, SIP1, SNF1, SOD1, SPS19*, SRV2*, STD1, SVL3, SWI6, TAH18, TDH1, TDH2, TDH3, TEL1, TOR2*, TPK1, TSC11, TSC3, TUB1, TUP1*, UBC5, UME6, UPC2, VMA2, VPS21, VPS30, VPS4*, YBR108W*, YBR159W*, YDL109C, YDR287W, YDR444W, YDR532C*, YDR541C*, YER024W, YFR016C, YGL039W, YGL144C*, YGR198W*, YHR001W, YHR046C*, YIR035C, YIR036C, YJL068C, YJL145W*, YJR083C, YJR107W*, YKL121W, YLR020C, YLR022C, YLR072W, YML131W, YMR210W*, YMR226C, YNL040W, YNL045W, YNL086W*, YNL094W, YNL134C, YPK1, YPL088W, YPR127W, YPT1, YSC84*, YSR3, ZTA1*

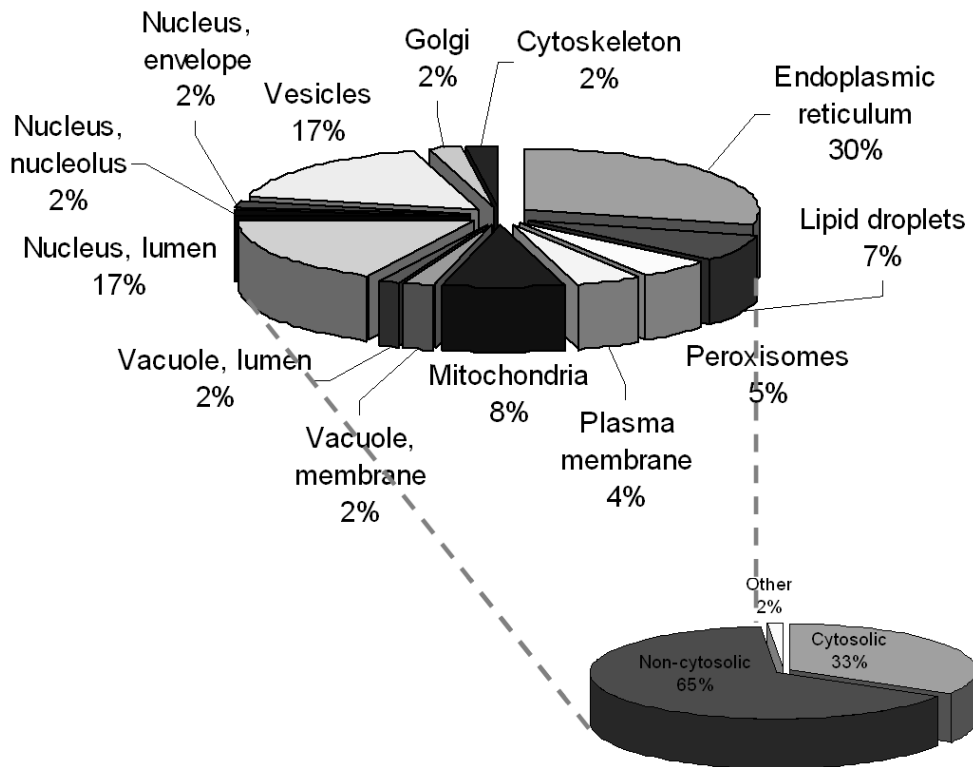


Figure 1.2 Abundance of lipid involved proteins in different compartments calculated from the *Subcellular distribution of the lipid proteome* data (Natter et al. 2005)

1.1.1 Fatty acids

Fatty acid (FA) is the major component of almost all lipid classes (except sterols) and also serves as carbon sources for energy production through β -oxidation and oxidative phosphorylation on shortage of glucose. The most abundant FA species in yeast cells are palmitoleic acid (16:1) and oleic acid (18: 1) followed by palmitic acid (16:0), stearic acids (18:0) , with minor amounts of myristic acids (14:0) are also found in yeast (Tuller et al. 1999; Tehlivets et al. 2007).

Table 1.3 Nomenclature and structures of common fatty acids in yeast

Numerical Symbol	Common Name	Systematic Name	Structure
14:0	Myristic acid	Tetradecanoic	
16:0	Palmitic acid	Hexadecanoic	
16:1 (n-7)	Palmitoleic acid	cis-9-hexadecenoic	
18:0	Stearic acid	Octadecanoic	
18:1 (n-9)	Oleic acid	cis-9-octadecenoic	
20:0	Arachidic acid	Eicosanoic	
20:1 (n-9)	Eicosenoic acid	cis-11-eicosenoic	

1.1.2 Phospholipids

The principal phospholipids in *S. cerevisiae* have been shown to be phosphatidic acid, phosphatidylethanolamine, phosphatidylinositol, phosphatidylserine, and phosphatidylcholine with fatty acid chains that are predominantly fatty acid 18:1 and 16:1, with smaller amounts of 18:0 and 16:0 (Swan and Watson 1997).

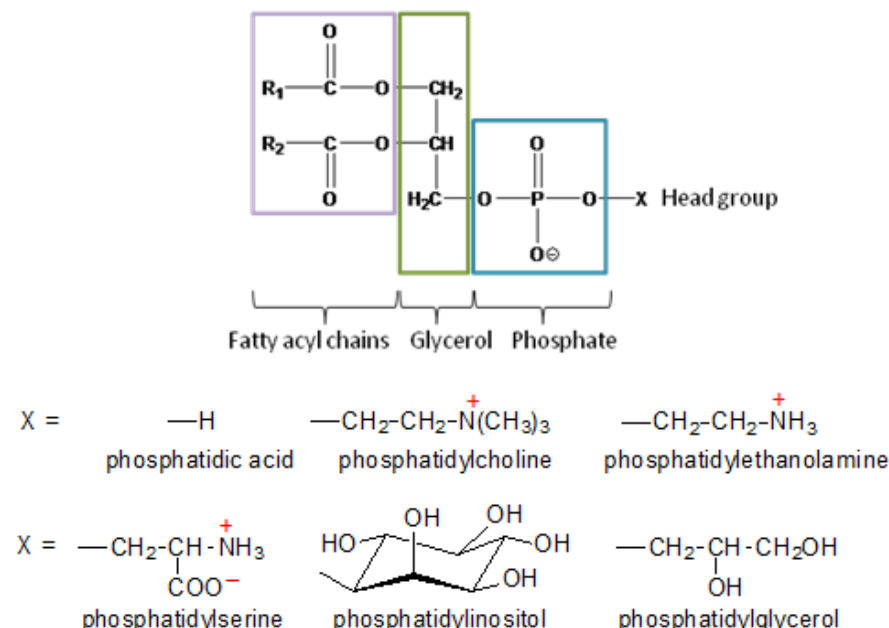


Figure 1.3 Variation of phospholipids in head group and also fatty acyl chains.
(Adopted from <http://lipidlibrary.acs.org/animbio/phospholipids/index.htm>)

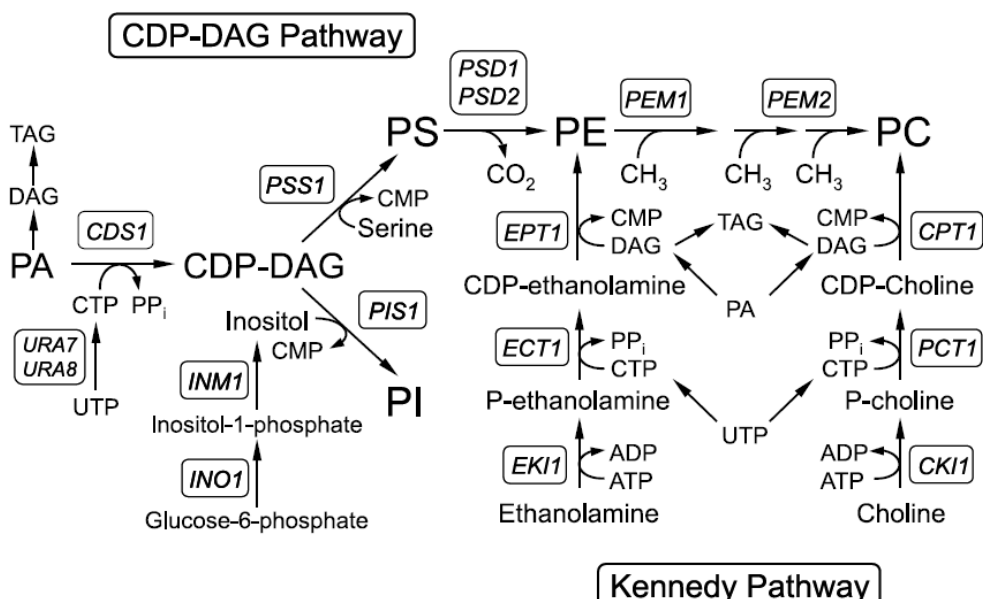


Figure 1.4 Pathways for the synthesis of phospholipids in *Saccharomyces cerevisiae*
(Carman and Kersting 2004). The pathways shown for the synthesis of phospholipids include the relevant steps discussed in the text. The CDP-DAG and Kennedy pathways are indicated. The known genes that code for enzymes catalyzing individual steps in the pathway are also indicated.

1.1.2 Sterol

The sterol component has been generally determined to range between 0.03 - 4.60% of yeast cell dry weight accounting for <1 to 10% of total cell lipid (el-Refai and el-Kady 1968; el-Refai and el-Kady 1968). *S. cerevisiae* is particularly rich in sterols with ergosterol accounting for over 90% of the total sterols (Dulaney et al. 1954; el-Refai and el-Kady 1968).

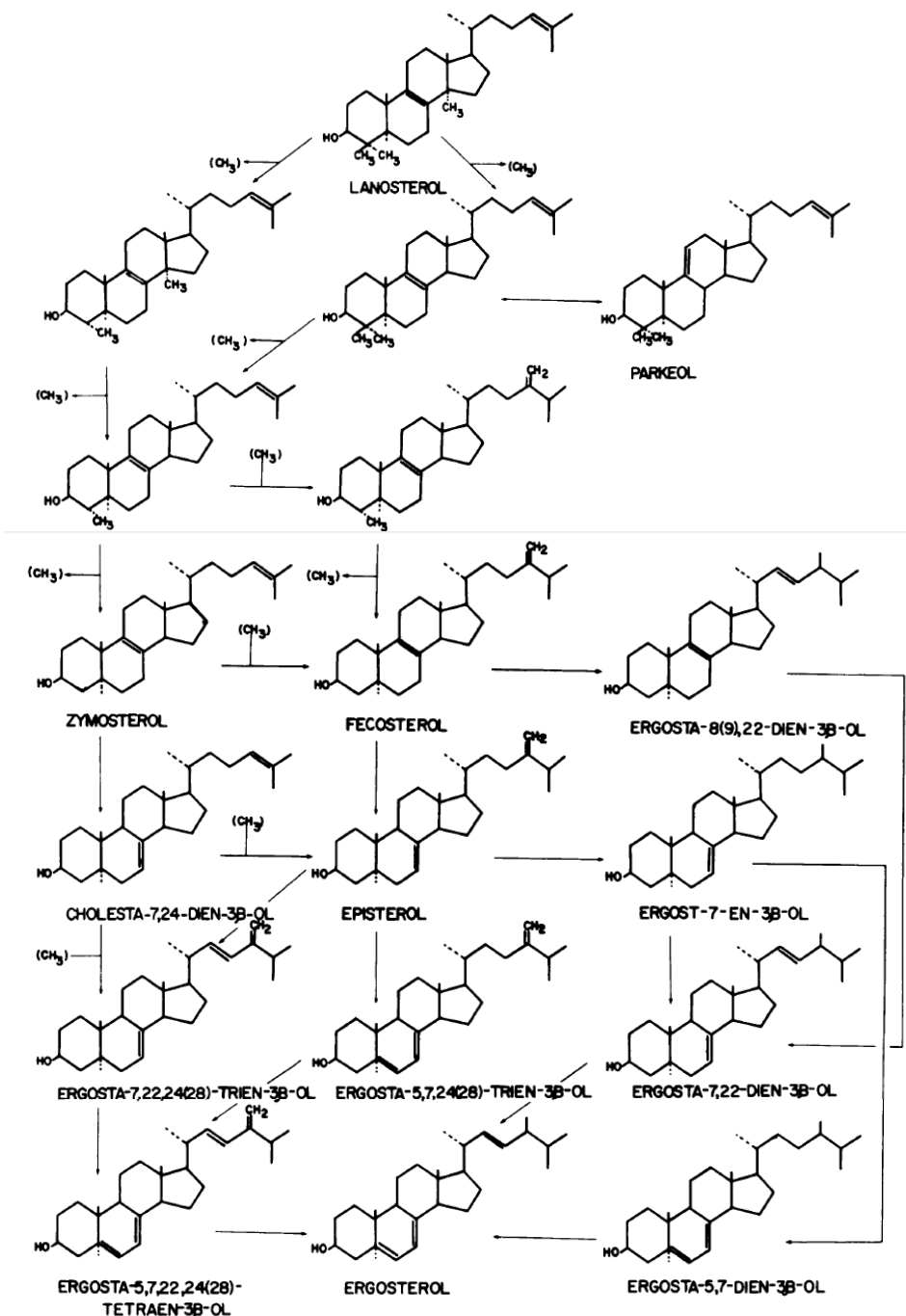


Figure 1.5 Sterols biosynthesis pathway in yeast; named compounds have been isolated from *S. cerevisiae* (Rattray et al. 1975)

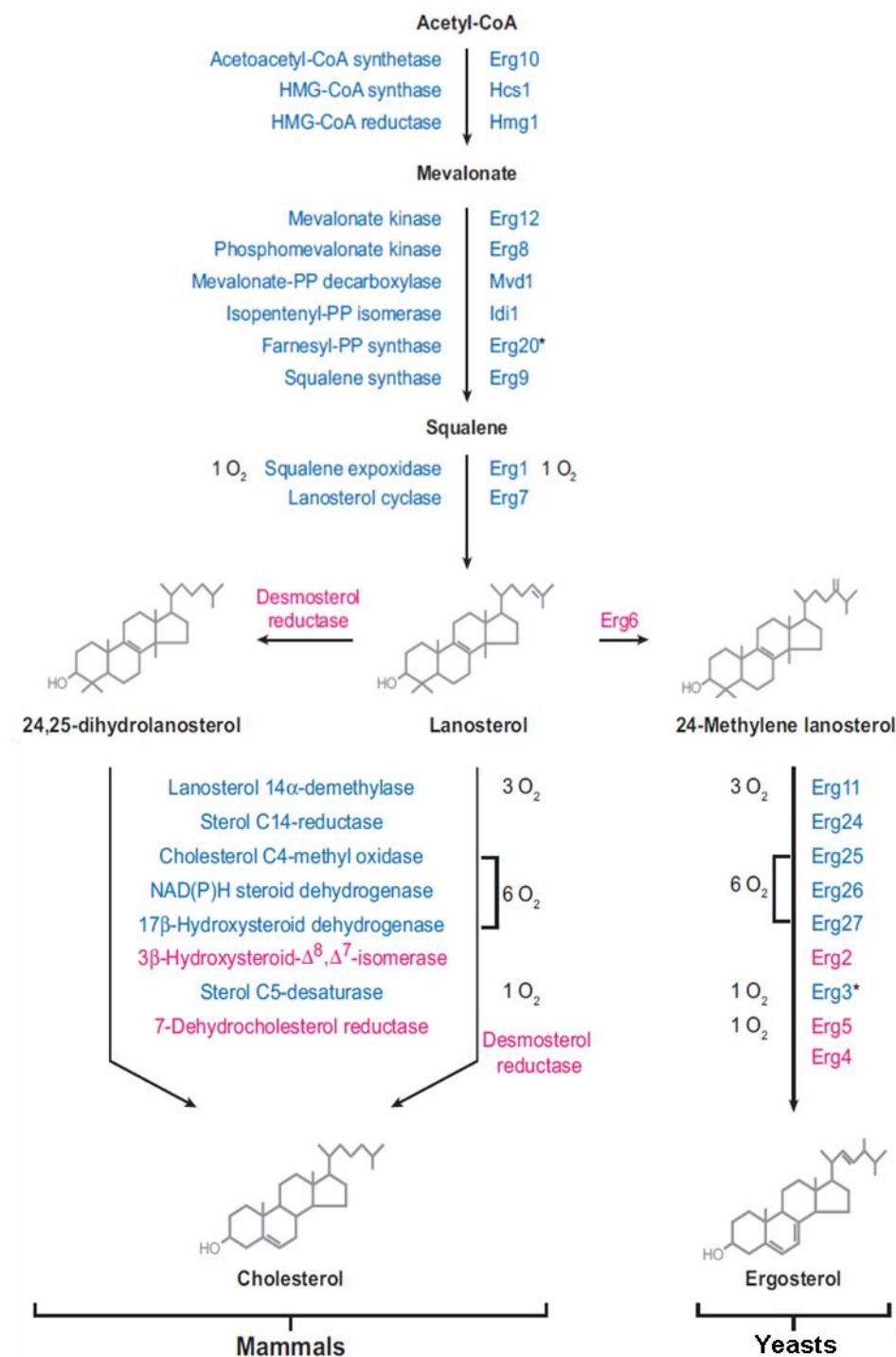


Figure 1.6 The sterol biosynthetic pathway in mammals and yeast. Enzymes in blue are conserved between yeast and mammals, while those in magenta are unique to each pathway. Oxygen requirements for oxygen-dependent enzymes are listed. *The yeast genome encodes two Erg20 and two Erg3 homologs. (Espenshade and Hughes 2007)

1.1.3 Storage lipids

All eukaryotic cells have a pool of neutral lipids stored as cytoplasmic droplets (also known as lipid droplets or lipid particles), which serve as reservoirs of cellular energy and building blocks for membrane lipids consisting of triacylglycerides (TAG) and sterol esters (SE) (Zweytick et al. 2000; Goodman 2009) surrounded by a monolayer of phospholipids and associated proteins (Brown 2001; Mullner and Daum 2004; Natter et al. 2005). In yeast, the lipid droplets consist of ~50% each of TAG and sterol esters (Schaffner and Matile 1981; Leber et al. 1994; Mullner and Daum 2004).

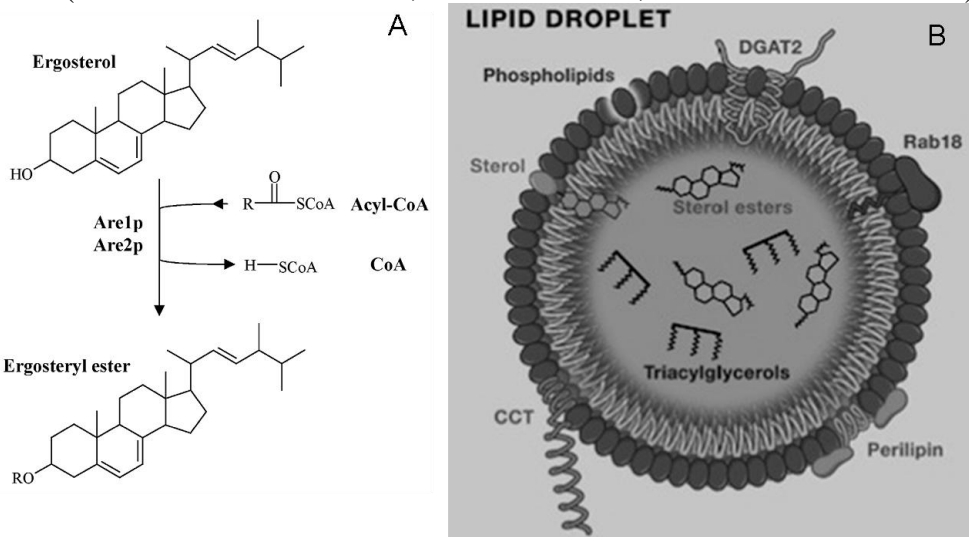


Figure 1.7 (A) Steryl ester formation in yeast (Mullner and Daum 2004) and (B) Lipid droplets composition (Krahmer et al. 2009)

Yeast SE has been characterized as having a high content of C18:1 and C16:1 fatty acid (Longley et al. 1968; Madyastha and Parks 1969; Hunter and Rose 1972) and account for 75% of the total sterol content in yeast.

1.2 Systems Biology of the Regulation in Yeast Lipid Metabolism

Lipid biosynthesis in the yeast *Saccharomyces cerevisiae* is a complex process that involves multilevel regulation by both genetic and biochemical mechanisms (Carman and Kersting 2004; Carman and Han 2009; Carman and Han 2011). In the light of systems biology, various high throughput techniques have been developed to quantify the different groups of biological molecules such as mRNA, protein, or metabolite at a global level (usually in the whole cell), which are normally referred to as “**transcriptome**”, “**proteome**”, or “**metabolome**”, respectively. For lipids (which is also a part of metabolome), the term “**lipidomics**” has been used, started by those working on lipid metabolism in mammalian systems (Han and Gross 2003; Lagarde et al. 2003; Pulfer and Murphy 2003; Spener et al. 2003; Wilson 2003; Han and Gross 2005; Spener 2005; Wenk 2005) to describe “**analysis of cellular lipids, as a whole, characterizing and quantifying the specific cell type under specific growth conditions**”. Taking into account the heterogeneity of major categories of phospholipids and neutral lipids with respect to acyl chain diversity, eukaryotic cells with their complex fatty acids, sterol, triacylglycerol, and other neutral lipids, sphingolipids, phospholipids, and glycolipids are estimated to have a thousand or more lipid species (Dowhan 1997; van der Meer et al. 2005).

The phospholipid synthesis enzymes are controlled by gene expression (e.g., transcription) and by other factors (i.e., lipids, water-soluble phospholipid precursors and products, and covalent modification of phosphorylation) that modulate catalysis. The effects from the nutritional level can lead to several changes at the kinase phosphorylation level, transcriptional level and also enzymatic reaction level. Environmental stimuli from outside the yeast cell, intracellular metabolites produced by itself (i.e. phospholipid, amino acid, fatty acids), and intermediates in lipid biosynthetic pathway can all effectively play a role in regulating lipid metabolism.

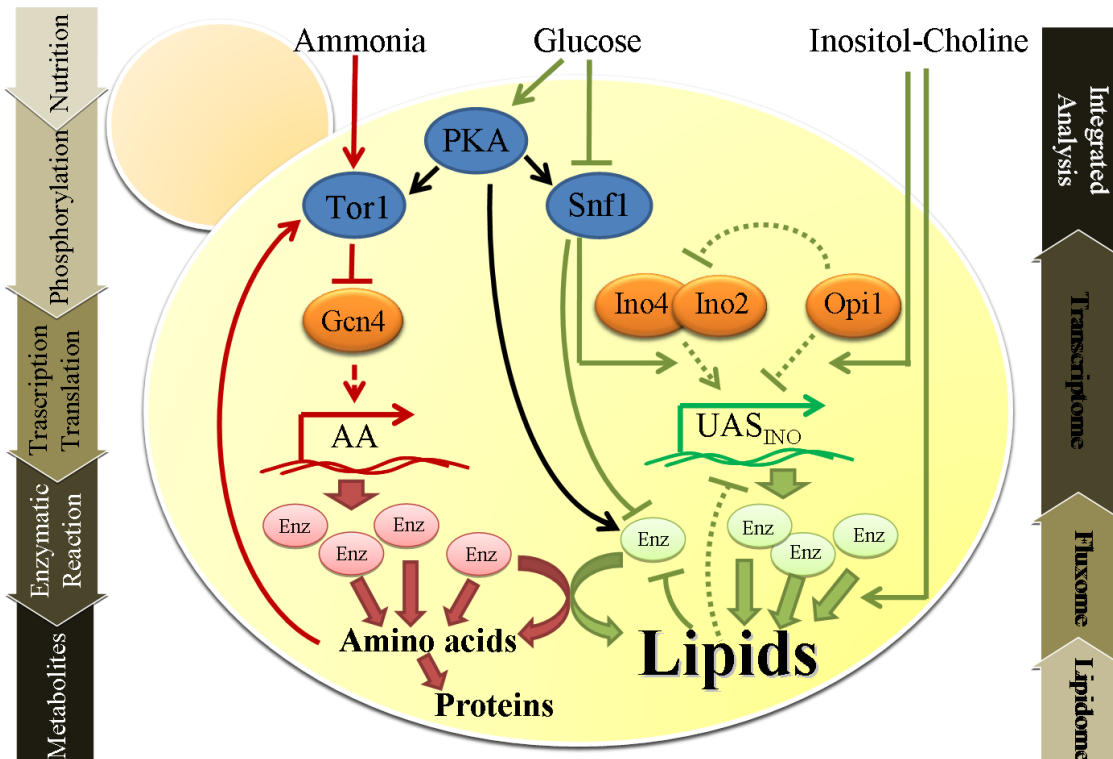


Figure 1.8 Overview of regulation of lipid metabolism at different levels.

1.2.1 Regulation by protein phosphorylation

Covalent modification by phosphorylation is a major mechanism by which the activity of enzymes or regulatory proteins are controlled and this kind of regulation is also found in phospholipid biosynthesis (Carman and Kersting 2004). Enzyme phosphorylation can affect the catalytic activity and (or) subcellular localization. Phosphorylation of a regulatory protein can control its localization, stability, or interaction with DNA or other proteins. Data indicate that phospholipid synthesis in yeast is regulated by protein phosphorylation. Some of this phosphorylation is mediated by the protein kinases A (PKA), protein kinases C (PKC), and the Snf1 protein kinase.

Table 1.4 Some phosphorylated proteins of yeast (*Saccharomyces cerevisiae*) phospholipid metabolism.

Enzyme	Gene	Protein kinase(s) involved	Phosphorylation site(s)	Effect on function
CTP synthetase	<i>URA7</i>	PKA	Ser424	Stimulation
		PKC	Ser36, Ser354, Ser424, and Ser454	Stimulation
			Ser330	Inhibition
Choline kinase	<i>CKII</i>	PKA	Ser30 and Ser85	Stimulation
45-kDa Mg ²⁺ -dependent PA phosphatase	Unknown	PKA	Unknown	Stimulation
PS synthase	<i>CHO1/PSSI</i>	PKA	Unknown	Inhibition
Opi1	<i>OPI1</i>	PKA PKC	Ser31 and Ser251Ser26	Stimulation Inhibition

In *S. cerevisiae*, PKA is the principal mediator of signals transmitted through the Ras-cAMP pathway (Broach and Deschenes 1990; Thevelein 1994). The activation of the Ras-cAMP pathway in *S. cerevisiae* results in a number of changes in lipid metabolism (Kinney et al. 1990; Quinlan et al. 1992). These changes include an increase in PI synthesis at the expense of PS synthesis and an increase in the synthesis of DAG. The decrease in PS synthesis may be attributed to inhibition of PS synthase by PKA mediated phosphorylation. The increase in DAG synthesis may be attributed to stimulation of Mg²⁺-dependent PA phosphatase by PKA mediated phosphorylation (Quinlan et al. 1992). The phosphorylation and stimulation of CTP synthetase, choline kinase, and PA phosphatase by protein kinase A is consistent with the increased utilization of the CDP-choline branch of the Kennedy pathway for PC synthesis under this condition. This hypothesis is supported by the fact that phosphorylation site mutants of CTP synthetase (Choi et al. 2003; Park et al. 2003) and choline kinase (Yu et al. 2002) exhibit a decrease in the synthesis of PC by the CDP-choline branch of the Kennedy pathway. In controlling of PKC, the yeast CTP synthetase and Opi1 are also regulated similar to PKA but phosphorylation at the different sites could have an opposite effects on the phospholipid pathway.

In yeast the Snf1 kinase complex is one of the key regulators in this regulatory network, and it belongs to a remarkably conserved serine/threonine kinase family called AMP-activated kinase (AMPK) that exists in all eukaryotes (Thomas and Polge 2007). The Snf1 kinase was firstly identified as a key enzyme in releasing glucose repression on glucose depletion (Celenza and Carlson 1984), and later found to be involved in the regulation of transcription through posttranslational modifications of histone H3 and Gcn5 (Lo et al. 2001; Liu et al. 2010) and interaction with RNA polymerase II holoenzyme (Kuchin et al. 2000). Snf1 is activated by phosphorylation on Thr210 by its upstream kinases in response to activation by the Snf4 subunit (Nath et al. 2003; Sutherland et al. 2003).

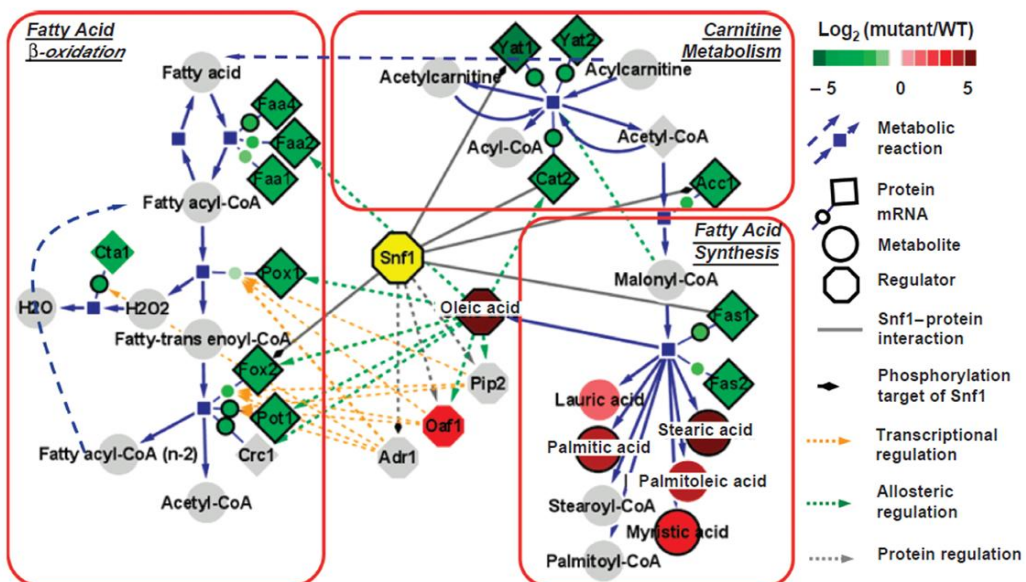


Figure 1.9 The impact of Snf1 kinase on fatty acid metabolism shows its role as a global energy regulator. (Usaite et al. 2009)

Once activated, Snf1 induces the genes in gluconeogenesis, glyoxylate cycle and β -oxidation of fatty acids (FA) by regulating a set of transcriptional factors (Soontorngun et al. 2007; Ratnakumar and Young 2010) and suppresses lipid biosynthesis by phosphorylation (inactivating) Acetyl-CoA carboxylase (Acc1), the committed step of FA synthesis pathway (Woods et al. 1994). Besides those aforementioned processes, Snf1 is also involved in other processes such as the carnitine metabolism, general stress response, pseudohyphal growth, ageing and ion homeostasis (Alepuz et al. 1997; Kuchin et al. 2002; Lin et al. 2003; Portillo et al. 2005; Hong and Carlson 2007; Shirra et al. 2008; Ye et al. 2008; Usaite et al. 2009).

1.2.2 Transcriptional level

It has been known that the transcription of the phospholipid biosynthetic genes is maximally repressed in the presence of the phospholipid precursors inositol and choline (IC) (Nikoloff and Henry 1991; Santiago and Mamoun 2003; Jesch et al. 2005). A highly conserved 10bp-element (5'-CATGTGAAAT-3'), in at least one copy is found in the promoters of the lipid co-regulated genes (such as *INO1*, *CHO1*, *CHO2*, *OPI3*, *FAS1*, *FAS2*, *ACS2*, *ACCI*, etc.) (Bailis et al. 1987; Lopes and Henry 1991; Schuller et al. 1992; Hasslacher et al. 1993; Schwank et al. 1995; Hiesinger et al. 1997). This element has been shown to be both necessary and sufficient for the IC response, so called “inositol/choline-responsive element” or “inositol-sensitive upstream activating sequence” (ICRE or UAS_{INO} motifs)(Bailis et al. 1987; Lopes and Henry 1991; Hoppen et al. 2005). These motifs are bound by a heterodimer of the positive regulators Ino2p and Ino4p containing basic helix-loop-helix (bHLH) structural motif (Hoshizaki et al. 1990; Nikoloff and Henry 1991; Schuller et al. 1992; Ambroziak and Henry 1994) which are necessary and sufficient for dimer formation and specific interaction with the UAS_{INO} motif (Hoshizaki et al. 1990; Dietz et al. 2003; Kumme et al. 2008).

Moreover, the ICRE-bound Ino2p can contact coactivator complexes such as the Snf1 kinase with its histone kinase function, the SAGA complex, and the TFIIB complex when *OPII* is disrupted or not present in the nucleus (Dietz et al. 2003; Lo et al. 2005). Opi1 is also necessary for repression of ICRE-dependent transcription when IC is present in excess (Greenberg et al. 1982; Wagner et al. 1999).

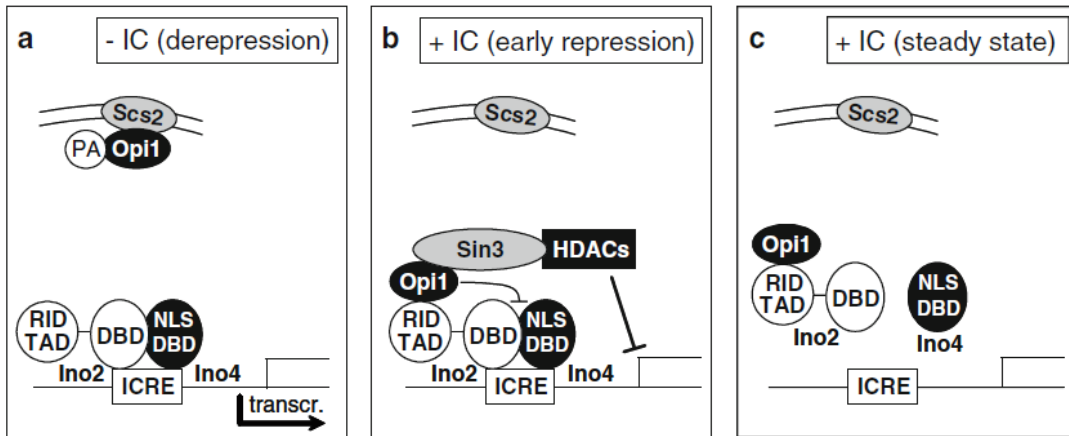


Figure 1.10 Hypothesis on regulatory transitions upon establishment of IC repression (Kumme et al. 2008). **(a)** Under conditions of IC limitation, accumulation of phosphatidic acid (*PA*) leads to retention of Opi1 at the ER and/or nuclear membrane via Scs2, allowing Ino2 + Ino4 to fully activate ICRE-driven target genes. **(b)** Opi1 is released from its membrane anchor upon increase of IC concentration and subsequent consumption of PA. Interaction with the RID of Ino2 specifically targets Opi1 to ICRE-containing genes. Since Opi1 simultaneously contacts the pleiotropic co-repressor Sin3, local modification of chromatin via histone deacetylases (HDACs) initiates repression. **(c)** Opi1 also weakens interaction of Ino2 and Ino4, leading to release of the heterodimer from its ICRE target sites in late repression and under steady state conditions. Auto-regulation of regulators as a putative means of the signal amplification is not considered here. *DBD* DNA-binding domain; *NLS* nuclear localization sequence; *RID* repressor interaction domain; *TAD* transcriptional activation domain

Table 1.5 Compilation of *Saccharomyces cerevisiae* genes containing ICRE or UAS_{INO} sequences in their upstream regions (Schuller et al. 1995)

Phospholipid biosynthesis:		Other functions:			Sequence
Gene	Function	Sequence	Gene	Function	Sequence
<i>FAS1</i>	Fatty acid synthase, β subunit	TTTTCACATGC	<i>ARG4</i>	Argininosuccinate lyase	TTTTCACATGT
<i>FAS1</i>	Fatty acid synthase, β subunit	ACTTCACATGC	<i>MET2</i>	Homoserine O-transacylase	TTTTCACGTGA
<i>FAS1</i>	Fatty acid synthase, α subunit	TTTTCACATGC	<i>MET78</i>	Bifunctional Dehydrogenase And Ferrochelatase	ATTTCACGTGT
<i>ACC1</i>	Acetyl-CoA carboxylase	TCTTCACATGG	<i>MET14</i>	ATP-adenylylsulfate reductase	ATTTCACGTGA
<i>FAA1</i>	Acyl-CoA synthetase	TATTTCACATGG	<i>MET16</i>	3'-Phosphoadenylylsulfate synthetase	ATTTCACGTGA
<i>FAA1</i>	Acyl-CoA synthetase	TCTTCATATTC	<i>SAM2</i>	S-adenosylmethionine synthetase	TCTTCACATGT
<i>ACB1</i>	Acyl-CoA binding protein	ATTTCACATGT	<i>MSW1</i>	Mitochondrial tryptophanyl-tRNA synthetase	TCTTCACGTGA
<i>ITR1</i>	Inositol permease	TCTTCACATGC	<i>ADE12</i>	Adenylosuccinate synthetase	TTTTCACGTGT
<i>ITR1</i>	Inositol permease	TTTTCACATGC	<i>CDC8</i>	Thymidylate kinase	ACTTCATATGC
<i>CTR1</i>	Choline permease	TTTTCACATGC	<i>CDC8</i>	Thymidylate kinase	TTTTCATATGA
<i>INO1</i>	Inositol-1-phosphate synthase	TTTTCACATGC	<i>CYC7</i>	Iso-2-cytochrome c	GTTTCA CATGC
<i>INO1</i>	Inositol-1-phosphate synthase	AATTTCACATGG	<i>COX4</i>	Cytochrome oxidase, subunit IV	TTTTCACATGA
<i>INO1</i>	Inositol-1-phosphate synthase	ATTTCACATTC	<i>SOD1</i>	Cu, Zn-Superoxidismutase	ATTTCACATGG
<i>INO1</i>	Inositol-1-phosphate synthase	TCATTCATATGC	<i>MAE61</i>	Maltose permease	TTTTCACATGT
<i>CHO1</i>	Phosphatidylserine synthase	CTTTCATCTGC	<i>FPP1</i>	Farnesylpyrophosphate synthetase	TTTTCACATGG
<i>CPT1</i>	Diacylglycerol cholinephosphotransferase	TTTTCACATGC	<i>MFa1</i>	α -factor precursor	TCTTCACATATG
<i>PSD1</i>	Phosphatidylserine decarboxylase	ATATTCACATGC	<i>STE2</i>	α -factor receptor	CCTTCACATGA
<i>PSD1</i>	Phosphatidylserine decarboxylase	TTCCTCACATGC	<i>STE4</i>	β -subunit of receptor-coupled G-protein	TTTTCATGTGT
<i>CK11</i>	Choline kinase	TATTTCACATGG	<i>CCL1</i>	Negative regulator of pheromone response	TTTTCACATGC
<i>PEM1</i>	Phosphatidylethanolamine N-methyltransferase	AATTTCACATGT	<i>SWI5</i>	Regulatory gene of mating type switch	TCTTCACATTC
<i>PEM1</i>	Phosphatidylethanolamine N-methyltransferase	TTTTCACATGC	<i>KAR1</i>	Nuclear fusion	TTTTCACATTC
<i>PEM1</i>	Phosphatidylethanolamine N-methyltransferase	TTTTCACATGC	<i>KSS1</i>	Protein kinase	TTTTCATATTC
<i>PEM1</i>	Phosphatidylethanolamine N-methyltransferase	TCTTCACATGC	<i>YCK1</i>	Casein kinase I	TTTTCATATGT
<i>PEM1</i>	Phosphatidylethanolamine N-methyltransferase	TTCATATGC	<i>NUF1</i>	Component of nucleoskeleton	ATTTCATATGT
<i>PEM2</i>	Phosphatidylethanolamine N-methyltransferase	TCTTCACATGC	<i>SAC6</i>	Fimbrin (Actin binding protein)	TTTTCACATGA
<i>PEM2</i>	Phosphatidylethanolamine N-methyltransferase	TCTTCACATGC	<i>MSB1</i>	Morphogenesis	ATTTCATGTGC
<i>PEM2</i>	Phosphatidylethanolamine N-methyltransferase	TCTTCATATGC	<i>RAD9</i>	Cell cycle arrest protein	TTTTCATATGT
<i>PIS1</i>	Phosphatidylinositol synthase	ACTTCATATGC	<i>RAD23</i>	Excision repair protein	ATTTCATATGT
<i>SLC1</i>	Long-chain acyl-CoA transferase	CCTTCACATTC	<i>RAD52</i>	Recombination protein	TTTTCA TATGT
<i>SLC1</i>	Long-chain acyl-CoA transferase	GCTTCACATTC	<i>GCR2</i>	Glycolysis regulator	TCTTCACATTC
<i>GUT1</i>	Glycerol kinase	TTTTCACATGG	<i>MCM3</i>	Minichromosome maintenance	TTTTCACATTC
<i>URA8</i>	CTP Synthetase	TCTTCACATTC	<i>CAP1</i>	Capping protein, α -subunit	TTTTCACGTGC
<i>INO2</i>	Positive regulator of phospholipid biosynthesis	AATTTCACATGT	<i>YEF3</i>	Elongation factor 3	ACTTCATATGC
<i>INO4</i>	Positive regulator of phospholipid biosynthesis	TATTTCACATGT	<i>PMA2</i>	Transport ATPase	TCTTCATATGT
<i>OPI1</i>	Negative regulator of phospholipid biosynthesis	TCTTCACATGC	<i>AFG2</i>	Putative ATPase	TTTTCATGTGA
			<i>PEP12</i>	Sorting of vacuolar proteins	CTTTCACATGC
			<i>PTP2</i>	Tyrosine phosphatase	

Under this condition, Opi1 is localized in the nucleus (Loewen et al. 2003) and prevent Ino2 from activation of target genes by recruitment of the pleiotropic co-repressors such as the Cyc8/Tup1 complex (Keleher et al. 1992; Smith and Johnson 2000) or Sin3p (Wang et al. 1990; Vidal et al. 1991; Wang and Stillman 1993; Kasten et al. 1997; Wagner et al. 2001).

Recent studies have shown that expression of several genes probably unrelated to phospholipid metabolism is also affected by Ino2p and Ino4p (Hoppen et al. 2005; Jesch et al. 2005; Chen and Lopes 2007). Importantly, over expression of *INO2* (but not of *INO4*) counteracts IC repression, suggesting Ino2p as a possible target of the signal transduction pathway triggering IC repression (Hosaka et al. 1994; Schwank et al. 1997)

At the transcription level, the heterodimeric Ino2/Ino4 activator and Opi1 are the global regulators of gene expression, affecting the expression of a large number of phospholipid biosynthetic genes (Ashburner and Lopes 1995; Ashburner and Lopes 1995; Santiago and Mamoun 2003). Opi1, containing a leucine zipper motif, has been known as a negative regulator phospholipid biosynthesis and it can also repress the transcription of *INO2* and *INO4* (White et al. 1991; Wagner et al. 1999). In the absence of Opi1, the transcriptional level of both *INO2* and *INO4* (so called “**INO-level**”) will be up-regulated compared to the reference strain. Consequently, Ino2 variants defective for interaction with Opi1 leads to the repression of phospholipid biosynthetic genes (Heyken et al. 2005).

1.2.3 Enzyme activity level

Several lipid involved enzymes and also some transcription factor can be controlled at the enzyme activity level by their own products or some other products in a competitive pathway. At the biochemical mechanism level, the level of phosphatidic acid (PA) is controlled by the biochemical regulation of key phospholipid biosynthetic enzymes (Loewen et al. 2003) and it plays a central role in the regulation of phospholipid synthesis gene expression (Loewen et al. 2004; Kumme et al. 2008; Carman and Han 2009). PA can, together with Sin3, inhibit Opi1 to pass through the nuclear membrane as mention above.

Between the competitive pathway like the CDP-DAG and Kennedy pathways, CTP and CDP-DAG seems to play an important role as a switch to control the flux through both pathways. Similarly, inositol is the key regulator at CDP-DAG branches which can either go to PI or PS. Not only at the transcriptional level as mentioned before, but inositol can also activate Pis1 and inhibit Cho1 (competitive enzyme) at the enzyme activity level. On the other hand, for the coupled-reaction pathway like methyltransferase steps required for PC synthesis, AdoHcy and AdoMet play the role as master regulators. CTP and AdoHcy are molecules that regulate UAS_{INO}-containing genes as well as the activities of phospholipid synthesis enzymes. CTP is essential for phospholipid synthesis; it is the direct precursor of the activated, energy-rich intermediates CDP-DAG, CDP-choline, and CDP-ethanolamine (Chang and Carman 2008). CTP is also used as the phosphate donor for the synthesis of PA by the *DGK1*-encoded DAG kinase (Han et al. 2008).

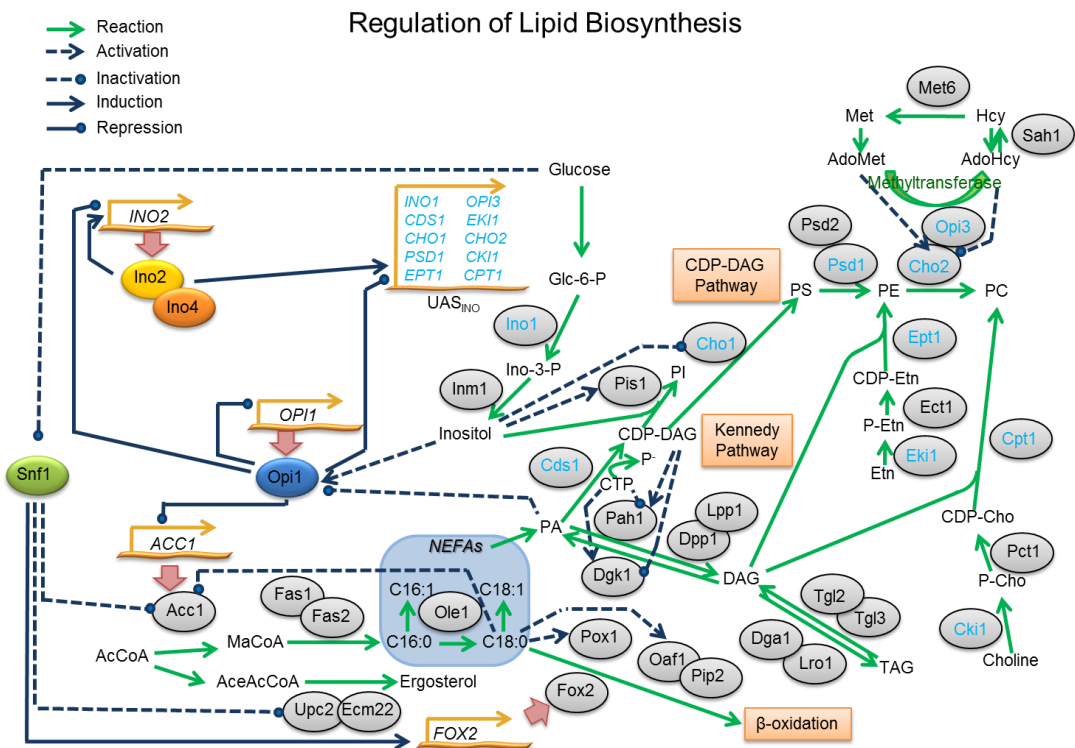


Figure 1.11 Overview of regulation of yeast lipid metabolism (Carman and Han 2009; Nielsen 2009)

Since the cellular levels of CTP are primarily controlled by product inhibition of CTP synthetase activity, expression of a mutant enzyme lacking this regulation results in elevated levels of CTP, as well as an increased rate of PA synthesis and the de-repression of UAS_{INO}-containing genes (Ostrander et al. 1998; Chang and Carman 2008). The increase in PA content and the inactivation of Opi1 repressor function (Han et al. 2008) may result from the stimulation of DAG kinase activity by increased availability of its substrate CTP. CTP also favors an elevation of PA content by inhibiting *PAHI*-encoded PA phosphatase2 activity (Wu and Carman 1996).

AdoHcy is a product of the AdoMet-dependent methylation reactions that are catalyzed by the *CHO2*-encoded PE methyltransferase and *OPI3*-encoded phospholipid methyltransferase in the CDP-DAG pathway (figure 1.11). AdoHcy, which is removed by the *SAH1*-encoded AdoHcy hydrolase (Malanovic et al. 2008), is a competitive inhibitor of the ethyltransferase enzymes (Gaynor and Carman 1990). Thus, down-regulation of the AdoHcy hydrolase causes the accumulation of AdoHcy and the inhibition of PC synthesis, which leads to an increase in PA content and the de-repression of UAS_{INO}-containing genes (Malanovic et al. 2008). Although the effects of AdoHcy on phospholipid composition have not been addressed, its accumulation causes an increase in TAG synthesis and lipid droplet content (Malanovic et al. 2008).

1.3 Yeast *Saccharomyces cerevisiae* as a model system for lipid metabolism

Budding yeast, *S. cerevisiae* is an important and widely utilized cell factory for biotechnological production. There is an increasing interest in bioengineering of lipids cell factory used for biotechnological production of a range of fuels, chemicals and food ingredients. This organism is tolerant to harsh industrial conditions, very well-characterized, and already used for large-scale production of different products. Moreover, it has been more widely used as a model organism for studying eukaryotic cell physiology and molecular events relevant even for human disease.

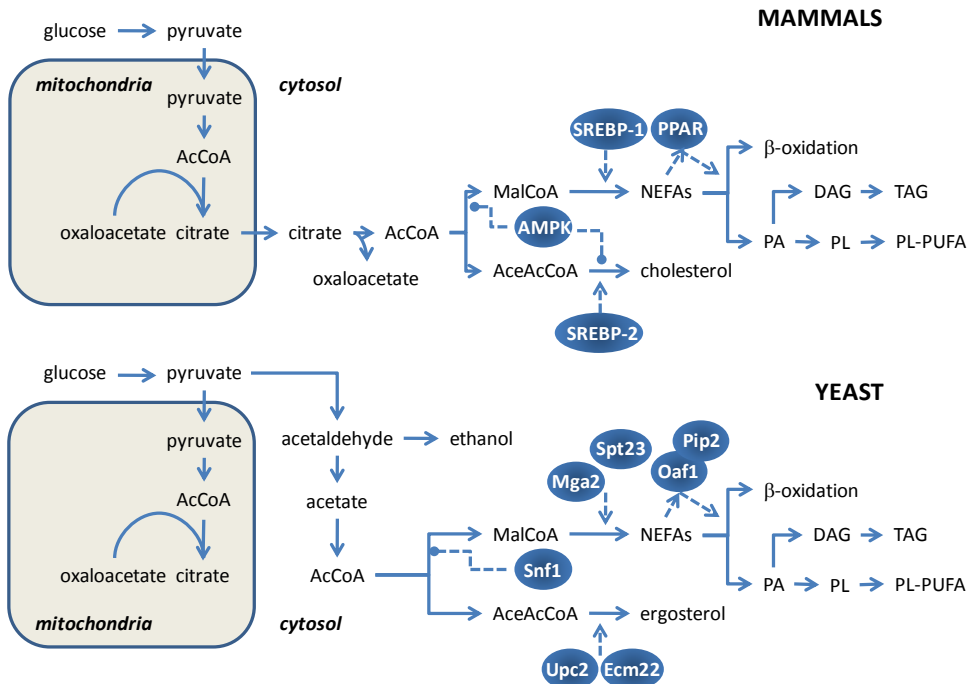


Figure 1.12 A comparison of lipid biosynthesis and its regulation in mammals and yeast (Nielsen 2009).

Yeast offers so many advantages that make it a good model organism for a study of lipid metabolism such as: 1) it has high accessibility of its molecular and classical genetics, 2) it is an unicellular microorganism that is easy to cultivate fast in inexpensive media which enables performing controlled experiments at many different conditions, 3) it comes both in haploid and diploid forms and the possibility for either sexual crossing or clonal division (budding) enable easy genetic manipulations and screenings, 4) yeast can express heterologous genes either from an episomal plasmid or from a chromosomal integration and it is possible to fairly easily insert, delete or mutate any sequence in the genome, 5) a collection of single deletion mutants is available for diploid cells and for non-essential genes also for haploid cells, 6) there is an extensive research infrastructure available with a well curated *Saccharomyces* Genome Database (SGD) (www.yeastgenome.org) and availability of a large number of technologies for high-throughput analysis (yeast has been used to pioneer transcriptome, proteome and interactome studies), and 7) a large fraction of the yeast genes have human orthologues (Nielsen 2009)

1.4 Challenging of lipid quantification

Undeniably, accurate quantitative determination of the different lipid classes in yeast cells is a key for lipid studies (e.g. lipids biosynthesis and accumulation, regulation of lipid metabolism, bioactive lipids, etc.).

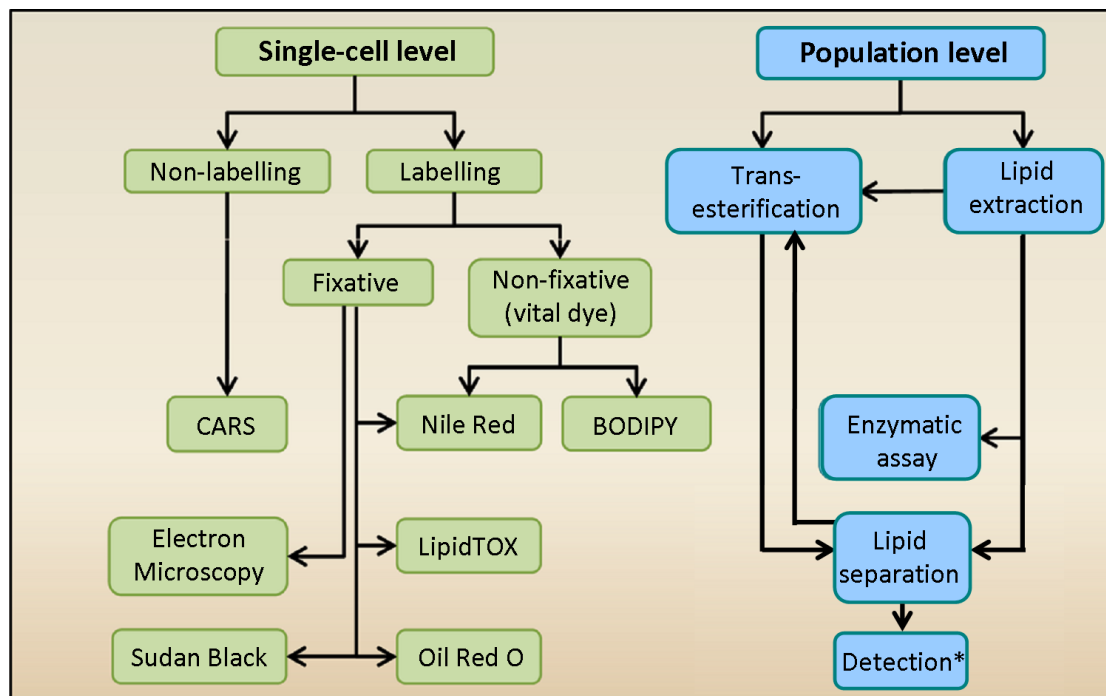


Figure 1.13 Overview of strategies and common methods to examine lipid amounts at different levels; single-cell and population level. Modified from (Elle et al. 2010).

Typically, Lipid separation can be done by TLC, SPE, or HPLC. Several detectors for lipid quantification can be used as the “**Detection***” step. The detection of TLC plates can be done by a TLC plate scanner that quantify absorption or fluorescent signal directly or after treatment with heating or reagent addition. Commonly, the detector for FAME analysis after trans-esterification and GC separation can be done with MS or FID while the detector for HPLC could be FID, ELSD, CAD, or MS. A comparison of these different detectors is summarized in table 1.6.

The microscopy strategies for single-cell level lipid monitoring (green side) can be roughly divided into non-labelling and labelling methods. So far, CARS (coherent anti-Stokes Raman scattering) is the only non-labelling method. If the strategy is labelling of lipid stores, there are two choices: Fixative (including electron microscopy, Sudan Black, Oil Red O, and LipidTOX) and non-fixative dyes (the most popular being C1-BODIPY-C12 and Nile Red). (Hellerer et al. 2007)

The biochemical strategies for lipid quantification at population level (blue side) start from total lipid extraction or directly go to trans-esterification (for total FA analysis) followed by GC-MS analysis. Lipid separation can be done using several techniques i.e. thin-layer chromatography (TLC)/solid-phase extraction (SPE), or high-performance liquid chromatography (HPLC) in combination with mass spectrometry (MS). Optionally, triacylglycerols (TAG) can also be quantified enzymatically using the commercial kits.

1.4.1 At single-cell level using CARS microscopy

To perform single-cell monitoring of the three-dimensional distribution and amounts of lipids stored in living, unlabeled cells, the Coherent Anti-Stokes Raman Scattering (CARS) microscopy has been used. This emerging technique has several advantages compared to present technology based on fluorescence microscopy (as illustrated in figure 1.13), whose main disadvantage is the requirement for labeling with fluorescent markers, resulting in a strong dependence on labeling efficiency or expression of fluorescent protein in the structure of interest. Together with the dependence on fluorescence yield, which is determined by the local chemical environment, this introduces variations and uncertainties in quantitative analysis, for example as reported for the commonly used lipid stains Nile red and Bodipy (Gocze and Freeman 1994). Furthermore, by using labeling the cells are studied in a modified state with possible effects on their properties and for lipids it has been shown that the use of alcohols in staining protocols influence the lipid droplet morphology (Fukumoto and Fujimoto 2002). It is often also of interest to co-localize visualized lipid droplets with other organelles by means of double labeling protocols. However, this possibility is often limited due to the broad fluorescence emission of Nile Red or the combined green and red fluorescence identified for Bodipy as recently discussed by Ohsaki *et al.* (Ohsaki *et al.* 2010). Fluorescence microscopy is also in many situations limited by sample photo-bleaching, in particular when using protein tagging. Nevertheless, intracellular lipid droplets in *S. cerevisiae* have been visualized using fluorescence tagging the protein Erg6 with green fluorescent protein (GFP) (Natter *et al.* 2005). Thus, the drawbacks of established technology make a label free method for lipid visualization and quantification without these limitations of high interest. CARS microscopy probes intrinsic molecular vibrations making it a label free technique allowing for live-cell studies under native conditions. In addition, it offers the advantages of three-dimensional imaging with high spatial resolution, good sample penetration, and low risk for photo-induced effects and damage.

CARS is a laser-induced nonlinear optical four-wave mixing process in which combined excitation and scattering generates blue-shifted anti-Stokes scattered photons in a sample. An enhanced CARS signal is achieved as the applied laser fields are tuned into resonance with a Raman-active molecular vibration, and thereby target specific species or molecular groups. Compared to spontaneous Raman scattering, which also allows for specific imaging probing molecular vibrations, CARS is induced by resonant vibrational excitation and results in coherent, directed signal emission that allows for efficient collection.

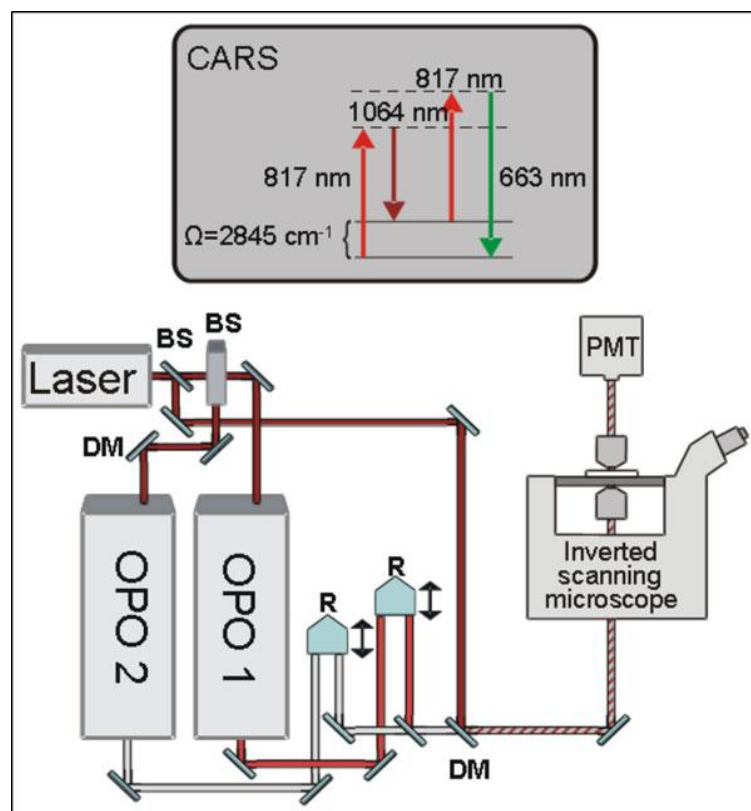


Figure 1.14 A schematic drawing of the CARS microscope. The instrument consists of a mirror-scanning optical microscope and two OPOs pumped by a Nd:VAN laser. The three excitation beams are overlapped in time and space by means of retroprisms and beam splitters. In this work, two of the beams (probe/pump: 817 nm and Stokes: 1064 nm) were coupled into the microscope to probe the C-H vibration at $2,845\text{ cm}^{-1}$, as illustrated by the excitation diagram (*Inset*). (Hellerer et al. 2007)

CARS signals are orders of magnitude higher compared to spontaneous Raman scattering, effectively reducing image acquisition times, clearly favorable for studies of living cells. CARS probing the symmetric stretch vibration of CH_2 groups in lipid acyl chains has become an established method for chemically specific imaging of lipids (Enejder et al. 2010; Le et al. 2010) and applied for studies in single cells (Nan et al. 2003), multi-cellular organisms (Hellerer et al. 2007), and tissues (Le et al. 2007; Huff et al. 2008). Specific imaging of intracellular lipid droplets in *S. cerevisiae* using CARS microscopy has also been presented (Brackmann et al. 2009).

1.4.2 At population level

1.4.2.1 Yeast Lipid Extraction

There are three lipid extraction methods which have been cited the most in the literature 1) Folch, Lees, and Stanley (Folch et al. 1957), 2) Bligh and Dyer (Bligh and Dyer 1959), and 3) Ways and Hanahan (Ways and Hanahan 1964). These methods use chloroform/methanol (2:1, v/v) as the extracting solvent and these protocols can be adapted for yeast lipid extraction by including a cell disruption step.

Briefly, the conventional lipid extraction procedure (Schneiter and Daum 2006) contains 4 steps; 1) cell disruption, 2) extraction of the lipids with chloroform/methanol (2:1, v/v), 3) removal of nonlipid contaminants by washing the extraction with aqueous salt solutions and 4) Drying of the extraction by removal of the organic solvent.

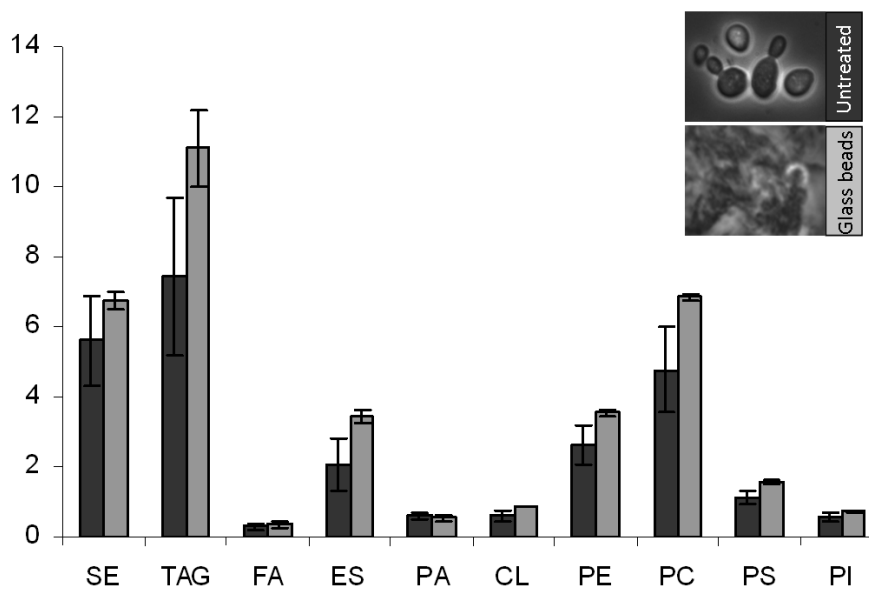


Figure 1.15 Comparison of the total lipid yield extracted from freeze-dried yeast cells with conventional extraction method with glass beads breaking and without cell disruption.

Due to the rigid cell wall of yeast, which can stand a high pressure of more than 300 Mpa, yeast samples are more difficult to handle in term of completeness of extraction compared to many other biological samples (Hartmann and Delgado 2004). Mechanical disintegration of the cells or cell disruption and drying yeast at appropriate temperatures also enhance lipid extraction (Letters 1966; Rattray et al. 1975). The cell disintegration process is usually done by either mechanical disintegration of the cells (sonication and bead mills) or by cell wall digestion (using zymolyase) (Letters 1966; Rattray et al. 1975; Engler and Robinson 1979). Moreover, lipid is most efficiently recovered from freeze-dried or freeze-thawed yeast cells (Souzu 1973) and this procedure is commonly employed.

1.4.2.2 Lipid classes analysis using HPLC-CAD

For lipid classes separation and quantification, numerous high performance liquid chromatography (HPLC) methods has been used and developed for quantitative analysis of plant, animal, and microbial lipids (Moreau and Asmann 1989; Moreau 1990). Hydrophilic interaction chromatography (HILIC) is one of the most useful columns not only in metabolomic profiling but also for lipid profiling (Zheng et al. 2010) . This column is a relatively recent development, also termed reverse normal phase chromatography, which uses a polar stationary phase and its associated layer of water to promote chromatographic

retention with partitioning against a mobile phase which has a high content of organic solvent.(Jandera 2008; Nesterenko et al. 2009) In this mode polar compounds are retained strongly and their elution is promoted by gradually increasing the aqueous content of the mobile phase.

Like ELSD, CAD allows HPLC detection of non-volatile or semi-volatile compounds and it has been used for lipid analysis (Moreau 2006). However, conventional UV detection is often not adequate and limited to chromophores (Schonherr et al. 2009) while other methods such as flame ionization detection (FID) or evaporative light-scattering detection (ELSD) have significant limitations in precision, sensitivity and dynamic range (Loughlin et al. 2007; Ramos et al. 2008). For detection purposes, the usual optical methods (UV and fluorescence) are not well adapted to the direct analyses of lipids.

Table 1.6: A comparison of common HPLC detectors.(Moreau 2009)

Detector	Destructive	Universal detector	Advantages	Disadvantages
UV-visible	No	No	Ease of use	Requires a chromophores
Fluorescence	No	No	Very sensitive	Requires a fluorophore
Radioisotope	Yes	No	Very sensitive	Requires a radiolabeled analyte
Electrochemical	Yes	No	Very sensitive	Analyte must be easily oxidized or reduced
Nitrogen	Yes	No	Very selective	Analyte must contain nitrogen
Mass spectrometric	Yes	Yes & No	Useful for structural determination	Costly, analyte must form ions
Refractive index	No	No	Ease of use	Requires isocratic Temperature Sensitive
Flame ionization	Yes	Yes	Linear mass to signal response	Solvents and buffers must be volatile
ELSD	Yes	Yes	Can be used with gradients	Solvents and buffers must be volatile, Nonlinear mass to signal response
CAD	Yes	Yes	Can be used with gradients	Solvents and buffers must be volatile, Nonlinear mass to signal response

Currently, ELSD and CAD detection methods are used for the direct analyses of lipid classes. Both detection methods share the same principle of operation: (1) the mobile phase leaving the column is sprayed using a pneumatic nebulizer, (2) the droplets enter the heated tube where the solvent (partially) evaporates, (3) the solute particles enter into the detection chamber. However, the principal difference between the two detection methods is the technology used for solute particles detection: light diffusion for ELSD and aerosol charging for CAD (Ramos et al. 2008). The CAD as a detector for lipid analysis has advantages over ELSD due to higher sensitivity and better precision judged by minimum limits of detection (LOD) and repeatability (RSD) values (Ramos et al. 2008; Moreau 2009). Comparing to another popular detector for lipid analysis mass spectrometry (MS) detector, CAD is cheaper and easier to use.

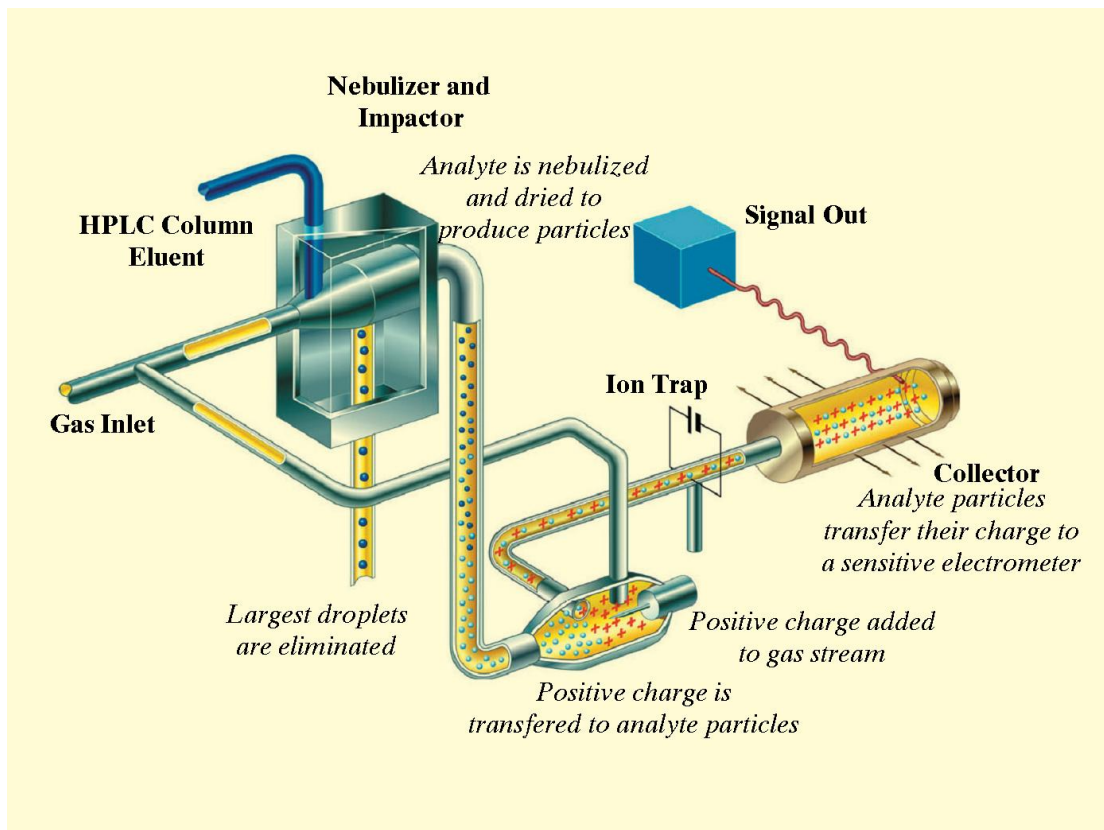


Figure 1.16 Demonstration of the working principle of the charged aerosol detector (CAD). Figure courtesy of ESA (Moreau 2009)

1.4.2.3 Fatty acids quantification and identification

The procedure for the determination of fatty acids by GC-MS consists of several steps such as esterification of lipids (sample preparation), sample injection, separation, identification and quantification (Eder 1995). The accuracy of total fatty acids quantification is generally influenced by a number of experimental factors. Esterification of lipids is the most critical step among those. Acid-catalyzed transesterification is the most common used method for preparation of fatty acid methyl esters (FAMEs), which is found in various applications (Abdulkadir and Tsuchiya 2008; Khoomrung et al. 2008; Glaser et al. 2010; Ichihara and Fukubayashi 2010). Although, preparation of FAMEs in this way delivers precise and accurate results, the reaction time to complete the conversion of lipids to FAMEs is considered as time consuming (from one to four hours) when using conventional heating method (Shimasaki et al. 1977; Ulberth and Henninger 1992; Masood et al. 2005). Recently, there has been growing interest in speeding up the reaction of chemical synthesis by microwave irradiation in different applications (Söderholm et al. 2010). The applications of microwave-assisted derivatization to prepare FAMEs from fatty acids (free & bound fatty acids) can be found in various types of biological samples (Jeyashoke et al. 1998; Zhang et al. 2000; Itonori et al. 2004; Tomas et al. 2009; Liebeke et al. 2010).

Briefly, bound fatty acids had to be split from lipids by saponification and then converted into methyl esters by esterification. Although this method delivers accurately quantitative results, having several steps of sample preparation (saponification, esterification, extraction, and base wash) is time consuming and also high possibility to have an error because of sample loss during the multi steps of sample preparation processes. To overcome those problems, the one-step method which combines saponification and esterification in one-step (Abdulkadir and Tsuchiya 2008), has been recently introduced for yeast FAMEs analysis (Zhang et al. 2011). Although the one-step method provides quantitative data and simplifies sample handling, the long reaction time (at least 1.5 hour) of FAME preparation remains an issue when dealing with a large number of samples. Besides, using of conventional heating (hot plate) cannot provide the effectively and homogeneously radiated heat to whole chamber area, leading to low precision of the measurement. Furthermore, the one- step method had been developed intentionally for marine animal samples, which are completely different matrices than yeast cells.

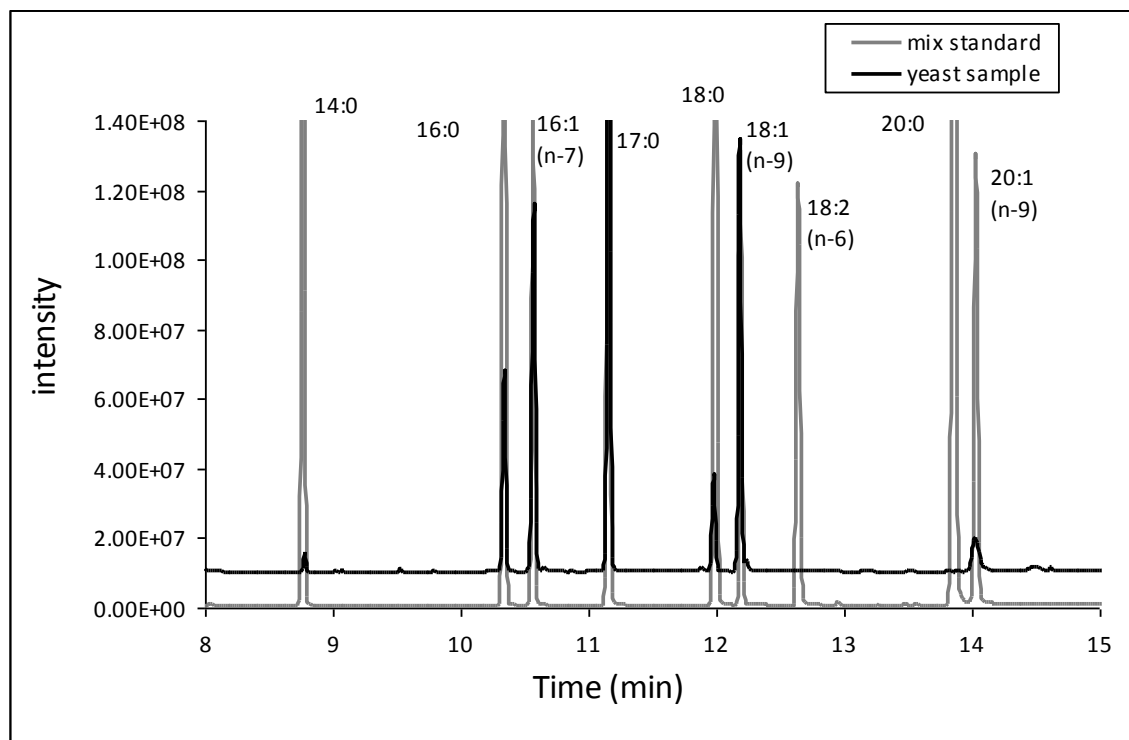


Figure 1.17 Identification of unknown FAME using GC-MS based on the retention time of the known standards.

The identification of unknown FAMEs from yeast cells was achieved by comparing their retention times and mass spectrum profiles with known standards.

1.4.2.4 Lipid fluxes calculation

To explore the carbon channeling in lipid metabolism, the fluxes in lipid biosynthesis (in units of $\mu\text{mol/gDW/h}$) can be calculated based on lipidome data from the measured lipid profiles of each condition. The metabolic flux information provides a clear picture of the changes in the flux distribution in response to the different factors evaluated.

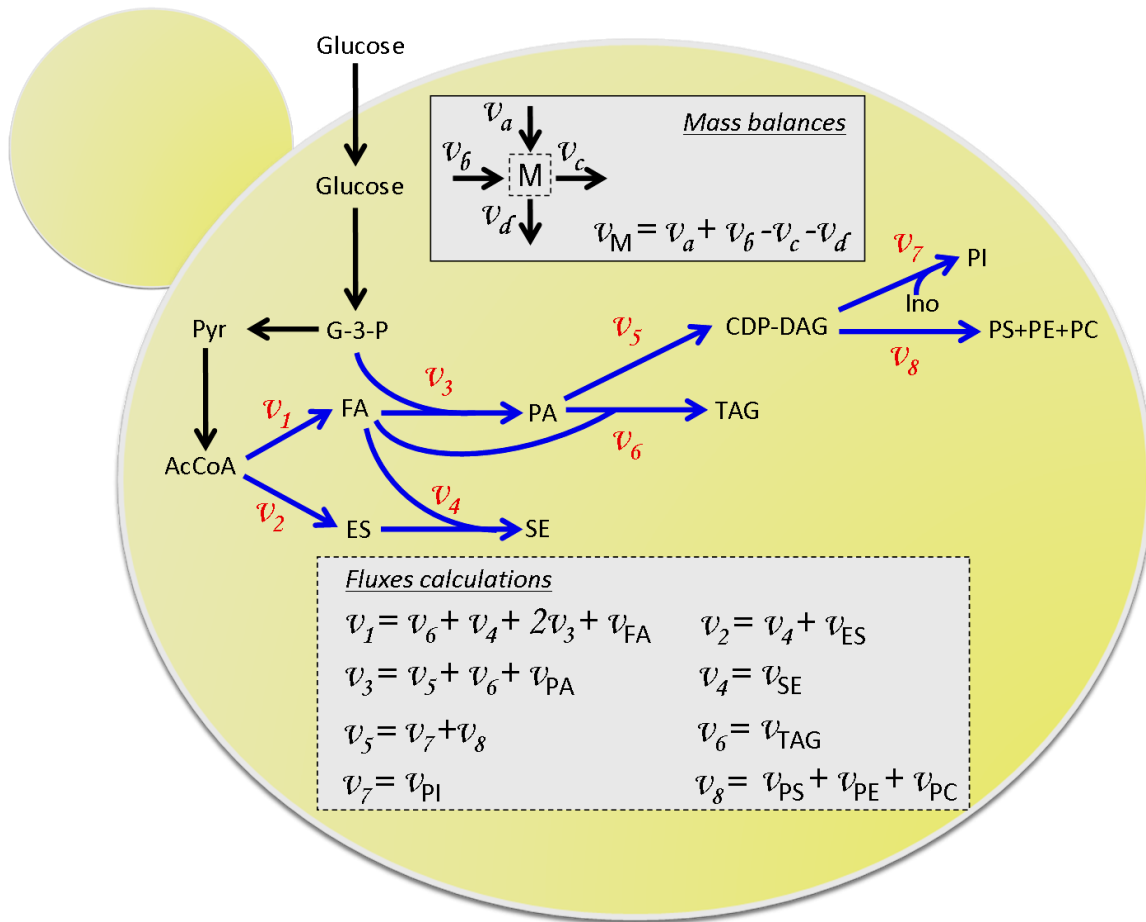


Figure 1.18: The calculation of fluxes through lipid synthesis pathway for lipid fluxes study in **paper I** and **paper II**.

The flux balances around each metabolite of the metabolic networks (Kauffman et al. 2003) consider the fluxes around each metabolite (**M**), mass balance for metabolite M and the flux of metabolite M (\mathbf{V}_M) at steady state are defined in figure 1.18.

Based on the flux balance concept mentioned above, all the fluxes through each lipid classes can be calculated using the flux calculation equations in figure 1.18.

Chapter 2 Results and Discussions

2.1 Integrated analysis reveals that regulation of lipid metabolism occurs at multiple levels

2.1.1 Co-influence of Snf1 and IC effects on yeast lipid metabolism

To elucidate the co-influence of Snf1 and inositol on lipid metabolism of *S. cerevisiae*, we undertook a global study of lipid metabolism by performing three perturbations following a robust factorial experimental design (**paper I**). The first factor is the level of inositol-choline (IC factor), which is known to directly influence lipid metabolism (Jesch et al. 2005). The second factor is a genetic difference factor or a strain factor (ST factor), which is the comparison of *SNF1* deficiency with the reference strain. The third factor is nutrient limitation (carbon and nitrogen) factor that results in a global perturbation of the lipid pool inside the cell (Sattur and Karanth 1989; Sattur and Karanth 1989). Using a systems biology approach (Canelas et al. 2010) a global regulatory model for lipid metabolism could be established, and in particular we could identify which genes involved in lipid biosynthesis that are correlated with the fluxes towards different lipid components.

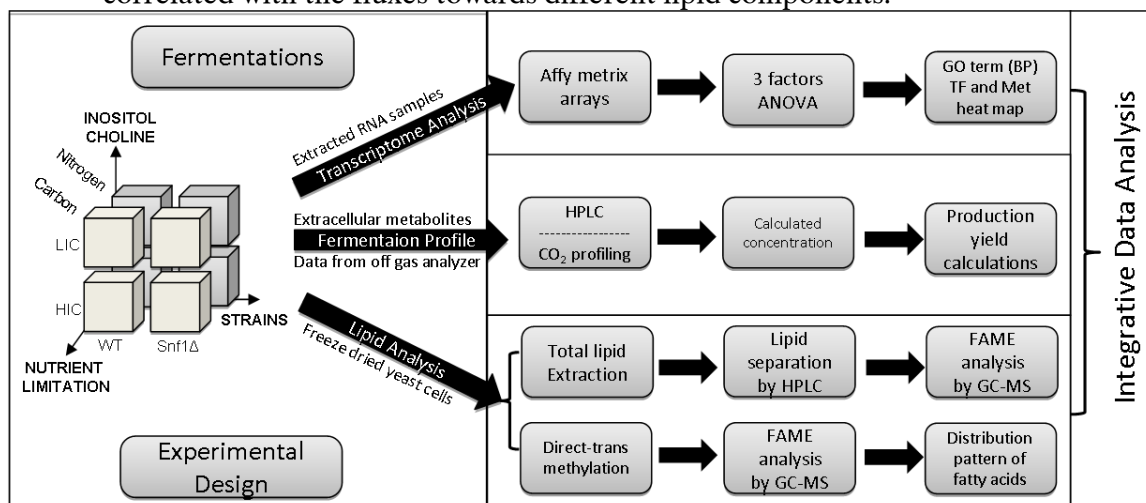


Figure 2.1 Illustration of the 3 factor factorial design and schematic analysis of our workflow for integrated analysis involving transcriptome-lipidome analysis of the inositol-choline effect on lipid biosynthesis in *snf1* Δ yeast strain

As previously described in the introduction part, the impact of IC and Snf1 individually on lipid metabolism and its regulations are substantial. Due to our factorial experimental design, the co-influences resulting from cross talk between inositol-choline and Snf1 could, however, also be evaluated. With our experimental setup in paper I, it is possible to see the effects from the knocking out of *SNF1* and also the substrate limitations that leads to changes in Snf1 activity (i.e. with the ST factor it is presence versus absence of Snf1 and for C-limitation Snf1 is active and for N-limitation it is inactive). So we have two slightly different co-influences of inositol-choline with active Snf1 and inositol-choline with inactive Snf1.

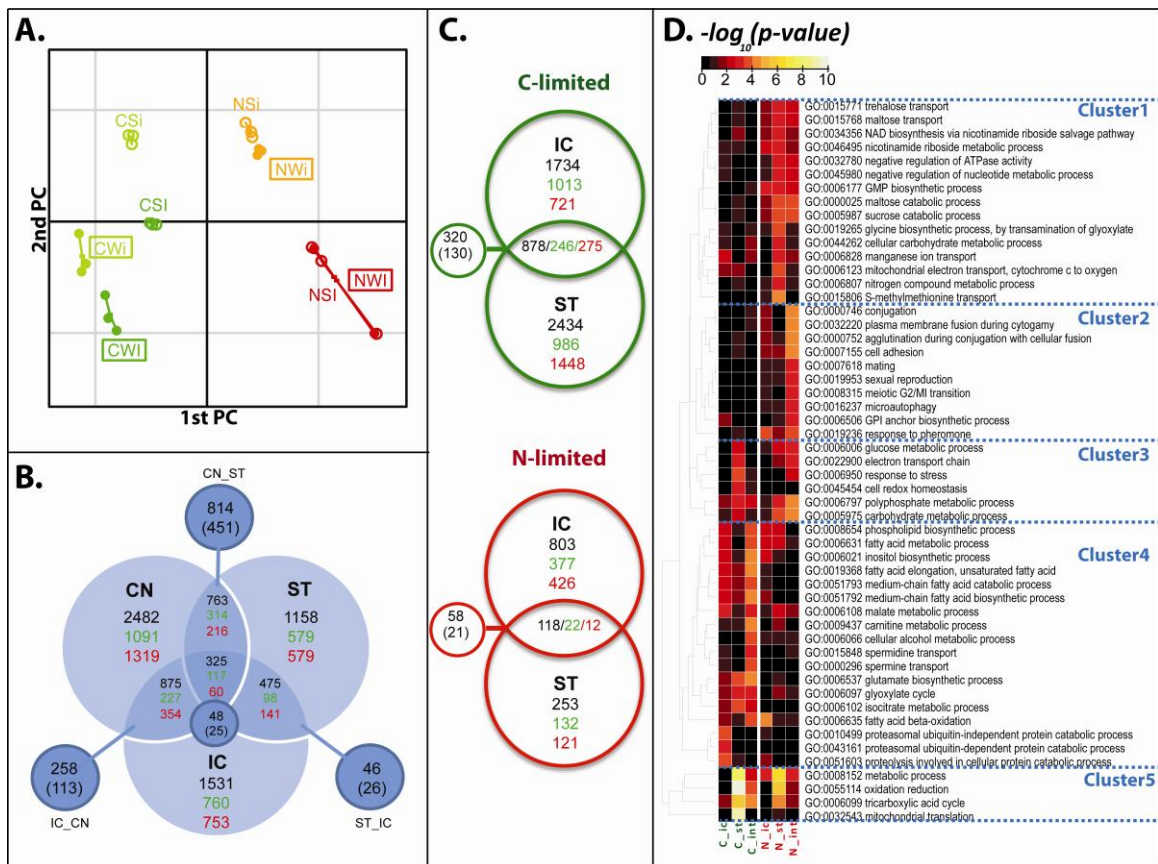


Figure 2.2 Transcription data analysis at a global view; (A) Principal component analysis of the transcriptome data. Each dot represents one biological replicate. The dots of same condition are connected by solid lines. C = C-limited , N = N-limited, W= wild type, S= snf1 Δ , i = LIC, and I = HIC. (B) Venn diagram of 3-factor ANOVA analysis i.e. carbon/nitrogen limited (CN), strain (ST), inositol-choline (IC) and their interactions, p -value < 0.01 was used. (C) Venn diagrams of 2 factors ANOVA analysis i.e. IC, ST and their interaction when focus on C-limitation and N-limitation separately, p -value < 0.01 was used. For figure 2B and 2C, the black numbers on top are the number of significant genes, green means down-regulated, red means up-regulated genes. In the intersection areas, only the genes that are down-regulated together or up-regulated together among those factors are represented. The small circles sticking out of the intersection areas represent the number of genes that are responded to each interaction effect deriving from those factors, and the numbers in the brackets show the number of overlapping genes which were also found in common with the intersection area. (D) A heat map of over-representation of GO terms (Biological Process) responded to each factor in the range of 0-10 of log(p -value).

We used the Affymetrix DNA microarray platform to measure the expression level of all genes and access the global effect caused by deletion of *SNF1*, by a high inositol-choline level, and the combination of the two at two different kinds of nutrient-limitation (C- and N-limitation). The transcriptome data of the 8 different conditions derived from 24 yeast 2.0 Affymetrix DNA microarrays were decomposed using principal component analysis (PCA) and 3-factor ANOVA analysis ($\alpha=0.01$) to obtain the global responses of gene expression at the different conditions. It is seen that the biological replicates are well grouped (Figure 2.2A), showing very high reproducibility.

Furthermore, the transcriptome data are presented in a Venn diagram (Figure 2.2B) showing that the number of significant genes in response to the nutrient limited (CN) factor was about 2 times of that in response to the Snf1 deficiency factor (ST) and the inositol-choline (IC) factors, showing that a change from carbon to nitrogen limitation is the dominant factor. This is in consistency with the PCA that also illustrated that the impact of nutrient limitation is the main factor separating the samples in the first principal component. We therefore re-analyzed the transcriptome data using 2-factor ANOVA analysis of the C-limited and N-limited data sets separately (Fig. 2C) to get better insight into the effect of the ST and IC factors. Based on this we found that there were more genes being significantly changed at C-limitation than at N-limitation. The variance between the reference and the *snf1Δ* strain (represented by the distance between reference-*snf1Δ*, Figure 2.2A) was very small at N-limited condition supported by the very small number of significant genes affected by the strain (ST) factor at N-limitation (see Venn diagram in Figure 2.2C). This is due to general inactivation of Snf1 at N-limited growth conditions (Usaite et al. 2009; Zhang et al. 2011), but still deletion of *SNF1* influences the transcription of around 250 genes.

Subsequently, functional enrichment in response to each perturbed factor was calculated using our reporter algorithm, and the results are summarized in Fig. 2D. With this approach we identify GO terms that are enriched in response to the different factors, and this allows for direct interpretation of which biological processes are affected in response to the different factors evaluated. It is seen that the identified GO terms (biological process) grouped into 5 main clusters (Figure 2.2D). Cluster 1 contains genes enriched in sugar transport and metabolism, which were mainly influenced by the ST factor and only at N-limited conditions. Cluster 2 contains genes involved in conjugation and reproduction, which were interaction effects of the ST and IC factors at N-limited condition only. Cluster 3 contains genes involving carbohydrate metabolism and stress response, which were mainly affected by the ST factor at C-limited conditions. Most biological processes of these three clusters are strongly influenced by a combination effect of the ST and IC factors that occur only in N-limited condition. Cluster 4 (The biggest group) contains genes mainly involved in fatty acid, phospholipids, inositol and biosynthesis process. Interestingly, not only individual factors like ST and IC influence the transcriptional changes of the processes in this cluster, there are also strong influences by the combination effect of the ST and IC factors indicating by the interaction *p*-values between ST and IC that only occurred at C-limited and not at N-limited condition. Cluster 5 contains genes involved in the TCA cycle and mitochondrial functions, which were strongly affected by the ST factor at both C-limited and N-limited conditions as previously known (Woods et al. 1994; Sanz 2003; Thomas and Polge 2007). The results of the reporter GO term analysis are in agreement with analysis of reporter metabolites and reporter transcription factors (TFs). The results of this analysis (reporter metabolites and TFs) are reported as heatmaps in **paper I** (Figure S4 and S5).

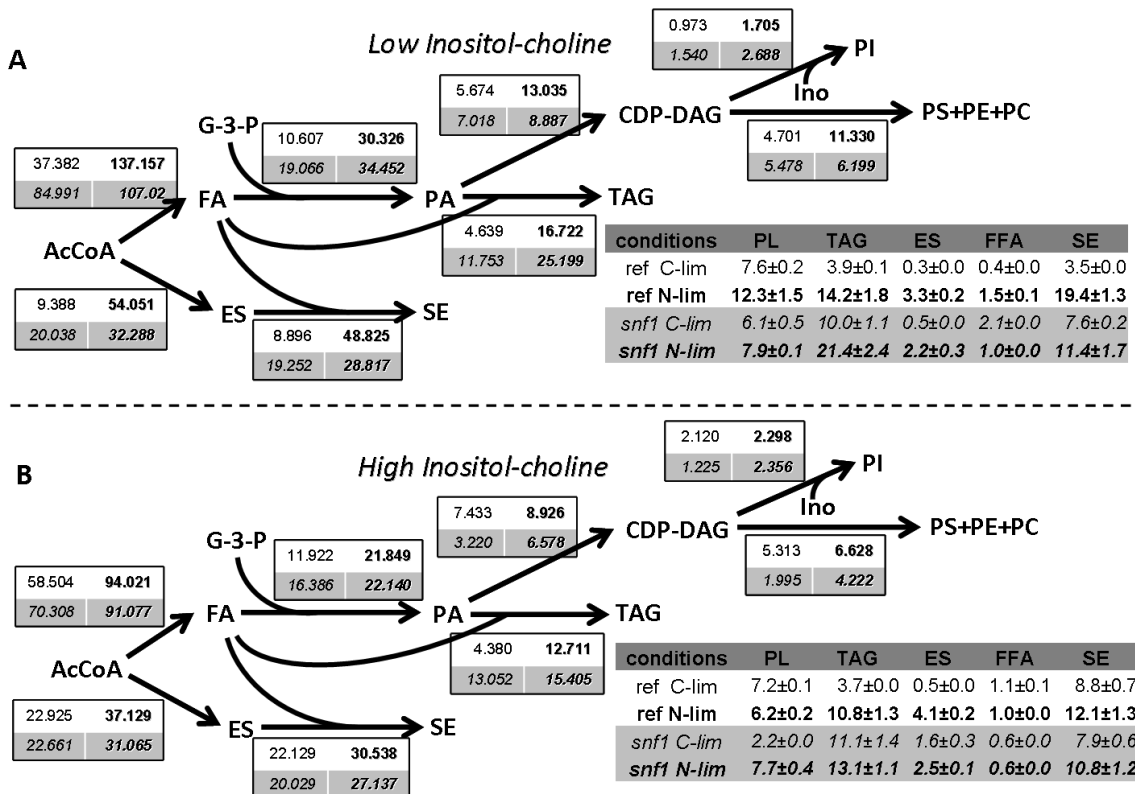


Figure 2.3 Fluxes through the different reactions of lipid biosynthetic pathway for LIC (A) and HIC (B). All fluxes are shown in units of $\mu\text{mol/gDW/h}$. The upper value (normal font) is for the reference strain, the lower (italic font) is for *snf1* Δ strain, normal font (left) and bold font (right) indicate the value from C-limitation and in N-limitation respectively. The level, in units of mg/gDW, of the different lipid species is shown in the table. (C = C-limited, N= N-limited, W= wild type, S= *snf1* Δ , i = LIC, and I = HIC)

As illustrated in Chapter 1, the lipid fluxes were affected by many factors at several levels, such as gene transcription, protein phosphorylation, and enzyme activity. Thus at N-limited condition, where there is excess glucose available, the fluxes from AcCoA were about 3 and 2 fold higher when compared to those at C-limited conditions for LIC and HIC conditions, respectively. According to the reporter metabolite analysis (**paper I**, Figure S4.), AcCoA was found to be significantly different in response to the IC factor. At LIC condition, the flux to the phospholipid pools is larger than that to the storage lipids (i.e. TAG and SE). On the other hand, the flux to storage lipids at HIC condition was greater than that at LIC (since the IC effect result in down-regulation of the whole set of phospholipid synthesis genes). Interestingly, we found Gis1 as one of the most significant TFs that were strongly affected by the ST factor at C-limitation and both the ST and IC factors at N-limited condition. Since Snf1 has protein-protein interaction with Gis1p as a repressor (Balciunas and Ronne 1999), the expression level of Gis1 genes were increasing at HIC condition only at N-limited conditions where Snf1 is inactive. Moreover, this TF has interactions (directly or indirectly) with several genes involved in lipid biosynthesis (i.e. *FAA2*, *ERG28*, and *DPP1*) and also carbohydrate metabolism (i.e. *PGM2*, *HOR2*, *TPK1*, *ICL1*, and *PCK1*). Moreover, we also found inositol-3-phosphate as a significant reporter metabolite in response to the IC factor at both C-limited and N-limited conditions. This directly resulted from addition of inositol-choline to the

culture medium. Thus, through our experimental design we obtained significant alteration in the fluxes of the different branches of lipid metabolism, and in the following we will discuss how the changes in these different fluxes are linked to the transcriptome and the different factorial effects.

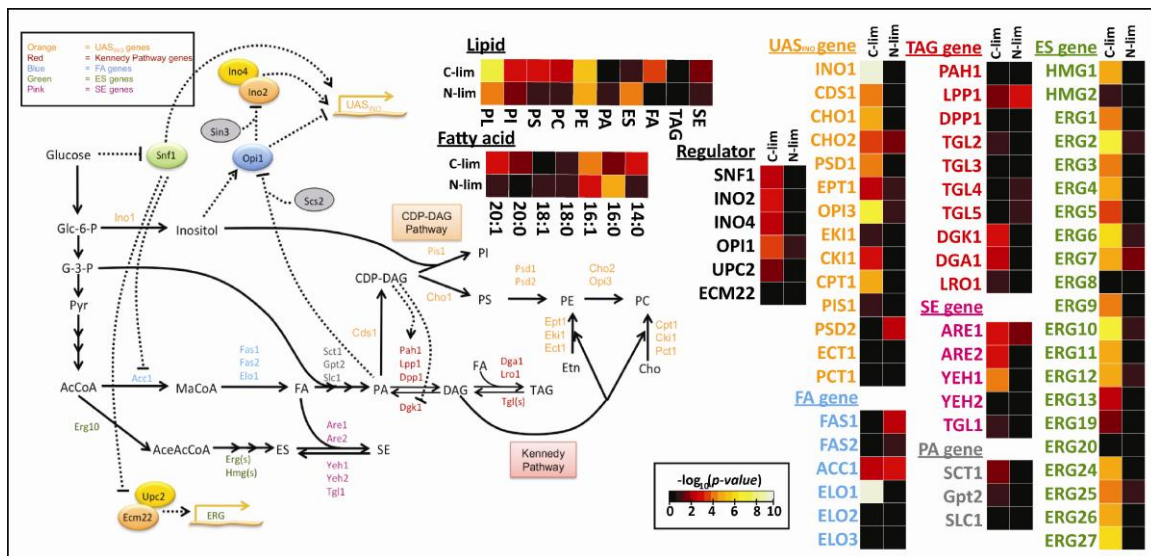


Figure 2.4 Biosynthetic pathway and regulation model of lipid metabolism in *S. cerevisiae*. The pathway shows the synthesis of neutral lipids (FA, ES, SE, DAG, and TAG) and phospholipids (PA, PI, PS, PE, and PC). The genes that are known to encode enzymes catalyzing individual steps in the lipid synthetic pathway are indicated. The co-influence levels on gene expression and lipid metabolites by the combination of inositol-choline and Snf1 are evaluated by interaction p-values presented as significance heatmaps.

Based on the integrative analysis, figure 2.4 summarizes the key regulation of the lipid biosynthesis pathways confirmed and identified by our study. The co-influences between Snf1 and inositol-choline are also reported as a heatmap in the figure for each gene expression and measured lipids (adjusted interaction p-values). The summarized figure provides compelling evidence of substantially co-influences of inositol-choline and Snf1 in terms of regulating the lipid metabolism. Noticeably, we found that the co-influence of inositol-choline and Snf1 depends on the active state of Snf1 at both the transcription and lipid metabolite levels. Interestingly, *INO1* was substantially influenced by both factors, which should be the consequence of the response of the regulators Ino2, Ino4 and Opi1, and this leads to changes in phospholipid metabolism. Transcription of genes in the ergosterol and sterol-ester synthesis pathway was also influenced by cross talking of inositol-choline and Snf1. Surprisingly, transcription of *ACC1*, encoding the rate controlling enzyme in fatty acid biosynthesis, was significantly influenced at both C- and N-limitation indicating a special response to the combination of IC and Snf1 (both in active or inactive form). This evidence may link to the fact that inositol auxotrophy in a *snf1Δ* strain can be rescued by inhibiting Acc1 activity (Woods et al. 1994), probably due to a decreased flux through fatty acid synthesis, which may allow the mutant to synchronize fatty acid synthesis with the reduction of inositol synthesis when Snf1 is absent, and hereby ensure that phospholipid biosynthesis is balanced with the demand for cellular growth. Besides, we found that the interaction between IC and Snf1 did not influence the

expression levels of most of the lipid genes much in N-limited condition (except a few genes e.g. *ACC1*, *CHO2*, *PSD2*, *LPP1* and *FASI*) since the global transcriptional responses caused by the ST factor were so small at N-limited conditions (where Snf1 were inactive).

2.1.2 The effects of *INO*-level on yeast lipid metabolism

The levels of *INO*-gene (*INO2* and *INO4*) expression in both C-limited and N-limited conditions and in different strains (reference, *ino2Δ*, *ino4Δ*, *ino2Δino4Δ*, *opi1Δ*) were evaluated using the expression level from micro array analysis (Figure 2.5). Even though there were metabolic cycle patterns with the *opi1Δ* strain grown at C-limited condition, the expressions of the *INO* genes were consistently high (Figure 2.5A). This evidence shows that *INO* genes are up-regulated when their repressor, Opi1, is absent. At C-limited condition, *INO* levels are low in both the two single and the double deletion strains (Figure 2.5A and C). Interestingly, the *INO4* gene seems to be expressed at a high level at N-limitation (Figure 2.5B) due to the nitrogen and/or amino acid and that it possibly also try to compensate the failure of *INO2* expression by up-regulating its expression in the *ino2Δ* strain at N-limitation (Figure 2.5D).

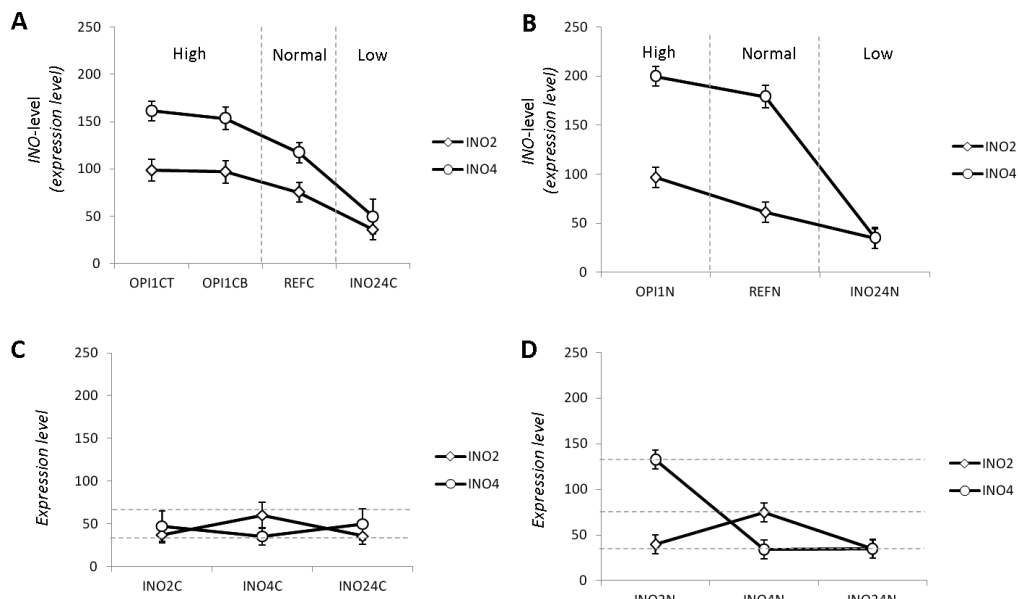


Figure 2.5 The normalized expression values of *INO2* and *INO4* (*INO*-level) for each strain. The key factor set shows the different *INO*-level at C-limitation (A) and N-limitation (B). The deficient factor group set shows the different *INO*-level at C-lim (C) and N-lim (D)

In paper II, we undertook a global study of lipid metabolism in response to different *INO*-levels (*INO2* and *INO4*): **i) normal *INO*-level** based on wild-type (CEN.PK113-7D), **ii) high *INO*-level** based on an *opi1Δ* strain, and **iii) low (or rather absent) *INO*-level** based on an *ino2Δ ino4Δ* double deletion strain. Moreover, we also focused on the deficient factors as a sub story comparing the individual knockout strains (*ino2Δ* and *ino4Δ*) with the double deletion strain.

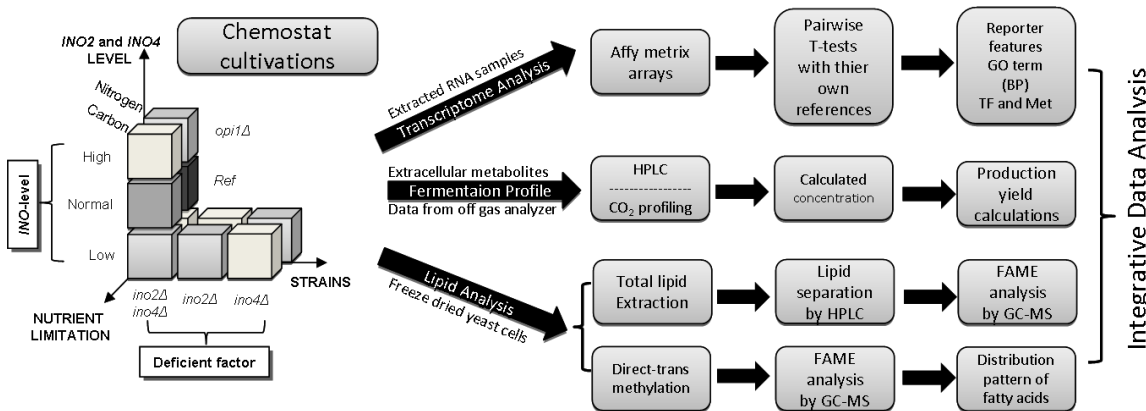


Figure 2.6 Schematic analysis of a workflow for integrated analysis, transcriptome-lipidome, of *INO*-level (key factor) and deficient factor effect on lipid biosynthesis

We used the Affymetrix DNA microarray platform to measure the expression level of all genes and access the global effect caused by the *INO*-level under nutrient-limited conditions (C-lim and N-lim). The transcriptome data were decomposed using principal component analysis (PCA) and student T-test analysis ($\alpha=0.001$). The transcriptome data are presented in Venn diagrams at C-limited (Figure 2.7A) and at N-limited (Figure 2.7B) showing that the high *INO*-level (*op1Δ*) strain had more genes being significantly changed at C-limitation. On the other hand, the low *INO*-level (*ino2Δino4Δ* double deletion) strain had more genes being significantly changed at N-limitation.

From clustering of reporter GO terms (biological process at $P<0.001$), there were 4 main clusters identified as shown in figure 2.7C. Cluster 1 (the largest group) contains the genes involving the phospholipid biosynthesis, myoinositol biosynthesis and transport, fatty acid metabolic process, cell conjugation, and ribonucleoside biosynthetic process which were highly up-regulated due to the deletion of *OPI1* (high *INO*-level), especially at N-limited condition, but down-regulated at low *INO*-level at both C- and N-limitation. Cluster 2 contains genes involving maltose and sucrose catabolic process which were highly up-regulated due to the C-limitations. Cluster 3 contains genes involving nitrogen compound metabolism, amino acid and peptide transport, and proton transport which were extremely down-regulated in the low *INO*-mutant at N-limited condition. Cluster 4 contains genes involving amino acid biosynthesis, mitochondria biogenesis, and endoplasmic reticulum associated unfolded protein responses (ER-UPR) which were highly significant in the double mutant strain. These genes were up-regulated at low *INO*-level and N-limitations but down-regulated at C-limitation.

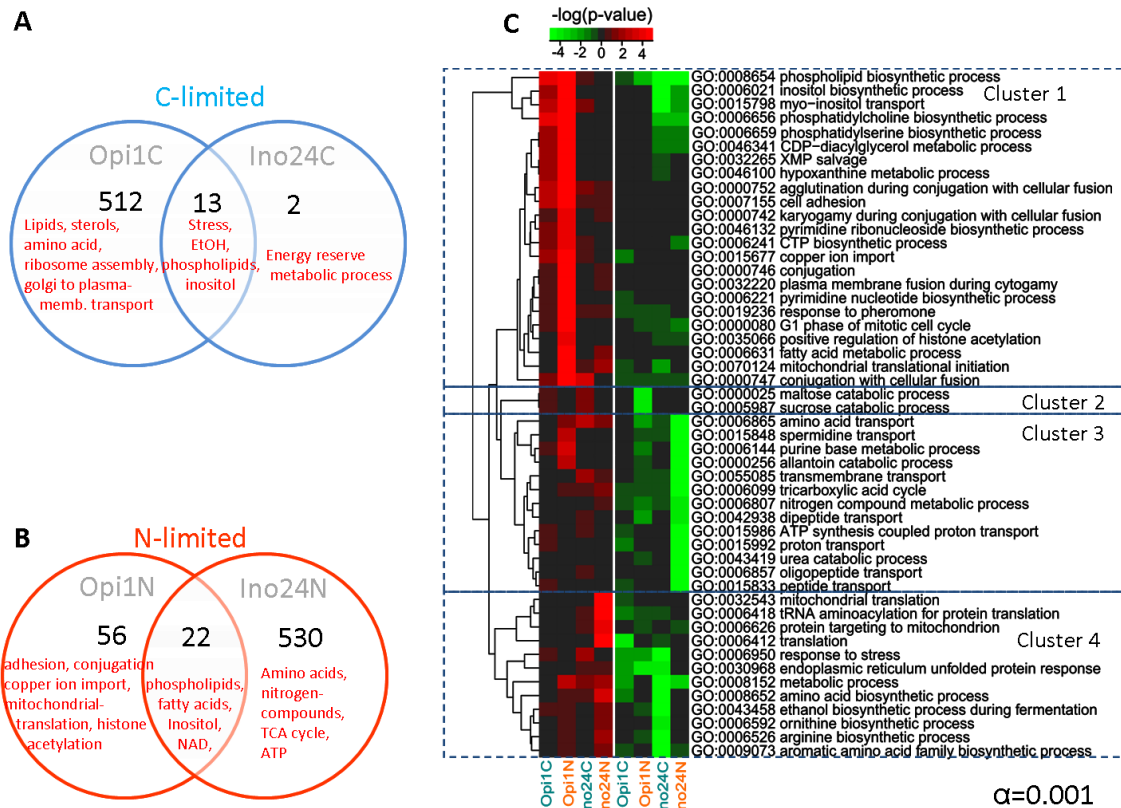


Figure 2.7 Transcriptional data analysis; Venn's diagram of significant genes of mutant strains caused by different *INO*-level when focus on C-limitation (A) and N-limitation (B) separately, p -value < 0.001 were considered. (C) A heat map of overrepresented GO terms (Biological Process) of each factor comparison showing in the range of -4 to 4 of $\log(p\text{-value})$. The green color indicates down-regulation and red indicates up-regulation compared to the reference strain.

To identify specific transcriptional regulation of metabolism in response to deletion of *INO2* and/or *INO4*, we performed transcriptome comparison of the three *INO* deficient mutants (defined as deficient factor in Figure 2.6). For each strain we identified genes with significantly changed expression compared with the reference strain and then presented the results for the three strain as Venn diagrams for both C-limited (Figure 2.7A) and N-limited (Figure 2.7B) conditions. Even though it has been known that Ino2 and Ino4 are heterodimeric transcription factor, we found some specific changes upon deletion of each of these genes (Figure 2.8A and B). Noticeably, *ino4Δ* has more significant genes due to the absent of *INO4* compared with the two other mutants at C-limitation. At N-limitation, on the other hand, the effect is when both *INO2* and *INO4* were deleted. In addition, most of the genes involving nitrogen compounds metabolism and carbon utilization (Figure 2.8C, Cluster 1) were down-regulated due to the absence of *INO2* and *INO4* but up-regulated when only *INO2* or *INO4* were individually knocked out at N-limitation. Moreover, we found that the genes involving ribosome biogenesis and rRNA processing (in cluster 2, Figure 2.8C) are dramatically down-regulated when *INO4* was knocked out especially at C-limited conditions.

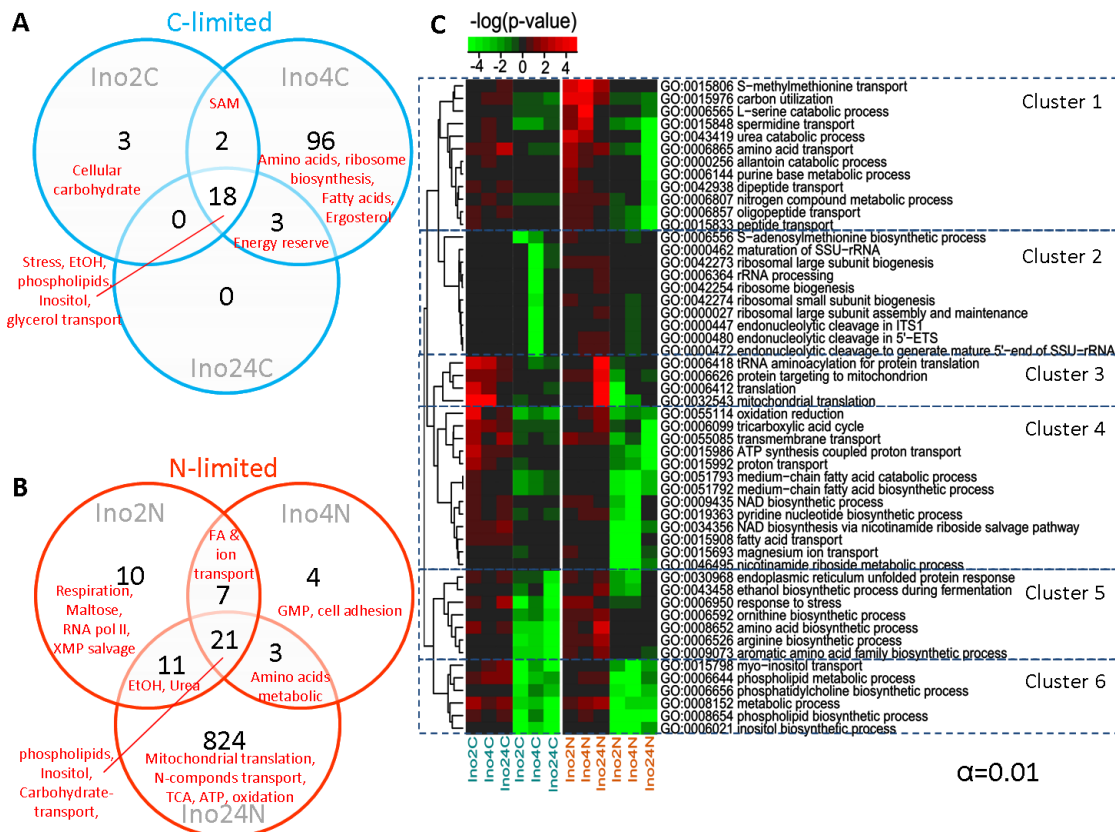


Figure 2.8 Transcriptional data analysis; Venn's diagram of significant genes of mutant strains caused by different deficient factors (single and double deletions) when focus on C-limitation (A) and N-limitation (B) separately, p -value < 0.01 were considered. (C) A heat map of overrepresented GO terms (Biological Process) of each factor comparison showing in range of -4 to 4 of $\log(p\text{-value})$. The green color indicates down-regulation and red indicates up-regulation compared to the reference strain.

Based on the transcriptome analysis results, it showed that Ino4 could possibly play role in repressing ribosome biogenesis (which basically supports protein synthesis). In addition, most of the genes involving protein translation (Cluster 3 in Figure 2.8C, including mitochondria translation) were up-regulated in the double mutant at N-limited conditions while they were only up-regulated when either *INO2* or *INO4* were deleted at C-limitation. Consistently, the genes involving phospholipid, inositol, and fatty acids (UAS_{INO}-contained genes in cluster 6, Figure 2.8C) were down regulated in all three strains at both C-limited and N-limited conditions. Nevertheless, they were 2 other clusters that also captured down-regulated genes in all three *INO*-deleted strains, but different for the two nutrient limitations. The first group listed in cluster 4 (involving fatty acids biosynthesis and β -oxidation, TCA cycle, ATP, NAD, magnesium ion, and proton transport) was mainly down-regulated at N-limited condition. Cluster 5, on the other hand, contains genes involving ER-UPR and stress response, ethanol and amino acids biosynthesis that were mainly down-regulated only at C-limitation.

Focusing on the deficient effects at metabolic flux level, double deletion of the *INO* genes (especially at N-limitation) can cause more effect to the dramatically reduction of phospholipids than the effect of single deletions (Figure 2.9).

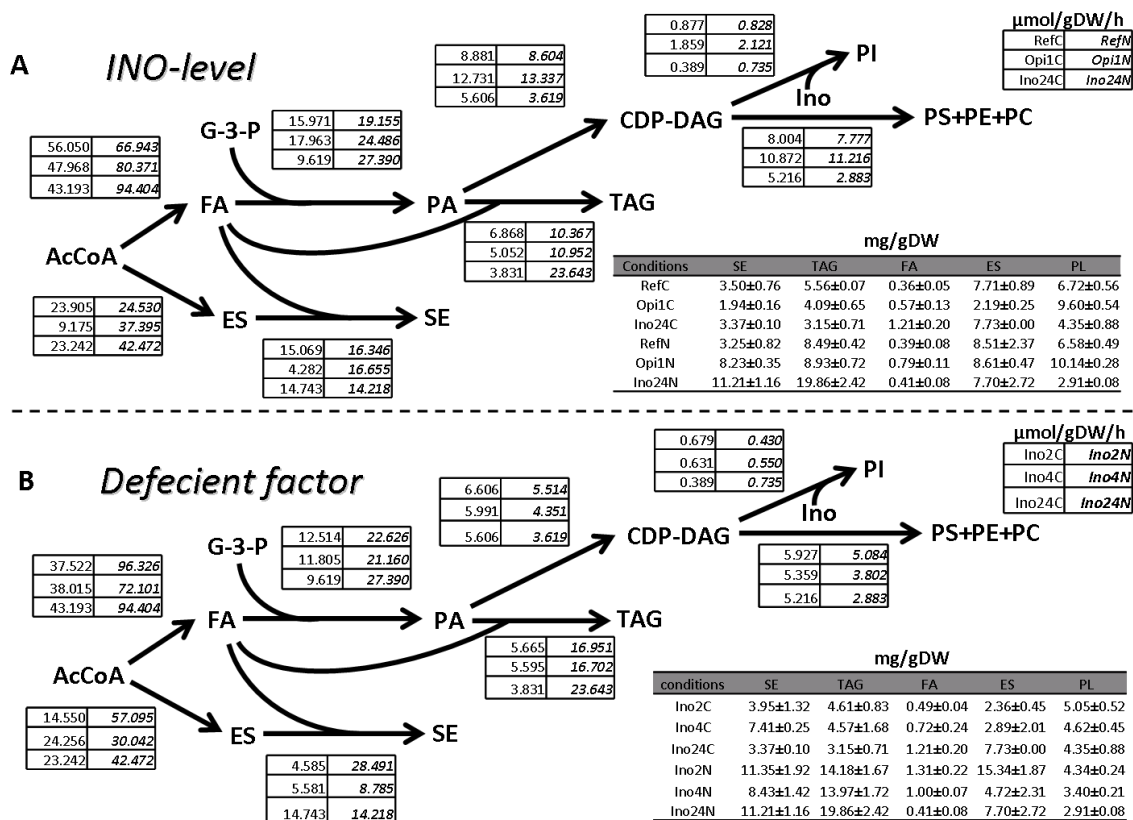


Figure 2.9. Fluxes through the different reactions of the lipid biosynthetic pathways for different *INO*-levels (A) and different deficient factors (B). All fluxes are shown in units of $\mu\text{mol/gDW/h}$. The normal font (left) and bold font (right) indicate the value from C-limitation and in N-limitation respectively. The levels, in units of mg/gDW ($\pm \text{SD}$), of the different lipid species are shown in the table. (C = C-limited, N= N-limited).

About a 70% decrease in PLs can be found when both *INO* genes were deleted, but there were only 50% or 60% decreasing in PLs when *INO2* or *INO4* were deleted respectively. Even though this double deletion effects did not make much changes in the PL pool at C-limitation, it still caused about 50% lower level of PI when compare to the single deletion strains. From the heatmap of reporter metabolites (figure S4 of **paper II**), S-adenosyl-L-methionine or SAM was strongly decreased in all low *INO*-level strains and this lead to a decrease of PLs (especially PC) since it is required for production of PC.

The production rate and accumulation of PC can cause ER stress and UPR activation which lead to the up-regulation of TAG and ES biosynthesis (Tehlivets 2011). At N-limitation, the low *INO*-level strain (double mutant) could produce and accumulate TAG and SE about 1.2 folds more when compared to the high *INO*-level strain (*opi1Δ*) and about 1.5 folds when compare to the reference strain (Figure 2.9). Interestingly, the double deletion strain showed a greater effect in increasing TAG only at N-limitation. This evidence was supported by the up-regulation of the *ARE1* gene which codes

for the enzyme for the first step of SE biosynthesis. At C-limited condition, on the other hand, *ino2Δ ino4Δ* has a larger effect on decreasing the TAG level compared with the single deletion strains. Moreover, the fluxes through ES of the *ino2Δ* strain was about 80% lower when compare to *INO4* deletion and double deletion at C-limited condition.

2.1.3 Linkage between lipid and amino acid (protein) biosynthesis

2.1.3.1 The role of Snf1-Tor1 on lipid metabolism

To map the co-influences of Snf1 and TORC1 on the regulation of FA metabolism, in **paper III**, we quantified the total FAs abundance, from both free and ester form (e.g., in TAG and SE), in the reference and mutant strains on both C- and N-limited conditions.

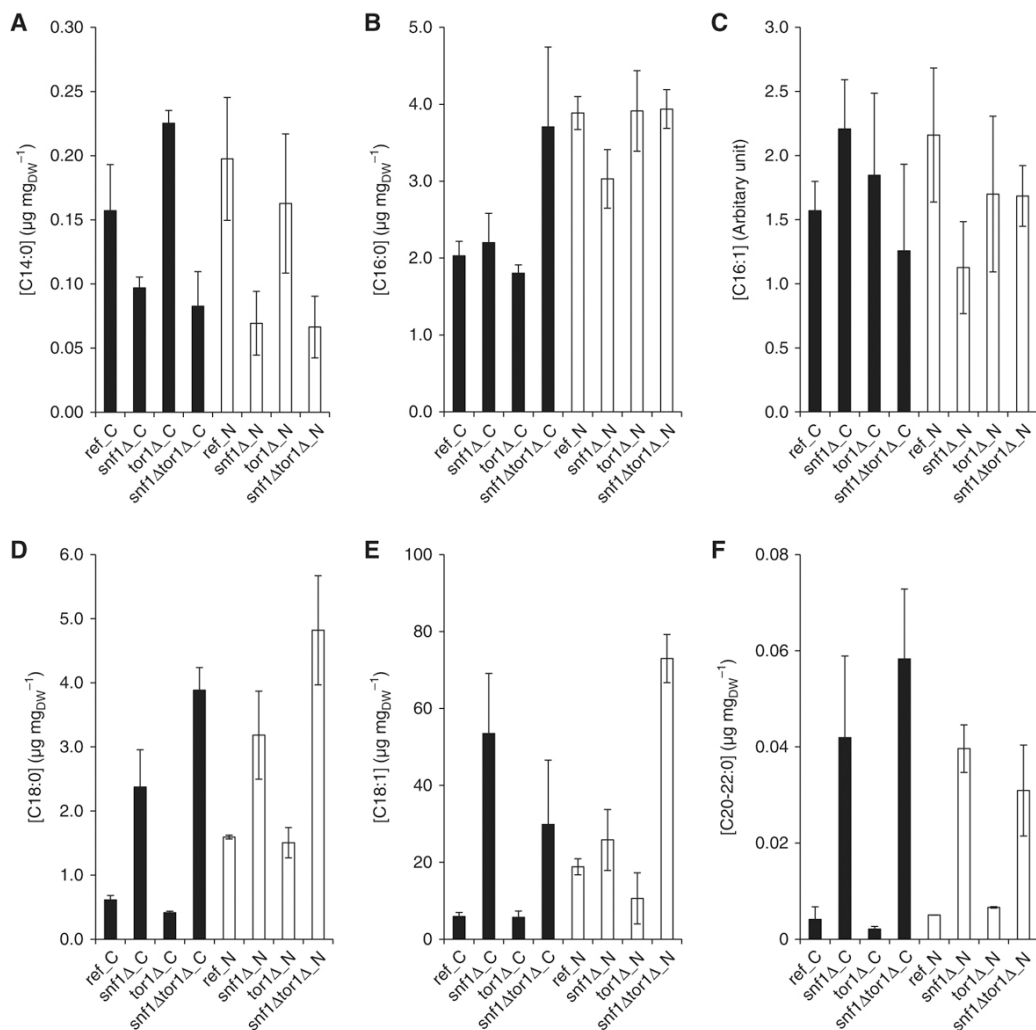


Figure 2.10 Abundance of fatty acids for all strains and two growth conditions (Zhang et al. 2011). The abundance is based on the sum of FAs in the free as well as ester form. The error bars represent the S.D. from at least three replicates. (A) C14:0—myristic acid; (B) C16:0—palmitic acid; (C) C16:1—palmitoleic acid; (D) C18:0—stearic acid; (E) C18:1—oleic acid and (F) C20:0—arachidic acid and C22:0— behenic acid. Black—C-limited condition and white—N-limited condition.

Since Snf1 regulates FA biosynthesis by inhibiting acetyl-CoA carboxylase (Acc1) under derepressive conditions (Woods et al, 1994), the significant increase of total FA in the *snf1Δ* and *snf1Δtor1Δ* strains on C-limited condition was expectable (Figure 2.10). However, there was a significant variation in the FA species between different strains and the two growth conditions. The most abundant species was C18:1, where the largest differences between strains were observed (Figure 2.10E). Interestingly, the *snf1Δ* and *snf1Δ tor1Δ* strains had higher levels of C18 (i.e., both C18:0 and C18:1) and longer FAs, on both C- and N-limited conditions, compared with the reference strain (Figure 2.10D–F), except for C14 where the result was contrary (Figure 4A). The *snf1Δtor1Δ* strain had higher amounts of C18 compared with the *snf1Δ* strain irrespective of the growth condition. The *tor1Δ* strain had higher C14 and C16 on N-limited condition, but the levels were lower on C-limited condition, compared with the reference strain. However, this was only observed for C18 and longer FAs in these two strains (Figure 2.10D and E), while the abundance of C14 was reduced in the mutant strains in which *SNF1* was deleted. There may be 2 possible reasons that can explain the different patterns between the FAs with different length.

The first reason could be that while the inhibition of Acc1 by Snf1 was relieved, and the FA synthetase (encoded by *FAS1* and *FAS2*) is constitutively functional and steadily converting short chain FAs to synthesize up to C16. Consistently, the elongase I (encoded by *ELO1*) that convert C12–16 to C18 was also found to be transcriptionally up-regulated in *snf1Δ* and *snf1Δtor1Δ*; therefore, C16 was not accumulated in the strain *snf1Δ* and *snf1Δtor1Δ* (Figure 2.10B and C). Second, it could also be that a lower peroxisome biogenesis, due to the loss of Snf1, leads to a lower level of β-oxidation of the long chain FAs (Ratnakumar and Young, 2010), therefore not only the biosynthesis, but also the degradation of FAs is regulated by Snf1. We also observed that the deletion of *TOR1* had some effect on the abundance of FAs, although to a lesser extent compared with those for *SNF1* deletion (Figure 2.10D and E). The deletion of *TOR1* in the *snf1Δ* background strengthened the changes caused by the deletion of *SNF1* for C18:0, but rather dampened the changes for C18:1 (the most abundant FA species). The FA data support the hypothesis that Tor1 has a role in the regulation of FAs.

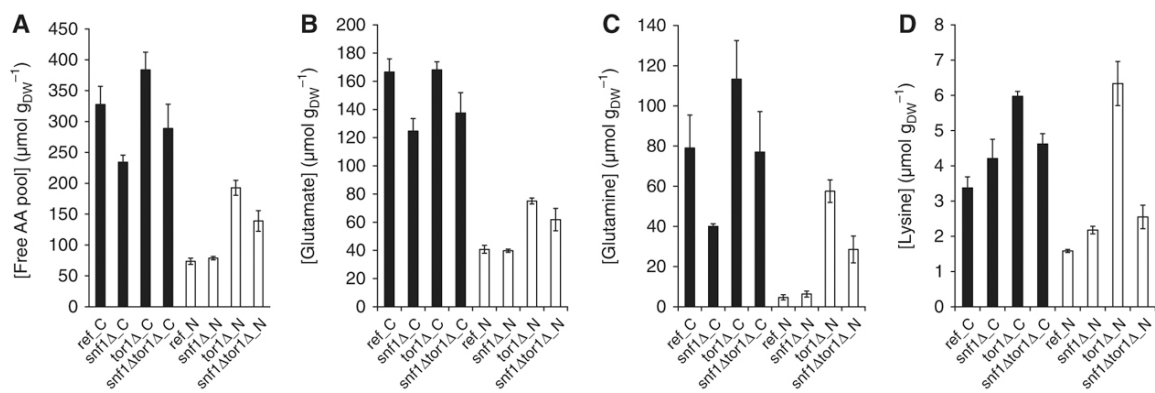


Figure 2.11 Intracellular levels of free amino acids (Zhang et al. 2011). (A) Free amino-acid pool; (B) glutamate; (C) glutamine and (D) lysine. The error bars represent the S.D. from biological replicates from three chemostat cultures. Black—C-limited condition and white—N-limited condition.

Noticeably, *TORC1* is unlikely involved in the regulation of acetyl-CoA carboxylase, and we suspect that the *TORC1* may have a role in the regulation of peroxisome and β -oxidation of FAs (figure 2.12). It is also interesting to see that although deletion of *TOR1* had not caused an evident change to the transcription and phosphorylation, many amino acids and FA species had changed significantly (Figures 2.10 and 2.11). This observation further supports the ideas that the intermediate metabolites are much more sensitive to mutations, while metabolic fluxes are rather robust (Cornish-Bowden and Cardenas, 2001; Raamsdonk et al. 2001).

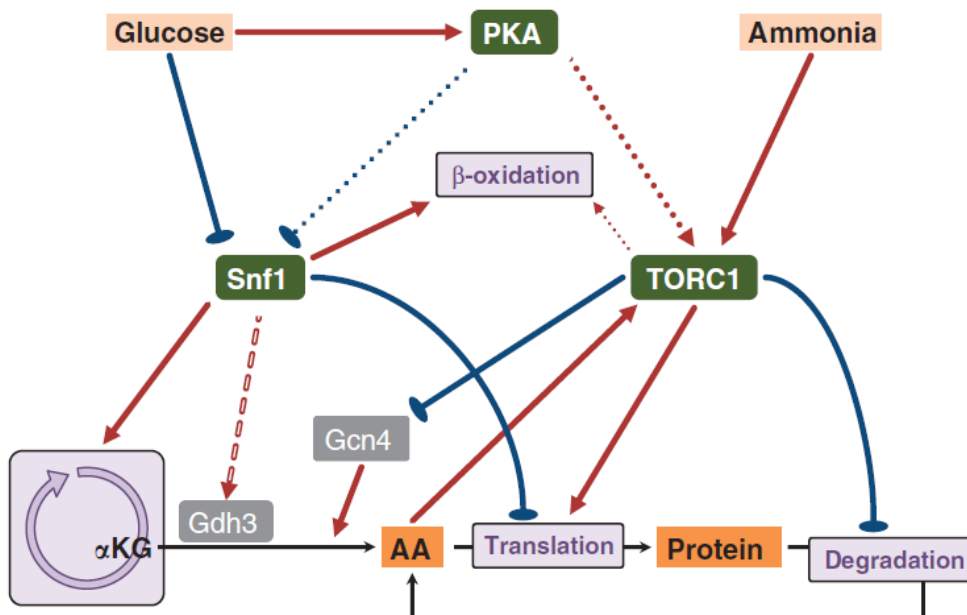


Figure 2.12 Summary of the main regulatory network of Snf1 and TORC1 (Zhang et al. 2011).

Even though our transcriptome results from **paper III** (figure 2.13) showed that deletion of *SNF1* (but not *TOR1*) is the main effect causing global change at transcriptional level, there are still some possible linkages between lipids and amino acids. We observed the co-influences of Snf1-Tor1 on ergosterol biosynthesis as one of the GO-term (biological processes) reporters.

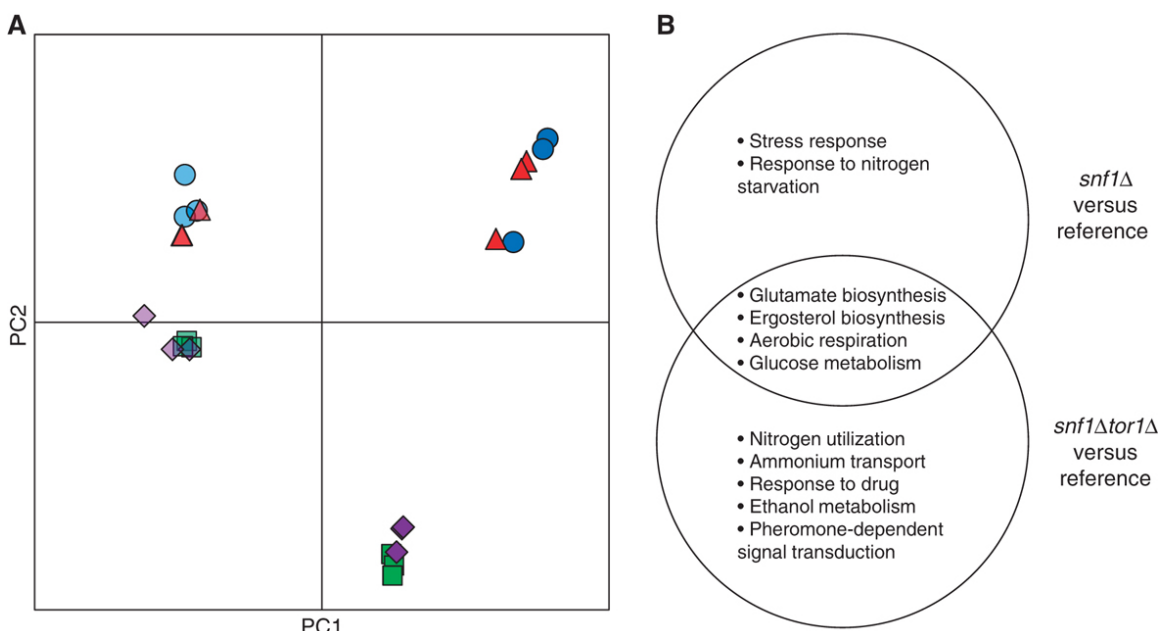


Figure 2.13 Deletion of *SNF1* but not *TOR1* caused global change in the transcriptome (Zhang et al. 2011). **(A)** Principal component analysis (PCA). Dark blue circles: reference on C-limited; dark green squares: *snf1Δ* on C-limited; dark red triangles: *tor1Δ* on C-limited; dark purple diamonds: *snf1Δtor1Δ* on C-limited; light blue circles: reference on N-limited; light green squares: *snf1Δ* on N-limited; light red triangles: *tor1Δ* on N-limited; light purple diamonds: *snf1Δtor1Δ* on N-limited. **(B)** The biological processes that were affected by deletion of *SNF1* (*snf1Δ* and *snf1Δtor1Δ*) on C-limited condition.

2.1.3.2 Linkage from phospholipids to amino acid metabolism and ER-UPR response

Interestingly, we found that the transcription of amino acid genes (including *MET6*) was up-regulated in the *SNF1* deletion strain and the *snf1Δtor1Δ* double deletion strain (Fig.2.14). Moreover, we found that the concentration of methionine (Met) was dramatically reduced while *MET6* was up-regulated in the *snf1Δ* and *snf1Δtor1Δ* strains pointing out that they potentially have more Hcy and AdoHcy. This may lead to increased synthesis and accumulation of FA and TAG and sterol esters (Fig. 2.15) which might affect ER-UPR (Tehlivets 2011).

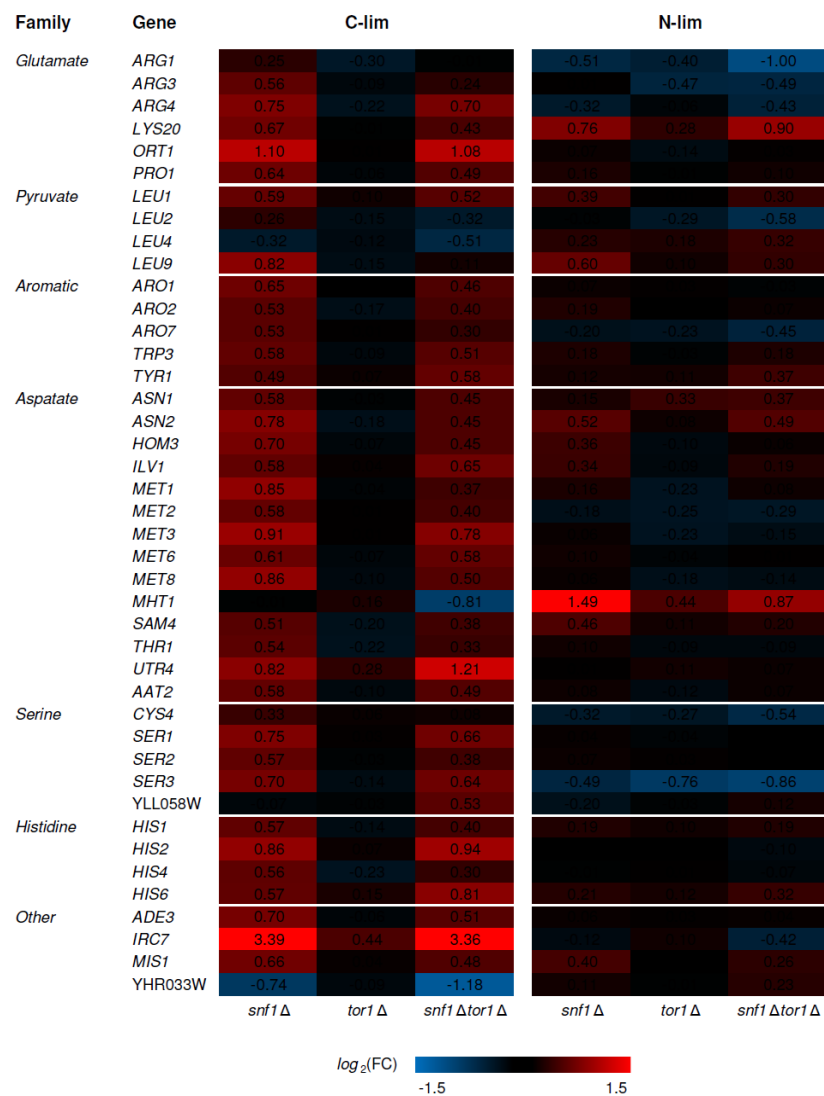


Figure 2.14 Expression of amino acid biosynthetic gene (Zhang et al. 2011). Numbers are average values from the biological replicates for all strains on both C- and N-limited conditions. Red (positive values) indicates higher expression while blue (negative values) indicates lower expression in mutant strain with respect to the reference strain.

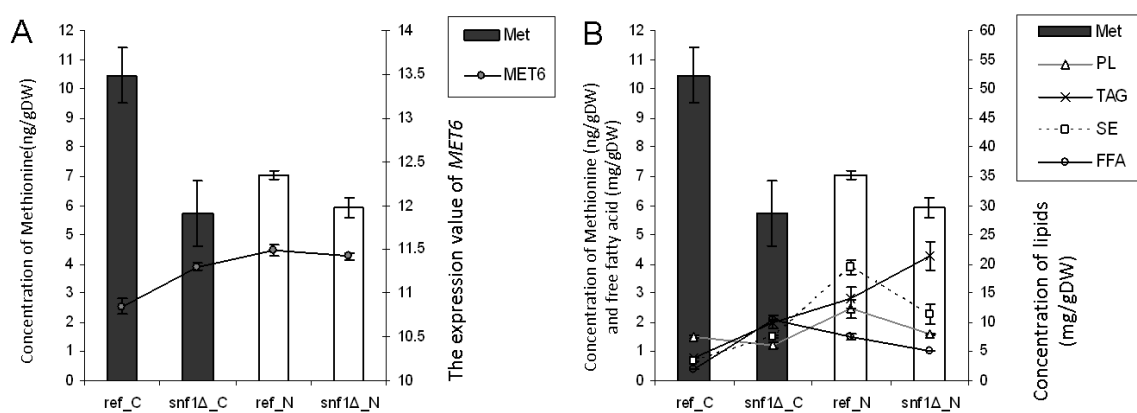


Figure 2.15 The effect of SNF1 deletion on sulfur-phospholipids pathway via MET6.

Moreover, we also found a key linkage among sulphur-phospholipids and ER-UPR at different *INO*-level condition (**paper II**). Double deletion of *INO2* and *INO4* (the low *INO*-level strain) at N-limitation showed some effects from amino acid starvation. UPR genes were also down-regulated when amino acids are decreasing (less missed fold proteins). It also has been known that the decreasing of PC biosynthesis, caused by the down-regulation of *CHO2* and *OPI3*, leads to the accumulation of saturated PC molecular species in ER membrane which causes ER stress, UPR activation and these evidences lead to the up-regulation of FA, TAG, and sterol biosynthesis in the end (Tehlivets 2011). Therefore, in the low *INO*-level strain, *KAR2* a key gene in the ER-UPR were up-regulated especially at N-limitation. The high *INO*-level on the other hand, showed a large decrease in expression of *KAR2* especially at C-limited condition. This shows that there is a linkage that plays a role in regulating a balance between amino acids biosynthesis, phospholipids biosynthesis, and function of the ER-UPR pathway (as illustrated in figure 2.16).

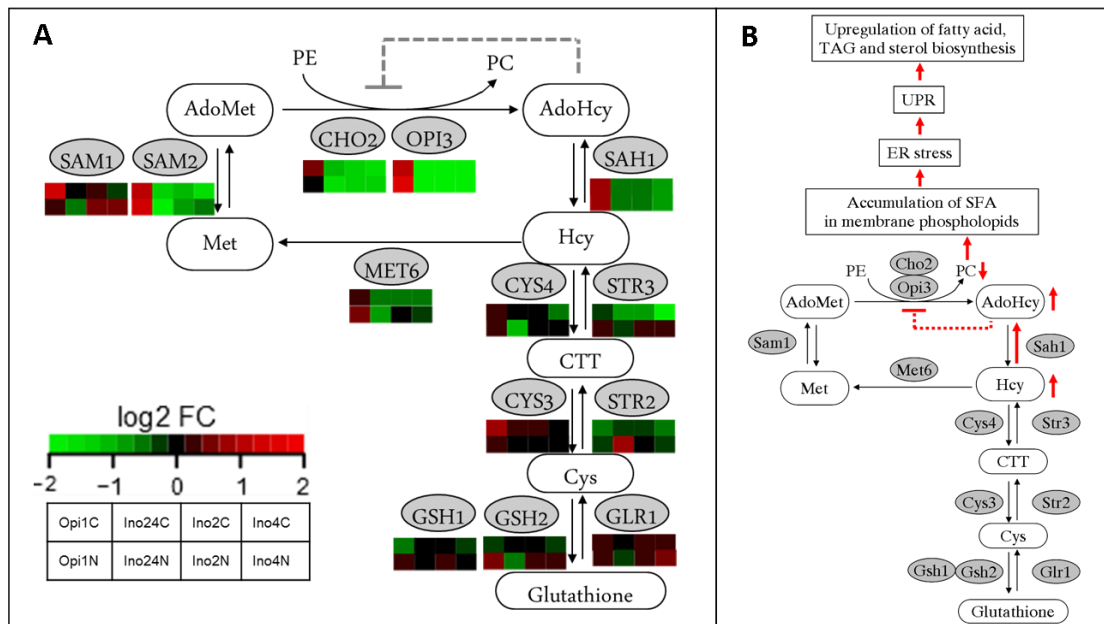


Figure 2.16 The coupled-reaction of methylations of phosphoethanolamine from S-adenosyl-L-methionine (AdoMet) by Cho2 and Opi3 enzymes. (A) A comparison of expression level (log₂ fold change) of each genes coding for sulfur-phospholipids couple d metabolism. (B) The effects of low *INO*-level on ER stress and UPR inducing the up-regulation of FA and storage lipids (Tehlivets 2011)

It is also possible that Ino4 plays a role as a regulator for amino acid metabolism. Unlike Ino2, Ino4 does not have a Trans-Activating Domain (TAD) which is recognized by the RNA polymerase II complex (Lee et al. 2002; Chen et al. 2007; Kumme et al. 2008). For *ino4Δ* the genes involving ribosome biogenesis and assembly were extremely down regulated especially at C-limited conditions (figure 2.8) and this was exactly the responsive process for amino acid (and of course nitrogen) starvation. This is consistent with suggestions that the induction of Ino4-regulated lipid biosynthesis genes may be connected to the immediate need of membranes used for the autophagocytosis process (Ernst et al. 2007). This process is utilized by yeast in order to regulate the equilibrium between proteins and the diminishing set of amino acids due to the starvation condition (Petiot et al. 2002). From the reporter metabolite heatmap, most of the amino acids were found to be greatly down-regulated (especially at N-limitation) in all low *INO*-level strains (paper II, figure S4) which pointed to the amino acid starvation phenomenon.

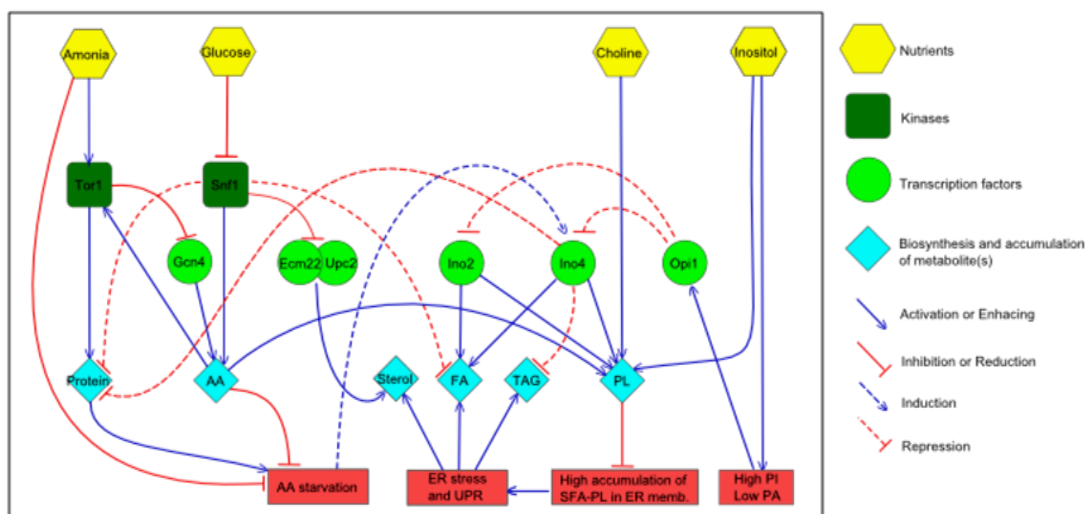


Figure 2.17 Summary of the multilevel regulation network among amino acids biosynthesis, protein synthesis, lipid metabolism, and ER-UPR.

2.2 High through-put techniques for lipid quantification

2.2.1 At single cell level using CARS microscope

The CARS microscopy results from **Paper IV** showed that the average trends of the CARS measurements are fairly consistent with those of the TAG levels (figure 2.18). However, the larger spread compared to the triacylglycerol levels based on measurements on populations of cells was found. It should be noted that the data spread does not represent the precision of the CARS technique, but rather cell-to-cell variations encountered with any microscopy technique based on single-cell measurements. More in-depth comparison between data evaluated from CARS microscopy images and TAG values needs to take lipid droplet sizes into further account and is dependent on the previously commented size accuracy. In addition, effects such as cell shrinking, resulting in a reduction in cell size without a decrease in cell mass, possibly needs to be considered for comparison of CARS and TAG results of the stationary phase.

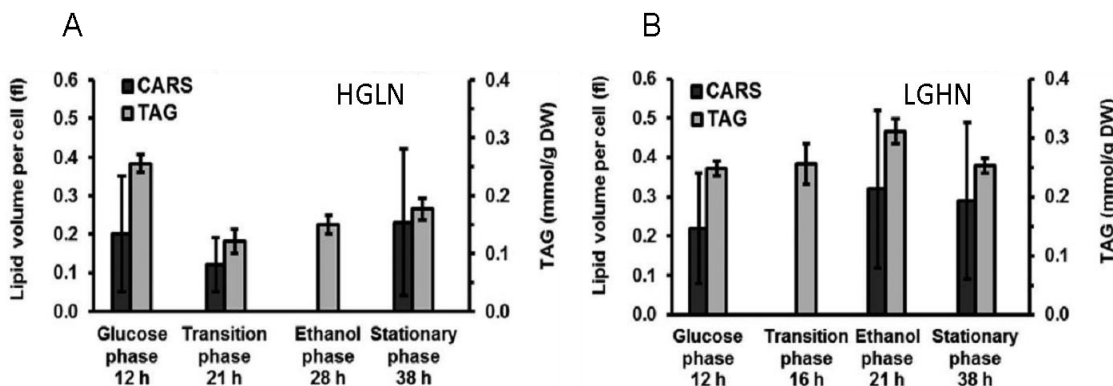


Figure 2.18 Comparison of storage lipid measurement at single cell level and population level. (A) Cellular lipid content during fermentation in HGLN condition presented as average lipid volume per cell with standard deviation, evaluated from CARS microscopy images ($n = 232$) and amount of TAG ($n = 6$). Data are presented as means \pm SD. The evaluated lipid volumes correspond to 4.5, 3.5, and 3.8 lipid droplets per cell for the time points 12, 21, and 38 h, respectively. (B) Cellular lipid content during fermentation in LGHN evaluated from CARS microscopy images ($n = 197$) and amount of TAG ($n = 6$). Data are presented as means \pm SD. The evaluated lipid volumes correspond to 3.8, 6.2, and 3.6 lipid droplets per cell for the time points 12, 21, and 38 h, respectively.

The higher average lipid content for the LGHN condition is represented by cells containing multiple lipid droplets indicated by an asterisk in figures 2.19C and D. The two conditions also show different lipid droplet distribution patterns. Whereas HGLN cells in the transition phase exhibit an even distribution of lipid droplets throughout the intracellular volume, LGHN cells enter the ethanol phase and lipid droplets can often be observed in the periphery surrounding larger vacuoles (indicated by arrows). This arrangement can also be seen in the rendered volume images, showing complete three-dimensional representations of yeast cells (magenta) and lipid droplets

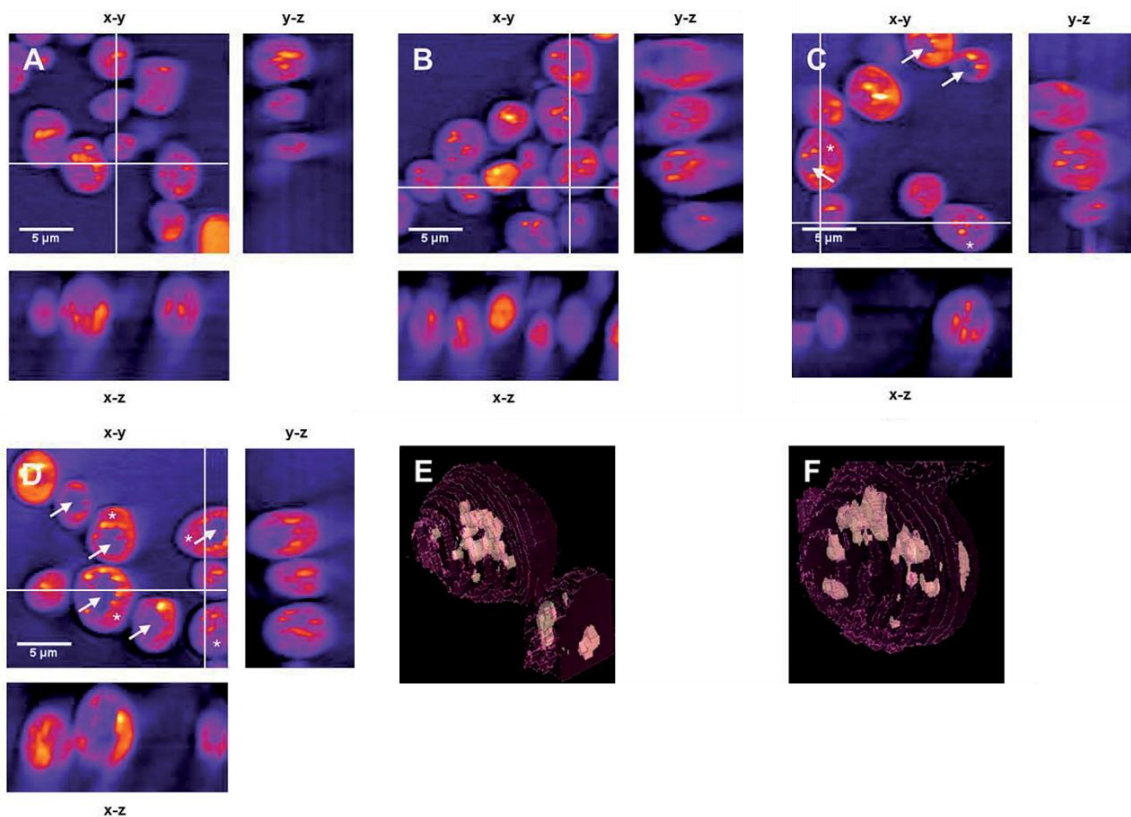


Figure 2.19 CARS microscopy images showing horizontal ($x-y$) and vertical ($x-z$, $y-z$) views of yeast cells measured after growth for 21 h. Positions of the vertical views are indicated by white lines. Image sizes, $20 \times 20 \mu\text{m}$ and $20 \times 10 \mu\text{m}$. Cells grown under HGLN conditions (**A** and **B**), LGHN conditions (**C** and **D**).

In addition to the quantitative measurements of the lipid content at single-cell level, the CARS microscopy z-stacks provide unique three-dimensional information on the lipid droplet distribution represented by the planar horizontal and vertical views shown in figure 2.19A-D and the volume images of figure 2.19E and F. This allows us to evaluate the intracellular arrangement of the lipid droplets and a significant difference was observed for the two nutritional conditions after 21 hours of growth. Whereas the lipid droplets were evenly distributed in cells with high access to glucose (HGLN, still in the transition phase at 21 hours) they were located in the periphery of cells exposed to glucose limitation (LGHN, early ethanol phase at 21 hours). This was most likely due to the formation of vacuoles in many LGHN cells, of which 89% exhibited a vacuole in contrast to the HGLN cells (18%). This trend can be seen in the images of figure 2.19A and B, where several of the LGHN cells in figure 2.19C and D show a vacuole, indicated by arrows. This difference in lipid droplet arrangement is also shown in the single-cell volume images of Figs. 3E and 3F (see supplementary information for 360 degree rendering movies at:-

*** <http://onlinelibrary.wiley.com/doi/10.1002/biot.201000386/suppinfo> ***)

2.2.2 At population level

2.2.2.1 Total lipid extraction

The closed-vessel system for microwave-assisted lipid extraction was modified from **paper V**, which is illustrated in figure 2.20. The ideal method used for sample preparation in biological research should be simple, rapid, precise and accurate. Besides these essential factors, sample preparation rate (number of samples that can be performed per hour or per day) is also important.

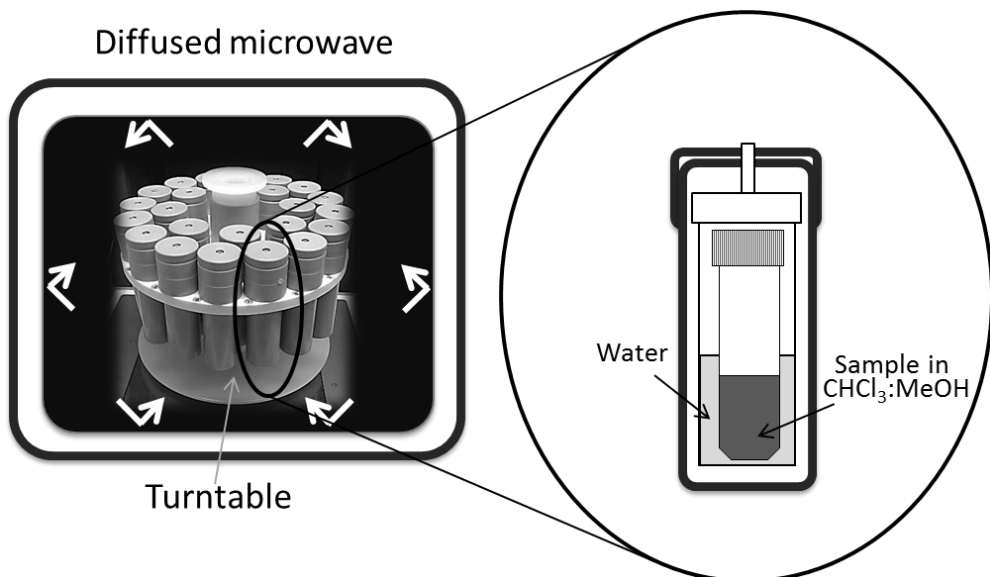


Figure 2.20 The modified closed-vessel system for total lipid extraction using microwave

Normally, the conventional lipid extraction procedure by Schneiter and Daum (Schneiter and Daum 2006) contains 4 key steps; (1) cell disruption, (2) extraction of the lipids with chloroform/methanol (2:1, v/v), (3) removal of nonlipid contaminants by washing the extraction with aqueous salt solutions, and (4) Drying of the extraction by removal of the organic solvent.

In order to perform fast sample preparation, we replaced the conventional extraction with microwave-assisted extraction that can extract the total lipid without the requirement of cell disruption step, which dramatically reduces the extraction time. Moreover, we increased the speed of sample preparation by using the modified closed-vessel systems from **paper IV** to be able to finish all the extraction process use within one Pyrex glass tubes. With this approach, we eliminated most of the time consuming steps for transferring of mixture solution from one extraction tube to the new glass tubes or flasks several times (at the glass beads removal, washing, and phase separation steps). Hereby we are able to reach a sample preparation rate of up to several hundred samples per day.

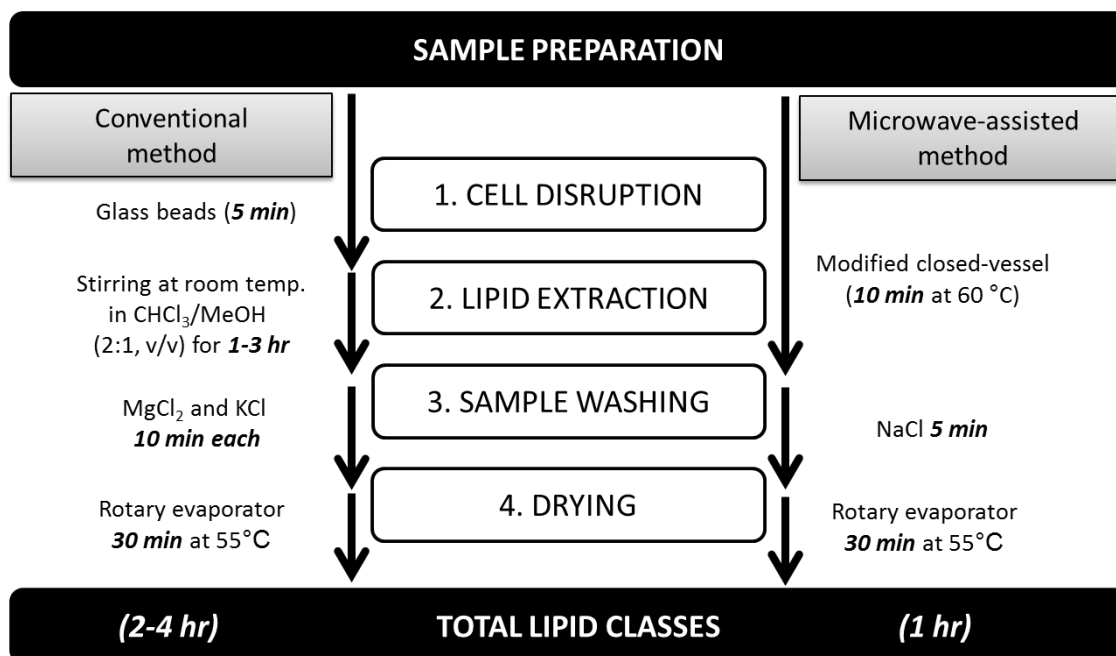


Figure 2.21 The comparison between conventional method and microwave-assisted method for total lipid extraction.

To validate the efficiency of our microwave extraction method, we compared the extracted lipid yields of each lipid class by our optimized method (60°C , 10 min) with the conventional method (figure 2.22). The results indicated that the microwave-assisted extraction method for total lipids was equally effective as compared to the conventional method. This could be due to the fact that the extraction occurred in closed-vessel microwave operated under higher temperature and pressure (60°C , 30 bars), and the yeast cell wall could simply be disrupted by this treatment. Clearly it is advantageous with lipid extraction using the microwave method as this is simple, rapid and involves little costs.

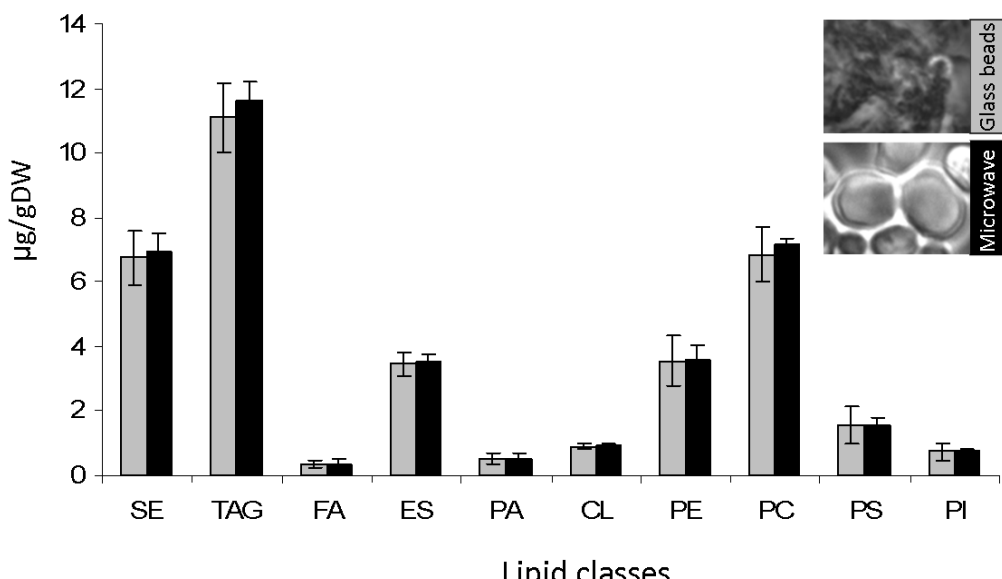


Figure 2.22 Comparison of microwave (10 min at 60 °C) and conventional method (3 hr at room temperature). Cholesterol was used as internal standard. Error bars correspond to standard deviation ($n = 3$).

Moreover, based on the recovery of the spiked CH standard, the efficiencies of total lipid obtained from both methods were found to be the same, i.e. there was an insignificant difference ($P>0.01$) in %recovery of CH (conventional closed-vessel: $92 \pm 6\%$ and modified closed-vessel: $93 \pm 8\%$). The high %recovery of CH and also TAG&FA (in the *Effect of the extraction temperature on bound and free FA* section) obtained from both methods indicates that these two methods are equally efficient for the lipid extraction , as shown by low amounts of spiked lipid standards lost during the entire process of sample preparation. In contrast, the reproducibility (judged by the standard deviations as error bars in figure 2.22) were significant higher with the modified method compared to the conventional method ($P>0.01$). Presumably, this is due to the non-homogenously disruption of using glass beads in the conventional method, probably because the efficiency of cell disruption were different in each extraction tubes

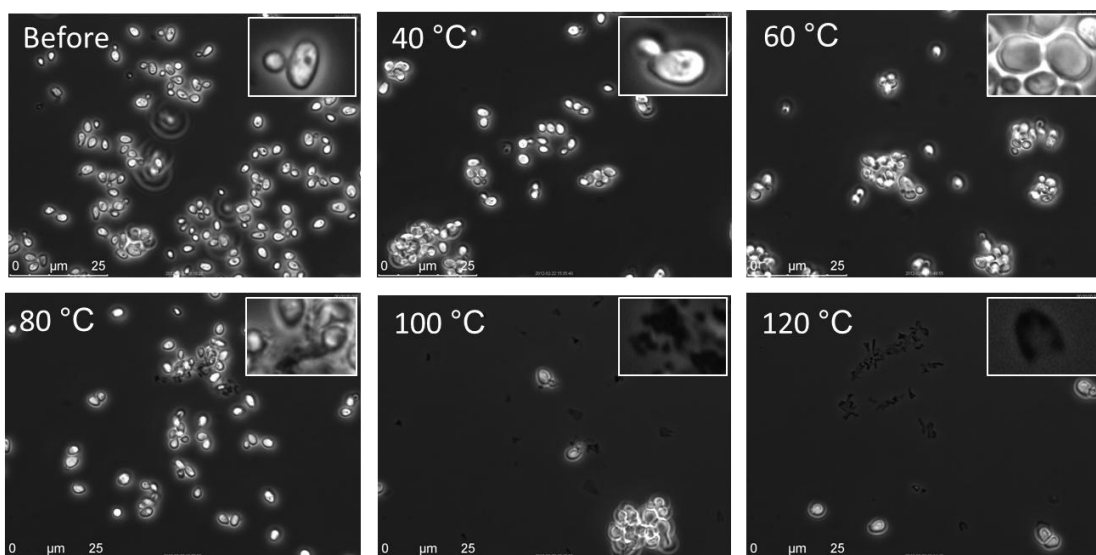


Figure 2.23 Microscopic results showing the effect of different extraction temperatures on cell disintegration.

From figure 2.23, the microscopic results proved that our microwave-assisted extraction at low extraction temperature (room temperature and 40°C) was not able to break the freeze-dried yeast cells and we can still see some subcellular compartments. At medium temperature 60°C , yeast cells seem to be disintegrated and the subcellular structure were not found inside the yeast cells, which indicate the leakage and infusion of extraction solvent into the cells. However, we started to see some cell debris caused by over heating at high temperature (80°C). Consequently, so much more damaged cell debris was found when higher temperatures ($100\text{-}120^{\circ}\text{C}$) were used for microwave-assisted extraction. Based on this evidence, we strongly believe that the extraction temperature of microwave must have some effects to the total lipid yields which can be detected by HPLC-CAD analysis in further step. Therefore, some more results on the extracted lipid yields caused by this effect will be discussed below.

2.2.2.2 Lipid separation and quantification by HPLC-CAD

One of the most investigated parameter for lipid separation using HPLC is the column temperature. To select a moderate temperature for lipid separation, we performed lipid analysis using a HILIC column in the range of 20 – 55 °C. The chromatographic results in figure 2.24 show the effects of column temperature to the separation of all lipid classes. For neutral lipids, the two yeast storage lipids such as steryl ester (SE) and triacylglycerol (TAG) seem to separate well only at $\geq 25^{\circ}\text{C}$ since the low column temperature effect the eluting time of TAG which makes the peak broad at 20 °C. However, this evidence was not found to affect the SE peak at all temperatures. The free fatty acid (FA) peak was sharper at higher column temperature and had peak tails problems at low column temperatures.

In our study, cholesterol (CH), which yeast cannot produce, was used as the spiked internal standard. Therefore, it is important to have a good separation between CH and ergosterol (ES) which is the main sterol in yeast. Focusing on the two sterol standards, CH and ES, just like TAG, were separated well only at $\geq 25^{\circ}\text{C}$ and the higher column temperature can speed up the eluting time. Therefore, the sterol peaks were sharper, came out faster, and separated better at higher column temperatures.

Phospholipid (PL) separation, on the other hand, could be separate well only at 30-35 °C. The lower column temperature affects PL separation, i.e. PA had peak tailed effect and there were co-elution problems for PE-PC and PS-PI. Higher column temperature, in contrast, resulted in increasing elution time. The PI peak was broad and low at high column temperature ($\geq 40^{\circ}\text{C}$).

Based on these column temperature effects, we selected the column temperature at 35°C as the most proper condition for further analysis. The chromatographic separation of all lipid classes with optimized condition has been shown in figure 2.25.

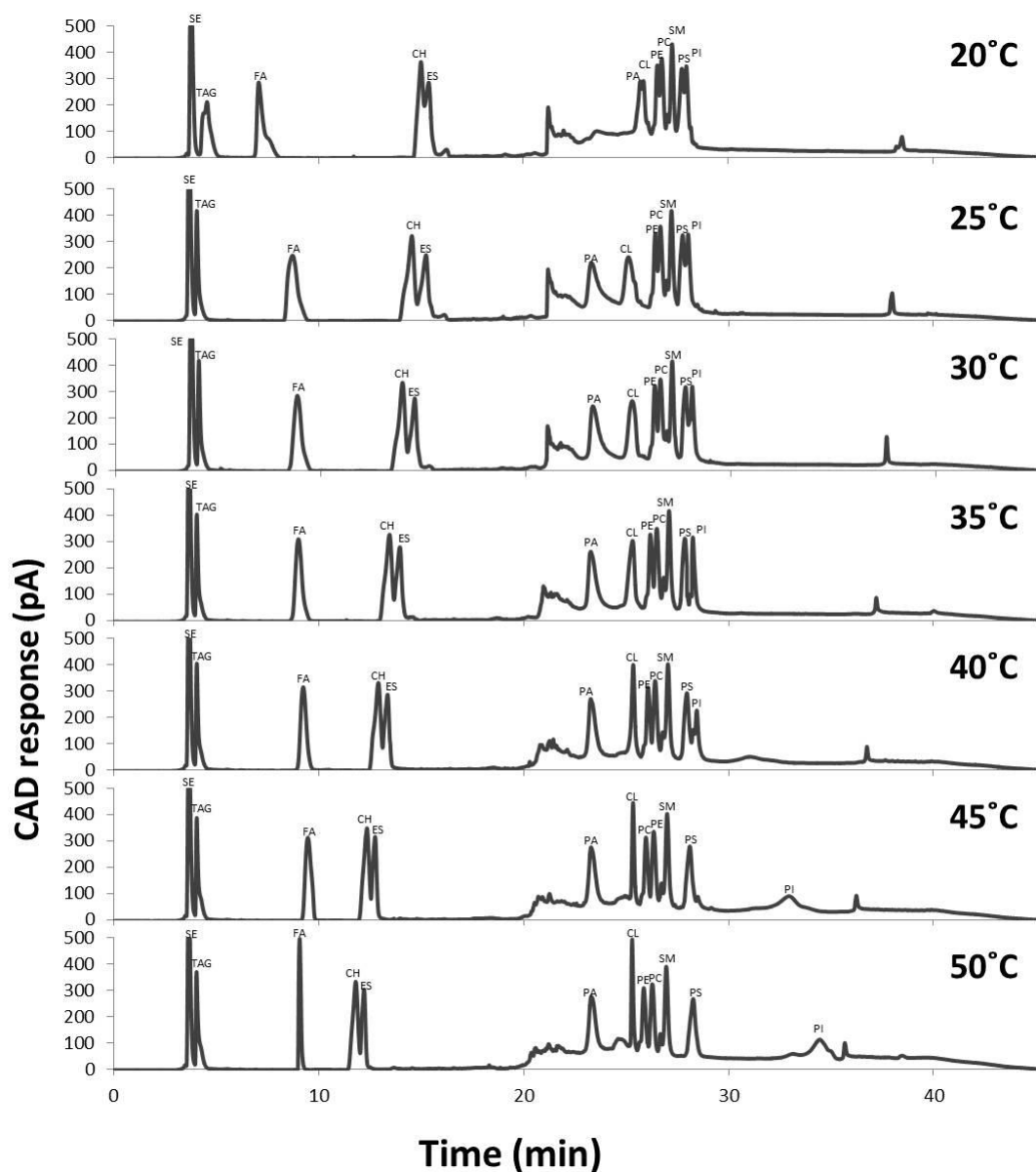


Figure 2.24 Effect of column temperature on the separation of all lipid classes, separated on a HILIC column (Luna 5 μ m 200 \AA 100 x 3.0 mm. 0.8 mL/min solvent flow rate) with triple gradient mobile phase.

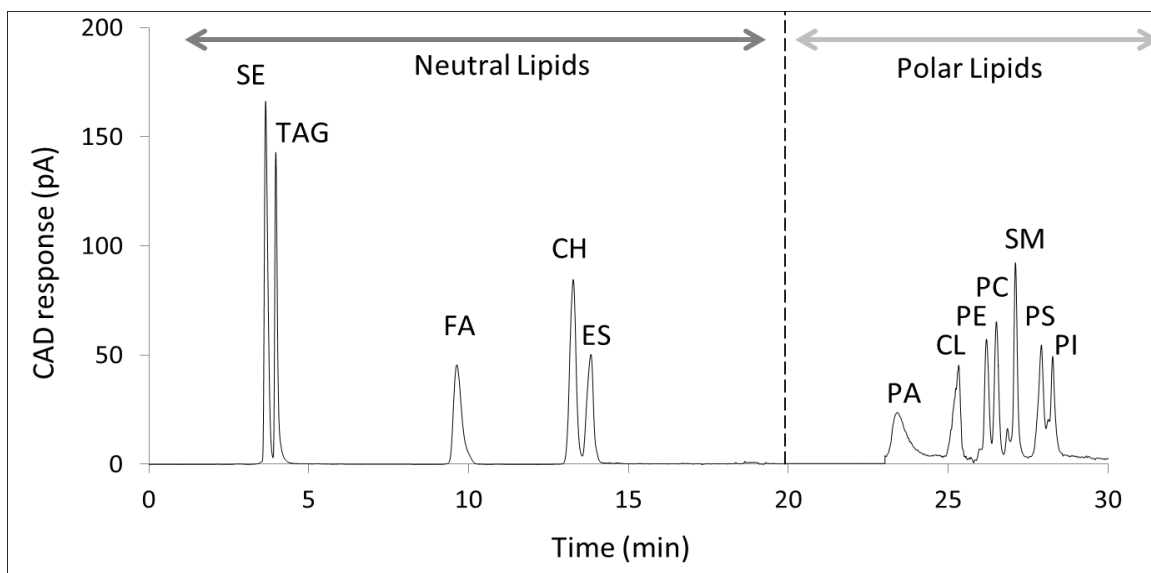


Figure 2.25 The chromatographic separation of all lipid classes with optimized condition, separated on a HILIC column (Luna 5 μ m 200 \AA 100 x 3.0 mm. 0.8 mL/min solvent flow rate at 35°C) with triple gradient mobile phase.

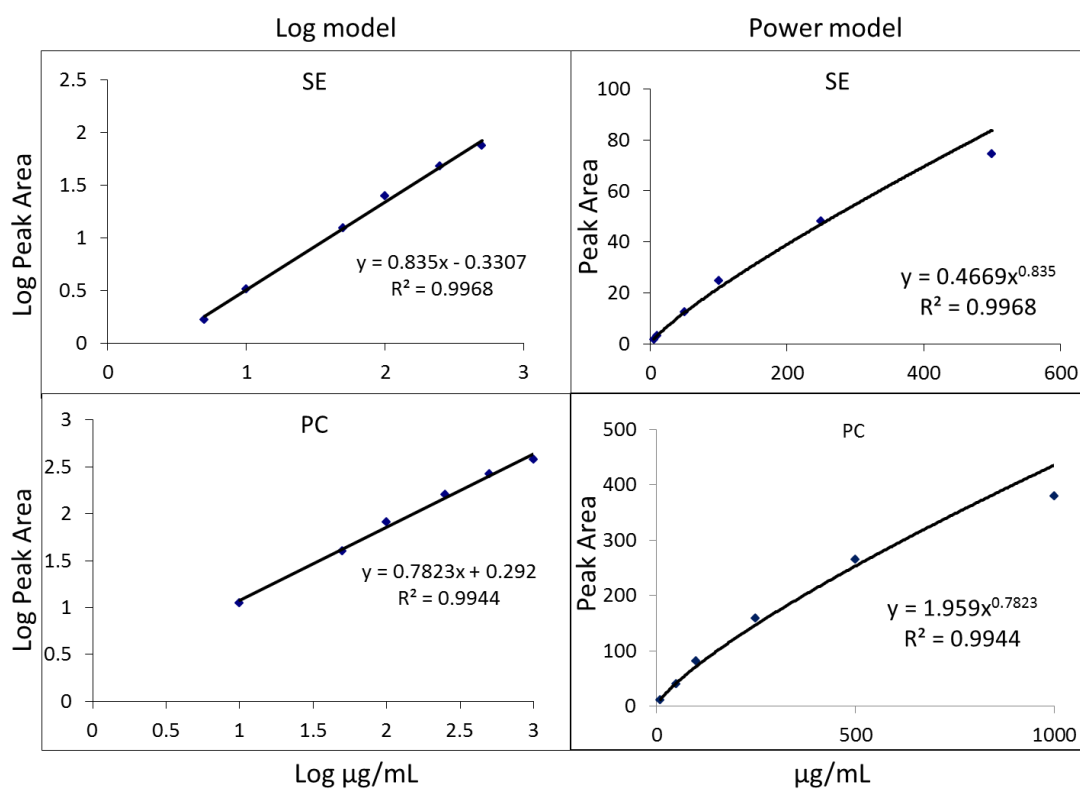


Figure 2.26 The example of calibration curves and response model for lipid analysis by HPLC-CAD.

The Calibration standards were diluted with chloroform-methanol (2:1, v/v) which was also used as blank and extraction solution through this lipid analysis study. Triplicate 5 μ L injections of each solution and the variable amount in the range of 5-1000 μ g/mL were investigated. The relationship between the lipid concentration and CAD response (peak area) has been reported as a non-linear pattern but Log model and power model can describe the detector response more accurately (Ramos et al. 2008; Moreau 2009). To select the right model to generate calibration curves for lipid class quantification, we evaluated both models in our mixed standard concentration ranges.

The examples of calibration curves for SE (neutral lipid) and PC (phospholipids) from figure 2.26 show that non-linear regression was preferred over the classical log-log transformation of both lipid concentration (on X-axis) and peak area (on Y-axis) instead the power model (which show poorly fitness to the plot).

Plotting $\log y = \log A + b \log x$ is also often used to linearize the ELSD response function (Ramos et al. 2008). Therefore, we selected the log model to generate our calibration curve for quantification process.

2.2.2.3 Microwave-assisted FAME extraction and derivatization

The ideal method used for sample preparation in biological research should be simple, rapid, precise and accurate. Besides these essential factors, sample preparation rate (number of samples that can be performed per hour or per day) is also important. In order to perform fast sample preparation, in **Paper VI**, we replaced the conventional heating (using hot plate or water bath) with microwave heating, which dramatically reduces the FAME reaction time. Moreover, we increased the speed of sample preparation by modifying the conventional closed-vessel to be able to use with Pyrex glass tubes (Fig. 2.27).

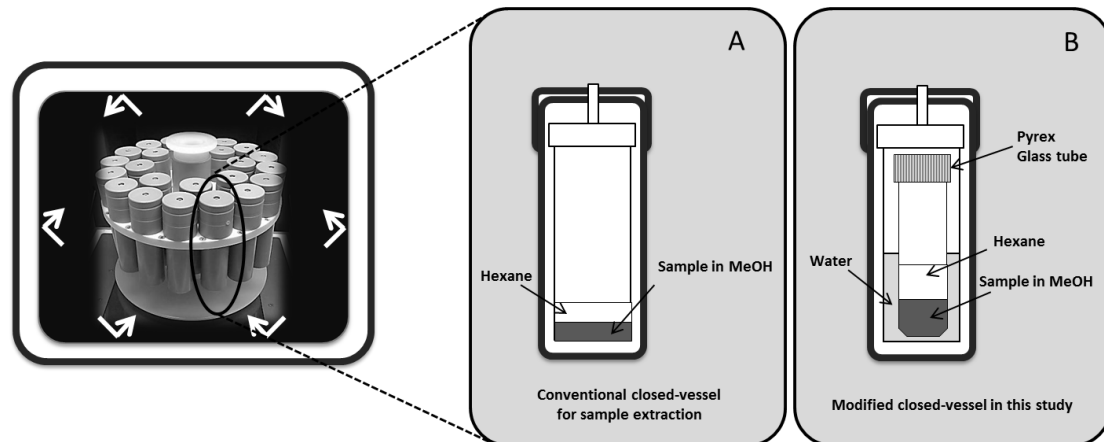


Figure 2.27 Experimental design. Conventional closed-vessel (A) and Modified closed vessel (B).

With this approach, we eliminated most of the time consuming steps for vessel preparation, such as cleaning or drying (vessel can be immediately reused for the next reaction) including the transferring of mixture solution from the vessel to the glass tube (at the separation state). Hereby we are able to reach a sample preparation rate of up to several hundred samples per day.

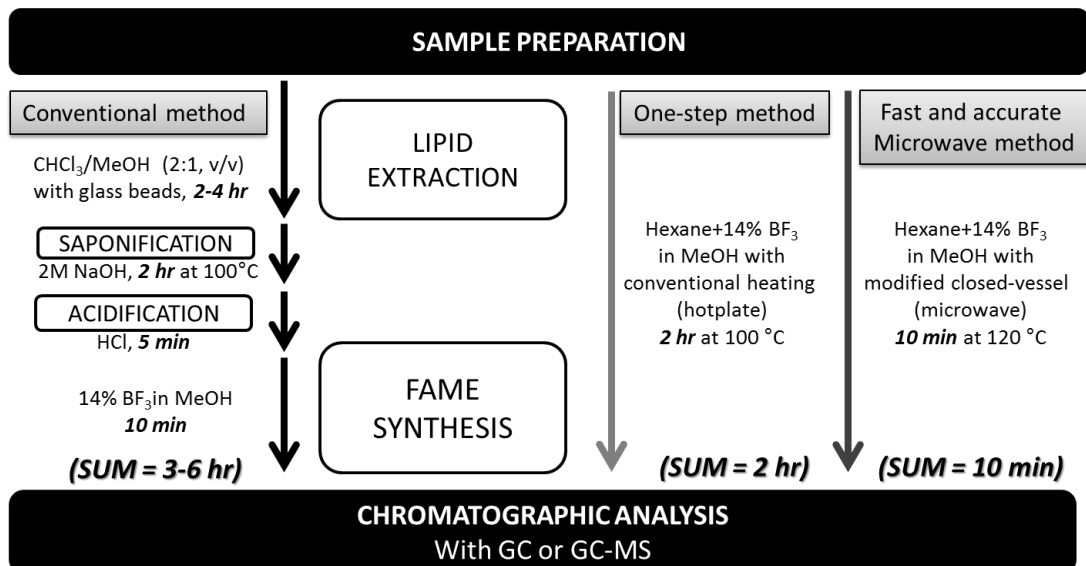


Figure 2.28 The comparison between conventional method (Meziane and Tsuchiya 2002), One-step method (Masood et al. 2005), and the fast and accurate microwave-assisted method (in our study) for FAME derivatization.

In general, bound fatty acids require longer time to complete the conversion as compared to free fatty acids (Ichihara and Fukubayashi 2010), and as mentioned above this could explain the similar results of 17:0 recovery obtained with the two methods and the different yields of 18:1 (n-9) and 20:1 (n-9) FAMEs from yeast samples (figure 2.29).

The selected optimum derivatization temperature in this study was in good agreement with what has been reported earlier using conventional heating (Eder 1995; Masood et al. 2005; Abdulkadir and Tsuchiya 2008; Ichihara and Fukubayashi 2010). Although the higher temperature may provide equal or higher yields of FAMEs, the operation of derivatization above 120 °C was not possible due to the damaging of the sample. The temperature at 120 °C was therefore selected as an optimum point and used for further investigation. The optimum reaction time for preparation of FAMEs depends on type and size of the sample. A sample in complex matrices may require longer time for complete conversion compared with a sample in a simple matrix. In general, derivatization time using microwave is very short compared to conventional heating because the solvents (water and MeOH) are directly absorbing the microwave energy and release it to the surrounding solution efficiently. Although a reaction time shorter than 5 min may also provide complete conversion, it would not make a significant difference in practice, and we therefore selected 5 min reaction time as the optimal condition.

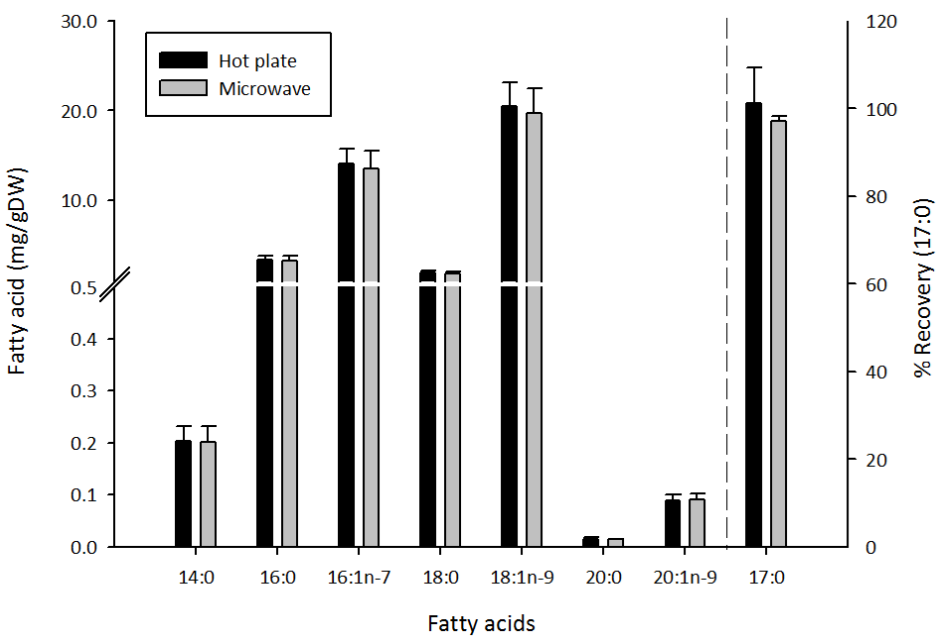


Figure 2.29 Comparison between conventional heating and microwave heating method.

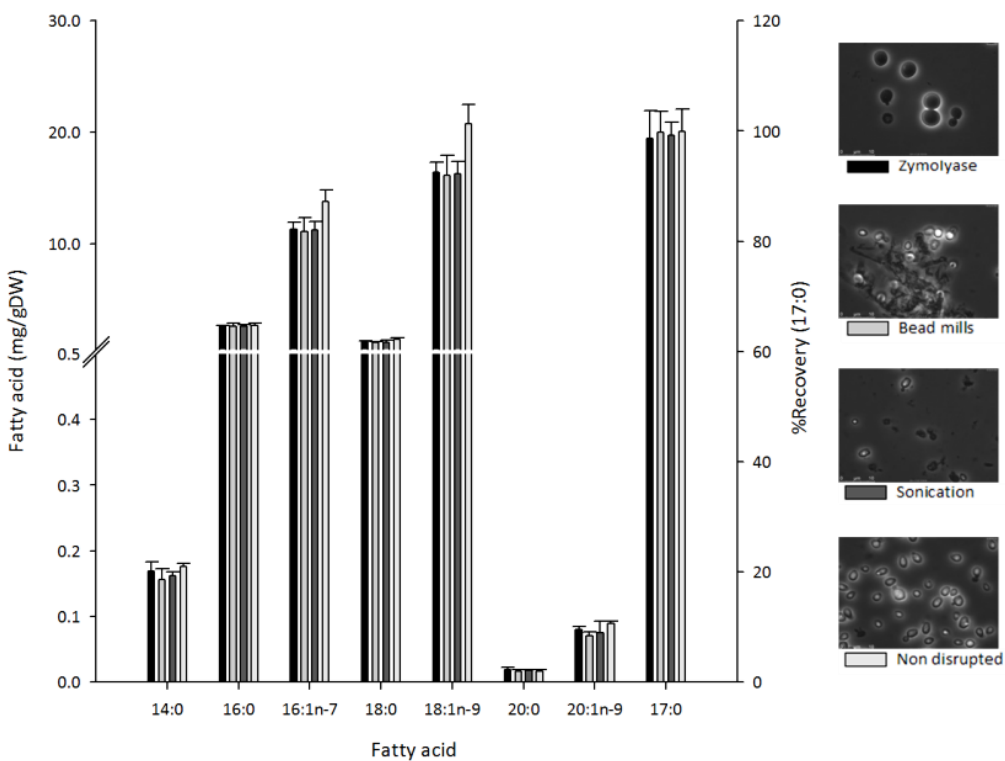


Figure 2.30 Comparison yields of FAMEs between non-disrupted cells and three different ways of sample pre-treatment (zymolyase digestion, bead mills, and sonication). All reactions were performed at 120 °C for 5 min.

According to the results in figure 2.30, we proved by our results that the modified closed-vessel system can also obtain the same yield of FAME even if the yeast cells are disrupted or not. Clearly it is advantageous with direct preparation of FAME using the microwave method as this is simple, rapid and involves little costs.

Chapter 3 Conclusions and Perspectives

Through integrated analysis of the transcriptome, lipidome, and fluxome derived from a robust experimental setup we were able to get insight into how gene expression is linked to the fluxes in lipid biosynthesis at the global level. Based on the results and findings as discussed in the previous chapter, we have advanced the understanding of global regulation of lipid metabolism and can make the following conclusions.

First, both **Snf1 and inositol-choline influence and also globally co-influence lipid metabolism**, especially phospholipid biosynthesis were affected via the transcription factors (i.e. Ino2, Ino4, and Opi1) or indirectly through other transcription factors e.g. Gis1, Mga2, Upc2, Ecm22, Pip2, Oaf1, Sut1, Hac1, etc. Our data also suggested that storage lipid synthesis and accumulation seem to be controlled at the enzyme activity level (i.e. Dpp1, Lpp1, Pah1, and Dgk1). Thus, through our genome-wide analysis of lipid metabolism we managed to both confirm earlier findings and map several novel regulatory circuits involved in controlling how carbon is directed into the different branches of lipid metabolism.

Second, we see **the global effect of INO-level on expression of the genes involved in lipid biosynthesis (both phospholipids and neutral lipids) and metabolic fluxes through lipid biosynthesis pathway**. Following our analysis by genome-wide strategy and analysis of generated complex data by integrated analysis approach enable us to explore correlations and association of changes in a concerted fashion.

Third, we found **a key linkage among ER-UPR and sulphur-phospholipids pathways**. Particularly, we found that i) an inositol-choline effect on the UPR pathway via the transcription factor Hac1, ii) an effect of Ino4, but not of Ino2, on the ribosome biogenesis and assembly which involves an amino acid starvation response especially at C-limited condition where Snf1 is always active, and iii) that Tor1 has a role on fatty acids metabolism. These evidences point to an interesting link between lipid metabolism and the amino acid starvation response and also the role of sulphur-phospholipids pathway effects on ER-UPR activation.

In the lipid analysis parts, we have demonstrated the strength and also the weak side of **the single-cell imaging using CARS microscopy** depending on the objective of individual study. Due to the large cell-to-cell variations, the lipid (TAG in particular) measured at the population level showed more accuracy and higher applicability for lipid profiling in yeasts. The CARS microscope, on the other hand, would be more useful for lipid monitoring in particularly for a dynamic study of living yeast cells.

To speed up analytical process for yeast lipid profiling at the population level and still ensuring a high accuracy, two fast and accurate methods for lipid extraction and quantification were developed. Hereby the sample preparation rate can reached several hundred samples per day and it is likely to also be applicable for other biological samples.

As the high throughput methods, **the modified closed-vessel microwave system for yeast total lipid extraction** showed that it is possible to carry out the cell disruption and extraction in Pyrex glass tubes kept inside the closed vessel at 60°C for 10 min which is extremely fast and simple compared to the conventional lipid extraction method. The optimized condition **for lipid class quantification using HPLC-CAD** is using a HILIC column operated at 35 °C for 45 min at a flow rate 0.8 mL/min and high

accuracy can be reached when log transformation is used to generate the calibration curves for quantifications of each lipid class.

For the yeast FA profiling, we present a **fast and accurate method for preparation of fatty acid methyl esters (FAMEs) using microwave-assisted derivatization of fatty acids**. The esterification of free/bound fatty acids to FAMEs was completed within 5 min, which is 24 times faster than with conventional heating methods. By performing a simple modification of closed-vessel microwave heating it was possible to carry out the esterification in Pyrex glass tubes kept inside the closed vessel while the pre-treated cell disruption steps are not required. Hereby we are able to increase the number of sample preparations to several hundred samples per day as the time for preparation of re-used vessels was eliminated.

With the hereby developed analytical methods and concepts for systems biology of yeast lipid metabolism, genome-wide high throughput data sets were generated and integratively analyzed providing biological information that could not be revealed by analyzing those data sets by reductionistic approaches. Noticeably, emerging properties derived from the integrated analysis enabled us to obtain a clearer picture of global regulation of lipid metabolism. The data sets we generated, both transcriptome and lipid profiles, will be really useful as a general resource which can be used in other studies also. In addition, we have shown that global studies are useful in forming working hypothesis and identifying molecular targets (such as amino acids, proteins, and lipid intermediates), which may be further investigated using more targeted analysis.

Acknowledgements

I sincerely would like to acknowledge the efforts of many people who contributed to the researches and particularly to this thesis. Without them, the work would never have been successfully completed.

I am proudly indebted to my supervisor Professor Jens Nielsen and my co-supervisor Dr. Intawat Nookaew for their valuable advice, guidance, correction, encouragement and being patient throughout my research and manuscript preparation.

I am very thankful to Dr. Jie Zhang and Dr. Goutham Vemuri for kindly assistance with fermentation and microarray data acquisition, to Dr. Sakda Khoomrung for guiding me to the whole new analytical chemistry world, to Dr. Subir K. Nandy and Dr. Christian Brackmann for being fantastic and helpful co-workers on the CARS paper, and also thank to Leif Väremo for kind assistances with R script for transcriptome data analysis.

I also thank Nils-Gunnar Carlsson and Suwanee Jansaard for valuable assistance with running the HPLC-CAD, Tobias Österlund and Klaas Buijs for helpful and kindly suggestions on manuscripts preparation. I wish to thank Erica Dahlin, Kanokarn Kocharin, Natapol Pornputtapong, Kwanjeera Wanichthanarak, Malin Nordvall, and Ximena R. Sevilla for always being so supportive and helpful to me. Undeniably, I must thank to all of my super cool office mates Bouke de Jong, Klaas Buijs, Stefan Tippman, Marta Papini, Christoph Knuf for spending the happy time together and sharing our “godis bank”.

I also would like to thank the Office of the Higher Education Commission, Thailand for support by a stipend for his Ph.D. program under the program “*Strategic Scholarships for Frontier Research Network*”.

Above all, it is a great pleasure for me to thank my mother for her moral support. Thanks are also given to my brothers and my friends for their encouragement throughout my research study.

Pramote Chumnanpuen
March 2012

References

- Abdulkadir, S. and M. Tsuchiya (2008). "**One-step method for quantitative and qualitative analysis of fatty acids in marine animal samples.**" *Journal of Experimental Marine Biology and Ecology* **354**(1): 1-8.
- Alepuz, P. M., K. W. Cunningham, et al. (1997). "**Glucose repression affects ion homeostasis in yeast through the regulation of the stress-activated ENA1 gene.**" *Mol Microbiol* **26**(1): 91-98.
- Ambroziak, J. and S. A. Henry (1994). "**INO2 and INO4 gene products, positive regulators of phospholipid biosynthesis in *Saccharomyces cerevisiae*, form a complex that binds to the INO1 promoter.**" *J Biol Chem* **269**(21): 15344-15349.
- Ashburner, B. P. and J. M. Lopes (1995). "**Autoregulated expression of the yeast INO2 and INO4 helix-loop-helix activator genes effects cooperative regulation on their target genes.**" *Mol Cell Biol* **15**(3): 1709-1715.
- Ashburner, B. P. and J. M. Lopes (1995). "**Regulation of yeast phospholipid biosynthetic gene expression in response to inositol involves two superimposed mechanisms.**" *Proc Natl Acad Sci U S A* **92**(21): 9722-9726.
- Bailis, A. M., M. A. Poole, et al. (1987). "**The Membrane-Associated Enzyme Phosphatidylserine Synthase Is Regulated at the Level of Messenger-Rna Abundance.**" *Mol Cell Biol* **7**(1): 167-176.
- Balciunas, D. and H. Ronne (1999). "**Yeast genes GIS1-4: multicopy suppressors of the Gal- phenotype of snf1 mig1 srb8/10/11 cells.**" *Mol Gen Genet* **262**(4-5): 589-599.
- Beopoulos, A., J. Cescut, et al. (2009). "**Yarrowia lipolytica as a model for bio-oil production.**" *Prog Lipid Res* **48**(6): 375-387.
- Bligh, E. G. and W. J. Dyer (1959). "**A Rapid Method of Total Lipid Extraction and Purification.**" *Can J Biochem Physiol* **37**(8): 911-917.
- Brackmann, C., J. Norbeck, et al. (2009). "**CARS microscopy of lipid stores in yeast: the impact of nutritional state and genetic background.**" *Journal of Raman Spectroscopy* **40**(7): 748-756.
- Broach, J. R. and R. J. Deschenes (1990). "**The function of ras genes in *Saccharomyces cerevisiae*.**" *Adv Cancer Res* **54**: 79-139.
- Brown, D. A. (2001). "**Lipid droplets: proteins floating on a pool of fat.**" *Curr Biol* **11**(11): R446-449.
- Canelas, A. B., N. Harrison, et al. (2010). "**Integrated multilaboratory systems biology reveals differences in protein metabolism between two reference yeast strains.**" *Nat Commun* **1**: 145.
- Carman, G. M. and G. S. Han (2009). "**Regulation of phospholipid synthesis in yeast.**" *J Lipid Res* **50 Suppl**: S69-73.
- Carman, G. M. and G. S. Han (2011). "**Regulation of phospholipid synthesis in the yeast *Saccharomyces cerevisiae*.**" *Annu Rev Biochem* **80**: 859-883.
- Carman, G. M. and M. C. Kersting (2004). "**Phospholipid synthesis in yeast: regulation by phosphorylation.**" *Biochem Cell Biol* **82**(1): 62-70.
- Celenza, J. L. and M. Carlson (1984). "**Cloning and genetic mapping of SNF1, a gene required for expression of glucose-repressible genes in *Saccharomyces cerevisiae*.**" *Mol Cell Biol* **4**(1): 49-53.
- Chang, Y. F. and G. M. Carman (2008). "**CTP synthetase and its role in phospholipid synthesis in the yeast *Saccharomyces cerevisiae*.**" *Prog Lipid Res* **47**(5): 333-339.
- Chen, M., L. C. Hancock, et al. (2007). "**Transcriptional regulation of yeast phospholipid biosynthetic genes.**" *Biochim Biophys Acta* **1771**(3): 310-321.

- Chen, M. and J. M. Lopes (2007). "*Multiple basic helix-loop-helix proteins regulate expression of the ENO1 gene of *Saccharomyces cerevisiae*.*" *Eukaryot Cell* **6**(5): 786-796.
- Choi, M. G., T. S. Park, et al. (2003). "*Phosphorylation of *Saccharomyces cerevisiae* CTP synthetase at Ser424 by protein kinases A and C regulates phosphatidylcholine synthesis by the CDP-choline pathway.*" *J Biol Chem* **278**(26): 23610-23616.
- Dietz, M., W. T. Heyken, et al. (2003). "*TFIIB and subunits of the SAGA complex are involved in transcriptional activation of phospholipid biosynthetic genes by the regulatory protein Ino2 in the yeast *Saccharomyces cerevisiae*.*" *Mol Microbiol* **48**(4): 1119-1130.
- Dowhan, W. (1997). "*Molecular basis for membrane phospholipid diversity: why are there so many lipids?*" *Annu Rev Biochem* **66**: 199-232.
- Dulaney, E. L., E. O. Stapley, et al. (1954). "*Studies on ergosterol production by yeasts.*" *Appl Microbiol* **2**(6): 371-379.
- Eder, K. (1995). "*Gas chromatographic analysis of fatty acid methyl esters.*" *J Chromatogr B Biomed Appl* **671**(1-2): 113-131.
- el-Refai, A. H. and I. A. el-Kady (1968). "*Sterol biosynthesis in *Saccharomyces fermentati*.*" *Z Allg Mikrobiol* **8**(5): 361-366.
- el-Refai, A. H. and I. A. el-Kady (1968). "*Sterol production of yeast strains.*" *Z Allg Mikrobiol* **8**(5): 355-360.
- Elle, I. C., L. C. Olsen, et al. (2010). "*Something worth dyeing for: molecular tools for the dissection of lipid metabolism in *Caenorhabditis elegans*.*" *FEBS Lett* **584**(11): 2183-2193.
- Enejder, A., C. Brackmann, et al. (2010). "*Coherent Anti-Stokes Raman Scattering Microscopy of Cellular Lipid Storage.*" *IEEE J Sel Top Quantum Electron* **16**(3): 506-515.
- Engler, C. R. and C. W. Robinson (1979). "*Disruption of *Candida-Utilis* Cell-Walls.*" *Abstracts of Papers of the American Chemical Society* (Sep): 47-8.
- Ernst, J., O. Vainas, et al. (2007). "*Reconstructing dynamic regulatory maps.*" *Mol Syst Biol* **3**: 74.
- Espenshade, P. J. and A. L. Hughes (2007). "*Regulation of sterol synthesis in eukaryotes.*" *Annu Rev Genet* **41**: 401-427.
- Folch, J., M. Lees, et al. (1957). "*A simple method for the isolation and purification of total lipides from animal tissues.*" *J Biol Chem* **226**(1): 497-509.
- Fukumoto, S. and T. Fujimoto (2002). "*Deformation of lipid droplets in fixed samples.*" *Histochem Cell Biol* **118**(5): 423-428.
- Gaynor, P. M. and G. M. Carman (1990). "*Phosphatidylethanolamine methyltransferase and phospholipid methyltransferase activities from *Saccharomyces cerevisiae*. Enzymological and kinetic properties.*" *Biochim Biophys Acta* **1045**(2): 156-163.
- Glaser, C., H. Demmelmair, et al. (2010). "*High-throughput analysis of total plasma fatty acid composition with direct in situ transesterification.*" *Plos One* **5**(8): e12045.
- Gocze, P. M. and D. A. Freeman (1994). "*Factors underlying the variability of lipid droplet fluorescence in MA-10 Leydig tumor cells.*" *Cytometry* **17**(2): 151-158.
- Goodman, J. M. (2009). "*Demonstrated and inferred metabolism associated with cytosolic lipid droplets.*" *J Lipid Res* **50**(11): 2148-2156.
- Greenberg, M. L., P. Goldwasser, et al. (1982). "*Characterization of a yeast regulatory mutant constitutive for synthesis of inositol-1-phosphate synthase.*" *Mol Gen Genet* **186**(2): 157-163.
- Han, G. S., L. O'Hara, et al. (2008). "*Characterization of the yeast DGK1-encoded CTP-dependent diacylglycerol kinase.*" *J Biol Chem* **283**(29): 20443-20453.

- Han, X. and R. W. Gross (2003). "Global analyses of cellular lipidomes directly from crude extracts of biological samples by ESI mass spectrometry: a bridge to lipidomics." *J Lipid Res* **44**(6): 1071-1079.
- Han, X. and R. W. Gross (2005). "Shotgun lipidomics: multidimensional MS analysis of cellular lipidomes." *Expert Rev Proteomics* **2**(2): 253-264.
- Hartmann, C. and A. Delgado (2004). "Numerical simulation of the mechanics of a yeast cell under high hydrostatic pressure." *J. Biomech.* **37**(7): 977-987.
- Hasslacher, M., A. S. Ivessa, et al. (1993). "Acetyl-CoA carboxylase from yeast is an essential enzyme and is regulated by factors that control phospholipid metabolism." *J Biol Chem* **268**(15): 10946-10952.
- Hellerer, T., C. Axang, et al. (2007). "Monitoring of lipid storage in *Caenorhabditis elegans* using coherent anti-Stokes Raman scattering (CARS) microscopy." *Proc Natl Acad Sci U S A* **104**(37): 14658-14663.
- Heyken, W. T., A. Repenning, et al. (2005). "Constitutive expression of yeast phospholipid biosynthetic genes by variants of *Ino2* activator defective for interaction with *Opi1* repressor." *Mol Microbiol* **56**(3): 696-707.
- Hiesinger, M., C. Wagner, et al. (1997). "The acetyl-CoA synthetase gene *ACS2* of the yeast *Saccharomyces cerevisiae* is coregulated with structural genes of fatty acid biosynthesis by the transcriptional activators *Ino2p* and *Ino4p*." *FEBS Lett* **415**(1): 16-20.
- Hong, S. P. and M. Carlson (2007). "Regulation of *snf1* protein kinase in response to environmental stress." *J Biol Chem* **282**(23): 16838-16845.
- Hoppen, J., A. Repenning, et al. (2005). "Comparative analysis of promoter regions containing binding sites of the heterodimeric transcription factor *Ino2/Ino4* involved in yeast phospholipid biosynthesis." *Yeast* **22**(8): 601-613.
- Hosaka, K., J. Nikawa, et al. (1994). "Cloning and characterization of the *SCS1* gene required for the expression of genes in yeast phospholipid synthesis." *J Biochem* **115**(1): 131-136.
- Hoshizaki, D. K., J. E. Hill, et al. (1990). "The *Saccharomyces cerevisiae* *INO4* gene encodes a small, highly basic protein required for derepression of phospholipid biosynthetic enzymes." *J Biol Chem* **265**(8): 4736-4745.
- Huff, T. B., Y. Shi, et al. (2008). "Multimodal Nonlinear Optical Microscopy and Applications to Central Nervous System Imaging." *IEEE J Sel Top Quantum Electron* **14**(1): 4-9.
- Huh, W. K., J. V. Falvo, et al. (2003). "Global analysis of protein localization in budding yeast." *Nature* **425**(6959): 686-691.
- Hunter, K. and A. H. Rose (1972). "Lipid composition of *Saccharomyces cerevisiae* as influenced by growth temperature." *Biochim Biophys Acta* **260**(4): 639-653.
- Ichihara, K. and Y. Fukubayashi (2010). "Preparation of fatty acid methyl esters for gas-liquid chromatography." *J Lipid Res* **51**(3): 635-640.
- Itonori, S., M. Takahashi, et al. (2004). "Microwave-mediated analysis for sugar, fatty acid, and sphingoid compositions of glycosphingolipids." *J Lipid Res* **45**(3): 574-581.
- Jandera, P. (2008). "Stationary phases for hydrophilic interaction chromatography, their characterization and implementation into multidimensional chromatography concepts." *J Sep Sci* **31**(9): 1421-1437.
- Jesch, S. A., X. Zhao, et al. (2005). "Genome-wide analysis reveals inositol, not choline, as the major effector of *Ino2p-Ino4p* and

- unfolded protein response target gene expression in yeast." *J Biol Chem* **280**(10): 9106-9118.**
- Jeyashoke, N., K. Krisnangkura, et al. (1998). "Microwave induced rapid transmethylation of fatty acids for analysis of food oil." *J. Chromatogr. A.* **818**(1): 133-137.
- Kasten, M. M., S. Dorland, et al. (1997). "A large protein complex containing the yeast *Sin3p* and *Rpd3p* transcriptional regulators." *Mol Cell Biol* **17**(8): 4852-4858.
- Kauffman, K. J., P. Prakash, et al. (2003). "Advances in flux balance analysis." *Curr Opin Biotechnol* **14**(5): 491-496.
- Keleher, C. A., M. J. Redd, et al. (1992). "*Ssn6-Tup1* is a general repressor of transcription in yeast." *Cell* **68**(4): 709-719.
- Khoomrung, S., K. Laoteng, et al. (2008). "Significance of fatty acid supplementation on profiles of cell growth, fatty acid, and gene expression of three desaturases in *Mucor rouxii*." *Appl. Microbiol. Biot.* **80**(3): 499-506.
- Kinney, A. J., M. Bae-Lee, et al. (1990). "Regulation of phospholipid biosynthesis in *Saccharomyces cerevisiae* by cyclic AMP-dependent protein kinase." *Journal of Bacteriology* **172**(2): 1133-1136.
- Krahmer, N., Y. Guo, et al. (2009). "SnapShot: Lipid Droplets." *Cell* **139**(5): 1024-1024 e1021.
- Kuchin, S., I. Treich, et al. (2000). "A regulatory shortcut between the *Snf1* protein kinase and RNA polymerase II holoenzyme." *Proc Natl Acad Sci U.S.A.* **97**(14): 7916-7920.
- Kuchin, S., V. K. Vyas, et al. (2002). "Snf1 protein kinase and the repressors Nrg1 and Nrg2 regulate *FLO11*, haploid invasive growth, and diploid pseudohyphal differentiation." *Mol Cell Biol* **22**(12): 3994-4000.
- Kumar, A., S. Agarwal, et al. (2002). "Subcellular localization of the yeast proteome." *Genes Dev* **16**(6): 707-719.
- Kumme, J., M. Dietz, et al. (2008). "Dimerization of yeast transcription factors *Ino2* and *Ino4* is regulated by precursors of phospholipid biosynthesis mediated by *Opi1* repressor." *Curr Genet* **54**(1): 35-45.
- Lagarde, M., A. Geloen, et al. (2003). "Lipidomics is emerging." *Biochim Biophys Acta* **1634**(3): 61.
- Le, T. T., I. M. Langohr, et al. (2007). "Label-free molecular imaging of atherosclerotic lesions using multimodal nonlinear optical microscopy." *Journal of Biomedical Optics* **12**(5).
- Le, T. T., S. Yue, et al. (2010). "Shedding new light on lipid biology with coherent anti-Stokes Raman scattering microscopy." *J Lipid Res* **51**(11): 3091-3102.
- Leber, R., E. Zinser, et al. (1994). "Characterization of lipid particles of the yeast, *Saccharomyces cerevisiae*." *Yeast* **10**(11): 1421-1428.
- Lee, T. I., N. J. Rinaldi, et al. (2002). "Transcriptional regulatory networks in *Saccharomyces cerevisiae*." *Science* **298**(5594): 799-804.
- Letters, R. (1966). "Phospholipids of yeast. II. Extraction, isolation and characterisation of yeast phospholipids." *Biochim Biophys Acta* **116**(3): 489-499.
- Liebeke, M., A. Wunder, et al. (2010). "A rapid microwave-assisted derivatization of bacterial metabolome samples for gas chromatography/mass spectrometry analysis." *Anal Biochem* **401**(2): 312-314.
- Lin, S. S., J. K. Manchester, et al. (2003). "Sip2, an N-myristoylated beta subunit of Snf1 kinase, regulates aging in *Saccharomyces cerevisiae* by affecting cellular histone kinase activity, recombination at rDNA loci, and silencing." *J Biol Chem* **278**(15): 13390-13397.
- Liu, Y., X. Xu, et al. (2010). "Snf1p Regulates Gcn5p Transcriptional Activity by Antagonizing Spt3p." *Genetics* **184**(1): 91-105.

- Lo, W. S., L. Duggan, et al. (2001). "*Snf1--a histone kinase that works in concert with the histone acetyltransferase Gcn5 to regulate transcription.*" *Science* **293**(5532): 1142-1146.
- Lo, W. S., E. R. Gamache, et al. (2005). "*Histone H3 phosphorylation can promote TBP recruitment through distinct promoter-specific mechanisms.*" *EMBO J* **24**(5): 997-1008.
- Loewen, C. J., M. L. Gaspar, et al. (2004). "*Phospholipid metabolism regulated by a transcription factor sensing phosphatidic acid.*" *Science* **304**(5677): 1644-1647.
- Loewen, C. J., A. Roy, et al. (2003). "*A conserved ER targeting motif in three families of lipid binding proteins and in Opi1p binds VAP.*" *EMBO J* **22**(9): 2025-2035.
- Longley, R. P., A. H. Rose, et al. (1968). "*Composition of the protoplast membrane from *Saccharomyces cerevisiae*.*" *Biochem J* **108**(3): 401-412.
- Lopes, J. M. and S. A. Henry (1991). "*Interaction of trans and cis regulatory elements in the INO1 promoter of *Saccharomyces cerevisiae*.*" *Nucleic Acids Res* **19**(14): 3987-3994.
- Loughlin, J., H. Phan, et al. (2007). "*Evaluation of charged aerosol detection (CAD) as a complementary technique for high-throughput LC-MS-UV-ELSD analysis of drug discovery screening libraries.*" *American Laboratory* **39**(16): 24-+.
- Madyastha, P. B. and L. W. Parks (1969). "*The effect of cultural conditons on the ergosterol ester components of yeast.*" *Biochim Biophys Acta* **176**(4): 858-862.
- Malanovic, N., I. Streith, et al. (2008). "*S-adenosyl-L-homocysteine hydrolase, key enzyme of methylation metabolism, regulates phosphatidylcholine synthesis and triacylglycerol homeostasis in yeast: implications for homocysteine as a risk factor of atherosclerosis.*" *J Biol Chem* **283**(35): 23989-23999.
- Masood, A., K. D. Stark, et al. (2005). "*A simplified and efficient method for the analysis of fatty acid methyl esters suitable for large clinical studies.*" *J Lipid Res* **46**(10): 2299-2305.
- Meziane, T. and M. Tsuchiya (2002). "*Organic matter in a subtropical mangrove-estuary subjected to wastewater discharge: Origin and utilisation by two macrozoobenthic species.*" *Journal of Sea Research* **47**(1): 1-11.
- Moreau, R. A. (1990). "*Plant Lipid Class Analysis by Hplc.*" *Plant Lipid Biochemistry, Structure and Utilization*: 20-22.
- Moreau, R. A. (2006). "*The analysis of lipids via HPLC with a charged aerosol detector.*" *Lipids* **41**(7): 727-734.
- Moreau, R. A. (2009). "*Lipid analysis via HPLC with a charged aerosol detector.*" *Lipid Technology* **21**(8-9): 191-194.
- Moreau, R. A. and P. T. Asmann (1989). "*Quantitative-Analysis of Lipids in Plastids by Hplc-Fid.*" *Physiology, Biochemistry, and Genetics of Nongreen Plastids* **2**: 274-276.
- Mullner, H. and G. Daum (2004). "*Dynamics of neutral lipid storage in yeast.*" *Acta Biochim Pol* **51**(2): 323-347.
- Nan, X., J. X. Cheng, et al. (2003). "*Vibrational imaging of lipid droplets in live fibroblast cells with coherent anti-Stokes Raman scattering microscopy.*" *J Lipid Res* **44**(11): 2202-2208.
- Nath, N., R. R. McCartney, et al. (2003). "*Yeast Pak1 kinase associates with and activates Snf1.*" *Mol Cell Biol* **23**(11): 3909-3917.
- Natter, K., P. Leitner, et al. (2005). "*The spatial organization of lipid synthesis in the yeast *Saccharomyces cerevisiae* derived from large scale green fluorescent protein tagging and high resolution microscopy.*" *Mol Cell Proteomics* **4**(5): 662-672.

- Nesterenko, E. P., P. N. Nesterenko, et al. (2009). "Zwitterionic ion-exchangers in ion chromatography: A review of recent developments." *Anal Chim Acta* **652**(1-2): 3-21.
- Nielsen, J. (2009). "Systems biology of lipid metabolism: from yeast to human." *FEBS Lett* **583**(24): 3905-3913.
- Nikoloff, D. M. and S. A. Henry (1991). "Genetic analysis of yeast phospholipid biosynthesis." *Annu Rev Genet* **25**: 559-583.
- Nurminen, T., E. Oura, et al. (1970). "The enzymic composition of the isolated cell wall and plasma membrane of baker's yeast." *Biochem J* **116**(1): 61-69.
- Ohsaki, Y., Y. Shinozawa, et al. (2010). "A pitfall in using BODIPY dyes to label lipid droplets for fluorescence microscopy." *Histochem Cell Biol* **133**(4): 477-480.
- Ostrander, D. B., D. J. O'Brien, et al. (1998). "Effect of CTP synthetase regulation by CTP on phospholipid synthesis in *Saccharomyces cerevisiae*." *J Biol Chem* **273**(30): 18992-19001.
- Park, T. S., D. J. O'Brien, et al. (2003). "Phosphorylation of CTP synthetase on Ser36, Ser330, Ser354, and Ser454 regulates the levels of CTP and phosphatidylcholine synthesis in *Saccharomyces cerevisiae*." *J Biol Chem* **278**(23): 20785-20794.
- Petiot, A., S. Pattingre, et al. (2002). "Diversity of signaling controls of macroautophagy in mammalian cells." *Cell Struct Funct* **27**(6): 431-441.
- Portillo, F., J. M. Mulet, et al. (2005). "A role for the non-phosphorylated form of yeast Snf1: tolerance to toxic cations and activation of potassium transport." *FEBS Lett* **579**(2): 512-516.
- Pulfer, M. and R. C. Murphy (2003). "Electrospray mass spectrometry of phospholipids." *Mass Spectrom Rev* **22**(5): 332-364.
- Quinlan, J. J., J. T. Nickels, Jr., et al. (1992). "The 45- and 104-kDa forms of phosphatidate phosphatase from *Saccharomyces cerevisiae* are regulated differentially by phosphorylation via cAMP-dependent protein kinase." *J Biol Chem* **267**(25): 18013-18020.
- Ramos, R. G., D. Libong, et al. (2008). "Comparison between charged aerosol detection and light scattering detection for the analysis of *Leishmania* membrane phospholipids." *J Chromatogr A* **1209**(1-2): 88-94.
- Ratnakumar, S. and E. T. Young (2010). "Snf1 dependence of peroxisomal gene expression is mediated by Adr1." *J Biol Chem* **285**(14): 10703-10714.
- Rattray, J. B., A. Schibeci, et al. (1975). "Lipids of yeasts." *Bacteriol Rev* **39**(3): 197-231.
- Santiago, T. C. and C. B. Mamoun (2003). "Genome expression analysis in yeast reveals novel transcriptional regulation by inositol and choline and new regulatory functions for Opi1p, Ino2p, and Ino4p." *J Biol Chem* **278**(40): 38723-38730.
- Sanz, P. (2003). "Snf1 protein kinase: a key player in the response to cellular stress in yeast." *Biochem Soc Trans* **31**(Pt 1): 178-181.
- Sattur, A. P. and N. G. Karanth (1989). "Production of microbial lipids: II. Influence of C/N ratio--model prediction." *Biotechnol Bioeng* **34**(6): 868-871.
- Sattur, A. P. and N. G. Karanth (1989). "Production of microbial lipids: III. Influence of C/N ratio--experimental observations." *Biotechnol Bioeng* **34**(6): 872-874.
- Schaffner, G. and P. Matile (1981). "Structure and Composition of Bakers-Yeast Lipid Globules." *Biochemie Und Physiologie Der Pflanzen* **176**(7): 659-666.
- Schnieder, R., B. Brugger, et al. (1999). "Electrospray ionization tandem mass spectrometry (ESI-MS/MS) analysis of the lipid molecular species composition of yeast subcellular membranes reveals acyl

- chain-based sorting/remodeling of distinct molecular species en route to the plasma membrane." J Cell Biol 146(4): 741-754.*
- Schneiter, R. and G. Daum (2006). "Extraction of yeast lipids." Methods Mol Biol 313: 41-45.
- Schonherr, C., S. Touchene, et al. (2009). "Simple and precise detection of lipid compounds present within liposomal formulations using a charged aerosol detector." J Chromatogr A 1216(5): 781-786.
- Schuller, H. J., A. Hahn, et al. (1992). "Coordinate genetic control of yeast fatty acid synthase genes FAS1 and FAS2 by an upstream activation site common to genes involved in membrane lipid biosynthesis." EMBO J 11(1): 107-114.
- Schuller, H. J., K. Richter, et al. (1995). "DNA binding site of the yeast heteromeric Ino2p/Ino4p basic helix-loop-helix transcription factor: structural requirements as defined by saturation mutagenesis." FEBS Lett 370(1-2): 149-152.
- Schuller, H. J., R. Schorr, et al. (1992). "Regulatory gene INO4 of yeast phospholipid biosynthesis is positively autoregulated and functions as a transactivator of fatty acid synthase genes FAS1 and FAS2 from *Saccharomyces cerevisiae*." Nucleic Acids Res 20(22): 5955-5961.
- Schwank, S., R. Ebbert, et al. (1995). "Yeast transcriptional activator INO2 interacts as an Ino2p/Ino4p basic helix-loop-helix heteromeric complex with the inositol/choline-responsive element necessary for expression of phospholipid biosynthetic genes in *Saccharomyces cerevisiae*." Nucleic Acids Res 23(2): 230-237.
- Schwank, S., B. Hoffmann, et al. (1997). "Influence of gene dosage and autoregulation of the regulatory genes INO2 and INO4 on inositol/choline-repressible gene transcription in the yeast *Saccharomyces cerevisiae*." Curr Genet 31(6): 462-468.
- Shimasaki, H., F. C. Phillips, et al. (1977). "Direct transesterification of lipids in mammalian tissue for fatty acid analysis via dehydration with 2,2'-dimethoxypropane." J Lipid Res 18(4): 540-543.
- Shirra, M. K., R. R. McCartney, et al. (2008). "A chemical genomics study identifies Snf1 as a repressor of GCN4 translation." J Biol Chem 283(51): 35889-35898.
- Smith, R. L. and A. D. Johnson (2000). "Turning genes off by Ssn6-Tup1: a conserved system of transcriptional repression in eukaryotes." Trends Biochem Sci 25(7): 325-330.
- Söderholm, S., M. Damm, et al. (2010). "Microwave-assisted derivatization procedures for gas chromatography/mass spectrometry analysis." Mol. Diversity 14(4): 869-888.
- Soontorngun, N., M. Larochelle, et al. (2007). "Regulation of gluconeogenesis in *Saccharomyces cerevisiae* is mediated by activator and repressor functions of Rds2." Mol Cell Biol 27(22): 7895-7905.
- Souzu, H. (1973). "Proceedings: The phospholipid degradation and cellular death caused by freeze-thawing or freeze-drying of yeast." Cryobiology 10(5): 427-431.
- Spener, F. (2005). "Lipidomics and consequences: a new classification system for lipids." European Journal of Lipid Science and Technology 107(5): 277-278.
- Spener, F., M. Lagarde, et al. (2003). "What is lipidomics?" European Journal of Lipid Science and Technology 105(9): 481-482.
- Sutherland, C. M., S. A. Hawley, et al. (2003). "Elm1p is one of three upstream kinases for the *Saccharomyces cerevisiae* SNF1 complex." Curr. Biol. 13: 1299.
- Swan, T. M. and K. Watson (1997). "Membrane fatty acid composition and membrane fluidity as parameters of stress tolerance in yeast." Can J Microbiol 43(1): 70-77.

- Tehlivets, O. (2011). "Homocysteine as a risk factor for atherosclerosis: is its conversion to s-adenosyl-L-homocysteine the key to deregulated lipid metabolism?" *J Lipids* **2011**: 702853.
- Tehlivets, O., K. Scheuringer, et al. (2007). "Fatty acid synthesis and elongation in yeast." *Biochim Biophys Acta* **1771**(3): 255-270.
- Thevelein, J. M. (1994). "Signal transduction in yeast." *Yeast* **10**(13): 1753-1790.
- Thomas, M. and C. Polge (2007). "SNF1/AMPK/SnRK1 kinases, global regulators at the heart of energy control?" *Trends in Plant Science* **12**(1): 20-28.
- Tomas, A., M. Tor, et al. (2009). "A rapid and reliable direct method for quantifying meat acylglycerides with monomode microwave irradiation." *J. Chromatogr. A.* **1216**(15): 3290-3295.
- Tuller, G., T. Nemec, et al. (1999). "Lipid composition of subcellular membranes of an FY1679-derived haploid yeast wild-type strain grown on different carbon sources." *Yeast* **15**(14): 1555-1564.
- Ulberth, F. and M. Henninger (1992). "One-step extraction/methylation method for determining the fatty acid composition of processed foods." *J. Am. Oil Chem. Soc.* **69**(2): 174-177.
- Usaite, R., M. C. Jewett, et al. (2009). "Reconstruction of the yeast Snf1 kinase regulatory network reveals its role as a global energy regulator." *Mol Syst Biol* **5**: 319.
- van der Meer, V., A. K. Neven, et al. (2005). "Diagnostic value of C reactive protein in infections of the lower respiratory tract: systematic review." *BMJ* **331**(7507): 26.
- Vidal, M., R. Strich, et al. (1991). "RPD1 (SIN3/UME4) is required for maximal activation and repression of diverse yeast genes." *Mol Cell Biol* **11**(12): 6306-6316.
- Wagner, C., M. Blank, et al. (1999). "Overproduction of the Opi1 repressor inhibits transcriptional activation of structural genes required for phospholipid biosynthesis in the yeast *Saccharomyces cerevisiae*." *Yeast* **15**(10A): 843-854.
- Wagner, C., M. Dietz, et al. (2001). "The negative regulator Opi1 of phospholipid biosynthesis in yeast contacts the pleiotropic repressor Sin3 and the transcriptional activator Ino2." *Mol Microbiol* **41**(1): 155-166.
- Wang, H., I. Clark, et al. (1990). "The *Saccharomyces cerevisiae* SIN3 gene, a negative regulator of HO, contains four paired amphipathic helix motifs." *Mol Cell Biol* **10**(11): 5927-5936.
- Wang, H. and D. J. Stillman (1993). "Transcriptional repression in *Saccharomyces cerevisiae* by a SIN3-LexA fusion protein." *Mol Cell Biol* **13**(3): 1805-1814.
- Ways, P. and D. J. Hanahan (1964). "Characterization and quantification of red cell lipids in normal man." *J Lipid Res* **5**(3): 318-328.
- Wenk, M. R. (2005). "The emerging field of lipidomics." *Nat Rev Drug Discov* **4**(7): 594-610.
- White, M. J., J. P. Hirsch, et al. (1991). "The OPI1 gene of *Saccharomyces cerevisiae*, a negative regulator of phospholipid biosynthesis, encodes a protein containing polyglutamine tracts and a leucine zipper." *J Biol Chem* **266**(2): 863-872.
- Wilson, J. F. (2003). "Long-suffering lipids gain respects." *Scientist* **17**(5): 34-36.
- Woods, A., M. R. Munday, et al. (1994). "Yeast SNF1 is functionally related to mammalian AMP-activated protein kinase and regulates acetyl-CoA carboxylase in vivo." *J Biol Chem* **269**(30): 19509-19515.
- Wu, W. I. and G. M. Carman (1996). "Regulation of phosphatidate phosphatase activity from the yeast *Saccharomyces cerevisiae* by

- phospholipids.*" Biochemistry **35**(12): 3790-3796.
- Ye, T., K. Elbing, et al. (2008). "The pathway by which the yeast protein kinase Snf1p controls acquisition of sodium tolerance is different from that mediating glucose regulation." Microbiology-Sgm **154**: 2814-2826.
- Yu, Y., A. Sreenivas, et al. (2002). "Phosphorylation of *Saccharomyces cerevisiae* choline kinase on Ser30 and Ser85 by protein kinase A regulates phosphatidylcholine synthesis by the CDP-choline pathway." J Biol Chem **277**(38): 34978-34986.
- Zhang, J., S. Vaga, et al. (2011). "Mapping the interaction of Snf1 with TORC1 in *Saccharomyces cerevisiae*." Mol Syst Biol **7**.
- Zhang, Z. X., G. H. Xiong, et al. (2000). "Sample pretreatment with microwave-assisted techniques." Anal. Sci. **16**(2): 221-224.
- Zheng, L., R. T'Kind, et al. (2010). "Profiling of lipids in *Leishmania donovani* using hydrophilic interaction chromatography in combination with Fourier transform mass spectrometry." Rapid Commun Mass Spectrom **24**(14): 2074-2082.
- Zinser, E., C. D. Sperka-Gottlieb, et al. (1991). "Phospholipid synthesis and lipid composition of subcellular membranes in the unicellular eukaryote *Saccharomyces cerevisiae*." Journal of Bacteriology **173**(6): 2026-2034.
- Zweytick, D., K. Athenstaedt, et al. (2000). "Intracellular lipid particles of eukaryotic cells." Biochim Biophys Acta **1469**(2): 101-120.

Paper I

Integrated analysis of the transcriptome-lipid profiling reveals the co-influences of inositol-choline and Snf1 in controlling lipid biosynthesis in yeast.

Chumnanpuen, P., J. Zhang, I. Nookaew, J. Nielsen

Under revision in Molecular Genetics and Genomics.

Integrated analysis of the transcriptome-lipid profiling reveals the co-influences of inositol-choline and Snf1 in controlling lipid biosynthesis in yeast

Pramote Chumnanpuen, Jie Zhang, Intawat Nookaew, and Jens Nielsen*

Department of Chemical and Biological Engineering,
Chalmers University of Technology,
Kemivägen 10, SE-412 96 Gothenburg, Sweden

*Corresponding Author:

Jens Nielsen

Systems and Synthetic Biology, Department of Chemical and Biological Engineering,
Chalmers University of Technology, Kemivägen 10, SE-412 96 Gothenburg, Sweden.

Email: nielsenj@chalmers.se

Tel: +46 31 772 38 04

List of Abbreviations

AcCoA = acetyl coenzyme A, AceAcCoA = acetoacetyl coenzyme A, CDP-DAG = cytidine diphosphate-diacylglycerol, Cho = choline, DAG = diacylglycerol, Etn = ethanolamine, ES = ergosterol, FA = fatty acid or fatty acyl-CoA, Glc-6-P = glucose 6-phosphate, G-3-P = glycerol 3-phosphate, HIC = high inositol-choline, IC = inositol-choline, LIC = low inositol-choline, MaCoA = malonyl coenzyme A, PA = phosphatidic acids, PC = phosphatidylcholine, PE = phosphatidylethanolamine, PI = phosphatidylinositol, PL = phospholipids, PS = phosphatidylserine, , Pyr = pyruvate, SE = sterylester, ST = strain factor, TAG = triacylglycerol, TF = transcription factor, UAS_{INO} = inositol-sensitive upstream activating sequence

Abstract

In the yeast *Saccharomyces cerevisiae* many genes involved in lipid biosynthesis are transcriptionally controlled by inositol-choline and the protein kinase Snf1. Here we undertook a global study on how inositol-choline and Snf1 interact in controlling lipid metabolism in yeast. Using both a reference strain (CEN.PK113-7D) and a *snf1* Δ strain cultured at different nutrient limitations (carbon and nitrogen) at a fixed specific growth rate of 0.1 h⁻¹ and at different inositol choline concentrations, we quantified the expression of genes involved in lipid biosynthesis and the fluxes towards the different lipid components. Through integrated analysis of the transcriptome, the lipid profiling and the fluxome, it was possible to obtain a high quality, large-scale dataset that could be used to identify correlations and associations between the different components. At the transcription level, Snf1 and inositol-choline interact either directly through the main phospholipid-involving transcription factors (i.e. Ino2, Ino4, and Opi1) or through other transcription factors e.g. Gis1, Mga2, and Hac1. However, there seems to be regulation in lipid's fluxes distribution at the enzyme levels of several lipid involving enzymes. The analysis showed the strength of using both transcriptome and lipid profiling analysis for mapping the co-influence of inositol-choline and Snf1 on phospholipid metabolism.

Introduction

Eukaryotic cells have evolved complex regulatory networks to control energy metabolism and the utilization of different carbon sources (Gancedo 1998; Usaite et al. 2009). In yeast the Snf1 kinase complex is one of the key regulators in this regulatory network, and it belongs to a remarkably conserved serine/threonine kinase family called AMP-activated kinase (AMPK) that exists in all eukaryotes (Thomas and Polge 2007). The Snf1 kinase was firstly identified as a key enzyme in releasing glucose repression on glucose depletion (Celenza and Carlson 1984), and later found to be involved in the regulation of transcription through posttranslational modifications of histone H3 and Gcn5 (Lo et al. 2001; Liu et al. 2010) and interaction with RNA polymerase II holoenzyme (Kuchin et al. 2000). Snf1 is activated by phosphorylation on Thr210 by its upstream kinases in response to activation by the Snf4 subunit (Nath et al. 2003; Sutherland et al. 2003). Once activated, Snf1 induces the genes in gluconeogenesis, glyoxylate cycle and β -oxidation of fatty acids (FA) by regulating a set of transcriptional factors (Soontorngun et al. 2007; Ratnakumar and Young 2010) and suppresses lipid biosynthesis by inactivating Acetyl-CoA carboxylase (Acc1), the committed step of FA synthesis pathway (Woods et al. 1994). Besides those aforementioned processes, Snf1 is also involved in other processes such as the general stress response, pseudohyphal growth, ageing and ion homeostasis (Alepuz et al. 1997; Hong and Carlson 2007; Kuchin et al. 2002; Lin et al. 2003; Ye et al. 2008; Shirra et al. 2008;

Portillo et al. 2005; Usaite et al. 2009). Considering the role of snf1 at the level of protein-protein interactions retrieved from the BioGRID database (Stark et al. 2011), Snf1 associates with 335 proteins, which are enriched in the GO-terms phosphorylation and proteins phosphorylation (hypergeometric test: $P=1.5E-5$) within the GO-terms transcription, DNA-dependent and regulation on transcription, DNA-dependent (hypergeometric test: $P=1.5E-5$). Remarkably, the GO term phospholipid metabolism is also over-represented within the Snf1 interaction network (hypergeometric test: $P=1.28E-3$), inferring the important role of Snf1 in controlling phospholipid metabolism.

Snf1 is involved in many stress response processes in yeast, including inositol biosynthesis. At high inositol concentrations, transcription of the *INO1* gene (a key gene required for an early rate-controlling step in phosphoinositol biosynthesis) is strongly repressed by the transcriptional repressor *OPI1* (Jackson and Lopes 1996). On the contrary, at low inositol concentrations, the basic helix-loop-helix proteins Ino2 and Ino4 heterodimerize and bind to the *INO1* promoter to activate its transcription (Ambroziak and Henry 1994). This kind of mechanism can also be observed in many phospholipid involving genes that contain the conserved UAS_{INO} (inositol-sensitive upstream activating sequence) element, also known as ICRE (inositol/choline responsive-element), in their promoters. Activation of *INO1*

and other UAS_{INO} -containing genes requires the transcription factors (TFs) Ino2 and Ino4, which bind as a heterodimer directly to UAS_{INO} sites (Ambroziak and Henry 1994; Lopes and Henry 1991; Schwank et al. 1995). Nevertheless, The negative regulator, Opi1, required for repression of the UAS_{INO} -containing genes (Greenberg et al. 1982; White et al. 1991), was shown to reside in the endoplasmic reticulum (ER) as a part of a protein complex that also contains the membrane spanning protein Scs2 under the signaling of inositol and PA (Gavin et al. 2002; Loewen et al. 2003). It has been known that the rate of phospholipid synthesis is dramatically increased when inositol is added to the growth medium (Kelley et al. 1988; Loewen et al. 2004). Recently, genome-wide transcription analysis revealed that growth in the presence of inositol also affects the expression level of over 100 genes (Jesch et al. 2005; Santiago and Mamoun 2003). However, the combination of inositol and choline increased the number of repressed genes compared with inositol alone and enhanced the repression level of a subset of genes whose expression are affected by inositol (Jesch et al. 2005).

The Snf1 kinase is able to directly activate the transcription of the *INO1* gene, encoding inositol-1-phosphate synthase required for inositol biosynthesis (Graves and Henry 2000; Donahue and Henry 1981). Since Snf1 is required for histone H3 modification at the promoter site of UAS_{INO}-genes (Arndt et al. 1995; Henry and Patton-Vogt 1998), the expression level of *INO1* is down regulated in a *snf1* deletion strain (Lo et al. 2005; Lo et al. 2001; Shirra et al. 2001). Consequently, a *snf1* Δ strain is inositol auxotrophic and addition of inositol into the culture medium is needed to compensate the failure of *INO1* expression. This indicates the co-influence of Snf1 and inositol on the yeast cell growth and lipid metabolism.

To elucidate the co-influence of Snf1 and inositol-choline on lipid metabolism of *S. cerevisiae*, we undertook a global study of lipid metabolism by performing three perturbations following a robust factorial experimental design. The first factor is the level of inositol-choline (IC factor), which is known to directly influence lipid metabolism (Jesch et al. 2005). The second factor is a genetic difference factor or a strain factor (ST factor), which is the comparison of *SNF1* deficiency with the reference strain. The third factor is nutrient limitation (carbon and nitrogen) factor that results in a global perturbation of the lipid pool inside the cell (Sattur and Karanth 1989b, a). Using a systems biology

approach (Canelas et al. 2010) a global regulatory model for lipid metabolism could be established, and in particular we could identify which genes involved in lipid biosynthesis that are correlated with the fluxes towards different lipid components.

Materials and methods

1. Materials

All chemicals were reagent grade. Phospholipids, fatty acid methyl ester and neutral lipids standards were purchased from Sigma.

2. Agar spot test on SD media with different inositol concentrations.

Both reference and *snf1* Δ strains were grown on SD agar plate (containing Yeast Nitrogen Base without amino acids and inositol, Formedium LTD, England). The SD agar plates were supplemented with 0, 1.39, 75 or 220 μ M of inositol.

3. Strains, cultivation, and fermentation profile.

The *S. cerevisiae* strains used in this study were a prototrophic strain CEN.PK 113-7D (*Mata Mal2-8c SUC2*) (van Dijken et al. 2000) and its derivative *snf1* Δ supplied by Peter Kötter (Frankfurt, Germany). Steady-state aerobic chemostat cultures were grown at 30 °C in 1.2 L bioreactors (DASGIP, Germany) with working volume of 0.5 L using a dilution rate of 0.10 (± 0.005) h⁻¹. For the C-limited cultures, the medium composition was the same as used by (Zhang et al. 2011). For N-limited cultivation, the medium was the same as the one used in C-limited cultivations except that the concentrations for (NH₄)₂SO₄ and glucose were 1.0 g/L and 60 g/L, respectively. The pH was controlled at 5.00 \pm 0.05 with 2M KOH and dissolved oxygen was kept above 30%. Chemostat cultivation ensured that metabolic and regulatory changes observed were specific to disruptions of Snf1 and also the addition of IC, and not complicated by external effects resulting from different growth rates. For HIC condition, the media contained 75 μ M of inositol and 1mM of choline (Klig et al. 1985; Bailis et al. 1987). The chemostat culture with low inositol concentration and associated data on transcription analysis were also used in a study

on the interaction of Snf1 and Tor1 (Zhang et al. 2011).

Samples were harvested from the cultivation media every second hour and immediately filtered through a 0.45 µm pore-size cellulose acetate filter (VWR) and stored at -20 °C until analysis. Biomass production was evaluated by measuring of optical density (OD_{600}) and dry cell weight. Glucose, glycerol, ethanol, and acetate concentrations were determined by HPLC analysis using an Aminex HPX-87H column (Biorad, Hercules, CA) (Zaldivar et al. 2002).

4. Transcriptome analysis

4.1 Transcriptome data acquisition

Samples for RNA extraction were taken after 50 h (i.e. 5 retention times) of steady-state by rapidly taking 20 ml of culture and mixing with 30 ml of crushed ice in a 50 ml Falcon tube to cool down the samples immediately. The cells were harvested by centrifuging at 4000 rpm and 2°C for 3 min, and then frozen in liquid nitrogen and stored at -80°C until subsequent RNA extraction. The cells were mechanically disrupted using FastPrep homogenizer (MP Biomedicals) and total RNA was isolated using the RNeasy Mini Kit (QIAGEN). The quality of total RNA was assessed using an Agilent 2100 Bioanalyzer (Agilent Technologies) with RNA 6000 Nano LabChip kit (Agilent Technologies). The labeled RNA was synthesized using the GeneChip 3' IVT Express Kit (Affymetrix), which was then hybridized onto the GeneChip Yeast Genome 2.0 Arrays (Affymetrix). Staining and washing of the hybridized arrays were carried out on the GeneChip® Fluidics Station 450 (Affymetrix) and scanned using the GeneChip Scanner 300 7G (Affymetrix). All transcriptome data of this study can be found at Gene Expression Omnibus with accession number GSE32418

*** Available for reviewer on private page at:
<http://www.ncbi.nlm.nih.gov/geo/query/acc.cgi?token=pjsfvwusiqaweb&acc=GSE32418>

4.2 Transcriptome data analysis

The transcriptome data were analyzed using Bioconductor in R. Raw data were normalized and processed together with Probe Logarithmic Intensity Error method. The 3-factor and 2-factor ANOVA analysis was performed to determine the genes whose expression level is significantly changed due

to three factors, limiting nutrient (CN), supplement inositol-choline (IC) and strains (ST), as well as their co-influence effect. The calculated P -values of different hypothesis were corrected for multiple testing by false discovery rate (FDR) method. A cut-off value of adjusted P value < 0.01 was set to assess statistical significance. Detailed summary of the results can be found in supplementary text file “C only Pval&FC” for C-limited conditions and “N only Pval&FC” for N-limited conditions. To evaluate intrinsic variation between transcriptome samples to assess quality of data and also robustness of biological replications, principal component analysis (PCA) was employed. Then, the result is visualized by two first principle components as illustrated on Figure 2A. All analyzes and plots were performed in R suite software.

5. Lipid data acquisition

5.1 Total lipid extraction

The lipid extraction method was adapted from Bligh and Dyer (Bligh and Dyer 1959). First, 15 mg of freeze-dried cell pellets were treated with 1 unit μl^{-1} of zymolyase digesting buffer (1.2 M glycerol, 100 mM sodium thioglycolate, 50 mM Tris-sulfate, pH 7.5) at 37°C for 15 min, followed by centrifugation at 3000 rpm for 3 min to collect the spheroplast, which was mixed with internal standards (heptadecanoic acid and glyceryl tri-heptadecanoate, 25 µg of each). After the addition of 7 ml of chloroform-methanol (2:1, v/v), the mixture was shaken horizontally at 300 rpm 4°C for 3 h, mixed with 1.7 ml of sodium chloride solution (0.73%) and centrifuged at 3000 rpm 4°C for 4 min for phase separation. The lower (organic)-phase was collected and the remaining was re-extracted with 5 ml of chloroform-methanol (85:15 v/v). The lower (organic)-phase was collected and pooled with the previous organic fraction and kept at -20°C until further analysis.

5.2 Lipid class separation, identification, and quantification using HPLC-CAD

Lipid separation and quantification were performed using the method modified from Silversand and Haux (Silversand and Haux 1997). Lipid separation was accomplished by HPLC (Dionex) equipped with charge aerosol detector; CAD (Corona) and the gas connected was nitrogen gas with 35 psi gas pressure. All

the separated fractions were then collected by automated fraction collector; AFC-3000 (Dionex). A 20 μ l volume of sample was injected in to the Luna 5 μ m HILIC 200 \AA 100 x 3.0 mm LC Column (Phenomenex). The flow-rate was 0.8 ml/min and the column temperature was kept at 25°C during all runs. The chromatogram was record at 10 Hz frequency and gain for 100 pA. The polar and neutral lipid classes were separated by two different solvent mixtures and gradient systems.

5.2.1 Polar lipids separation

For polar lipids, the two solvents in the binary gradient used for the separation of polar lipid classes were as follows: (A) hexane-isopropanol-acetic acid (70:29:1, v/v/v); (B) isopropanol-water-acetic acid (85:14:1, v/v/v). Triethylamine (0.08%, v/v) was added to the solvents. The samples were injected at time 0 and the gradient profile started at 5% of Solvent B and was increased to 60% in 15 min, after which it was kept at 60% in 5 min. Finally, the gradient was reduced from 60% to 5% of Solvent B in 10 min and then maintained at 5% for 5 min. In total, the solvent program for the separation of polar lipids took 35 min. All samples analyzed for polar lipid class separation were dissolved in Solvent A prior to chromatography. However, the total lipids were kept dissolved in chloroform-methanol (2:1, v/v) while stored and just before HPLC analysis evaporated to dryness and dissolved in Solvent A. All phospholipids fractions collected by AFC-3000 were processed by FAME analysis to quantify their FA contents.

5.2.2 Neutral lipids separation

The first fraction from polar lipids separation, which was all neutral lipids, was evaporated to dryness and dissolved in 200 μ l of Solvent C, which is hexane-acetic acid (99:1, v/v), prior to chromatography. After resuspended in Solvent C, 20 μ l of samples were re-injected and analyzed by neutral lipid separation program. For neutral lipids, Solvent A and Solvent C were used as binary gradient for neutral lipids. The samples were injected at time 0 and the gradient profile started at 0% for Solvent C and was changed to 5% A in 5 min. The gradient then continued from 5% to 100% in 15 min, after which it was kept at 100% A for 5 min. Finally, the gradient was reduced to 0% A in 10 min and then maintained at 100% C for 5 min. The solvent program for the separation of neutral lipid classes took 40 min in total.

5.3 Identification and quantification

Pure lipid standards were analyzed individually using chromatography to confirm their retention times and purity. Lipid standards were also co-eluted together with samples to identify peaks in unknown samples. Solutions of known concentrations of different lipid classes were mixed and lipid standard curves were generated to study the linearity of the detection method and to quantify lipid classes in unknown samples. Calibration curves were prepared for 5-500 μ g ml⁻¹ of PA, PE, PC, PS, PI, ES, TAG, FA, and ES. Each concentration of the standard solutions was injected twice and the average log₁₀ peak area for each lipid was plotted against the log₁₀ amount of lipid. Correlation (r^2) was determined for all curves by linear regression.

5.4 FAMEs analysis

We used standard procedure developed in our laboratory which is based on the our developed protocol (Khoomrung et al. 2012) . Briefly, 10 mg of freeze-dried samples was mixed with 4 mL of hexane, 2 mL of 14 % BF₃ (in Methanol) and 5 μ g of internal standard (17:0 fatty acid standard was added. The sample was then flushed into the tube's head space with nitrogen gas for 30s and closed tightly with a Teflon screw cap. The tube was placed in a vessel containing 30 mL of milliQ water and then sealed with TFM screw cap. The tube was heated using microwave digestion system (milestone start D, Sorisole Bergamo, Italy) equipped with rotor PRO-24. The temperature programming of microwave digestion was ramped (from room temperature) to 120 °C within 6 min and maintained for 10 min. After cooling down sample at the room temperature, 2 mL of milliQ water was added and shaken vigorously for 1 min and centrifuged at 2500 rpm for 5 min. The upper phase (hexane phase which contained the FAMEs) was analysed by GC-MS.

The FAMEs were separated and quantified using Focus GC ISQ single quadrupole GC-MS (Thermo Fisher scientific, Germany). The separation of FAMEs was performed on Zebron (ZB-WAX) GC column (30 m x 0.25 mm I. D., 0.25 μ m film thickness) from Phenomenex, Macclesfield, UK. Sample was injected in splitless injection mode (1 μ L at 240 °C) and Helium was a carrier gas (1 mL/min). The column temperature was initially set at 50 °C (1.5 min), then temperature was

ramped to 180 °C (25°C/min) for 1 min, then increased to 220 °C (10°C/min) and held for 1 min. Finally, temperature was increased to 250 °C (15°C/min) and held for 3.0 min. Mass transfer line and ion source were set at 250 °C and 200 °C, respectively. The FAMEs were detected with electron ionization (70 eV) in scan mode (50-650 m/z) and selected ion monitoring mode at m/z 55, 67, 74 and 79 (for quantitative analysis). The identification of unknown FAMEs was achieved by comparing their retention times and mass spectrum profiles with known standards (Sigma-Aldrich, USA). The quantification of FAMEs was performed using QuanBrowser function in Xcalibur software version 2.0 (Thermo Fisher Scientific). According to the serial dilution of FAME mix standards and were normalized according to the internal standard fatty acid C17:0. The average molecular weights of each PL (Table.S1) were used for mg/gDW and mmol/gDW units conversion (were later used for metabolic fluxes analysis).

6. Integrated analysis

The statistical adjusted P -values of each hypothesis testing were overlaid on the three curetted biological networks graph of Gene Ontology (Ashburner et al. 2000), Transcription factor-gene interaction (Abdulrehman et al. 2011) and genome-scale metabolic model iIN800 (Nookaew et al. 2008) (metabolite-gene interaction). Briefly, the networks were transformed to be bipartite graph then the adjusted p -values derived from each hypothesis as previously described in transcriptome in analysis section. After that, reporter algorithm (Oliveira et al. 2008) was performed to evaluate the functional enrichment of cellular responses based on each statistical hypothesis. The algorithm estimated meta-significant values (reporter p -value) of each GO term, Transcription factors (TF) and metabolites (feature) that are in response to each perturbation factor. Features that have reporter P -value < 0.001 were considered and presented in heatmaps. The list of gene members associated within the three features can be found in supplementary text file “C only Pval&FC” for C-limited conditions and “N only Pval&FC” for N-limited conditions.

Results

High and Low inositol-choline condition and media design

As previously reported for yeast, inositol is essential in a *snf1Δ* deletion strain (Shirra et al. 2001; Sanz 2003). To quantify the required inositol levels for a *snf1Δ* yeast strain, a spot test of *snf1Δ* on different concentrations of inositol were performed (Fig. 1A). Since Snf1 kinase regulates positively the expression of *INO1* (Lo et al. 2005; Shirra et al. 2001), the *snf1Δ* yeast strain could, as reported earlier, not grow on SD agar media without inositol (see Fig. 1A). However, myo-inositol is included in a concentration of 25 mg/L (corresponding to about 139 μM) in the minimal medium we normally use in our laboratory (Verduyn et al. 1992), and the spot test showed that even a 100 times lower amount (1.39 μM) is enough to support the growth of *snf1Δ* while higher concentrations (up to 200 μM) only provide marginal improvements in growth. Based on this we used an experimental design where 1.39 μM inositol and 0 mM choline represent low inositol-choline (LIC) condition and 75 μM inositol and 1 mM choline represent high inositol-choline (HIC) condition (see Fig. 1B).

Strains, cultivation, and fermentation profile

Two strains (the reference and *snf1Δ*) were grown in aerobic chemostat cultures were grown at 30 °C in 1.2 L bioreactors (DASGIP, Germany) with working volume of 0.5 L using a dilution rate of 0.10 (± 0.005) h⁻¹. According to the key physiology information of all conditions in table 1, the effects of *SNF1* deletion and IC obviously influenced to the cell growth reflected on biomass yields. At C-limited condition, deletion of *SNF1* resulted in substantial reduction in biomass yields by 34% and 22% at HIC and LIC conditions, respectively. At N-limited, in contrast, all the wild type strain and *snf1Δ* seemed to have no significant different in biomass yield at both HIC and LIC condition. This evidence pointed to the similar responsive patterns of the yeast cells due to inactivated Snf1 at N-limited compared to the *SNF1* deletion. Focusing on the IC effects on the cell growth of both reference and *snf1Δ*, we found about 5% to 15% increasing in biomass yield and about 30% to 60% increasing in biomass yield for C-limited and N-limited respectively. At HIC conditions, both strains produced a relatively high concentration of ethanol, glycerol and acetate compared to LIC by approximately 50% to 100% during chemostat.

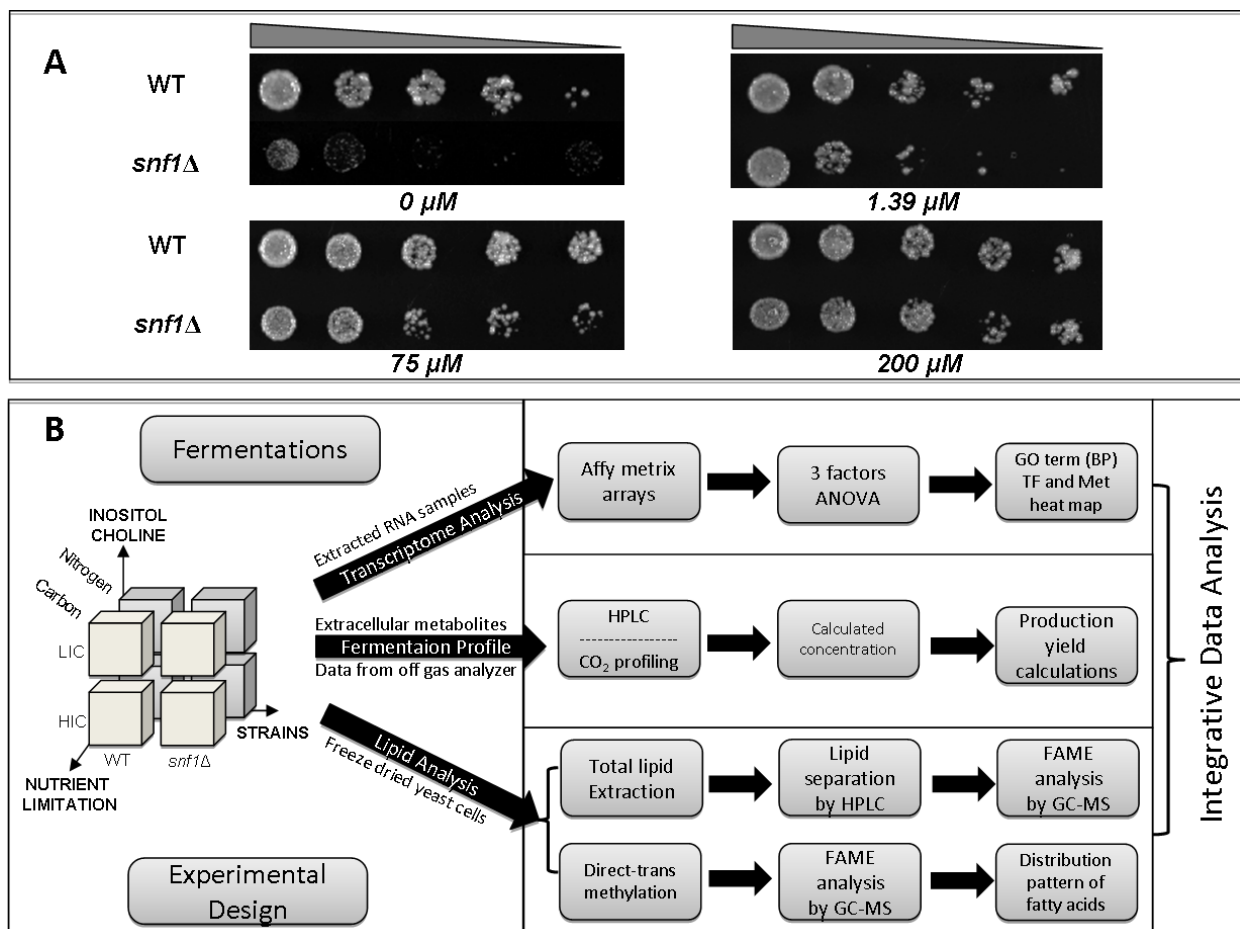


Figure 1. Spot test on SD agar plates with different inositol concentrations after 24 h (A). Illustration of the 3 factor factorial design and schematic analysis of our workflow for integrated analysis involving transcriptome-lipid profiling analysis of the inositol-choline effect on lipid biosynthesis in *snf1Δ* yeast strain (B).

Table 1. Key physiological parameters for all conditions in chemostat cultivations.

Strains	Conditions	Y_{SX}^1	Y_{SE}^2	Y_{SG}^3	Y_{SA}^4
reference	LIC, C-limited	0.515±0.007	n.d.	0.008±0.001	n.d.
reference	LIC, N-limited	0.097±0.002	0.292±0.029	0.002±0.000	0.004±0.001
<i>snf1Δ</i>	LIC, C-limited	0.384±0.003	n.d.	0.014±0.002	n.d.
<i>snf1Δ</i>	LIC, N-limited	0.102±0.000	0.252±0.044	0.007±0.000	0.005±0.001
reference	HIC, C-limited	0.539±0.010	n.d.	0.019±0.001	n.d.
reference	HIC, N-limited	0.128±0.004	0.485±0.0479	0.008±0.000	0.007±0.001
<i>snf1Δ</i>	HIC, C-limited	0.442±0.008	n.d.	0.021±0.001	n.d.
<i>snf1Δ</i>	HIC, N-limited	0.164±0.011	0.483±0.030	0.012±0.001	0.010±0.002

¹ Biomass yield on glucose (unit: g biomass formed/g glucose consumed)

² Ethanol yield on glucose (unit: g ethanol formed/g glucose consumed)

³ Glycerol yield on glucose (unit: g glycerol formed/g glucose consumed)

⁴ Acetate yield on glucose (unit: g acetate formed/g glucose consumed)

Global transcriptome changes due to IC level and deletion of Snf1 in nutrient-limited condition

We used the Affymetrix DNA microarray platform to measure the expression level of all genes and access the global effect caused by deletion of *SNF1*, by a high inositol-choline level, and the combination of the two under two different kinds of nutrient-limitation (C- and N-limitation). The transcriptome data of the 8 different conditions derived from 24 yeast 2.0 Affymetrix DNA microarrays were decomposed using principal component analysis (PCA) and 3-factor ANOVA analysis ($\alpha=0.01$) to obtain the global responses of gene expression at the different conditions. It is seen that the biological replicates are well grouped (Fig. 2A), showing very high reproducibility. Furthermore, the transcriptome data are presented in a Venn diagram (Fig. 2B) showing that the number of significant genes in response to the nutrient limited (CN) factor was about 2 times of that in response to the Snf1 deficiency factor (ST) and the inositol-choline (IC) factors, showing that a change from carbon to nitrogen limitation is the dominant factor. This is in consistency with the PCA that also illustrated that the impact of nutrient limitation is the main factor separating the samples in the first principal component. We therefore re-analyzed the transcriptome data using 2-factor ANOVA analysis of the C-limited and N-limited data sets separately (Fig. 2C) to get better insight into the effect of the ST and IC factors. Based on this we found that there were more genes being significantly changed at C-limitation than that at N-limitation. The variance between the reference and the *snf1* Δ strain (represented by the distance between reference-*snf1* Δ , Fig.2A) was very small at N-limited condition supported by the very small number of significant genes affected by the strain (ST) factor at N-limitation (see Venn diagram in Fig. 2C). This is due to general inactivation of Snf1 at N-limited growth conditions (Usaite et al. 2009; Zhang et al. 2011), but still deletion of *SNF1* influences the transcription of around 250 genes.

Subsequently, functional enrichment in response to each perturbed factor was calculated using our reporter algorithm, and the results are summarized in Fig. 2D. With this approach we identify GO terms that are enriched in response to the different factors, and this allows for direct interpretation of which biological processes are

affected in response to the different factors evaluated. It is seen that the identified GO terms (biological process) grouped into 5 main clusters (Fig. 2D). Cluster 1 contains genes enriched in sugar transport and metabolism, which were mainly influence by the ST factor and only at N-limited conditions. Cluster 2 contains genes involved in conjugation and reproduction, which were interaction effects of the ST and IC factors at N-limited condition only. Cluster 3 contains genes involving carbohydrate metabolism and stress response, which were mainly affected by the ST factor at C-limited conditions. Most biological processes of these three clusters are strongly influenced by a combination effect of the ST and IC factors that occur only in N-limited condition. Cluster 4 (The biggest group) contains genes mainly involved in fatty acid, phospholipids, inositol and biosynthesis process.

Interestingly, not only individual factors like ST and IC influence the transcriptional changes of the processes in this cluster, there are also strong influences by the combination effect of the ST and IC factors indicating by the interaction *p*-values between ST and IC that only occurred at C-limited and not at N-limited condition. Cluster 5 contains genes involved in the TCA cycle and mitochondrial functions, which were strongly affected by the ST factor at both C-limited and N-limited conditions as previously known (Sanz 2003; Thomas and Polge 2007; Woods et al. 1994).

To identify transcriptional regulation of metabolism in response to deletion of *SNF1* and/or IC effect, we overlaid the transcriptome onto a genome-scale metabolic model of *S. cerevisiae* “iIN800” (Nookaew et al. 2008). This method (Oliveira et al. 2008; Patil and Nielsen 2005) is really useful for the identification of “reporter feature” (metabolites, transcription factors, etc) around which significant transcriptional activity occurred and also sub-networks of coordinated transcriptional changes. The results of the reporter GO term analysis are in agreement with analysis of reporter metabolites and reporter transcription factors (TFs). The results of this analysis (reporter metabolites and TFs) are reported as heatmaps in Fig. S4 and S5. The list of gene members corresponded by each reporter GO term and each TFs can be found in supplementary text files “GO_member.txt” and “TF_member.txt”, respectively.

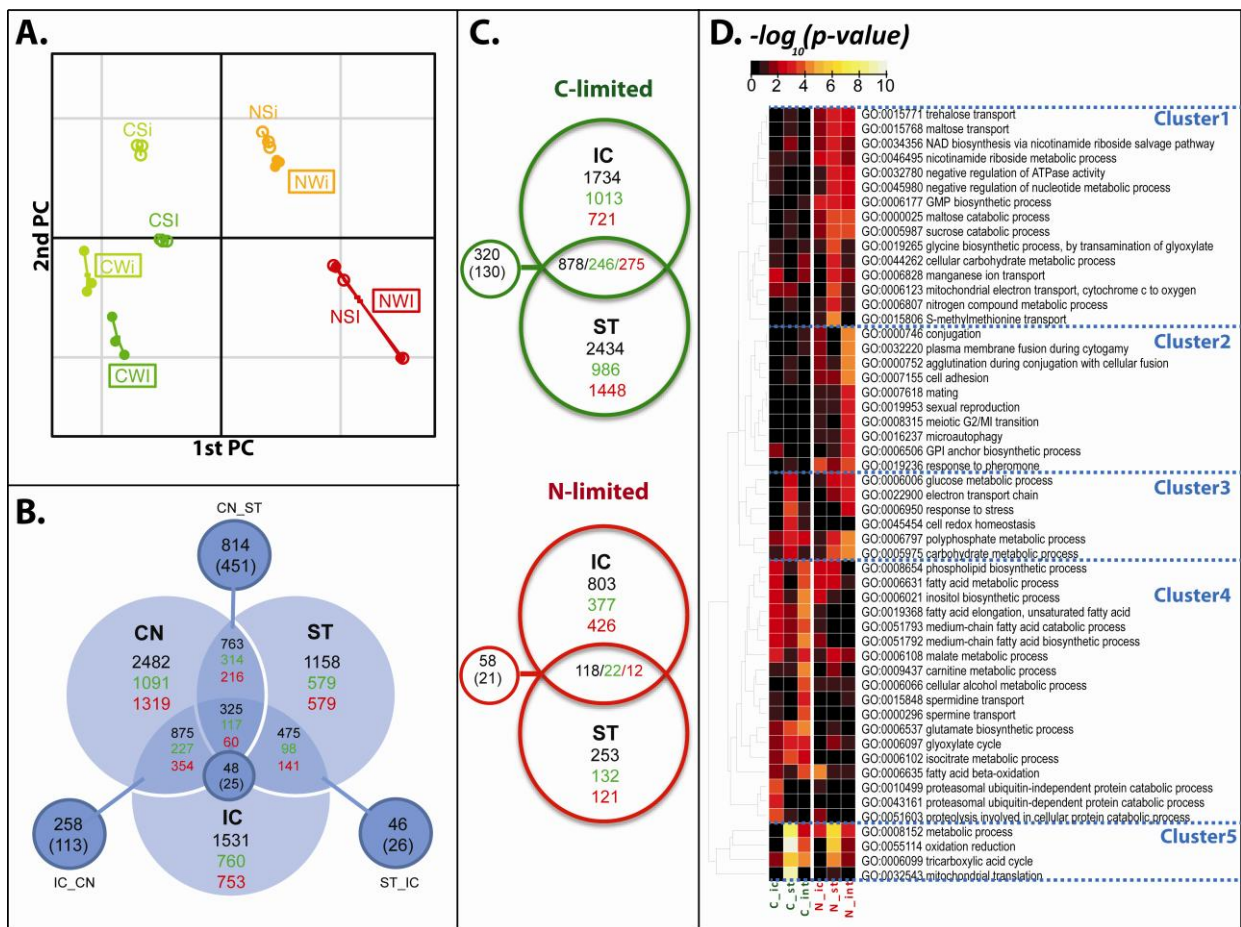


Figure 2. Transcription data analysis at a global view; (A) Principal component analysis of the transcriptome data. Each dot represents one biological replicate. The dots of same condition are connected by solid lines. C = C-limited, N = N-limited, W= wild type, S= snf1 Δ , i = LIC, and I = HIC. (B) Venn diagram of 3-factor ANOVA analysis i.e. carbon/nitrogen limited (CN), strain (ST), inositol-choline (IC) and their interactions, p -value < 0.01 was used. (C) Venn diagrams of 2 factors ANOVA analysis i.e. IC, ST and their interaction when focus on C-limitation and N-limitation separately, p -value < 0.01 was used. For figure 2B and 2C, the black numbers on top are the significant genes, green means down-regulated, red means up-regulated genes. In the intersection areas, only the genes that are down-regulated together or up-regulated together among those factors are represented. The small circles sticking out of the intersection areas represent the number of genes that are responded to each interaction effect deriving from those factors, and the numbers in the brackets show the number of overlapping genes which were also found in common with the intersection area. (D) A heat map of over-representation of GO terms (Biological Process) responded to each factor in the range of 0-10 of $\log(p\text{-value})$.

Lipid composition and content

To link the transcription level to alterations in the cellular lipid composition, we measured different lipid classes at all conditions (with biological triplicate samples). This also allowed us to obtain insight into how the inositol-choline level and the Snf1 activity affected the lipid biosynthesis at the metabolic level. For each sample, four neutral lipids (i.e. SE, TAG, FA, and ES) and five phospholipids (such as PA, PE, PC,

PS, and PI) were separated and quantified (see Fig. S2-3). Moreover, the FA distributions in each phospholipid class and total fatty acids were monitored (supp. table 4-8). The FA analysis of the total lipid pool confirmed that the C16 and C18 fatty acids were the two major FAs in yeast. About 70-80% of yeast FAs are monounsaturated (Fig. S1) via a reaction catalysed by the ER-bound $\Delta 9$ desaturase Ole1 (Tehlivets et al. 2007). The major parts of the lipid composition were

phospholipids and storage lipids (TAG and ES), each in the range of 20-40% at all conditions. Both SE and free FAs were detected in very small amounts, around 2-8%, at all conditions. The IC effect had influence on the total lipid composition,

and we found that at HIC conditions, the percentages of phospholipids were lower whereas the storage lipids (such as TAG and ES) were higher compared with LIC.

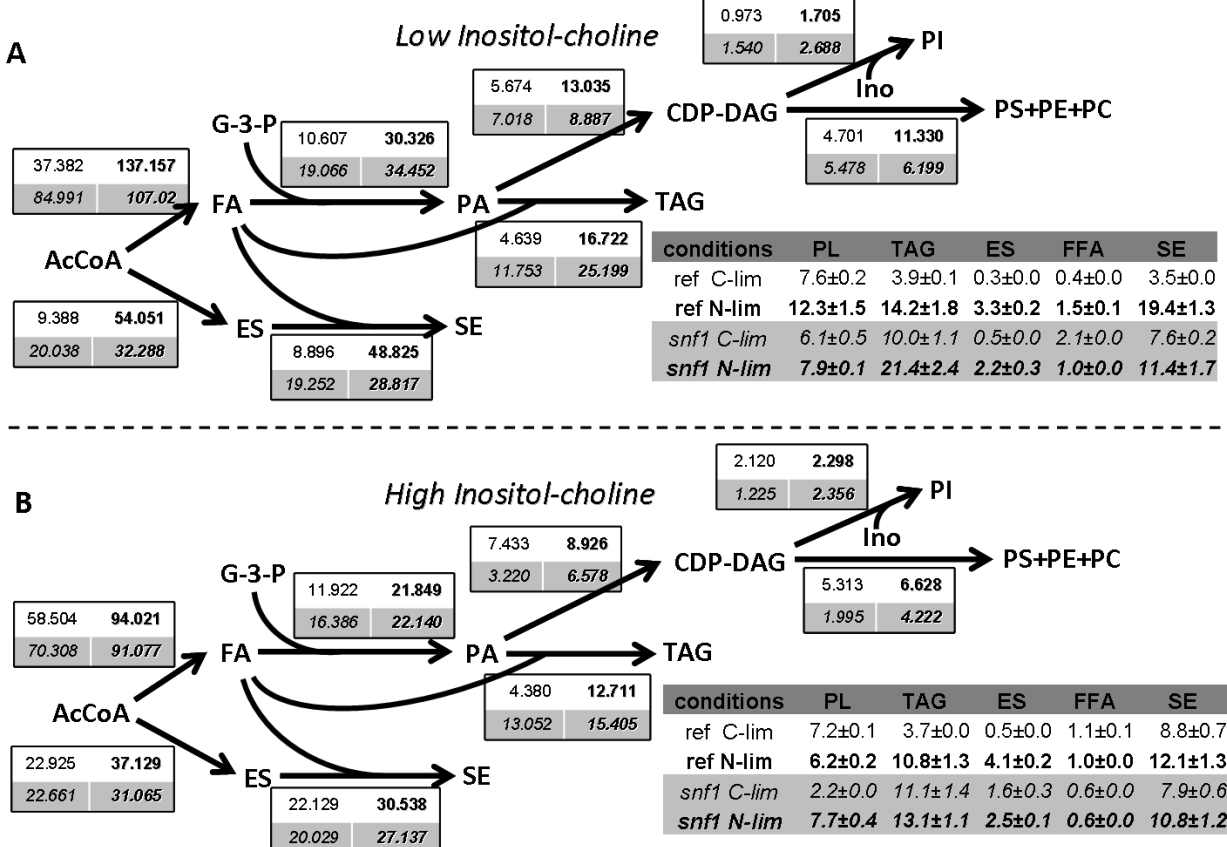


Figure 3. Fluxes through the different reactions of lipid biosynthetic pathway for LIC (A) and HIC (B). All fluxes are shown in units of $\mu\text{mol/gDW/h}$. The upper value (normal font) is for the reference strain, the lower (italic font) is for *snf1* Δ strain, normal font (left) and bold font (right) indicate the value from C-limitation and in N-limitation respectively. The level, in units of mg/gDW, of the different lipid species is shown in the table. (C = C-limited, N= N-limited, W= wild type, S= *snf1* Δ , i = LIC, and I = HIC)

Flux distribution in lipid pathway is highly influenced by IC and Snf1

To explore the carbon channeling in lipid metabolism, the fluxes in lipid biosynthesis (in units of $\mu\text{mol/gDW/h}$) were calculated from the measured lipid profiles at all conditions (Fig. 3) and this provides a clear picture of the changes in the flux distribution in response to the different factors evaluated. These fluxes were affected by many factors at several levels, such as gene transcription, protein phosphorylation, and enzyme activity. Thus at N-limited condition, where there is excess glucose available, the fluxes from AcCoA were about 3 and 2 fold higher when compared to those at C-limited conditions for LIC and HIC conditions,

respectively. According to the reporter metabolite analysis (Fig S4.), AcCoA was found to be significantly different in response to the IC factor. At LIC condition, the flux to the phospholipid pools is larger than that to the storage lipids (i.e. TAG and SE). On the other hand, the flux to storage lipids at HIC condition was greater than that at LIC (since the IC effect result in down-regulation of the whole set of phospholipid synthesis genes). Interestingly, we found Gis1 as one of the most significant TFs that were strongly affected by the ST factor at C-limitation and both the ST and IC factors at N-limited condition. Since Snf1 has protein-protein interaction with Gis1p as a repressor (Balciunas and Ronne 1999), the expression level of Gis1 genes were increasing at HIC condition only at N-limited

conditions where Snf1 is inactive. Moreover, this TF has interactions (directly or indirectly) with several genes involved in lipid biosynthesis (i.e. *FAA2*, *ERG28*, and *DPP1*) and also carbohydrate metabolism (i.e. *PGM2*, *HOR2*, *TPK1*, *ICL1*, and *PCK1*). Moreover, we also found inositol-3-phosphate as a significant reporter metabolite in response to the IC factor at both C-limited and N-limited conditions. This directly resulted from addition of inositol-choline to the culture medium. Thus, through our experimental design we obtained significant alteration in the fluxes of the different branches of lipid metabolism, and in the following we will discuss how the changes in these different fluxes are linked to the transcriptome and the different factorial effects.

Discussions

Effect of inositol-choline, Snf1, and nutrient limitations on FA biosynthesis

According to reporter GO terms as presented in Fig 2D, FA synthesis related genes (i.e. *ELO1* and *OLE1*) had significant changes in expression in response to the IC factor (especially at C-limited conditions). It has been

known that β -oxidation happens in the peroxisome associated with lipid droplets, so called pexopedia. At N-limited conditions there is accumulation of ethanol (table 1), and this could repress the synthesis of Fox1-3 proteins that are the core enzymes of fatty acid β -oxidation in the peroxisome (Hiltunen et al. 2003). This repression of β -oxidation may explain the accumulation of TAG at these conditions. Pip2 and Oaf1 were found to be significant reporter TFs in response to the IC factor and these transcription factors are regulating genes involved in FA β -oxidation, and these genes are also found to be significantly regulated only in response to the IC factor. This is supported by findings by Jesch et al. (2005), who showed that the IC factor results in down regulation of FA β -oxidation genes (Jesch et al. 2005). Interestingly, we also found Mga2, which is the TF controlling the expression of *OLE1* gene (Zhang et al. 1999), as a significant reporter TF at C-limited condition in response to the IC factor. This explains the increased *OLE1* expression (Fig. 4A); i.e. the expression level is higher at C-limited condition than at N-limited condition and seems to be up regulated at HIC condition (especially in the *snf1* Δ strain).

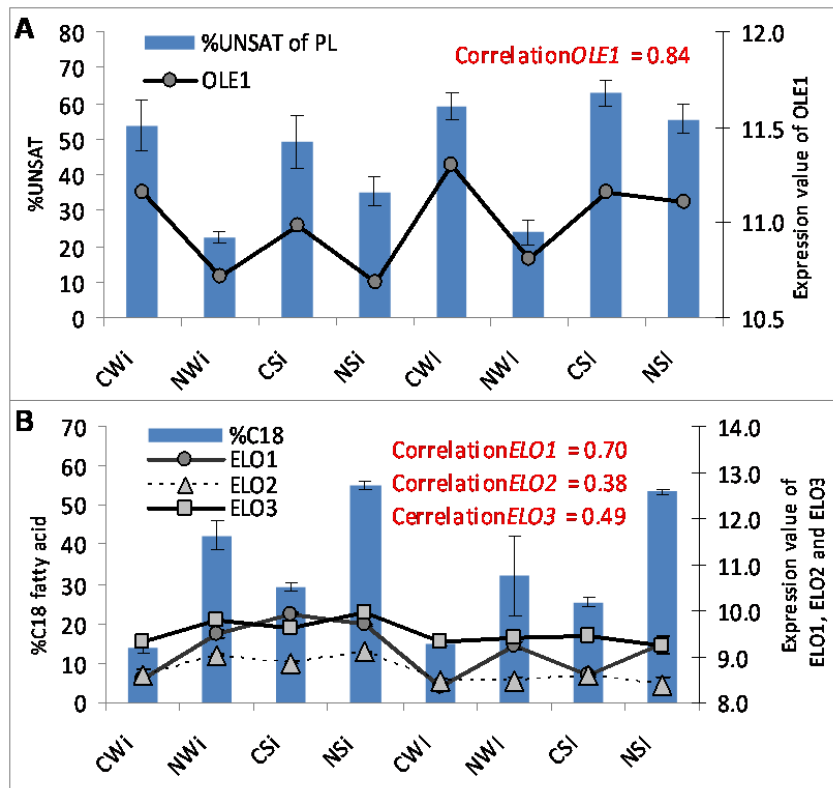


Figure 4. Correlation between fatty acid ratio and their specific enzyme coding genes (C = C-limited, N = N-limited, W = wild type, S = *snf1* Δ , i = LIC, and I = HIC). (A) Correlation between %unsaturation and *OLE1* expression. (B) Correlation between %C18 FA and each FA elongase coding genes (*ELO1*, *ELO2*, and *ELO3*) expression.

This result supports the evidence that inositol can induce *OLE1* expression but repress *INO1* expression (Gaspar et al. 2006). Furthermore, the correlation between the *OLE1* gene and %unsaturation of phospholipids and total lipid were examined, and a Pearson's correlation coefficient of 0.84 (*p*-value about 2.55e-7) was found between *OLE1* gene expression and %unsaturation of phospholipid, whereas there was no correlation found to the %unsaturation of the total lipids. Normally, the expression value captured by Microarray measurement has lesser dynamic range compared with quantitative real time PCR (QPCR). However, the significantly change derived from the both method are generally agreed (Canelas et al. 2010). As seen in the figure 4 the expression of *OLE1* (in Log2 scale) has small changes in low magnitude however the statistical different derived from one way ANOVA analysis indicates significantly different (*P*=1.86E-13). This strongly suggests that the %unsaturation of FA in phospholipids were highly regulated at the transcriptional level. This may be an important factor for controlling membrane fluidity that is exquisitely regulated by the ubiquitin/proteasome system (Braun et al. 2002), which is in agreement with our integrated analysis of the transcriptome data as illustrated in Figure 2, where we found a GO term associated

with proteasomal ubiquitin dependent and independent protein catabolic processes in response to the IC factor at both C-limitation and N-limitation. Consequently, the correlations between the genes coding for fatty acid elongase enzyme i.e. *ELO1*, *ELO2*, and *ELO3* against %C18 FA in total lipid were also calculated and the Pearson's correlation coefficient of 0.70, 0.38 and 0.49 were found between *ELO1*, *ELO2* and *ELO3* on %C18 FA, respectively (figure 4B). Moreover, Hac1, which is the key transcription factor controlling the unfolded protein response (UPR), was also found to be significantly responding to IC (Fig. S5). This shows that the IC effects on fatty acid desaturation process is also linked to the UPR pathway through the OLE pathway as reported by Jesch et al.(2005) (Jesch et al. 2005).

It has been reported that Snf1 kinase regulates negatively the activity of acetyl-CoA carboxylase Acc1 (the first enzyme of the fatty acid synthesis pathway), resulting in the inhibition of lipid biosynthesis (Woods et al. 1994; Usaite et al. 2009) (see Fig. 5). There is, however, also a transcriptional response as we also found several types of AcylCoA as significant reporter metabolites as well as malonyl-CoA, which is the key precursor for FA biosynthesis (Fig. S4). Several FA types were significant reporter metabolites in response to the IC factor at C-limited condition and both the IC and ST factors at N-limited conditions.

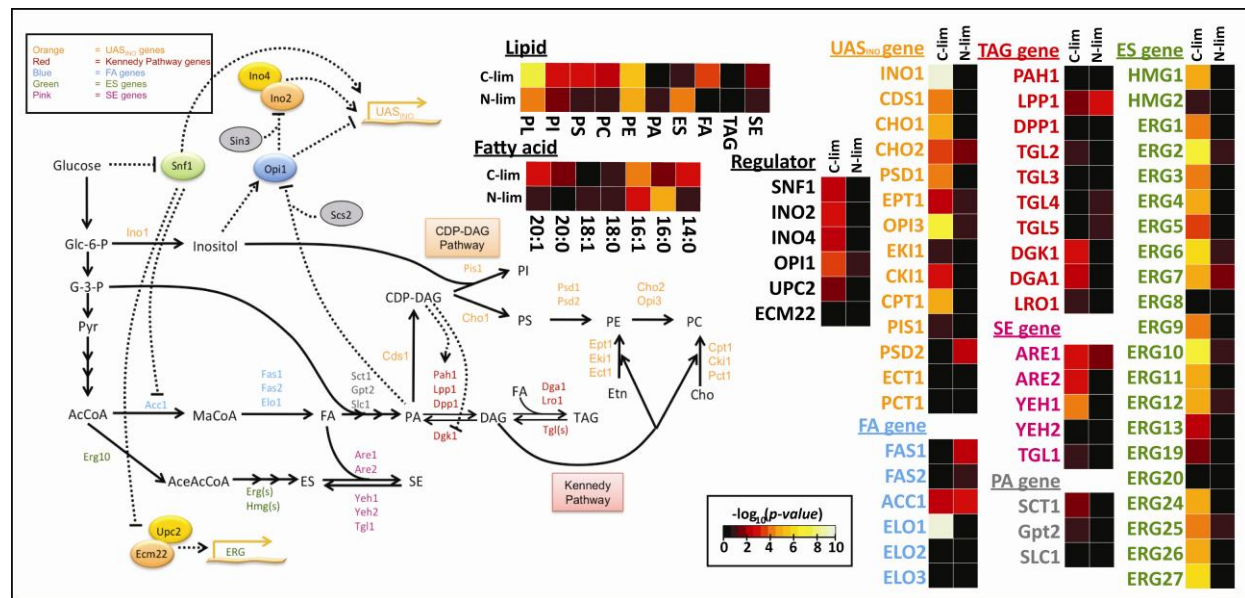


Figure 5. Biosynthetic pathway and regulation model of lipid metabolism in *S. cerevisiae*. The pathway shows the synthesis of neutral lipids (FA, ES, SE, DAG, and TAG) and phospholipids (PA, PI, PS, PE, and PC). The genes that are known to encode enzymes catalyzing individual steps in the lipid synthetic pathway are indicated. The co-influence levels on gene expression and lipid metabolites by the combination of inositol-choline and Snf1 are evaluated by interaction *p*-values presented as significance heatmaps.

IC and Snf1 in controlling phospholipids biosynthesis

The rate of phospholipid synthesis is substantially decreased when inositol is added to the growth medium (Kelley et al. 1988; Loewen et al. 2004). At all HIC conditions, UAS_{INO}-containing genes were significantly down regulated, at 70% on average (for more information, please see supplementary text files) when compared with LIC. Since Snf1 is active at C-limitation (Usaite et al. 2009; Zhang et al. 2011), this shows that Snf1 substantially affects the expression of the whole set of UAS_{INO}-containing genes when compared with N-limited conditions where Snf1 is not active (Usaite et al. 2009; Zhang et al. 2011) (mean adjusted P-value = 1.39 E-4, 3.33E-2 for C- and N-limited, respectively (for more information, please see supplementary text file “Specific Pval&FC Lipids and genes”). Furthermore, when Snf1 is active it will inhibit Acc1 and hereby result in reduced level of lipids in the cell as seen in Fig. 3. The expression of UAS_{INO}-containing genes in the reference strain at C-limitation and LIC condition were therefore not as high as those in the *snf1Δ* strain and the reference strain at N-limitation where there is increased activity of Acc1 (see Fig. 3). There therefore seems to be co-ordination between regulation of the Acc1 activity and expression of down-stream UAS_{INO} genes. Recently, it has been found that mutations in *ACC1* (encoding acetylCoA carboxylase) and *FASI* (encoding fatty acid synthase) suppress the inositol auxotrophy of the *snf1Δ* mutants, indicating that this auxotroph arises in part from increased Acc1 activity in the mutant (Sanz 2003). Considering the lipid content at all conditions, the reference strain at C-limitation and LIC condition still was the one that had the highest level of phospholipid (almost 50% w/w total lipid). This may be caused by the high PA level since it this was found to be highest at this condition (Fig. 3 and Fig. S3). This may lead to inhibition of the master negative regulator of phospholipid biosynthesis, Opi1, which is associated with the nuclear/ER membrane through interaction with the integral membrane protein Scs2 (Fig. 5). At HIC conditions the PA will be consumed to produce PI, and this may resulted in reduced levels of PA in the cells (Fig. S3 and table S3). This can be directly sensed by Opi1, a component of the endoplasmic reticulum (ER)-localized lipid sensing complex (Loewen et al. 2003). Since Opi1 is free and hence able to migrate into the nucleus, where it interacts with Sin3 to

inhibit the Ino2/Ino4 complex, and this results in down-regulation of the whole set of UAS_{INO}-containing genes (Loewen et al. 2004; Kumme et al. 2008) leading to a 40% reduction in the phospholipid pool at HIC condition (see Fig. 3 and Fig. S2). Moreover, the lack of Snf1 activity in the *snf1Δ* strain also resulted in a 50% reduced phospholipid pools due to down regulation of *INO1* at both C- and N- limited conditions. These effects are captured by our integrative analysis where Ino2, Ino4 and Opi1 were all found as reporter TFs in both IC and ST conditions (Fig.S6), but Opi1 had the highest significant score derived from the integrated analysis (Fig.S6), which is probably due to the fact that Opi1 is the direct target of the PA levels as a result of the IC effect while Ino2 and Ino4 are affected by Opi1, and hence are both lower in the regulatory cascade (Fig. 5).

IC and Snf1 in controlling neutral lipid biosynthesis and accumulation

In yeast, the neutral storage lipids are accumulated in lipid droplets consisting of TAG and SE, each consisting of about 50% (Leber et al. 1994; Mullner and Daum 2004; Schaffner and Matile 1981). These storage lipids are normally synthesized in hydrophobic region of the ER membrane and later incorporated into lipid droplets and then released into the cytosol (Mullner and Daum 2004). Both TAG and ES synthesis are regulated and affected by IC and Snf1 at different levels, such as the transcription level, protein kinase level, and enzyme activity level. Even though the expression level of phosphatidic acid phosphatase (PAPs) genes coding for storage lipid enzyme (e.g. Pah1, Dpp1, and Lpp1) were not significantly changed at HIC condition, the percentage of storage lipids such as TAG and SE were still 11-14% higher than those at LIC and C-limited condition in both the *snf1Δ* and the reference strain. This must be due to changes at the metabolite and/or protein level, and not at the transcriptional level. Once PA has been converted to PI via the CDP-DAG intermediate, PAPs will be activated. We found CDP-DAG as well as PA as the top significant reporter metabolites (Fig. S4), and since CDP-DAG is the main regulator that can activate the enzyme activity of PAPs (Loewen et al. 2004) (Fig. 5), the fluxes through TAG were increased in HIC, which has a higher amount of CDP-DAG (Fig. 3). For ES biosynthesis, a similar pattern of expression levels of genes involved in ES synthesis was observed,

i.e. expression was not significantly changed in response to the IC factor. Moreover, we found key TFs involved in sterol biosynthesis (*Upc2* and *Ecm22*) as reporter TFs in response to the ST factor, but only at C-limited conditions, and *Sut1* (involved in sterol uptake) as a reporter TF in response to both the IC and ST factors at N-limited condition (Fig S6). Since *Upc2* and *Ecm22* can be repressed by *Snf1* (Nielsen 2009; Zhang et al. 2010), ES genes (*Erg1-27* and *HMG1-2*) had higher expression value at N-limitation and in the *snf1Δ* strain especially at HIC condition (supplementary text file “Specific Pval&FC Lipids and genes”). In addition, mevalonate and AceAcCoA were identified as reporter metabolites for the ST and IC factors, especially at C-limited condition (Fig S4), and this is consistent with the observed higher fluxes towards ES at HIC condition, in particular for the *snf1Δ* strain (Fig. 3).

Co-influences of inositol-choline and Snf1 on lipid metabolism

As previously described, the impact of IC and *Snf1* individually on lipid metabolism and its regulations is substantial. Due to our factorial experimental design, the co-influences resulting from cross talking between inositol-choline and *Snf1* could, however, also be evaluated. With our experimental setup it is possible to see the effects from the knocking out of *SNF1* and also the substrate limitations that leads to changes in *Snf1* activity (i.e. with the ST factor it is presence versus absence of *Snf1* and for C-limitation *Snf1* is active and for N-limitation it is inactive). So we have two slightly different co-influences of inositol-choline with active *Snf1* and inositol-choline with inactive *Snf1*. Based on the integrative analysis Figure 5 summarizes the key regulation of the lipid biosynthesis pathways confirmed and identified by our study. The co-influences between *Snf1* and inositol-choline are also reported as a heatmap in the figure for each gene expression and measured lipids (adjusted interaction *p*-values). The summarized figure provides compelling evidence of substantially co-influences of inositol-choline and *Snf1* in terms of regulating the lipid metabolism. We can conclude that the co-influence of inositol-choline and *Snf1* depends on the active state of *Snf1* at both the transcription and lipid metabolite levels. Interestingly, *INO1* was substantially influenced by both factors, which should be the consequence of the response of the regulators *Ino2*, *Ino4* and *Opi1*, and this leads to changes in phospholipid metabolism. Transcription

of genes in the ergosterol and sterol-ester synthesis pathway was also influenced by cross talking of inositol-choline and *Snf1*. Surprisingly, transcription of *ACCI*, encoding the rate controlling enzyme in fatty acid biosynthesis, was significantly influenced at both C- and N-limitation indicating a special response to the combination of IC and *Snf1* (both in active or inactive form). This evidence may link to the fact that inositol auxotrophy in a *snf1Δ* strain can be rescued by inhibiting *Acc1* activity (Woods et al. 1994), probably due to a decreased flux through fatty acid synthesis, which may allow the mutant to synchronize fatty acid synthesis with the reduction of inositol synthesis when *Snf1* is absent, and hereby ensure that phospholipid biosynthesis is balanced with the demand for cellular growth. Besides, we found that the interaction between IC and *Snf1* did not influence the expression levels of most of the lipid genes much in N-limited condition (except a few genes e.g. *ACCI*, *CHO2*, *PSD2*, *LPP1* and *FASI*) since the global transcriptional responses caused by the ST factor were so small at N-limited conditions (where *Snf1* were inactive).

Through integrated analysis of the transcriptome, lipid profiling, and fluxome derived from a robust experimental setup we were able to get insight into how gene expression is linked to the fluxes in lipid biosynthesis at the global level. Among the interesting findings is an effect of inositol-choline, but not by *Snf1*, on the UPR pathway via the transcription factor *Hac1*. This evidence points to an interesting link between lipid metabolism and the protein secretory pathway, both involving activities in the endoplasmic reticulum. Globally, both *Snf1* and inositol-choline influence and also co-influence lipid metabolism, especially phospholipid biosynthesis were affected via the transcription factors (i.e. *Ino2*, *Ino4*, and *Opi1*) or indirectly through other transcription factors e.g. *Gis1*, *Mga2*, *Upc2*, *Ecm22*, *Pip2*, *Oaf1*, *Sut1*, *Hac1*, etc. Our data also suggested that storage lipid synthesis and accumulation seem to be controlled at the enzyme activity level (i.e. *Dpp1*, *Lpp1*, *Pah1*, and *Dgk1*). Thus, through our genome-wide analysis of lipid metabolism we managed to both confirm earlier findings and map several novel regulatory circuits involved in controlling how carbon is directed into the different branches of lipid metabolism.

Acknowledgements

Part of this work was financed by Chalmers Foundation, the Knut and Alice Wallenberg Foundation and the Swedish Research Council (Vetenskapsrådet). We also acknowledge funding from the EU-funded project UNICELLSYS. Pramote Chumnanpuen also would like to thank the Office of the Higher Education Commission, Thailand for support by a stipend for his Ph.D. program under the program Strategic Scholarships for Frontier Research Network. We also thank Nils-Gunnar Carlsson for valuable assistance with running the HPLC-CAD, Tobias Österlund and Klaas Buijs for helpful suggestions on manuscript preparation.

References

- Abdulrehman D, Monteiro PT, Teixeira MC, Mira NP, Lourenco AB, dos Santos SC, Cabrito TR, Francisco AP, Madeira SC, Aires RS, Oliveira AL, Sa-Correia I, Freitas AT (2011) YEASTRACT: providing a programmatic access to curated transcriptional regulatory associations in *Saccharomyces cerevisiae* through a web services interface. *Nucleic Acids Res* 39 (Database issue):D136-140. doi:10.1093/nar/gkq964
- Alepuz PM, Cunningham KW, Estruch F (1997) Glucose repression affects ion homeostasis in yeast through the regulation of the stress-activated ENA1 gene. *Mol Microbiol* 26 (1):91-98
- Ambroziak J, Henry SA (1994) INO2 and INO4 gene products, positive regulators of phospholipid biosynthesis in *Saccharomyces cerevisiae*, form a complex that binds to the INO1 promoter. *J Biol Chem* 269 (21):15344-15349
- Arndt KM, Ricupero-Hovasse S, Winston F (1995) TBP mutants defective in activated transcription *in vivo*. *EMBO J* 14 (7):1490-1497
- Ashburner M, Ball CA, Blake JA, Botstein D, Butler H, Cherry JM, Davis AP, Dolinski K, Dwight SS, Eppig JT, Harris MA, Hill DP, Issel-Tarver L, Kasarskis A, Lewis S, Matese JC, Richardson JE, Ringwald M, Rubin GM, Sherlock G (2000) Gene ontology: tool for the unification of biology. *The Gene Ontology Consortium*. *Nat Genet* 25 (1):25-29. doi:10.1038/75556
- Bailis AM, Poole MA, Carman GM, Henry SA (1987) The Membrane-Associated Enzyme Phosphatidylserine Synthase Is Regulated at the Level of Messenger-Rna Abundance. *Mol Cell Biol* 7 (1):167-176
- Balciunas D, Ronne H (1999) Yeast genes GIS1-4: multicopy suppressors of the Gal-phenotype of snf1 mig1 srb8/10/11 cells. *Mol Gen Genet* 262 (4-5):589-599
- Bligh EG, Dyer WJ (1959) A Rapid Method of Total Lipid Extraction and Purification. *Can J Biochem Physiol* 37 (8):911-917
- Braun S, Matuschewski K, Rape M, Thoms S, Jentsch S (2002) Role of the ubiquitin-selective CDC48(UFD1/NPL4)chaperone (segregase) in ERAD of OLE1 and other substrates. *EMBO J* 21 (4):615-621
- Canelas AB, Harrison N, Fazio A, Zhang J, Pitkanen JP, van den Brink J, Bakker BM, Bogner L, Bouwman J, Castrillo JI, Cankorur A, Chumnanpuen P, Daran-Lapujade P, Dikicioglu D, van Eunen K, Ewald JC, Heijnen JJ, Kirdar B, Mattila I, Mensonides FI, Niebel A, Penttila M, Pronk JT, Reuss M, Salusjarvi L, Sauer U, Sherman D, Siemann-Herzberg M, Westerhoff H, de Winde J, Petranovic D, Oliver SG, Workman CT, Zamboni N, Nielsen J (2010) Integrated multilaboratory systems biology reveals differences in protein metabolism between two reference yeast strains. *Nat Commun* 1:145. doi:10.1038/ncomms1150
- Celenza JL, Carlson M (1984) Cloning and genetic mapping of SNF1, a gene required for expression of glucose-repressible genes in *Saccharomyces cerevisiae*. *Mol Cell Biol* 4 (1):49-53
- Donahue TF, Henry SA (1981) myo-Inositol-1-phosphate synthase. Characteristics of the enzyme and identification of its structural gene in yeast. *J Biol Chem* 256 (13):7077-7085
- Gancedo JM (1998) Yeast carbon catabolite repression. *Microbiol Mol Biol Rev* 62 (2):334-361

- Gaspar ML, Aregullin MA, Jesch SA, Henry SA (2006) Inositol induces a profound alteration in the pattern and rate of synthesis and turnover of membrane lipids in *Saccharomyces cerevisiae*. *J Biol Chem* 281 (32):22773-22785. doi:10.1074/jbc.M603548200
- Gavin AC, Bosche M, Krause R, Grandi P, Marzioch M, Bauer A, Schultz J, Rick JM, Michon AM, Cruciat CM, Remor M, Hofert C, Schelder M, Brajenovic M, Ruffner H, Merino A, Klein K, Hudak M, Dickson D, Rudi T, Gnau V, Bauch A, Bastuck S, Huhse B, Leutwein C, Heurtier MA, Copley RR, Edelmann A, Querfurth E, Rybin V, Drewes G, Raida M, Bouwmeester T, Bork P, Seraphin B, Kuster B, Neubauer G, Superti-Furga G (2002) Functional organization of the yeast proteome by systematic analysis of protein complexes. *Nature* 415 (6868):141-147
- Graves JA, Henry SA (2000) Regulation of the yeast INO1 gene. The products of the INO2, INO4 and OPI1 regulatory genes are not required for repression in response to inositol. *Genetics* 154 (4):1485-1495
- Greenberg ML, Goldwasser P, Henry SA (1982) Characterization of a yeast regulatory mutant constitutive for synthesis of inositol-1-phosphate synthase. *Mol Gen Genet* 186 (2):157-163
- Henry SA, Patton-Vogt JL (1998) Genetic regulation of phospholipid metabolism: yeast as a model eukaryote. *Prog Nucleic Acid Res Mol Biol* 61:133-179
- Hiltunen JK, Mursula AM, Rottensteiner H, Wierenga RK, Kastaniotis AJ, Gurvitz A (2003) The biochemistry of peroxisomal beta-oxidation in the yeast *Saccharomyces cerevisiae*. *FEMS Microbiol Rev* 27 (1):35-64
- Hong SP, Carlson M (2007) Regulation of snf1 protein kinase in response to environmental stress. *J Biol Chem* 282 (23):16838-16845. doi:10.1074/jbc.M700146200
- Jackson JC, Lopes JM (1996) The yeast UME6 gene is required for both negative and positive transcriptional regulation of phospholipid biosynthetic gene expression. *Nucleic Acids Research* 24 (7):1322-1329
- Jesch SA, Zhao X, Wells MT, Henry SA (2005) Genome-wide analysis reveals inositol, not choline, as the major effector of Ino2p-Ino4p and unfolded protein response target gene expression in yeast. *J Biol Chem* 280 (10):9106-9118. doi:10.1074/jbc.M411770200
- Kelley MJ, Bailis AM, Henry SA, Carman GM (1988) Regulation of phospholipid biosynthesis in *Saccharomyces cerevisiae* by inositol. Inositol is an inhibitor of phosphatidylserine synthase activity. *J Biol Chem* 263 (34):18078-18085
- Khoomrung S, Chumnanpuen P, Jansa-ard S, Nookaei I, Nielsen J (2012) Fast and accurate preparation fatty acid methyl esters by microwave-assisted derivatization in yeast *Saccharomyces cerevisiae*. Submitted to *Applied Microbiology and Biotechnology*
- Klig LS, Homann MJ, Carman GM, Henry SA (1985) Coordinate Regulation of Phospholipid Biosynthesis in *Saccharomyces-Cerevisiae* - Pleiotropically Constitutive Opi1 Mutant. *J Bacteriol* 162 (3):1135-1141
- Kuchin S, Treich I, Carlson M (2000) A regulatory shortcut between the Snf1 protein kinase and RNA polymerase II holoenzyme. *Proc Natl Acad Sci U S A* 97 (14):7916-7920. doi:10.1073/pnas.140109897
- Kuchin S, Vyas VK, Carlson M (2002) Snf1 protein kinase and the repressors Nrg1 and Nrg2 regulate FLO11, haploid invasive growth, and diploid pseudohyphal differentiation. *Mol Cell Biol* 22 (12):3994-4000
- Kumme J, Dietz M, Wagner C, Schuller HJ (2008) Dimerization of yeast transcription factors Ino2 and Ino4 is regulated by precursors of phospholipid biosynthesis mediated by Opi1 repressor. *Curr Genet* 54 (1):35-45. doi:10.1007/s00294-008-0197-7
- Leber R, Zinser E, Zellnig G, Paltauf F, Daum G (1994) Characterization of lipid particles of the yeast, *Saccharomyces cerevisiae*.

- Yeast 10 (11):1421-1428.
doi:10.1002/yea.320101105
- Lin SS, Manchester JK, Gordon JI (2003) Sip2, an N-myristoylated beta subunit of Snf1 kinase, regulates aging in *Saccharomyces cerevisiae* by affecting cellular histone kinase activity, recombination at rDNA loci, and silencing. *J Biol Chem* 278 (15):13390-13397.
doi:10.1074/jbc.M212818200
- Liu Y, Xu X, Kuo M-H (2010) Snf1p Regulates Gcn5p Transcriptional Activity by Antagonizing Spt3p. *Genetics* 184 (1):91-105. doi:10.1534/genetics.109.110957
- Lo WS, Duggan L, Emre NC, Belotserkovskya R, Lane WS, Shiekhattar R, Berger SL (2001) Snf1--a histone kinase that works in concert with the histone acetyltransferase Gcn5 to regulate transcription. *Science* 293 (5532):1142-1146. doi:10.1126/science.1062322
- Lo WS, Gamache ER, Henry KW, Yang D, Pillus L, Berger SL (2005) Histone H3 phosphorylation can promote TBP recruitment through distinct promoter-specific mechanisms. *EMBO J* 24 (5):997-1008. doi:10.1038/sj.emboj.7600577
- Loewen CJ, Gaspar ML, Jesch SA, Delon C, Ktistakis NT, Henry SA, Levine TP (2004) Phospholipid metabolism regulated by a transcription factor sensing phosphatidic acid. *Science* 304 (5677):1644-1647. doi:10.1126/science.1096083
- Loewen CJ, Roy A, Levine TP (2003) A conserved ER targeting motif in three families of lipid binding proteins and in Opi1p binds VAP. *EMBO J* 22 (9):2025-2035. doi:10.1093/emboj/cdg201
- Lopes JM, Henry SA (1991) Interaction of trans and cis regulatory elements in the INO1 promoter of *Saccharomyces cerevisiae*. *Nucleic Acids Res* 19 (14):3987-3994
- Mullner H, Daum G (2004) Dynamics of neutral lipid storage in yeast. *Acta Biochim Pol* 51 (2):323-347. doi:035001323
- Nath N, McCartney RR, Schmidt MC (2003) Yeast Pak1 kinase associates with and activates Snf1. *Mol Cell Biol* 23 (11):3909-3917
- Nielsen J (2009) Systems biology of lipid metabolism: from yeast to human. *FEBS Lett* 583 (24):3905-3913. doi:10.1016/j.febslet.2009.10.054
- Nookae I, Jewett MC, Meechai A, Thammarongtham C, Laoteng K, Cheevadhanarak S, Nielsen J, Bhumiratana S (2008) The genome-scale metabolic model iIN800 of *Saccharomyces cerevisiae* and its validation: a scaffold to query lipid metabolism. *BMC Syst Biol* 2:71. doi:10.1186/1752-0509-2-71
- Oliveira AP, Patil KR, Nielsen J (2008) Architecture of transcriptional regulatory circuits is knitted over the topology of bio-molecular interaction networks. *BMC Syst Biol* 2:17. doi:10.1186/1752-0509-2-17
- Patil KR, Nielsen J (2005) Uncovering transcriptional regulation of metabolism by using metabolic network topology. *Proc Natl Acad Sci U S A* 102 (8):2685-2689. doi:0406811102 [pii]
- 10.1073/pnas.0406811102**
- Portillo F, Mulet JM, Serrano R (2005) A role for the non-phosphorylated form of yeast Snf1: tolerance to toxic cations and activation of potassium transport. *FEBS Lett* 579 (2):512-516. doi:10.1016/j.febslet.2004.12.019
- Ratnakumar S, Young ET (2010) Snf1 dependence of peroxisomal gene expression is mediated by Adr1. *J Biol Chem* 285 (14):10703-10714. doi:10.1074/jbc.M109.079848
- Santiago TC, Mamoun CB (2003) Genome expression analysis in yeast reveals novel transcriptional regulation by inositol and choline and new regulatory functions for Opi1p, Ino2p, and Ino4p. *J Biol Chem* 278 (40):38723-38730. doi:10.1074/jbc.M303008200
- Sanz P (2003) Snf1 protein kinase: a key player in the response to cellular stress in yeast. *Biochem Soc Trans* 31 (Pt 1):178-181. doi:10.1042/
- Sattur AP, Karanth NG (1989a) Production of microbial lipids: II. Influence of C/N ratio-model prediction. *Biotechnol Bioeng* 34 (6):868-871. doi:10.1002/bit.260340617
- Sattur AP, Karanth NG (1989b) Production of microbial lipids: III. Influence of C/N

- ratio--experimental observations. *Biotechnol Bioeng* 34 (6):872-874. doi:10.1002/bit.260340618
- Schaffner G, Matile P (1981) Structure and Composition of Bakers-Yeast Lipid Globules. *Biochemie Und Physiologie Der Pflanzen* 176 (7):659-666
- Schwank S, Ebbert R, Rautenstrauss K, Schweizer E, Schuller HJ (1995) Yeast transcriptional activator INO2 interacts as an Ino2p/Ino4p basic helix-loop-helix heteromeric complex with the inositol/choline-responsive element necessary for expression of phospholipid biosynthetic genes in *Saccharomyces cerevisiae*. *Nucleic Acids Res* 23 (2):230-237
- Shirra MK, McCartney RR, Zhang C, Shokat KM, Schmidt MC, Arndt KM (2008) A chemical genomics study identifies Snf1 as a repressor of GCN4 translation. *J Biol Chem* 283 (51):35889-35898. doi:10.1074/jbc.M805325200
- Shirra MK, Patton-Vogt J, Ulrich A, Liuta-Tehlivets O, Kohlwein SD, Henry SA, Arndt KM (2001) Inhibition of acetyl coenzyme A carboxylase activity restores expression of the INO1 gene in a snf1 mutant strain of *Saccharomyces cerevisiae*. *Mol Cell Biol* 21 (17):5710-5722
- Silversand C, Haux C (1997) Improved high-performance liquid chromatographic method for the separation and quantification of lipid classes: application to fish lipids. *J Chromatogr B Biomed Sci Appl* 703 (1-2):7-14
- Soontorngun N, Laroche M, Drouin S, Robert F, Turcotte B (2007) Regulation of gluconeogenesis in *Saccharomyces cerevisiae* is mediated by activator and repressor functions of Rds2. *Mol Cell Biol* 27 (22):7895-7905. doi:10.1128/MCB.01055-07
- Stark C, Breitkreutz BJ, Chatr-Aryamontri A, Boucher L, Oughtred R, Livstone MS, Nixon J, Van Auken K, Wang X, Shi X, Reguly T, Rust JM, Winter A, Dolinski K, Tyers M (2011) The BioGRID Interaction Database: 2011 update. *Nucleic Acids Res* 39 (Database issue):D698-704. doi:10.1093/nar/gkq1116
- Sutherland CM, Hawley SA, McCartney RR, Leech A, Stark MJ (2003) Elm1p is one of three upstream kinases for the *Saccharomyces cerevisiae* SNF1 complex. *Curr Biol* 13:1299
- Tehlivets O, Scheuringer K, Kohlwein SD (2007) Fatty acid synthesis and elongation in yeast. *Biochim Biophys Acta* 1771 (3):255-270. doi:10.1016/j.bbaply.2006.07.004
- Thomas M, Polge C (2007) SNF1/AMPK/SnRK1 kinases, global regulators at the heart of energy control? *Trends Plant Sci* 12 (1):20-28. doi:10.1016/j.tplants.2006.11.005
- Usaite R, Jewett MC, Oliveira AP, Yates JR, 3rd, Olsson L, Nielsen J (2009) Reconstruction of the yeast Snf1 kinase regulatory network reveals its role as a global energy regulator. *Mol Syst Biol* 5:319. doi:10.1038/msb.2009.67
- van Dijken JP, Bauer J, Brambilla L, Duboc P, Francois JM, Gancedo C, Giuseppin MLF, Heijnen JJ, Hoare M, Lange HC, Madden EA, Niederberger P, Nielsen J, Parrou JL, Petit T, Porro D, Reuss M, van Riel N, Rizzi M, Steensma HY, Verrips CT, Vindelov J, Pronk JT (2000) An interlaboratory comparison of physiological and genetic properties of four *Saccharomyces cerevisiae* strains. *Enzyme Microb Tech* 26 (9-10):706-714
- Verduyn C, Postma E, Scheffers WA, Vandijken JP (1992) Effect of Benzoic-Acid on Metabolic Fluxes in Yeasts - a Continuous-Culture Study on the Regulation of Respiration and Alcoholic Fermentation. *Yeast* 8 (7):501-517
- White MJ, Hirsch JP, Henry SA (1991) The OPI1 gene of *Saccharomyces cerevisiae*, a negative regulator of phospholipid biosynthesis, encodes a protein containing polyglutamine tracts and a leucine zipper. *J Biol Chem* 266 (2):863-872
- Woods A, Munday MR, Scott J, Yang X, Carlson M, Carling D (1994) Yeast SNF1 is functionally related to mammalian AMP-activated protein kinase and regulates acetyl-CoA carboxylase in vivo. *J Biol Chem* 269 (30):19509-19515

- Ye T, Elbing K, Hohmann S (2008) The pathway by which the yeast protein kinase Snf1p controls acquisition of sodium tolerance is different from that mediating glucose regulation. *Microbiol-Sgm* 154:2814-2826. doi:DOI 10.1099/mic.0.2008/020149-0
- Zaldivar J, Borges A, Johansson B, Smits HP, Villas-Boas SG, Nielsen J, Olsson L (2002) Fermentation performance and intracellular metabolite patterns in laboratory and industrial xylose-fermenting *Saccharomyces cerevisiae*. *Appl Microbiol Biotechnol* 59 (4-5):436-442. doi:10.1007/s00253-002-1056-y
- Zhang J, Olsson L, Nielsen J (2010) The beta-subunits of the Snf1 kinase in *Saccharomyces cerevisiae*, Gal83 and Sip2, but not Sip1, are redundant in glucose derepression and regulation of sterol biosynthesis. *Mol Microbiol* 77 (2):371-383. doi:10.1111/j.1365-2958.2010.07209.x
- Zhang J, Vaga S, Chumnanpuen P, Kumar R, Vemuri GN, Aebersold R, Nielsen J (2011) Mapping the interaction of Snf1 with TORC1 in *Saccharomyces cerevisiae*. *Mol Syst Biol* 7. doi:http://www.nature.com/msb/journal/v7/n1/supplinfo/msb201180_S1.html
- Zhang S, Skalsky Y, Garfinkel DJ (1999) MGA2 or SPT23 is required for transcription of the delta9 fatty acid desaturase gene, OLE1, and nuclear membrane integrity in *Saccharomyces cerevisiae*. *Genetics* 151 (2):473-483

Supplementary Information to

Integrated analysis of the transcriptome-lipid profiling reveals the co-influences of inositol-choline and Snf1 in controlling lipid biosynthesis in yeast

Pramote Chumnanpuen, Jie Zhang, Intawat Nookaew, and Jens Nielsen*

Department of Chemical and Biological Engineering,
Chalmers University of Technology,
Kemivägen 10, SE-412 96 Gothenburg, Sweden

*Corresponding Author:

Jens Nielsen

Email: nielsenj@chalmers.se

Tel: +46 31 772 38 04

Figure S1. Abundance of fatty acids from the total lipid including neutral and phospholipids for all conditions in units of mg/gDW biomass. The abundance is based on the sum of Fas in the free as well as ester form. The error bar represent the SD from triplicate. (A) C14:0 – myristic acid; (B) C16:0 – palmitic acid; (C) C16:1 – palmitoleic acid; (D) C18:0 – stearic acid; (E) C18:1 – oleic acid; (F) C20:0 – arachidic acid; (G) C20:1 – eicosenoic acid.

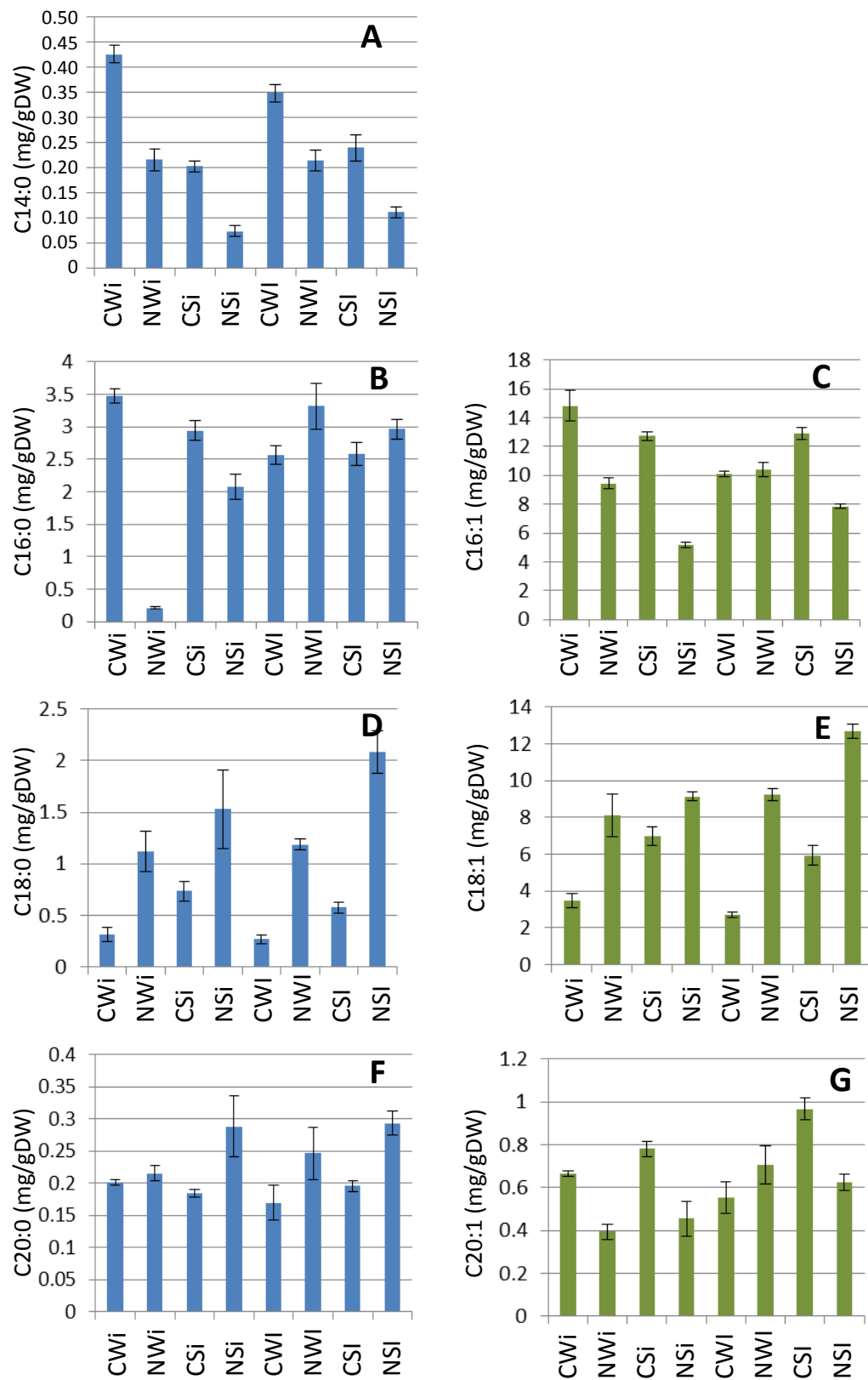


Figure S2. Abundance of different lipid species in units of %content w/w of total lipids

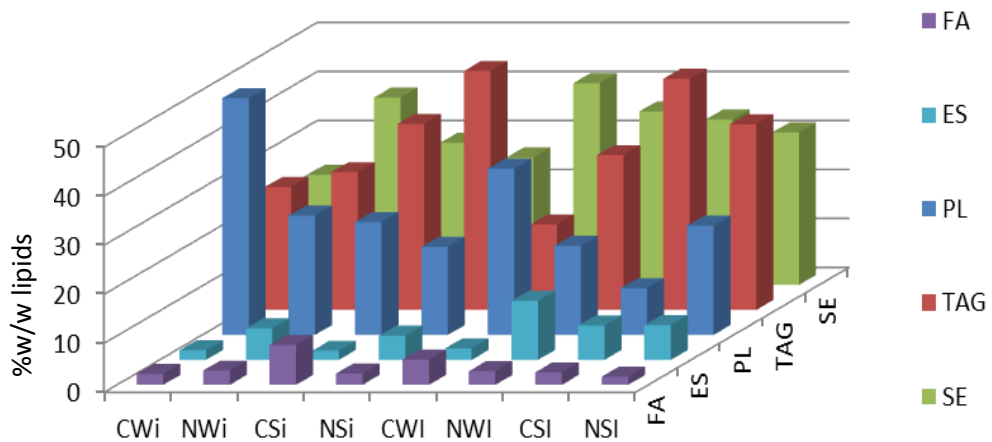


Figure S3. Abundance of different lipid species in units of mmol/gDW of phospholipids

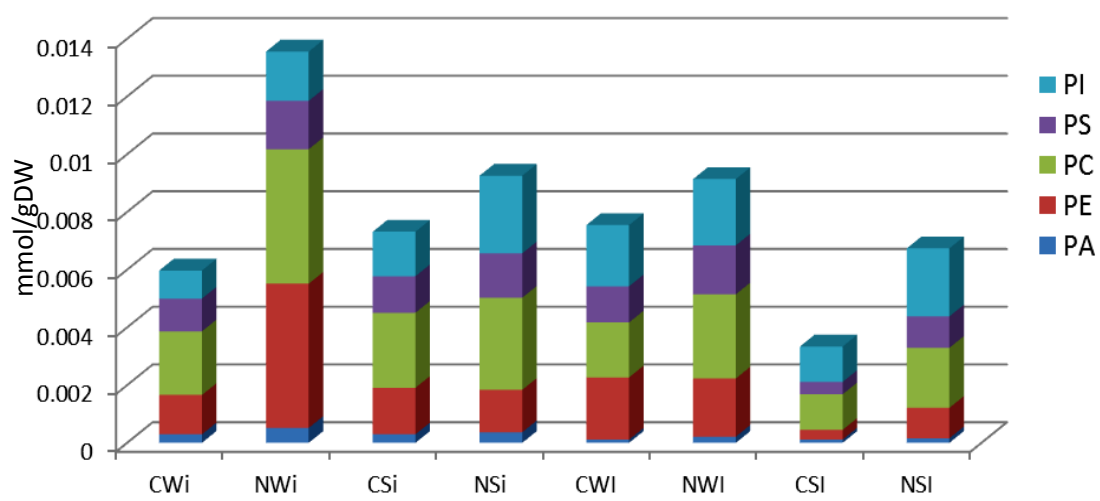


Figure S4. A heat map of reporter Metabolites of each factor comparison showing in range of 0-4 of log(p-value).

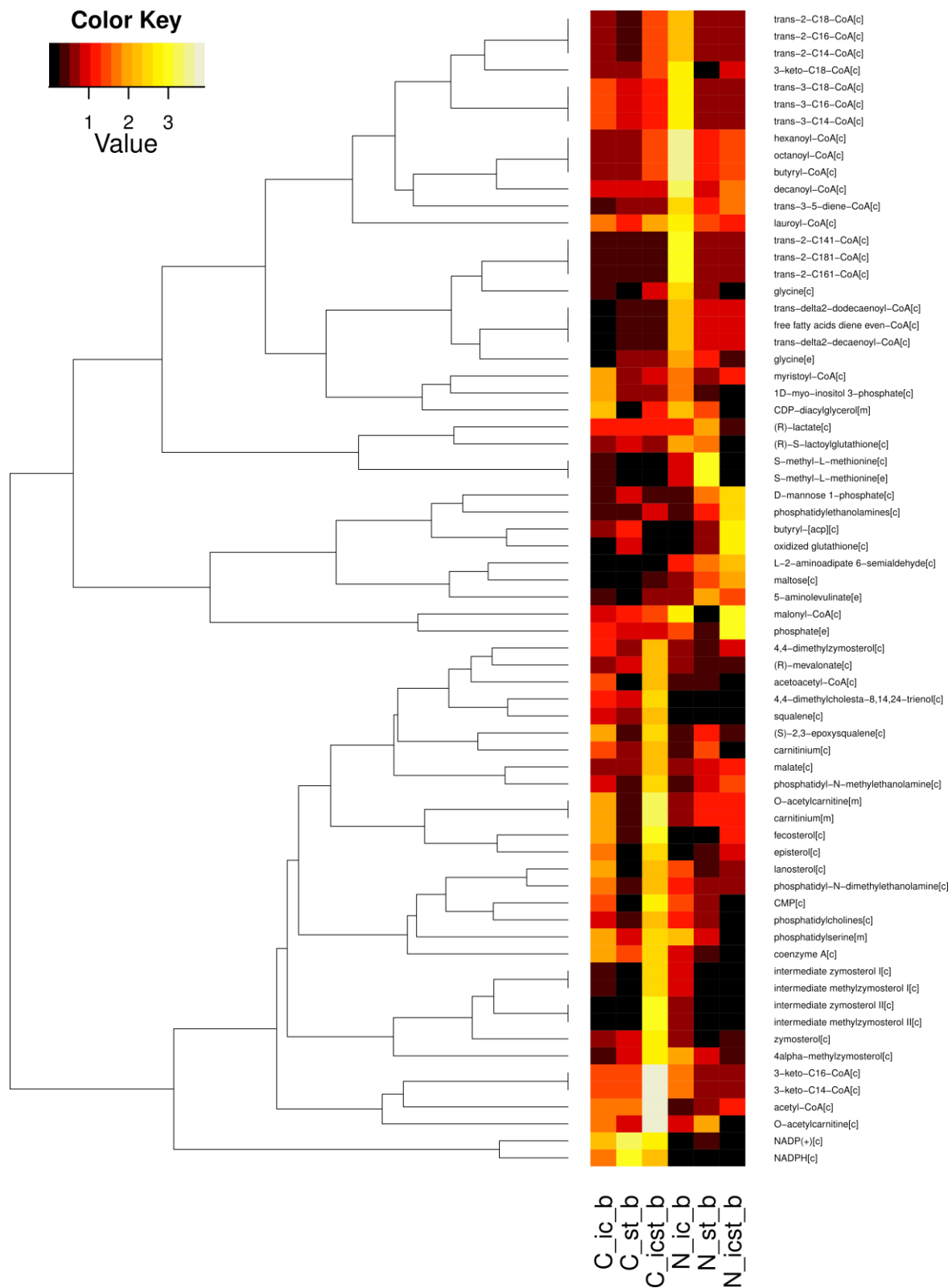


Figure S5. A heat map of reporter TF of each factor comparison showing in range of 0-20 of log(p-value).

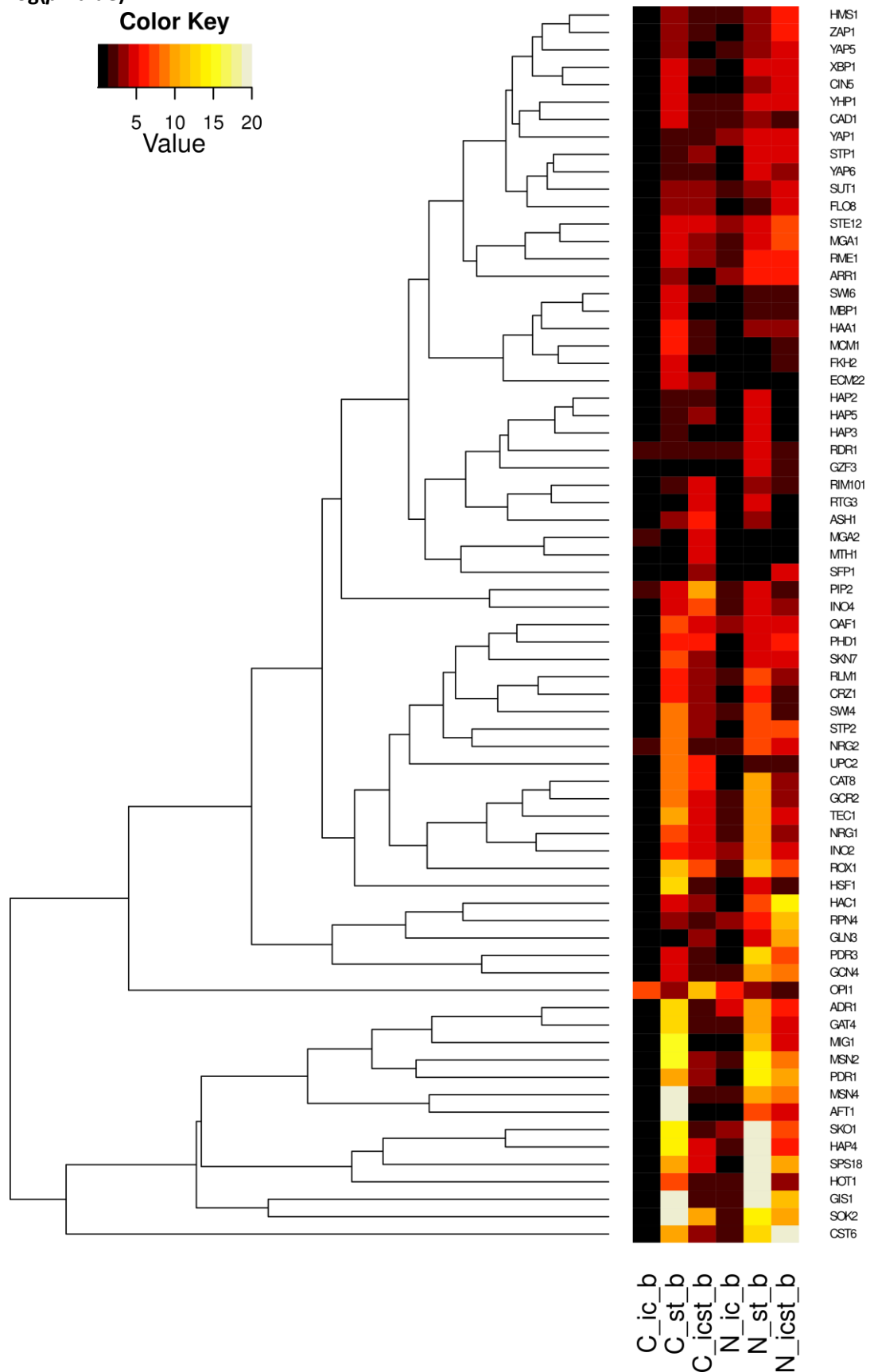


Figure S6. The chromatographic separation of all lipid classes with optimized condition, separated on a HILIC column (Luna 5 μ m 200Å 100 x 3.0 mm. 0.8 mL/min solvent flow rate at 35°C) with triple gradient mobile phase. Cholesterol (CH) was used as an internal standard and the recovery was above 95%.

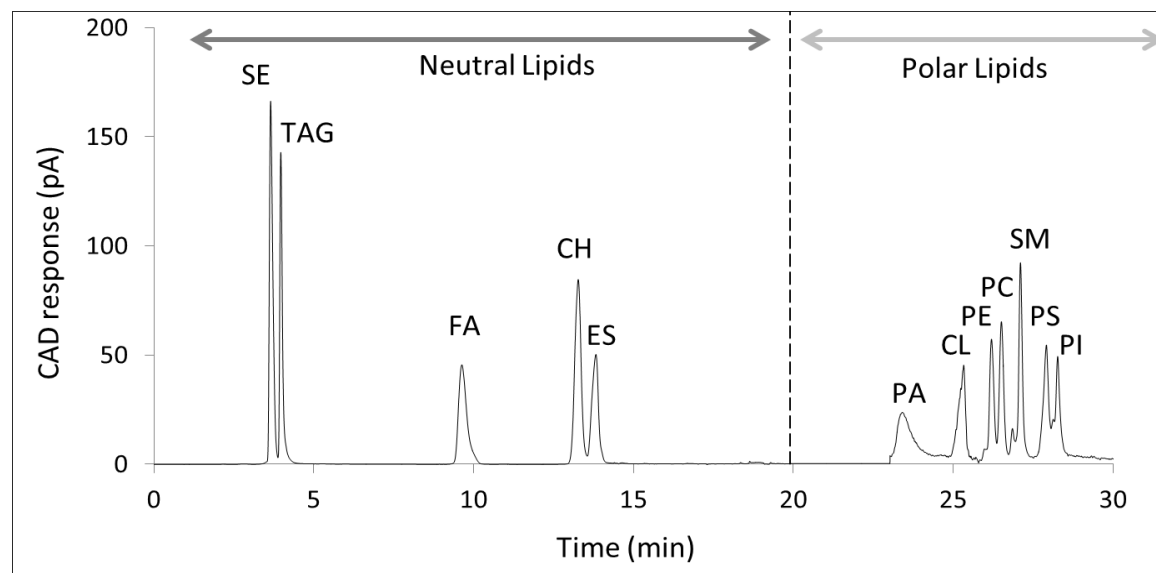


Figure S7. Identification of unknown FAME from yeast sample using GC-MS based on the retention time of the known standards. 17:0 FA was used as an internal standard and the recovery was above 95%.

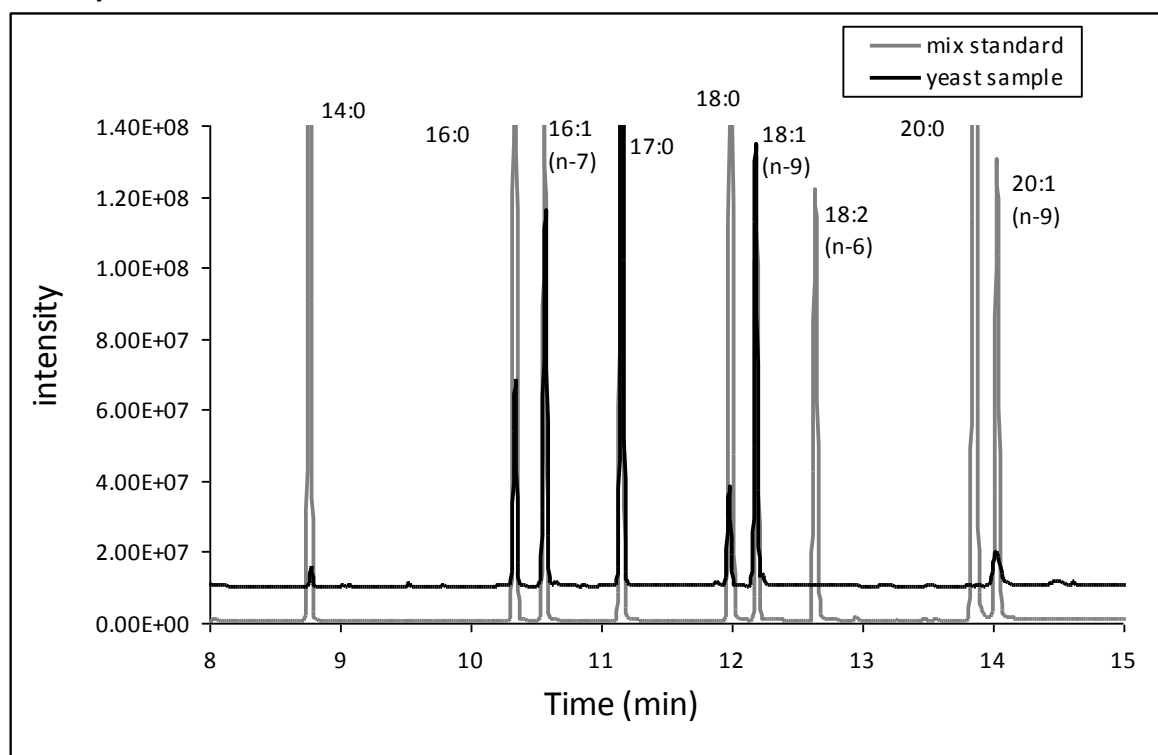


Figure S8. Abundance of fatty acids from the total lipid including neutral and phospholipids for all conditions. The abundance is based on the sum of Fas in the free as well as bound fatty acid.

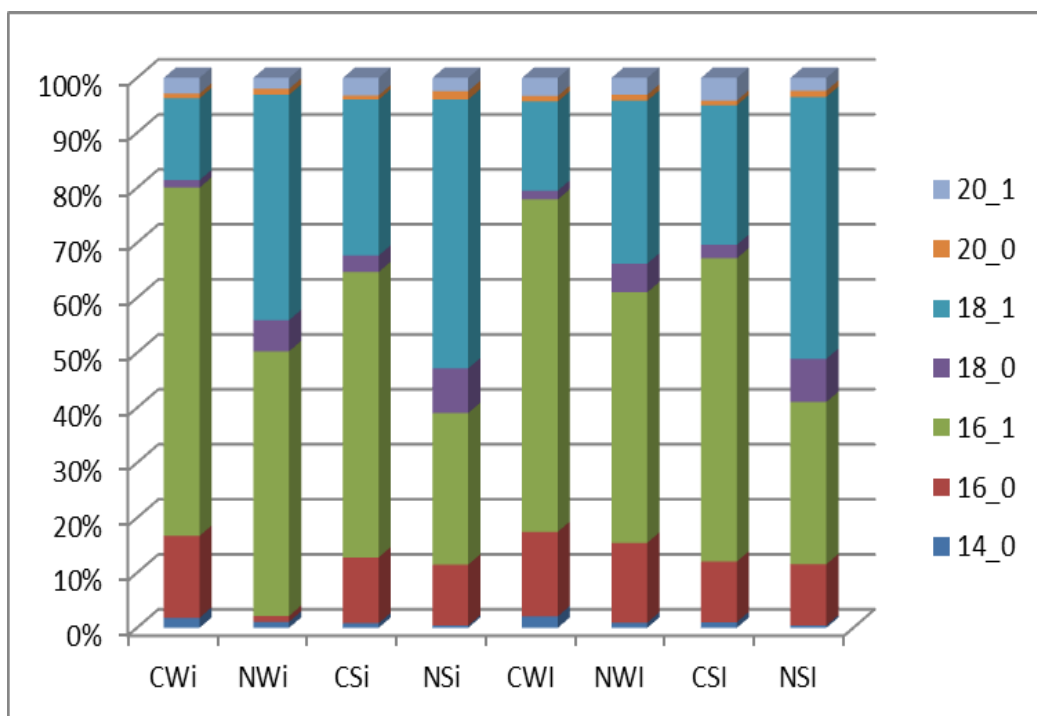


Table S1. Average molecular weight for phospholipid amount calculation.

Phospholipids	Avg MW (g/mol)
PA	691.53±39.62
PE	712.61±40.83
PC	754.70±43.22
PS	778.61±44.59
PI	848.72±48.58

Table S2. The level of different phospholipid species in units of %content (w/w phospholipids)

conditions	PA	PE	PC	PS	PI
CWi	4.364±0.293	21.528±0.286	36.838±0.256	19.028±0.449	18.243±0.410
NWi	3.424±0.445	35.126±0.413	34.687±0.639	12.527±0.421	14.236±0.181
CSi	3.543±0.939	20.618±0.890	35.217±0.656	17.225±0.072	23.397±0.366
NSi	3.436±0.108	14.677±0.483	33.719±0.180	16.310±2.367	31.859±0.110
CWI	1.265±0.260	26.561±0.323	24.823±0.599	16.361±1.210	30.989±0.139
NWI	2.022±0.668	20.529±0.631	31.396±0.593	18.302±0.476	27.751±0.177
CSI	2.937±0.747	9.137±0.472	35.656±1.242	12.487±0.631	39.783±0.120
NSI	2.011±0.500	14.316±0.468	29.924±0.489	15.729±0.432	38.019±1.864

Table S3. The distribution of FA content in PA in units of %content (w/w fatty acids)

Condition	14_0	16_0	16_1	18_0	18_1
CWi	6.17±0.16	26.32±0.16	17.14±0.12	19.1±0.12	31.27±0.07
NWi	2.82±0.42	27.75±0.24	9.81±0.20	39.99±0.16	19.63±0.17
CSI	3.47±0.12	31.40±0.11	11.64±0.10	32.86±0.06	20.64±0.05
NSi	14.35±0.09	25.44±0.08	8.75±0.08	29.16±0.04	22.30±0.04
CWI	4.54±0.04	24.14±0.04	25.88±0.02	27.60±0.02	17.84±0.02
NWI	3.82±0.11	34.88±0.08	9.30±0.08	30.32±0.06	21.68±0.04
CSI	4.24±0.02	34.36±0.02	9.28±0.02	37.89±0.01	14.22±0.01
NSI	5.44±0.05	35.74±0.02	10.64±0.02	31.14±0.02	17.05±0.02

Table S4. The distribution of FA content in PE in units of %content (w/w fatty acids)

Condition	14_0	16_0	16_1	18_0	18_1
CWi	2.85±0.10	31.17±0.09	11.2±0.09	20.9±0.08	33.88±0.04
NWi	2.67±0.49	25.93±0.45	12.33±0.44	30.07±0.19	29.00±0.21
CSI	2.68±0.06	27.87±0.06	17.48±0.04	27.18±0.04	24.80±0.02
NSi	7.02±0.21	28.30±0.19	11.17±0.18	23.95±0.16	29.56±0.08
CWI	6.68±0.21	25.27±0.21	21.94±0.16	23.23±0.14	22.88±0.09
NWI	4.57±0.35	35.35±0.34	8.55±0.32	27.48±0.31	24.05±0.14
CSI	3.48±0.03	23.33±0.03	17.24±0.02	39.29±0.01	16.66±0.01
NSI	4.80±0.17	30.42±0.17	14.36±0.17	28.29±0.17	22.13±0.07

Table S5. The distribution of FA content in PC in units of %content (w/w fatty acids)

Condition	14_0	16_0	16_1	18_0	18_1
CWi	2.86±0.18	32.94±0.09	14.34±0.09	24.25±0.09	25.61±0.07
NWi	3.48±0.52	28.42±0.46	15.29±0.46	10.50±0.45	42.30±0.21
CSI	1.55±0.28	23.1±0.28	28.45±0.17	21.44±0.16	25.48±0.12
NSi	3.68±0.17	20.16±0.18	25.38±0.17	24.42±0.15	26.36±0.07
CWI	2.67±0.11	20.04±0.11	44.75±0.06	12.19±0.05	20.35±0.05
NWI	3.16±0.46	37.12±0.43	15.72±0.42	21.81±0.42	22.19±0.19
CSI	4.88±0.36	25.74±0.35	23.27±0.23	26.92±0.2	19.19±0.15
NSI	2.97±0.40	18.74±0.40	20.82±0.38	21.48±0.38	35.99±0.17

Table S6. The distribution of FA content in PS in units of %content (w/w fatty acids)

Condition	14_0	16_0	16_1	18_0	18_1
CWi	2.24±0.06	32.79±0.06	11.74±0.06	25.81±0.05	27.41±0.02
NWi	4.70±0.17	24.58±0.16	14.24±0.15	21.54±0.13	34.94±0.07
CSi	5.23±0.00	35.48±0.10	14.84±0.00	27.65±0.02	16.80±0.01
NSi	12.31±0.65	34.55±0.60	9.00±0.56	23.1±0.40	21.03±0.26
CWI	2.63±0.17	21.79±0.16	40.88±0.07	19.74±0.07	14.97±0.07
NWI	3.60±0.23	36.48±0.23	9.22±0.22	34.90±0.18	15.80±0.09
CSI	3.87±0.08	26.79±0.07	25.63±0.03	27.85±0.03	15.85±0.03
NSI	10.16±0.09	26.6±0.09	9.44±0.09	23.04±0.09	30.77±0.04

Table S7. The distribution of FA content in PI in units of %content (w/w fatty acids)

Condition	14_0	16_0	16_1	18_0	18_1
CWi	3.43±0.52	30.4±0.49	7.99±0.49	28.33±0.47	29.85±0.21
NWi	5.37±0.21	26.94±0.22	16.38±0.18	23.90±0.18	27.41±0.09
CSi	3.73±0.21	33.42±0.19	5.69±0.18	36.70±0.08	20.46±0.09
NSi	3.43±0.25	27.91±0.21	6.57±0.20	33.94±0.17	28.15±0.09
CWI	3.38±0.13	29.07±0.12	8.88±0.12	35.26±0.12	23.40±0.05
NWI	5.99±0.03	28.94±0.02	10.27±0.02	31.29±0.02	23.50±0.02
CSI	5.43±0.02	36.96±0.21	13.22±0.01	28.24±0.01	16.16±0.02
NSI	3.50±0.53	27.62±0.53	12.13±0.52	26.59±0.52	30.17±0.22

Paper II

Integrated analysis, transcriptome-lipid profiling, reveals the effects of *INO2* and *INO4* level on lipid metabolism in yeast.

Chumnanpuen, P., I. Nookaew, J. Nielsen

Submitted for publication

Integrated analysis, transcriptome-lipidome, reveals the effects of *INO*-level (*INO2* and *INO4*) on lipid metabolism in yeast

Pramote Chumnanpuen, Intawat Nookaew, and Jens Nielsen*

Systems and Synthetic Biology,
Department of Chemical and Biological Engineering,
Chalmers University of Technology,
Kemivägen 10, SE-412 96 Gothenburg, Sweden

*Corresponding Author:
Jens Nielsen

Systems and Synthetic Biology, Department of Chemical and Biological Engineering,
Chalmers University of Technology, Kemivägen 10, SE-412 96 Gothenburg, Sweden.
Email: nielsenj@chalmers.se

Tel: +46 31 772 38 04

Abstract

Background: In the yeast *Saccharomyces cerevisiae*, genes containing UAS_{INO} sequences are regulated by the Ino2/Ino4 and Opi1 transcription factors, and this regulation controls lipid biosynthesis. The expression level of *INO2* and *INO4* genes (*INO*-level) at different nutrient limited conditions might lead to several responds in yeast lipid metabolism.

Results: In this study, we undertook a global study on how *INO*-levels (transcription level of *INO2* and *INO4*) affect lipid metabolism in yeast and we also studied the effects of single and double deletions of the two *INO*-genes (deficient effect). Using 2 types of nutrient limitations (carbon and nitrogen) in chemostat cultures operated at a fixed specific growth rate of 0.1 h⁻¹ and strains having different *INO*-level, we were able to see the effect on expression level of the genes involved in lipid biosynthesis and the fluxes towards the different lipid components. Through combined measurements of the transcriptome, metabolome, and lipidome it was possible to obtain a large dataset that could be used to identify how the *INO*-level controls lipid metabolism and also establish correlations between the different components.

Conclusion: Our analysis showed the strength of using a combination of transcriptome and lipidome analysis to illustrate the effect of *INO*-levels on phospholipid metabolism and based on our analysis we established a global regulatory map.

Key words: phospholipid synthesis, gene regulation, enzyme regulation, phosphatidic acid, yeast

Introduction

Phospholipid synthesis in the yeast *Saccharomyces cerevisiae* is a complex process that involves regulation by both genetic and biochemical mechanisms [1-3]. The activity levels of phospholipid synthesis enzymes are controlled by gene expression, e.g., transcription, and by other factors, i.e., lipids, water-soluble phospholipid precursors and products, and covalent modification by phosphorylation.

At the transcription level, the heterodimeric Ino2/Ino4 activator and the transcription factor Opi1 are global regulators affecting the expression of a large number of phospholipid biosynthetic genes [4-6]. Opi1, containing a leucine zipper motif, has been known as a negative regulator of phospholipid biosynthesis and it can also repress the transcription of *INO2* and *INO4* [7, 8]. In the absence of Opi1, the transcriptional level of both *INO2* and *INO4* (so called “**INO-level**”) will be up-regulated compared to the reference strain. Ino2p and Ino4p binds to so-called inositol-choline response elements (ICRE), and ICRE-bound Ino2p can interact with coactivator complexes such as Snf1 kinase that has histone kinase function, the SAGA complex, and the TFIIB complex when *OPII* is disrupted or not presented in the nucleus [9, 10]. Opi1 is also necessary for repression of ICRE-dependent transcription when inositol-choline is present in excess [8, 11]. Under this condition, Opi1 is localized in the nucleus [12] and prevent Ino2 from activation of target genes by recruiting the pleiotropic co-repressors such as the Cyc8/Tup1 complex[13, 14] or Sin3p[15-19]. Consequently, Ino2 variants those are defective in interacting with Opi1 leads to the repression of phospholipid synthetic genes [20]. However, a genome wide transcription analysis of the effect of varying *INO*-levels that effect lipid metabolism has never been studied before.

It is known that the transcription of the phospholipid biosynthetic genes is maximally repressed in the presence of the phospholipid precursors inositol and choline (IC) [4, 21, 22]. A highly conserved 10bp-element (5'-CATGTGAAAT-3’), in at least one copy is found in the promoters of the lipid co-regulated genes such as *INO1*, *CHO1*, *CHO2*, *OPI3*, *FAS1*, *FAS2*, *ACS2*, and *ACCI* [23-28]. This element has been shown to be both necessary and sufficient for the IC response, the so called “inositol/choline-responsive element” or “inositol-sensitive upstream activating sequence” (ICRE or UAS_{INO} motifs)[23, 24, 29]. These motifs are bound by a heterodimer of positive regulators Ino2p and Ino4p containing a basic helix-loop-helix (bHLH) structural motif [21, 30-32] which are necessary and sufficient for dimer formation and specific interaction with the UAS_{INO} motif [10, 32, 33]. Recent studies have shown that expression of several genes, probably unrelated to phospholipid metabolism, is also affected by Ino2p and Ino4p [22, 29, 34]. Importantly, over-expression of *INO2* (but not of *INO4*) counteracts IC repression, suggesting Ino2p as a possible target of the signal transduction pathway triggering IC repression [35, 36]

At the biochemical mechanism level, the level of phosphatidic acid (PA) is controlled by the biochemical regulation of key phospholipid synthesis enzymes [12] and it plays a central role in the regulation of phospholipid synthesis gene expression) [1, 33, 37].

In this study, we undertook a global study of lipid metabolism in response to different *INO*-levels (*INO2* and *INO4*): (1) normal *INO*-level using wild-type (CEN.PK113-7D), (2) high *INO*-level using a *opi1Δ* strain, and (3) low (or rather absent) *INO*-level using a *ino2Δ ino4Δ* double deletion strain. Moreover, we also focus on the deficient factors as a sub story comparing the individual knockout strains (*ino2Δ* and *ino4Δ*) with the double deletion strain. Using a systems biology approach [38] a global

regulatory model for lipid metabolism could be established. With 2 types of nutrient limitations (carbon and nitrogen) and different *INO*-level, we were able to see the effect on expression level of the genes involved in lipid biosynthesis and the fluxes towards the different lipid components. Through combined measurements of the transcriptome, metabolome, and lipidome it was possible to obtain a large dataset that could be useful to identify the effect of *INO*-level and also establish correlations between the different components.

Materials and Methods

1. Materials

All chemicals were reagent grade. Phospholipids, fatty acid methyl ester and neutral lipids standards were purchased from Sigma.

2. Agar spot test on SD media with different inositol concentrations.

The reference strain CEN.PK 113-7D and 5 mutants as shown in table 1 were grown on SD agar plate (containing Yeast Nitrogen Base without amino acids and inositol, Formedium LTD, England) for 48 hours. The SD agar plates were supplemented with 0, 1.39, 75 or 220 μM of inositol.

3. Strains, cultivation, and fermentation profile.

The *S. cerevisiae* strains used in this study were a prototrophic strain CEN.PK 113-7D (*Mata Mal2-8c SUC2*) [39] and its derivative (*opi1 Δ , ino2 Δ , ino4 Δ , and ino2 Δ ino4 Δ*) supplied by Peter Kötter (Frankfurt, Germany). All strains in this study were prototrophic and with mating type a (Table 1). Steady-state aerobic chemostat cultures were grown at 30 °C in 1.2 L bioreactors (DASGIP, Germany) with working volume of 0.5 L using a dilution rate of 0.10 (± 0.005) h^{-1} . For the C-lim and N-limit cultures, the medium composition was the same as in a previous study [40, 41] which contained

75 μM of inositol and 1mM of choline [24, 42]. The pH was controlled at 5.00 \pm 0.05 with 2M KOH and dissolved oxygen was kept above 30%. Chemostat cultivation ensured that metabolic and regulatory changes observed were specific to the *INO*-level and also the disruptions of *INO2* and/or *INO4*, and not complicated by external effects resulting from different specific growth rates.

Samples were harvested from the cultivation media every second hour and immediately filtered through a 0.45 μm pore-size cellulose acetate filter (VWR) and stored at -20 °C until analysis. Biomass production was evaluated by measuring of optical density (OD_{600}) and dry cell weight. Glucose, glycerol, ethanol, and acetate concentrations were determined by HPLC analysis using an Aminex HPX-87H column (Biorad, Hercules,CA) [43].

4. Transcriptome analysis

4.1 Transcriptome data acquisition

Samples for RNA extraction were taken after 50 h (i.e. 5 retention times) of steady-state by rapidly taking 20 ml of culture and mixing with 30 ml of crushed ice in a 50 ml Falcon tube to cool down the samples immediately. The cells were harvested by centrifuging at 4000 rpm and 2°C for 3 min, and then frozen in liquid nitrogen and stored at -80°C until subsequent RNA extraction. The cells were mechanically disrupted using FastPrep homogenizer (MP Biomedicals) and total RNA was isolated using the RNeasy Mini Kit (QIAGEN). The quality of total RNA was assessed using an Agilent 2100 Bioanalyzer (Agilent Technologies) with RNA 6000 Nano LabChip kit (Agilent Technologies). The labeled RNA was synthesized using the GeneChip 3' IVT Express Kit (Affymetrix), which was then hybridized onto the GeneChip Yeast Genome 2.0 Arrays (Affymetrix). Staining and washing of the hybridized arrays were carried out on the GeneChip® Fluidics

Station 450 (Affymetrix) and scanned using the GeneChip Scanner 300 7G (Affymetrix). All transcriptome data of this study can be found at Gene Expression Omnibus with accession number GSE36298.

***Available for reviewer on private page at:
<http://www.ncbi.nlm.nih.gov/geo/query/acc.cgi?token=hxqdbkcoeuskyfq&acc=GSE36298>

4.2 Transcriptome data analysis

The transcriptome data were analyzed using Bioconductor in R. Raw data were normalized and processed together with Probe Logarithmic Intensity Error (PLIER http://media.affymetrix.com/support/technical/technotes/plier_technote.pdf).

Pairwise T-test analysis was performed to determine the genes whose expression level is significantly changed due to *INO*-level, as well as the sufficiency factor. The calculated *P*-values were corrected for multiple testing by FDR method. A cut-off value of adjusted *P* value<0.01 was set to assess statistical significance.

5. Lipid data acquisition

5.1 Total lipid extraction

The lipid extraction method was adapted from Bligh and Dyer[44]. First, 15 mg of freeze-dried cell pellets were treated with 1 unit μl^{-1} of zymolyase digesting buffer (1.2 M glycerol, 100 mM sodium thioglycolate, 50 mM Tris-sulfate, pH 7.5) at 37°C for 15 min, followed by centrifugation at 3000 rpm for 3 min to collect the spheroplast, which was mixed with internal standards (heptadecanoic acid and glyceryl tri-heptadecanoate, 25 μg of each). After the addition of 7 ml of chloroform-methanol (2:1, v/v), the mixture was shaken horizontally at 300 rpm 4°C for 3 h, mixed with 1.7 ml of sodium chloride solution (0.73%) and centrifuged at 3000 rpm 4°C for 4 min for phase separation. The lower (organic)-phase was collected and the remaining was re-extracted with 5 ml of chloroform-methanol (85:15 v/v). The lower

(organic)-phase was collected and pooled with the previous organic fraction and kept at -20°C until further analysis.

5.2 Lipid class separation, identification, and quantification using HPLC-CAD

Lipid separation and quantification were performed using the method modified from Silversand and Haux [45]. Lipid separation was accomplished by HPLC (Dionex) equipped with charge aerosol detector; CAD (Corona) and the gas connected was nitrogen gas with 35 psi gas pressure. All the separated fractions were then collected by automated fraction collector; AFC-3000 (Dionex). A 20 μl volume of sample was injected in to the Luna 5 μm HILIC 200 Å 100 x 3.0 mm LC Column (Phenomenex). The flow-rate was 0.8 ml/min and the column temperature was kept at 25°C during all runs. The chromatogram was record at 10 Hz frequency and gain for 100 pA. The polar and neutral lipid classes were separated by three solvent mixtures and gradient systems as follow: (A) hexane-acetic acid (99:1, v/v); (B) acetone-isopropanol-acetic acid (29:70:1, v/v/v); (C) water-acetone-isopropanol-acetic acid (9:20:70:1, v/v/v/v). Triethylamine (0.08%, v/v) was added to the solvent C to adjust pH. The samples were injected at time 0 and the gradient profile started at 100% of Solvent A and the solvent B was gradually increased to 5% in 14 min and it was always kept at 5% along the process. At 15 min time point, solvent C was slowly entering to the system and rising up to 40 % in 5 min. Then solvent C was slowly increased until 45% in 20 min. Finally, the gradient was reduced from 5% to 0% of solvent B and from 45% to 0% of solvent C in 5 min and then maintained at 100% of solvent A for 5 min. In total, the solvent program for the separation of all lipid classes took 45 min.

5.3 Identification and quantification

Pure lipid standards were analyzed individually using chromatography to confirm their

retention times and purity. Lipid standards were also co-eluted together with samples to identify peaks in unknown samples. Solutions of known concentrations of different lipid classes were mixed and lipid standard curves were generated to study the linearity of the detection method and to quantify lipid classes in unknown samples. Calibration curves were prepared for 5-1000 µg ml⁻¹ of PA, PE, PC, PS, PI, ES, TAG, FA, and ES. Each concentration of the standard solutions was injected twice and the average log₁₀ peak area for each lipid was plotted against the absolute amount of lipid. Correlation (r^2) was determined for all curves by linear regression.

5.4 FAMEs analysis

We used standard procedure developed in our laboratory which is based on the previous protocol by Khoomrung *et al.* [46]. Briefly, 10 mg of freeze-dried samples was mixed with 4 mL of hexane, 2 mL of 14 % BF₃ (in Methanol) and 5 µg of internal standard (17:0 fatty acid standard was added. The sample was then flushed into the tube's head space with nitrogen gas for 30s and closed tightly with a Teflon screw cap. The tube was placed in a vessel containing 30 mL of milliQ water and then sealed with TFM screw cap. The tube was heated using microwave digestion system (milestone start D, Sorisole Bergamo, Italy) equipped with rotor PRO-24. The temperature programming of microwave digestion was ramped (from room temperature) to 120 °C within 6 min and maintained for 10 min. After cooling down sample at the room temperature, 2 mL of milliQ water was added and shaken vigorously for 1 min and centrifuged at 2500 rpm for 5 min. The upper phase (hexane phase which contained the FAMEs) was analysed by GC-MS.

The FAMEs were separated and quantified using Focus GC ISQ single quadrupole GC-MS (Thermo Fisher scientific, Germany). The separation of FAMEs was performed on Zebron (ZB-

WAX) GC column (30 m x 0.25 mm I.D., 0.25 µm film thickness) from Phenomenex, Macclesfield, UK. Sample was injected in splitless injection mode (1µL at 240 °C) and Helium was a carrier gas (1 mL/min). The column temperature was initially set at 50 °C (1.5 min), then temperature was ramped to 180 °C (25°C/min) for 1 min, then increased to 220 °C (10°C/min) and held for 1 min. Finally, temperature was increased to 250 °C (15°C/min) and held for 3.0 min. Mass transfer line and ion source were set at 250 °C and 200 °C, respectively. The FAMEs were detected with electron ionization (70 eV) in scan mode (50-650 m/z) and selected ion monitoring mode at m/z 55, 67, 74 and 79 (for quantitative analysis). The identification of unknown FAMEs was achieved by comparing their retention times and mass spectrum profiles with known standards (Sigma-Aldrich, USA). The quantification of FAMEs was performed using QuanBrowser function in Xcalibur software version 2.0 (Thermo Fisher Scientific). According to the serial dilution of FAME mix standards and were normalized according to the internal standard fatty acid C17:0. The average molecular weights of each PL (Table.S1) were used for mg/gDW and mmol/gDW units conversion (were later used for metabolic fluxes analysis).

6. Integrated analysis

The statistical adjusted P-values of each hypothesis testing were overlaid on the three networks graph of Gene Ontology, Transcription factor-gene interaction and genome-scale metabolic model iIN800 [47] (metabolite-gene interaction). Then reporter algorithm [48] was performed to obtain significant values (reporter p-value) of GO terms, Transcription factors (TF) and metabolites. All the features presented in heatmaps are those features that have reporter P-value < 0.001 and P-value < 0.01 were considered for INO-level and deficient factors, respectively.

Table 1 List of strains used in this study and their genotypes.

Strain	Genotype	Remark
CEN.PK113-7D	MATa URA3 HIS3 LEU2 TRP1 SUC2	Reference
CEN.PK1029-1A	MATa URA3 HIS3 LEU2 TRP1 SUC2 <i>opi1Δ::loxP-Kan-loxP</i>	<i>opi1Δ</i> (high <i>INO</i>)
CEN.PK1033-9A	MATa URA3 HIS3 LEU2 TRP1 SUC2 <i>ino2Δ::loxP-Kan-loxP</i> <i>ino4Δ::loxP-Kan-loxP</i>	<i>ino2Δino4Δ</i> (low <i>INO</i>)
CEN.PK1027-1B	MATa URA3 HIS3 LEU2 TRP1 SUC2 <i>ino2Δ::loxP-Kan-loxP</i>	<i>ino2Δ</i>
CEN.PK1028-2A	MATa URA3 HIS3 LEU2 TRP1 SUC2 <i>ino4Δ::loxP-Kan-loxP</i>	<i>ino4Δ</i>

Results and Discussions

Inositol is essential in the low *INO*-level yeast

To estimate the required inositol concentration for low *INO*-level (either *ino2Δ*, or *ino4Δ*, or double deletion of them), a spot test with the 5 yeast strains on different concentrations of inositol were performed (Fig.1A). Since the Ino2-Ino4 heterodimer regulates positively the expression of *INO1* (a structural gene for inositol-1-phosphate synthase which is required for inositol synthesis) and other phospholipid genes containing UAS_{INO} element [31, 49], deletion of *INO2* and *INO4* results in a requirement for supplementation of myo-inositol. However, myo-inositol is included in our minimal medium in a concentration of 250 µg/L (corresponding to about 1.39 µM) [41]. The spot test showed that *opi1Δ* as well as reference strain are prototroph for inositol but at least 75 µM of inositol is sufficient for low *INO*-level strains (either single or double deletion of *INO2* and *INO4*) to grow. However, higher concentrations of inositol (even 200 µM) did not make much difference in term of growth. Based on this we conclude that the low *INO*-level strains are auxotroph for inositol, and this leads us to an experimental design using 75 µM of inositol in the medium for all the chemostat cultures.

Cell physiology and carbon metabolism

To see the effects on cell growth of each mutant strain, 5 strains (the reference, *opi1Δ*, *ino2Δino4*, *ino2Δ*, *ino4Δ*) were grown in batch cultivations using a defined minimum medium and switched to chemostat immediately after glucose was depleted. Table 2 summarizes the basic physiological parameters for growth on glucose for all the strains in either C-limited or N-limited conditions. During the batch, *ino2Δ ino4Δ* double deletion had the highest maximum specific growth rate in the C-limited medium but the lowest maximum specific growth rate in the N-limited medium (Fig. 1B). However, it was clear that the double deletion strain had longer lag phase during batch cultivation in both C-limited and N-limited conditions (25h and 60h, respectively). Interestingly, during the chemostat cultivation we found this double deletion strain had the lowest biomass yields compared to the other strains. Interestingly, we found that the *opi1Δ* strain exhibited metabolic oscillations in the glucose limited chemostat cultures. We therefore sampled at two time points, at the maximum and minimum level of CO₂ production.

These two samples represent reductive-building (R/B) and reductive-

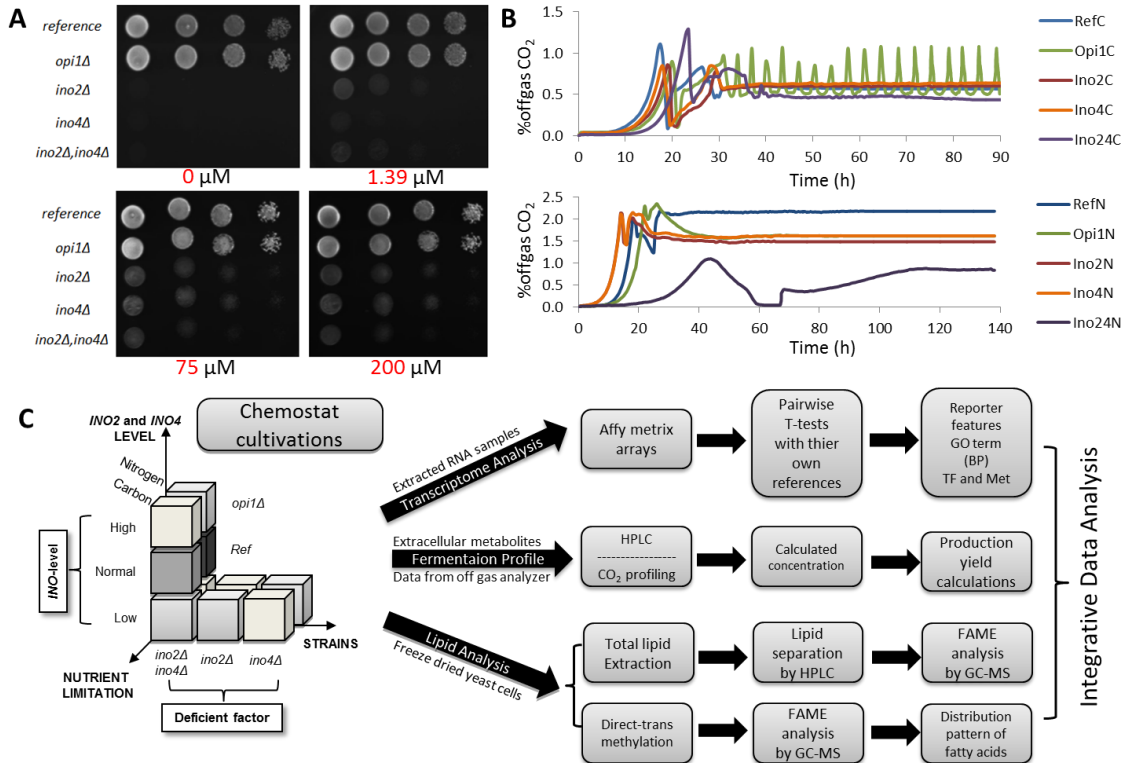


Figure 1. Spot test of all strains on SD agar plates with different inositol concentrations (A). Off gas CO₂ profile of each mutant strain during the chemostat cultivation at C-lim and N-lim (B). Schematic analysis of a workflow for integrated analysis, transcriptome-lipidome, of *INO*-level (key factor) and deficient factor effect on lipid biosynthesis (C).

Table 2 Physiological parameters of reference and mutants in chemostat cultivation.

Strains	μ_{\max}^1	Left Glc (g/L)	RQ	Y_{SX}^2	Y_{SE}^3	Y_{SG}^4	Y_{SA}^5	Y_{ss}^6	Y_{sc}^7
RefC	0.384±0.001	0.015±0.000	0.817±0.007	0.539±0.010	n.d.	0.019±0.001	n.d.	n.d.	0.124±0.003
Opi1CT	0.343±0.001	0.009±0.001	1.058±0.020	0.557±0.002	0.004±0.000	0.019±0.000	0.003±0.000	n.d.	0.208±0.004
Opi1CB	0.343±0.001	0.009±0.001	0.819±0.003	0.550±0.001	n.d.	0.019±0.000	n.d.	n.d.	0.106±0.003
Ino2C	0.340±0.000	0.018±0.001	0.805±0.011	0.597±0.020	n.d.	0.018±0.001	0.003±0.000	n.d.	0.129±0.006
Ino4C	0.369±0.001	0.010±0.000	0.837±0.009	0.571±0.007	n.d.	0.018±0.002	n.d.	n.d.	0.135±0.002
Ino24C	0.436±0.000	0.039±0.001	0.889±0.013	0.362±0.028	0.098±0.011	0.022±0.003	0.019±0.000	0.002±0.000	0.101±0.002
RefN	0.486±0.000	20.387±1.667	1.286±0.008	0.128±0.004	0.485±0.048	0.008±0.000	0.007±0.001	0.002±0.000	0.124±0.004
Opi1N	0.499±0.001	15.521±1.809	1.260±0.001	0.096±0.003	0.316±0.017	0.005±0.000	0.005±0.000	n.d.	0.075±0.017
Ino2N	0.495±0.001	28.286±0.877	1.159±0.008	0.168±0.002	0.305±0.015	0.009±0.000	0.006±0.001	n.d.	0.102±0.005
Ino4N	0.494±0.001	28.837±0.427	1.261±0.017	0.164±0.003	0.337±0.010	0.008±0.000	0.006±0.000	n.d.	0.103±0.001
Ino24N	0.410±0.000	35.944±1.867	1.269±0.010	0.058±0.008	0.370±0.026	0.017±0.001	0.038±0.001	n.d.	0.076±0.005

Note: All values are average ± SD from three biological replicates.

¹ maximum specific growth rate on glucose during batch cultivation (with 10 g/L and 60 g/L initial glucose for C-limited and N-limited conditions, respectively)

² Biomass yield on glucose in chemostat cultures (g biomass formed/g glucose consumed)

³ Ethanol yield on glucose in chemostat cultures (g ethanol formed/g glucose consumed)

⁴ Glycerol yield on glucose in chemostat cultures (g glycerol formed/g glucose consumed)

⁵ Acetate yield on glucose in chemostat cultures (g acetate formed/g glucose consumed)

⁶ Succinate yield on glucose in chemostat cultures (g succinate formed/g glucose consumed)

⁷ CO₂ yield on glucose in chemostat cultures (mg CO₂ formed/g glucose consumed)

charging (R/C) of the yeast metabolic cycle respectively [50] and the transcriptional data analysis for both of them were performed to see the differences from 2 metabolic phases (Fig. S1). The heatmap of reporter shows that the differences between these 2 metabolic phases mainly affects genes associated with differences in cell cycles period. According to the respiratory quotient (RQ) from Table 2, the phase of the population at maximum CO_2 production showed about 20% higher RQ compared with all the other strains at C-limitation. Based on this we therefore decided to exclude this sample and only use the sample from the minimum CO_2 production as a high *INO*-level representative at C-limitation condition.

Double deletion of *Ino2* and *Ino4* resulted in a substantial reduction (about 35% in C-limited and 55% in N-limited conditions) in biomass yield compared with the reference strain (Table 2). Interestingly, deletion of *Opi1* resulted in a small reduction (approx. 25%) in

biomass only at N-limited but not at C-limited conditions.

INO-level in nutrient-limited conditions

The levels of *INO*-gene (*INO2* and *INO4*) expression in both C-limited and N-limited conditions were investigated according to the expression level from micro array results (Fig. 2). Even though there were metabolic cycle patterns with the *opi1Δ* strain grown at C-limited condition, the expressions of the *INO* genes were consistently high (Fig. 2A). This evidence shows that *INO* genes are up-regulated when their repressor, *Opi1*, is absent. At C-limited condition, *INO* levels are low in both the two single and the double deletion strains (Fig. 2A and 2C). Interestingly, the *INO4* gene seems to be expressed at a high level at N-limitation (Fig. 2B) and it possibly also try to compensate the failure of *INO2* expression by up-regulating its expression in the *ino2Δ* strain at N-limitation (Fig. 2D).

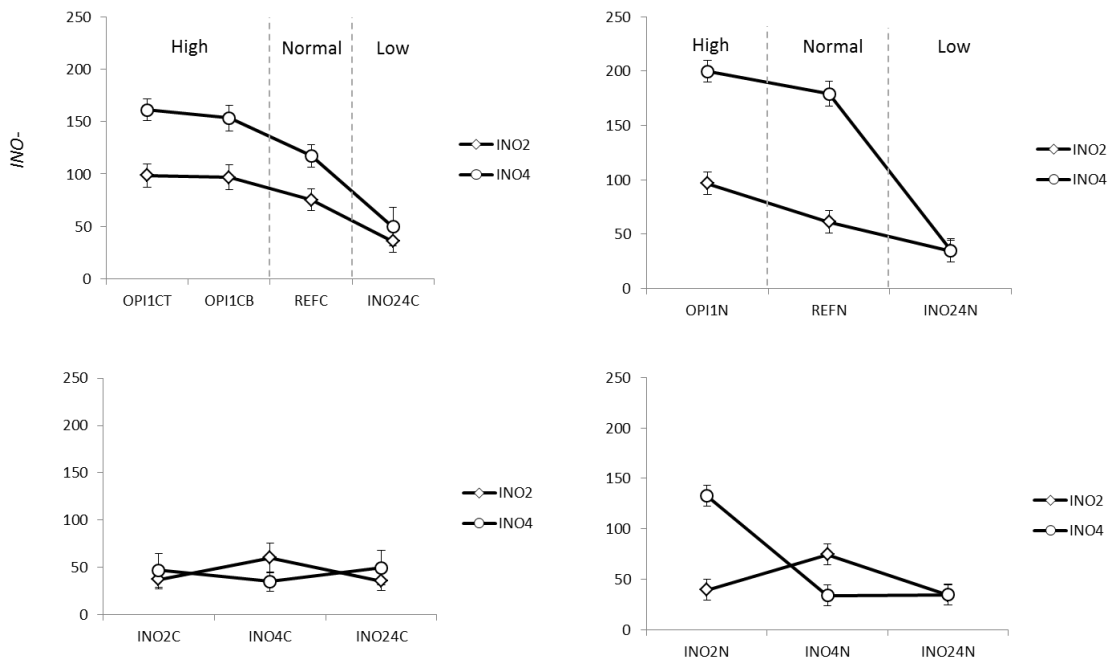


Figure 2. The normalized expression values of *INO2* and *INO4* (*INO*-level) for each strain. The key factor set shows the different *INO*-level at C-limitation (A) and N-limitation (B). The deficient factor group set shows the different *INO*-level at C-lim (C) and N-lim (D)

Global transcriptome changes due to *INO*-level in nutrient-limited conditions

We used the Affymetrix DNA microarray platform to measure the expression level of all genes and access the global effect caused by the *INO*-level under nutrient-limited conditions (C-lim and N-lim). The transcriptome data were decomposed using principal component analysis (PCA) and student T-test analysis ($\alpha=0.001$). The transcriptome data are presented in Venn diagrams at C-limited (Fig. 3A) and at N-limited (Fig. 3B) showing that the high *INO*-level (*opi1Δ*) strain had more genes being significantly changed at C-limitation. On the other hand, the low *INO*-level (*ino2Δino4Δ* double deletion) strain had

more genes being significantly changed at N-limitation.

From clustering of reporter GO terms (biological process at $P<0.001$), 4 main clusters were identified (Fig. 3C). Cluster 1 which is the largest group contains the genes involving the phospholipid biosynthesis, myo-inositol biosynthesis and transport, fatty acid metabolic process, cell conjugation, and ribonucleoside biosynthetic process which were highly up-regulated due to the deletion of *OPI1* (high *INO*-level), especially at N-limited condition, but down-regulated at low *INO*-level at both C- and N-limitation. Cluster 2 contains genes involving maltose and sucrose catabolic process which were highly up-regulated due to the C-limitations. Cluster 3 contains genes involving

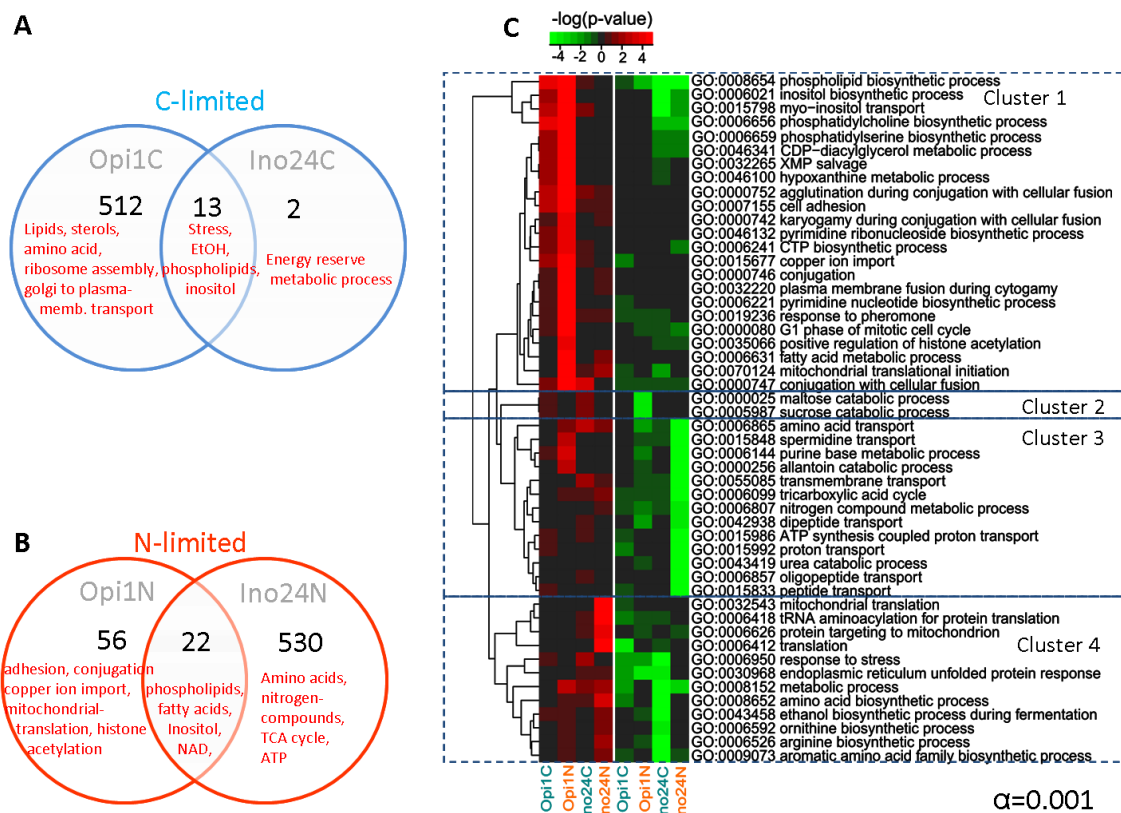


Figure 3. Transcriptional data analysis; Venn's diagram of significant genes of mutant strains caused by different *INO*-level when focus on C-limitation (A) and N-limitation (B) separately, p -value < 0.001 were considered. (C) A heat map of overrepresented GO terms (Biological Process) of each factor comparison showing in the range of -4 to 4 of $\log(p\text{-value})$. The green color indicates down-regulation and red indicates up-regulation compared to the reference strain.

nitrogen compound metabolism, amino acid and peptide transport, and proton transport which were down-regulated in the double mutant at N-limited condition. Cluster 4 contains genes involving amino acid biosynthesis, mitochondria biogenesis, and endoplasmic reticulum associated unfolded protein responses (ER-UPR) which were highly significant in the double mutant strain. These genes were up-regulated at low *INO*-level and N-limitations but down-regulated at C-limitation.

To identify specific transcriptional regulation of metabolism in response to deletion of *INO2* and/or *INO4*, we performed transcriptome comparison of the three *INO* deficient mutants (defined as deficient factor in Fig. 1C). For each strain we identified

genes with significantly changed expression compared with the reference strain and then presented the results for the three strain as Venn diagrams for both C-limited (Fig. 4A) and N-limited (Fig. 4B) conditions. Even though it has been known that Ino2 and Ino4 are heterodimeric transcription factor, we found some specific changes upon deletion of each of these genes (Fig. 4A and 4C). Interestingly, *ino4Δ* has more significant genes due to the absent of *INO4* compared with the two other mutants at C-limitation. At N-limitation, on the other hand, the effect is when both *INO2* and *INO4* was deleted. Interestingly, most of the genes involving nitrogen compounds metabolism and carbon utilization (Fig. 4C, Cluster 1) were down-regulated due to the absence of *INO2* and *INO4* but up-regulated

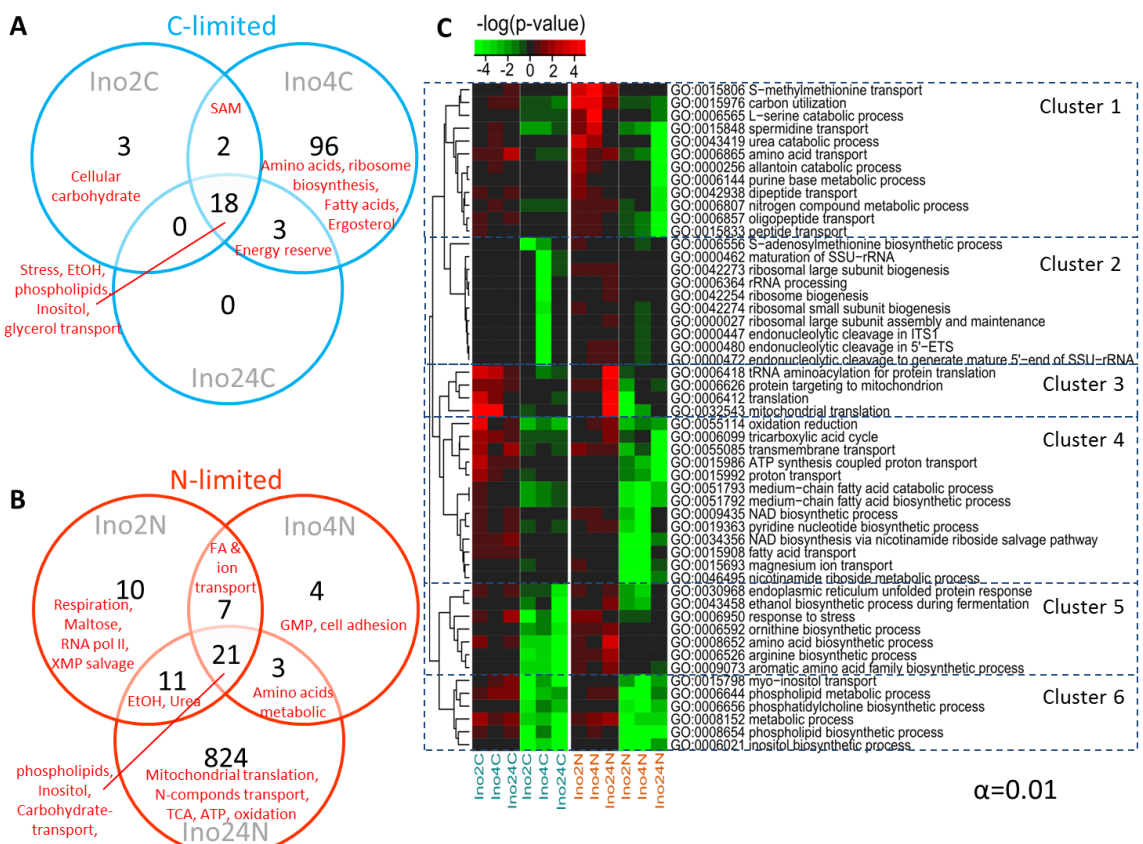


Figure 4. Transcriptional data analysis; Venn's diagram of significant genes of mutant strains caused by different deficient factors (single and double deletions) when focus on C-limitation (A) and N-limitation (B) separately, p -value < 0.01 were considered. (C) A heat map of overrepresented GO terms (Biological Process) of each factor comparison showing in range of -4 to 4 of $\log(p\text{-value})$. The green color indicates down-regulation and red indicates up-regulation compared to the reference strain.

when only *INO2* or *INO4* were knocked out individually at N-limitation. Moreover, we found that the genes involving ribosome biogenesis and rRNA processing (in cluster 2 Fig. 4C) are dramatically down-regulated when *INO4* was knocked out especially at C-limited conditions. The evidence showed that Ino4 (probably together with other TFs) could possibly play role in ribosome biogenesis (which supports protein synthesis). Surprisingly, most of the genes involving protein translation (Cluster 3 in Fig. 4C, including mitochondria translation) were up-regulated in the double mutant at N-limited conditions while they were only up-regulated when either *INO2* or *INO4* were deleted at C-limitation. Consistently, the genes involving phospholipid, inositol, and fatty acids (*UAS_{INO}*-contained genes in cluster 6, Fig. 4C) were down regulated in all three

strains at both C-limited and N-limited conditions. However, they were 2 other clusters that also captured down-regulated genes in all three *INO*-deleted strains, but different for the two nutrient limitations. The first group listed in cluster 4 (involving fatty acids biosynthesis and β -oxidation, TCA cycle, ATP, NAD, magnesium ion, and proton transport) were mainly down-regulated at N-limited condition. Cluster 5, on the other hand, contains genes involving ER-UPR and stress response, ethanol and amino acids biosynthesis that were mainly down-regulated only at C-limitation.

Effects of *INO*-level on fatty acid biosynthesis

With *UAS_{INO}* sites in their promoters, the expression of fatty acid synthase genes such as *ACC1*, *FAS1*, and

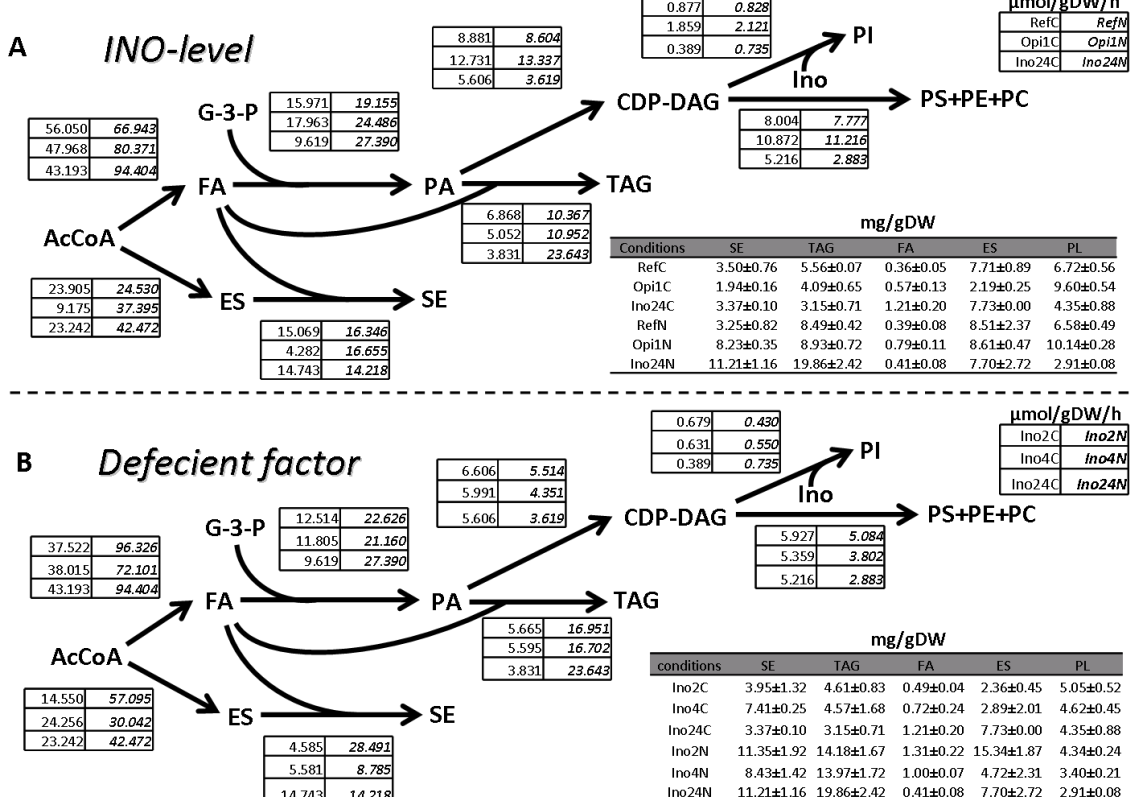


Figure 5. Fluxes through the different reactions of the lipid biosynthetic pathways for different *INO*-levels (A) and different deficient factors (B). All fluxes are shown in units of $\mu\text{mol/gDW/h}$. The normal font (left) and bold font (right) indicate the value from C-limitation and in N-limitation respectively. The level, in units of mg/gDW ($\pm\text{SD}$), of the different lipid species are shown in the table. (C = C-limited, N= N-limited).

FAS2 are subject to control by the Ino2/Ino4 and Opi1 transcription factors [26, 51, 52]. At low *INO*-level strain, the fatty acid synthase genes (*FAS1* and *FAS2*) were down-regulated at both C-limited and N-limited condition (Fig. S8). However, single deletion of each *INO* gene seems to have effect only at C-limitation when *FAS1*, *FAS2*, and also *ACC1* were down-regulated (Fig. S8). In contrast, the high *INO*-level strains especially at N-limited condition showed an increase in *FAS2* expression and none of the fatty acid synthase genes were down-regulated. This enhanced the ability to produce more FA needed for phospholipid biosynthesis. From the reporter metabolite heatmap (Fig. S2), the FA pools and also fatty acyl-ACP were increasing for high *INO*-level strains especially at N-limited condition. All the low *INO*-level strains showed a dramatic decrease in FA and fatty acyl-ACP pools as reporter metabolites. However, it seems like the effects of lacking *INO* genes have higher effect at C-limited than at N-limited conditions (Fig. S2). The transcription factors involving beta-oxidation, *OAF1* and *PIP2*, were found as reporter TF which were highly up-regulated at high *INO*-level but down-regulated at low *INO*-level (Fig. S3). Moreover, we found a significant increase in the free fatty acid (FA) pool of all the mutants compared to the reference strain (Fig. 5). However, the low *INO*-level strains showed slightly higher amount of accumulated FAs due to the lower fluxes towards PLs. From the plots of correlation between each fatty acid chain and their elongase enzyme coding genes (Fig. S7), we found a correlation between C18 fatty acid products (stearic and oleic acid) and the expression value of *ELO1* to be about 0.65 while the correlation between C20 fatty acids and *ELO2-ELO3* transcription were found in a negative direction (about -0.42 and -0.27, respectively). Presumably, C20 fatty acid might have a regulatory mechanism by repression their own elongase genes.

Effects of *INO*-level on phospholipids biosynthesis and accumulation

As mentioned above the whole set of UAS_{INO}-contained genes were extremely up-regulated at high *INO*-level (Fig. S8). However, to get a clearer picture about the carbon channeling in lipid metabolism at the metabolite level, the fluxes in lipid biosynthesis (in units of $\mu\text{mol/gDW/h}$) were calculated from the measured lipid profiles at all conditions (Fig. 5) and this provides a clear picture of the changes in the flux distribution in response to the different factors evaluated. These fluxes were affected by many factors at several levels, such as gene transcription, protein phosphorylation, and enzyme activity. At high *INO*-level, the fluxes through CDP-DAG and phospholipids synthesis pathway were higher than the reference about 45-55 % at C-limitation and N-limitation, respectively. Moreover, the expression of the genes coding for myo-inositol transporter (*ITR1*) and choline transporter (*HNM1*) were highly up-regulated in *opi1Δ*. This supported the synthesis of PI and also enhanced the Kennedy's pathway to produce more PC using choline and DAG as precursors and it was consistent with the highly up-regulation of the genes coding for Kennedy's pathway enzymes such as *CPT1* and *CKII* (Fig. S8). On the other hand, the *ITR1* were constantly down-regulated in all low *INO*-level strains either double or single deletion in both limitation conditions. The low *INO*-level strain showed about 40-60% decreasing fluxes through the CDP-DAG pathway which caused a dramatically decrease in the phospholipid pool especially at N-limitation. The metabolite reporter heat map showed a large increase of PL pools in the high *INO*-level strain. In contrast, we found a dramatically decreasing of PLs in low *INO*-level compared to the reference strain.

Focusing on the deficient effects, double deletion of *INO* genes (especially at N-limitation) can cause more effect to the dramatically reduction of

phospholipids than the effect of single deletions (Fig. 5). About a 70% decrease in PLs can be found when both *INO* genes were deleted, but there were only 50% or 60% decreasing in PLs when *INO2* or *INO4* were deleted respectively. Even though this double deletion effects did not make much changes in the PLs pool at C-limitation, it still caused about 50% lower level of PI when compare to the single deletion strains. From the heatmap of reporter metabolites (Fig. S4), S-adenosyl-L-methionine or SAM (the only donor of PE methylation reaction) was strongly decreased in all low *INO*-level strains and this lead to a decrease of PLs (especially PC) since it is required for production of PC by Cho2 and Opi3.

Effects of *INO*-level on storage lipids biosynthesis and accumulation

The production rate and accumulation of PC can cause ER stress and UPR activation which lead to the up-regulation of TAG and ES biosynthesis [53]. At N-limitation, the low *INO*-level strain (double mutant) could produce and accumulate TAG and SE about 1.2 folds more when compared to the high *INO*-level strain (*opi1Δ*) and about 1.5 folds when compare to the reference strain (Fig. 5). Presumably, the down-regulation of *LPP1* at both C- and N-limitation for the high *INO*-level strain led to a decrease in TAG biosynthesis and accumulation compared to the reference strain and other mutants (Fig. S8). Consistently, almost the whole set of the ES genes (the green group in Fig. S8) were down-regulated compared to the reference and this was associated with a dramatically decreasing levels of ES and SE. This correlation between transcription of ES genes and ES level was also supported by the up-regulation of several ES genes in all low *INO*-level strains especially at N-limited condition (Fig. S8). Interestingly, the double deletion strain showed a greater effect in increasing TAG only at N-limitation. This evidence was supported by the up-regulation of the *ARE1* gene in the

double deletion strain (Fig. S8) which codes for the enzyme for the first step of SE biosynthesis. At C-limited condition, on the other hand, *ino2Δ ino4Δ* has a larger effect on decreasing the TAG level compared with the single deletion strains. Moreover, the fluxes through ES of the *ino2Δ* strain was about 80% lower when compare to *INO4* deletion and double deletion at C-limited condition.

Ino4 might have an extra function, beside the regulator of phospholipid biosynthesis, response to nitrogen starvation and amino acids starvations

It is possible that Ino4, but not Ino2, plays a role as a regulator for amino acid metabolism. It may not be Ino4 alone since Ino4, unlike Ino2, does not have a trans-activating domain (TAD) which is recognized for the RNA polymerase II complex [33, 54, 55]. In *ino4Δ*, the genes involving ribosome biogenesis and assembly were extremely down regulated especially at C-limited conditions and this was exactly the responsive process for amino acids (and of cause nitrogen) starvation. There are indications that the induction of Ino4-regulated lipid biosynthesis genes may be connected to the immediate need of membrane material used for the autophagocytosis process [56]. This process is utilized by yeast in order to regulate the equilibrium between proteins and the diminishing set of amino acids due to starvation conditions [57]. From the reporter metabolite heatmap (Fig. S4), most of the amino acids were found to be greatly down-regulated (especially at N-limitation) in all low *INO*-level strains which pointed an amino acid starvation response.

To identify the extra function of Ino4 on protein biosynthesis, we also performed the Pearson correlation analysis of *INO4* to all other genes based on the normalized expression values from transcriptome data of all strains and all conditions. Using the cut off at 0.50 absolute correlation value, about 470 genes were selected as the high correlated genes of *INO4* (91 genes were

positively correlated and 380 genes were negatively correlated). The overrepresentation of gene ontology categories (biological process) were identified and analyzed using BiNGO, a Cytoscape plugin [58]. From the *INO4* positively correlated genes listed in table S2, it confirmed the main function of Ino4 (together with Ino2 as listed in table S4) as a positive regulators of lipid biosynthesis and inositol-choline transport involved genes as it has been reported before by many researchers. However, the list of *INO4* negatively correlated genes in table S3 showed the new findings that Ino4 is actually play an extra role as the negative regulator of the translation process, protein biosynthesis and assembly, and also involves in mitochondrial translation. Ino2, on the other hand, had about 200 negatively correlated genes that passed through the cut off at 0.50 absolute Pearson correlation value. This particular group contains many interesting genes involving protein transport, protein catabolic process, and proteolysis which might also responds for amino acid starvation as summarized in table S5.

Linkage among sulfur-phospholipis, protein synthesis, and ER-UPR pathway.

The double deletion of *INO2* and *INO4* at N-limitation showed some effects from amino acid starvation. UPR genes were also down-regulated when amino acids are decreasing (less missed fold proteins). It also has been known that decreasing PC levels leads to the accumulation of saturated PC molecular species in the ER membrane which causes ER stress, UPR activation and these evidences lead to the up-regulation of FA, TAG, and sterol biosynthesis in the end [53]. Therefore, in the low *INO-*

level strain, the *KAR2* gene which is a responsive gene for ER-UPR were up-regulated especially at N-limitation. The high *INO*-level on the other hand, showed a large decrease in expression of *KAR2* especially at C-limited condition. These evidences show that there is a linkage which plays a role in regulating the homeostasis among amino acids biosynthesis, phospholipids biosynthesis, and the ER-UPR pathway. As it has been reported before most of the genes coding for enzymes involved in cysteine-methionine biosynthesis, i.e. *MET2*, *MET8*, *MET14*, *MET16*, *SAH1*, *SAH2*, contain ICRE or UAS_{INO} sequences in their upstream regions [52], and these genes were up-regulated at high *INO*-level while *OPI1* (the repressor) was disturbed. Consequently, we found down-regulation of *MET6* and *SAH1* and especially *SAH2* in all low *INO*-level mutants, especially at C-limited condition. This leads to reduced synthesis and accumulation of storage lipids at C-limited condition compared to their references (Fig. 6). This pointed out that amino acid synthesis genes might be controlled by the regulation of Snf1 kinase (via Gln3 or Gdh3) which is always activated at low glucose (C-limited) condition and consistent with our previous study [40]. Consistently, *MET6* and *SAH1* were up-regulated at high *INO*-level at N-limitations where Snf1 is consistently repressed by excess glucose in the culture media, and this leads to the slightly higher biosynthesis of TAG and hence TAG accumulation (Fig. 6). Based on our findings and some supporting knowledge from the previous study [40], the overall regulation systems linking amino acids-protein synthesis, lipid metabolism and ER-UPR is summarised in Fig. 7 which has kinase proteins and several transcription factors involved.

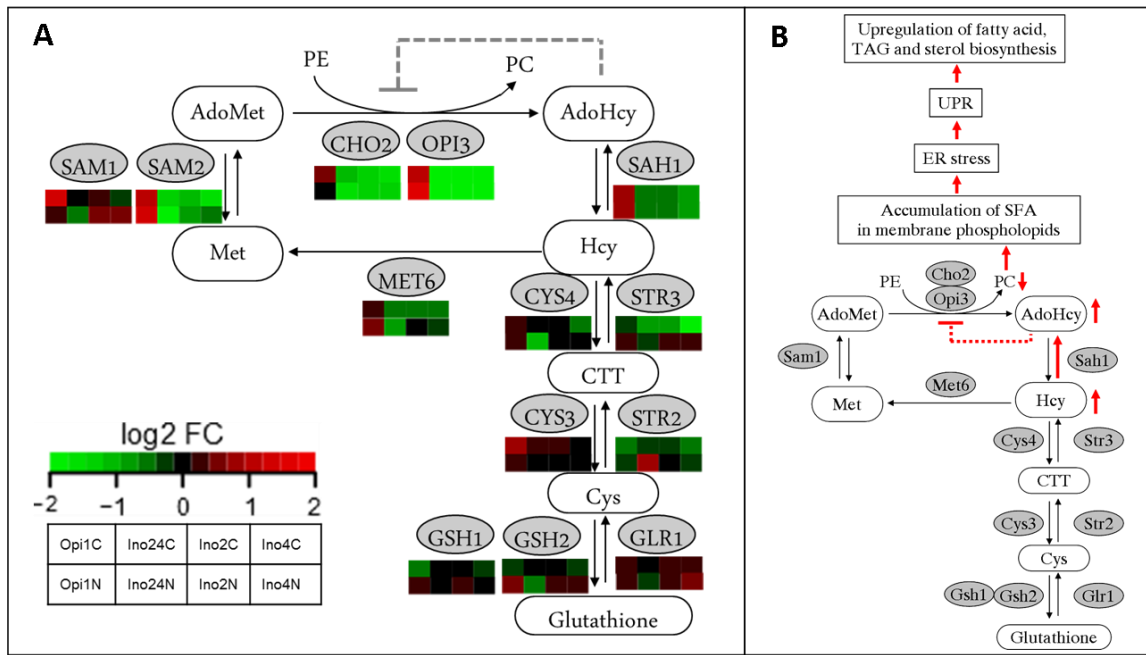


Figure 6. The coupled-reaction of methylations of phosphoethanolamine from *S*-adenosyl-*L*-methionine (AdoMet) by Cho2 and Opi3 enzymes. (A) A comparison of expression level (log₂ fold change) of each genes coding for sulfur-phospholipids couple d metabolism. (B) The effects of low INO-level on ER stress and UPR inducing the up-regulation of FA and storage lipids [53]

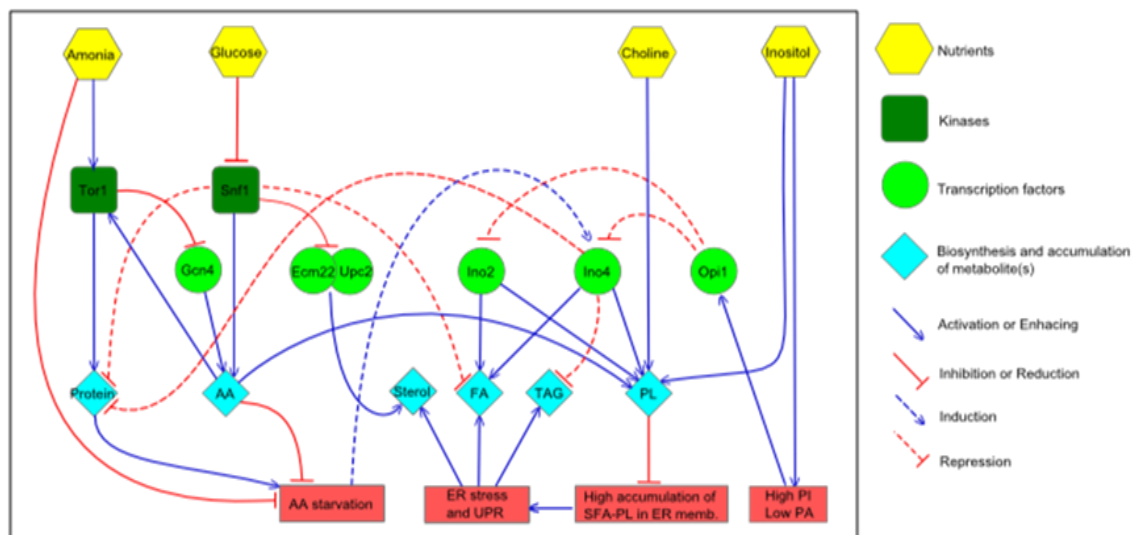


Figure 7. Summary of the multilevel regulation network among amino acids biosynthesis, lipid metabolism, and ER-UPR.

Conclusions

Through integrated analysis of transcriptome and lipidome derived from robust experimental setup, it was possible to obtain a large-scale dataset that could be used to systematically identify correlations and associations between the different components. We were able to see the effect on expression of the genes involved in lipid biosynthesis and metabolic fluxes through lipid biosynthesis pathway. We found that there is an effect of Ino4, but not by Ino2, on the ribosome biogenesis and assembly which involves an amino acid starvation response. It points to an interesting link between lipid metabolism and the amino acid starvation response and we also found an effect of phospholipids on ER-UPR activation. Moreover, we found a close linkage among *INO* genes, amino acid genes, and probably Snf1 kinase in controlling lipid biosynthesis and accumulation. Following our analysis by genome-wide strategy and analysis of generated complex data by integrated analysis approach enable us to explore correlations and association of changes in a concerted fashion.

Acknowledgements

Part of this work was financed by Chalmers Foundation, the Knut and Alice Wallenberg Foundation and the Swedish Research Council (Vetenskapsrådet). We also acknowledge funding from the EU-funded project UNICELLSYS. Pramote Chumnanpuen also would like to thank the Office of the Higher Education Commission, Thailand for supporting with a stipend for his Ph.D. program under the program Strategic Scholarships for Frontier Research Network. We also thank Dr. Jie Zhang and Dr. Goutham Vemuri for kindly assistance with fermentation and microarray data acquisition, and Leif Varemo for kindly help with R script for transcriptome data analysis package.

References

1. Carman GM, Han GS: Regulation of phospholipid synthesis in yeast. *J Lipid Res* 2009, 50 Suppl:S69-73.
2. Carman GM, Han GS: Regulation of phospholipid synthesis in the yeast *Saccharomyces cerevisiae*. *Annu Rev Biochem* 2011, 80:859-883.
3. Carman GM, Kersting MC: Phospholipid synthesis in yeast: regulation by phosphorylation. *Biochem Cell Biol* 2004, 82:62-70.
4. Santiago TC, Mamoun CB: Genome expression analysis in yeast reveals novel transcriptional regulation by inositol and choline and new regulatory functions for Opi1p, Ino2p, and Ino4p. *J Biol Chem* 2003, 278:38723-38730.
5. Ashburner BP, Lopes JM: Regulation of yeast phospholipid biosynthetic gene expression in response to inositol involves two superimposed mechanisms. *Proc Natl Acad Sci U S A* 1995, 92:9722-9726.
6. Ashburner BP, Lopes JM: Autoregulated expression of the yeast *INO2* and *INO4* helix-loop-helix activator genes effects cooperative regulation on their target genes. *Mol Cell Biol* 1995, 15:1709-1715.
7. White MJ, Hirsch JP, Henry SA: The OPI1 gene of *Saccharomyces cerevisiae*, a negative regulator of phospholipid biosynthesis, encodes a protein containing polyglutamine tracts and a leucine zipper. *J Biol Chem* 1991, 266:863-872.
8. Wagner C, Blank M, Strohmann B, Schuller HJ: Overproduction of the Opi1 repressor inhibits transcriptional activation of structural genes required for phospholipid biosynthesis in the yeast *Saccharomyces cerevisiae*. *Yeast* 1999, 15:843-854.
9. Lo WS, Gamache ER, Henry KW, Yang D, Pillus L, Berger SL: Histone H3 phosphorylation can promote TBP recruitment through distinct promoter-specific mechanisms. *EMBO J* 2005, 24:997-1008.
10. Dietz M, Heyken WT, Hoppen J, Geburtig S, Schuller HJ: TFIIB and

- subunits of the SAGA complex are involved in transcriptional activation of phospholipid biosynthetic genes by the regulatory protein Ino2 in the yeast *Saccharomyces cerevisiae*. *Mol Microbiol* 2003, 48:1119-1130.
11. Greenberg ML, Goldwasser P, Henry SA: Characterization of a yeast regulatory mutant constitutive for synthesis of inositol-1-phosphate synthase. *Mol Gen Genet* 1982, 186:157-163.
 12. Loewen CJ, Roy A, Levine TP: A conserved ER targeting motif in three families of lipid binding proteins and in Opi1p binds VAP. *EMBO J* 2003, 22:2025-2035.
 13. Keleher CA, Redd MJ, Schultz J, Carlson M, Johnson AD: Ssn6-Tup1 is a general repressor of transcription in yeast. *Cell* 1992, 68:709-719.
 14. Smith RL, Johnson AD: Turning genes off by Ssn6-Tup1: a conserved system of transcriptional repression in eukaryotes. *Trends Biochem Sci* 2000, 25:325-330.
 15. Wagner C, Dietz M, Wittmann J, Albrecht A, Schuller HJ: The negative regulator Opi1 of phospholipid biosynthesis in yeast contacts the pleiotropic repressor Sin3 and the transcriptional activator Ino2. *Mol Microbiol* 2001, 41:155-166.
 16. Wang H, Stillman DJ: Transcriptional repression in *Saccharomyces cerevisiae* by a SIN3-LexA fusion protein. *Mol Cell Biol* 1993, 13:1805-1814.
 17. Vidal M, Strich R, Esposito RE, Gaber RF: RPD1 (SIN3/UME4) is required for maximal activation and repression of diverse yeast genes. *Mol Cell Biol* 1991, 11:6306-6316.
 18. Wang H, Clark I, Nicholson PR, Herskowitz I, Stillman DJ: The *Saccharomyces cerevisiae* SIN3 gene, a negative regulator of HO, contains four paired amphipathic helix motifs. *Mol Cell Biol* 1990, 10:5927-5936.
 19. Kasten MM, Dorland S, Stillman DJ: A large protein complex containing the yeast Sin3p and Rpd3p transcriptional regulators. *Mol Cell Biol* 1997, 17:4852-4858.
 20. Heyken WT, Repenning A, Kumme J, Schuller HJ: Constitutive expression of yeast phospholipid biosynthetic genes by variants of Ino2 activator defective for interaction with Opi1 repressor. *Mol Microbiol* 2005, 56:696-707.
 21. Nikoloff DM, Henry SA: Genetic analysis of yeast phospholipid biosynthesis. *Annu Rev Genet* 1991, 25:559-583.
 22. Jesch SA, Zhao X, Wells MT, Henry SA: Genome-wide analysis reveals inositol, not choline, as the major effector of Ino2p-Ino4p and unfolded protein response target gene expression in yeast. *J Biol Chem* 2005, 280:9106-9118.
 23. Lopes JM, Henry SA: Interaction of trans and cis regulatory elements in the INO1 promoter of *Saccharomyces cerevisiae*. *Nucleic Acids Res* 1991, 19:3987-3994.
 24. Bailis AM, Poole MA, Carman GM, Henry SA: The Membrane-Associated Enzyme Phosphatidylserine Synthase Is Regulated at the Level of Messenger-Rna Abundance. *Mol Cell Biol* 1987, 7:167-176.
 25. Hiesinger M, Wagner C, Schuller HJ: The acetyl-CoA synthetase gene ACS2 of the yeast *Saccharomyces cerevisiae* is coregulated with structural genes of fatty acid biosynthesis by the transcriptional activators Ino2p and Ino4p. *FEBS Lett* 1997, 415:16-20.
 26. Hasslacher M, Ivessa AS, Paltauf F, Kohlwein SD: Acetyl-CoA carboxylase from yeast is an essential enzyme and is regulated by factors that control phospholipid metabolism. *J Biol Chem* 1993, 268:10946-10952.
 27. Schwank S, Ebbert R, Rautenstrauss K, Schweizer E, Schuller HJ: Yeast transcriptional activator INO2 interacts as an Ino2p/Ino4p basic helix-loop-helix heteromeric complex with the inositol/choline-responsive element necessary for expression of phospholipid biosynthetic genes in *Saccharomyces cerevisiae*. *Nucleic Acids Res* 1995, 23:230-237.

28. Schuller HJ, Hahn A, Troster F, Schutz A, Schweizer E: Coordinate genetic control of yeast fatty acid synthase genes FAS1 and FAS2 by an upstream activation site common to genes involved in membrane lipid biosynthesis. *EMBO J* 1992, 11:107-114.
29. Hoppen J, Repenning A, Albrecht A, Geburtig S, Schuller HJ: Comparative analysis of promoter regions containing binding sites of the heterodimeric transcription factor Ino2/Ino4 involved in yeast phospholipid biosynthesis. *Yeast* 2005, 22:601-613.
30. Schuller HJ, Schorr R, Hoffmann B, Schweizer E: Regulatory gene INO4 of yeast phospholipid biosynthesis is positively autoregulated and functions as a transactivator of fatty acid synthase genes FAS1 and FAS2 from *Saccharomyces cerevisiae*. *Nucleic Acids Res* 1992, 20:5955-5961.
31. Ambroziak J, Henry SA: INO2 and INO4 gene products, positive regulators of phospholipid biosynthesis in *Saccharomyces cerevisiae*, form a complex that binds to the INO1 promoter. *J Biol Chem* 1994, 269:15344-15349.
32. Hoshizaki DK, Hill JE, Henry SA: The *Saccharomyces cerevisiae* INO4 gene encodes a small, highly basic protein required for derepression of phospholipid biosynthetic enzymes. *J Biol Chem* 1990, 265:4736-4745.
33. Kumme J, Dietz M, Wagner C, Schuller HJ: Dimerization of yeast transcription factors Ino2 and Ino4 is regulated by precursors of phospholipid biosynthesis mediated by Op1 repressor. *Curr Genet* 2008, 54:35-45.
34. Chen M, Lopes JM: Multiple basic helix-loop-helix proteins regulate expression of the ENO1 gene of *Saccharomyces cerevisiae*. *Eukaryot Cell* 2007, 6:786-796.
35. Hosaka K, Nikawa J, Kodaki T, Yamashita S: Cloning and characterization of the SCS1 gene required for the expression of genes in yeast phospholipid synthesis. *J Biochem* 1994, 115:131-136.
36. Schwank S, Hoffmann B, Schuller HJ: Influence of gene dosage and autoregulation of the regulatory genes INO2 and INO4 on inositol/choline-repressible gene transcription in the yeast *Saccharomyces cerevisiae*. *Curr Genet* 1997, 31:462-468.
37. Loewen CJ, Gaspar ML, Jesch SA, Delon C, Ktistakis NT, Henry SA, Levine TP: Phospholipid metabolism regulated by a transcription factor sensing phosphatidic acid. *Science* 2004, 304:1644-1647.
38. Canelas AB, Harrison N, Fazio A, Zhang J, Pitkanen JP, van den Brink J, Bakker BM, Bogner L, Bouwman J, Castrillo JI, et al: Integrated multilaboratory systems biology reveals differences in protein metabolism between two reference yeast strains. *Nat Commun* 2010, 1:145.
39. van Dijken JP, Bauer J, Brambilla L, Duboc P, Francois JM, Gancedo C, Giuseppin MLF, Heijnen JJ, Hoare M, Lange HC, et al: An interlaboratory comparison of physiological and genetic properties of four *Saccharomyces cerevisiae* strains. *Enzyme and Microbial Technology* 2000, 26:706-714.
40. Zhang J, Vaga S, Chumnanpuen P, Kumar R, Vemuri GN, Aebersold R, Nielsen J: Mapping the interaction of Snf1 with TORC1 in *Saccharomyces cerevisiae*. *Mol Syst Biol* 2011, 7.
41. Chumnanpuen P, Zhang J, Nookae I, Nielsen J: Integrated analysis of the transcriptome-lipidome reveals the co-influences of inositol-choline and Snf1 in controlling lipid biosynthesis in yeast. *Submitted to Molecular Genetics and Genomics* 2012.
42. Klig LS, Homann MJ, Carman GM, Henry SA: Coordinate Regulation of Phospholipid Biosynthesis in *Saccharomyces-Cerevisiae* - Pleiotropically Constitutive Op1 Mutant. *Journal of Bacteriology* 1985, 162:1135-1141.
43. Zaldivar J, Borges A, Johansson B, Smits HP, Villas-Boas SG, Nielsen J, Olsson L: Fermentation performance and intracellular metabolite patterns in

- laboratory and industrial xylose-fermenting *Saccharomyces cerevisiae*. *Appl Microbiol Biotechnol* 2002, 59:436-442.
44. Bligh EG, Dyer WJ: A rapid method of total lipid extraction and purification. *Can J Biochem Physiol* 1959, 37:911-917.
45. Silversand C, Haux C: Improved high-performance liquid chromatographic method for the separation and quantification of lipid classes: application to fish lipids. *J Chromatogr B Biomed Sci Appl* 1997, 703:7-14.
46. Khoomrung S, Chumnanpuen P, Jansa-ard S, Nookaew I, Nielsen J: Fast and accurate preparation fatty acid methyl esters by microwave-assisted derivatization in yeast *Saccharomyces cerevisiae*. Submitted to *Applied Microbiology and Biotechnology* 2012.
47. Nookaew I, Jewett MC, Meechai A, Thammarongtham C, Laoteng K, Cheevadhanarak S, Nielsen J, Bhumiratana S: The genome-scale metabolic model iIN800 of *Saccharomyces cerevisiae* and its validation: a scaffold to query lipid metabolism. *BMC Syst Biol* 2008, 2:71.
48. Oliveira AP, Patil KR, Nielsen J: Architecture of transcriptional regulatory circuits is knitted over the topology of bio-molecular interaction networks. *BMC Syst Biol* 2008, 2:17.
49. Graves JA, Henry SA: Regulation of the yeast INO1 gene. The products of the INO2, INO4 and OPI1 regulatory genes are not required for repression in response to inositol. *Genetics* 2000, 154:1485-1495.
50. Tu BP, Kudlicki A, Rowicka M, McKnight SL: Logic of the yeast metabolic cycle: temporal compartmentalization of cellular processes. *Science* 2005, 310:1152-1158.
51. Chirala SS, Zhong Q, Huang W, al-Feel W: Analysis of FAS3/ACC regulatory region of *Saccharomyces cerevisiae*: identification of a functional UASINO and sequences responsible for fatty acid mediated repression. *Nucleic Acids Res* 1994, 22:412-418.
52. Schuller HJ, Richter K, Hoffmann B, Ebbert R, Schweizer E: DNA binding site of the yeast heteromeric Ino2p/Ino4p basic helix-loop-helix transcription factor: structural requirements as defined by saturation mutagenesis. *FEBS Lett* 1995, 370:149-152.
53. Tehlivets O: Homocysteine as a risk factor for atherosclerosis: is its conversion to s-adenosyl-L-homocysteine the key to deregulated lipid metabolism? *J Lipids* 2011, 2011:702853.
54. Chen M, Hancock LC, Lopes JM: Transcriptional regulation of yeast phospholipid biosynthetic genes. *Biochim Biophys Acta* 2007, 1771:310-321.
55. Lee TI, Rinaldi NJ, Robert F, Odom DT, Bar-Joseph Z, Gerber GK, Hannett NM, Harbison CT, Thompson CM, Simon I, et al: Transcriptional regulatory networks in *Saccharomyces cerevisiae*. *Science* 2002, 298:799-804.
56. Ernst J, Vainas O, Harbison CT, Simon I, Bar-Joseph Z: Reconstructing dynamic regulatory maps. *Mol Syst Biol* 2007, 3:74.
57. Petiot A, Pattingre S, Arico S, Meley D, Codogno P: Diversity of signaling controls of macroautophagy in mammalian cells. *Cell Struct Funct* 2002, 27:431-441.
58. Maere S, Heymans K, Kuiper M: BiNGO: a Cytoscape plugin to assess overrepresentation of gene ontology categories in biological networks. *Bioinformatics* 2005, 21:3448-3449.

Supplementary Information to

Title: Integrated analysis of the transcriptome-lipidome reveals the effects of *INO*-level (*INO2* and *INO4*) on lipid metabolism in yeast

Pramote Chumnanpuen, Intawat Nookaew, and Jens Nielsen*

Department of Chemical and Biological Engineering,
Chalmers University of Technology,
Kemivägen 10, SE-412 96 Gothenburg, Sweden

*Corresponding Author:

Jens Nielsen

Email: nielsenj@chalmers.se

Tel: +46 31 772 38 04

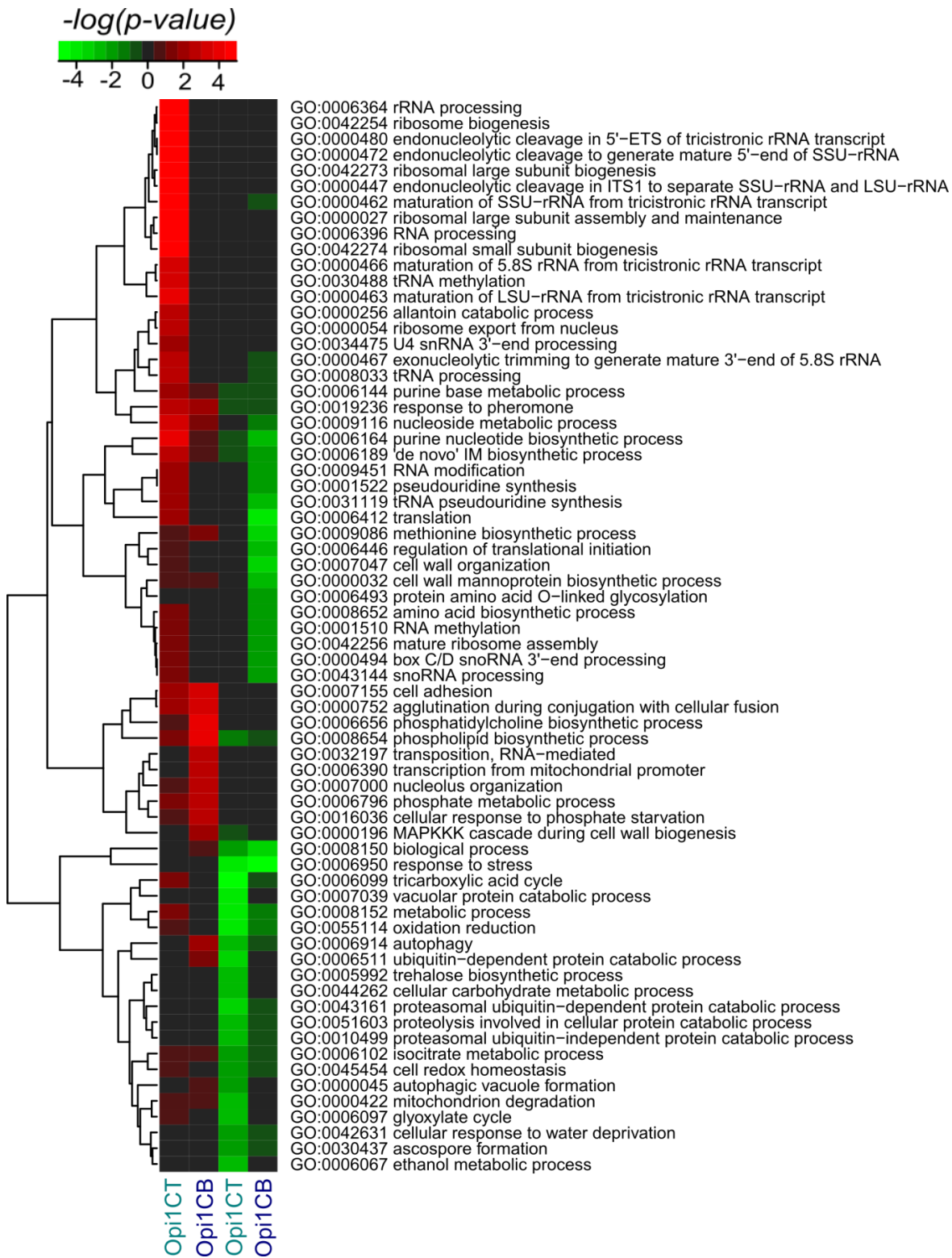


Figure S1. A heat map of over-representation of GO terms (Biological Process) responded to the 2 different phases of *opi1Δ* at C-limitation (top phase and bottom phase of CO₂ profile)

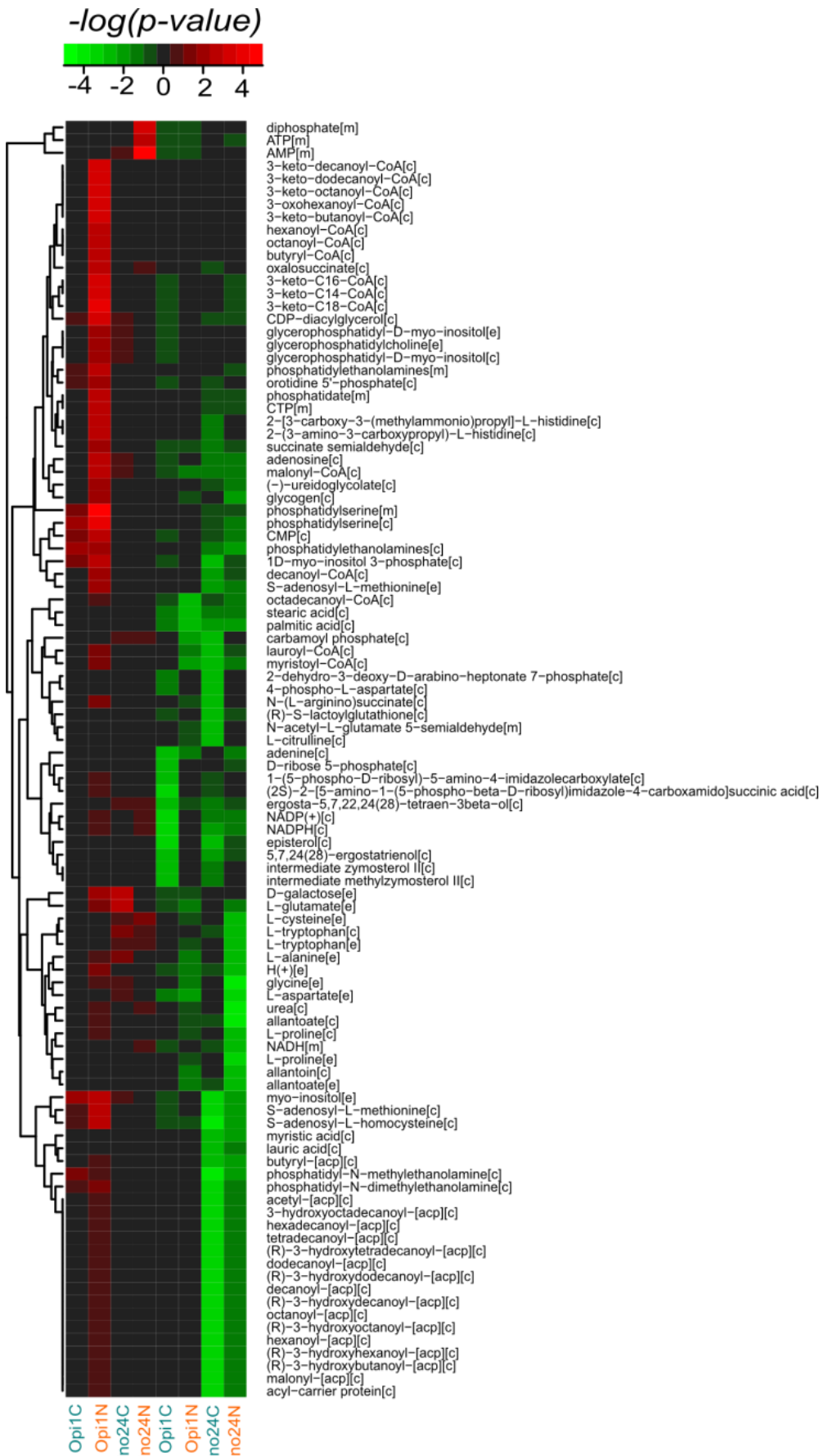


Figure S2. A heat map of reporter Metabolites of *INO*-level comparison

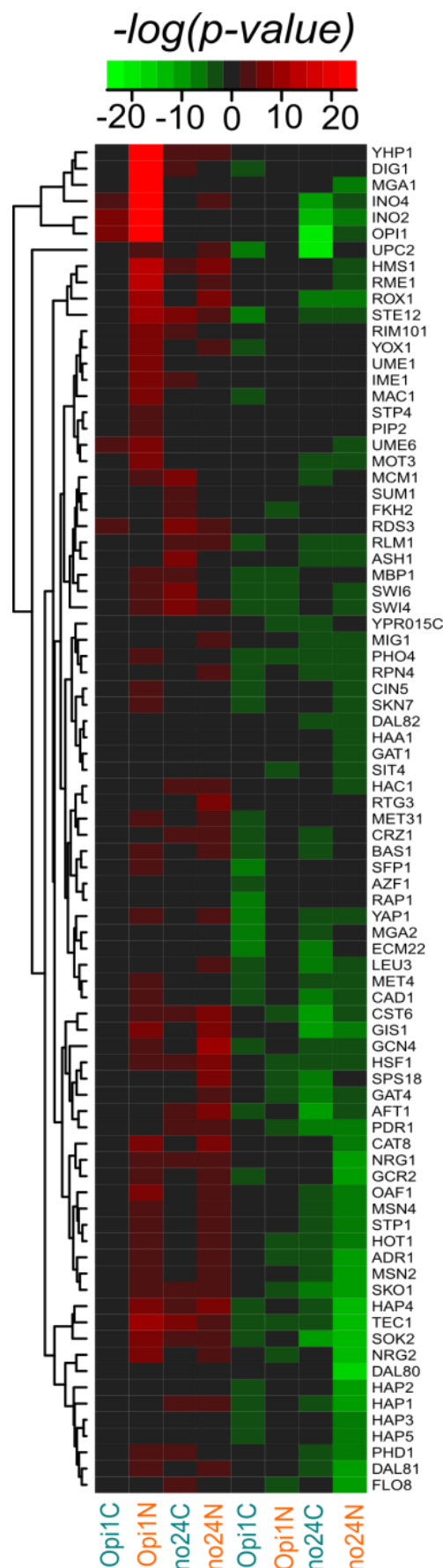


Figure S3. A heat map of reporter transcription factors of *INO*-level comparison

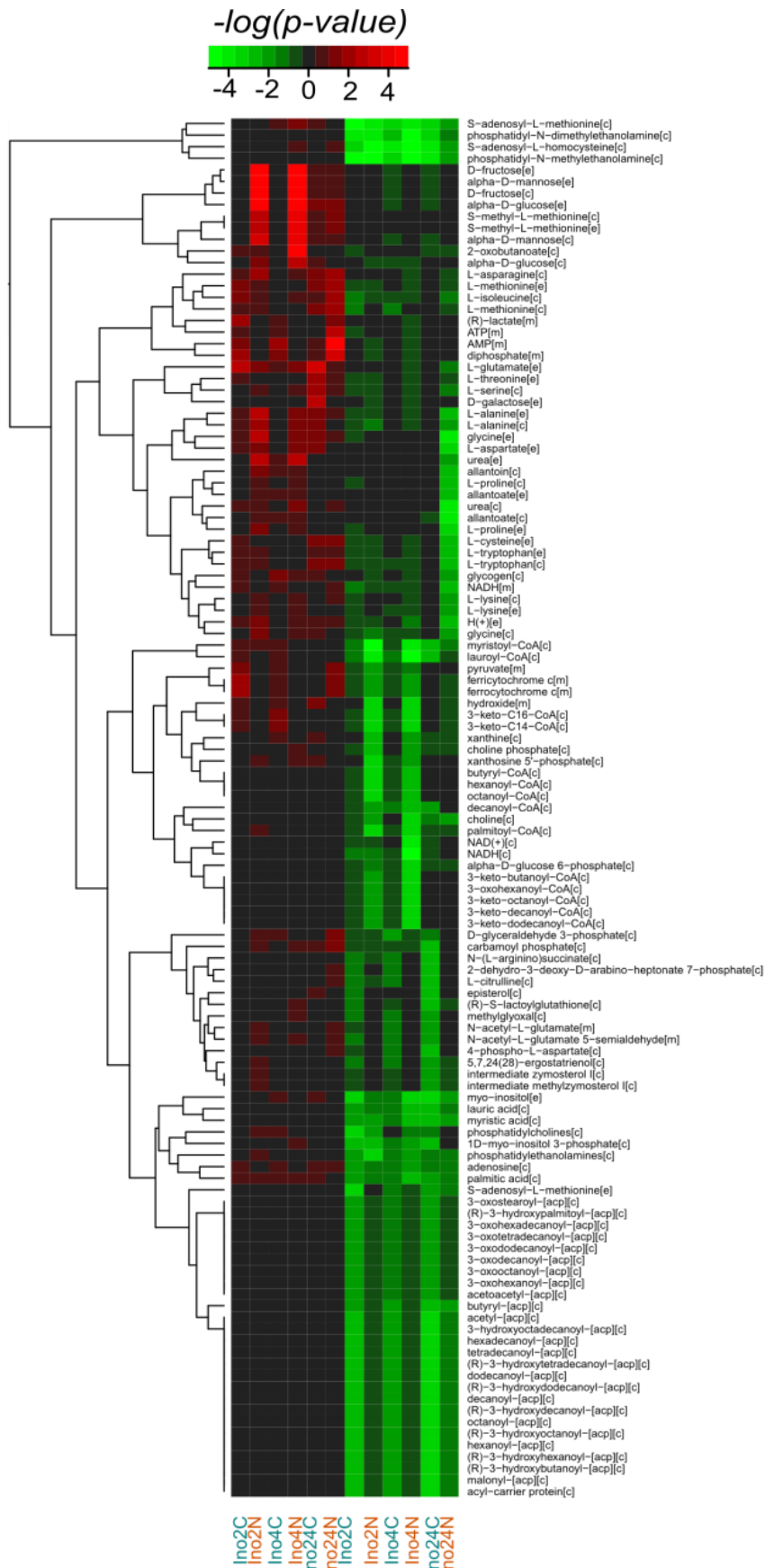


Figure S4. A heat map of reporter metabolites of deficient effects comparison

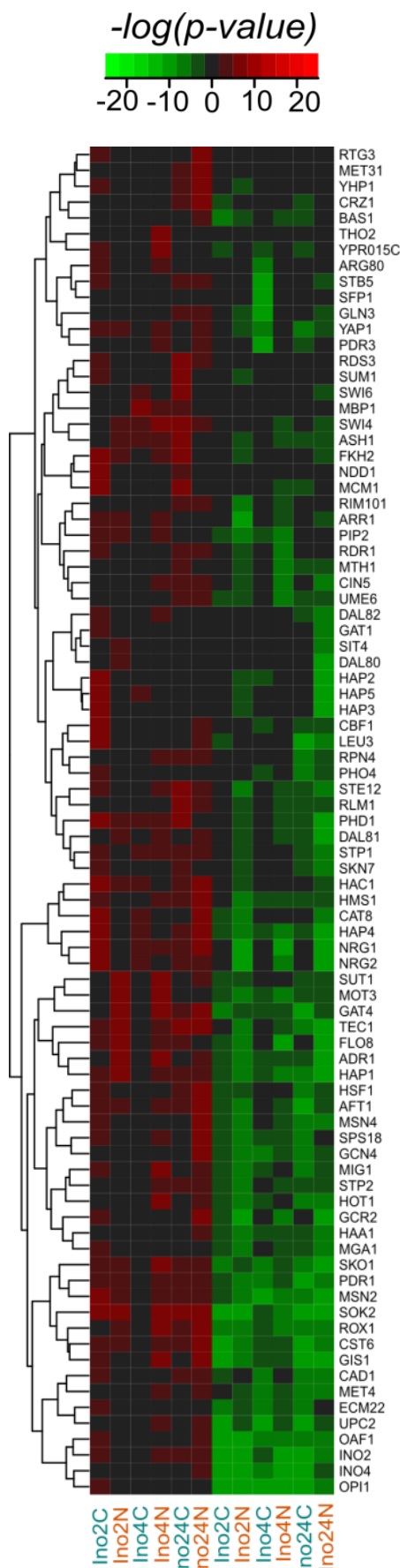


Figure S5. A heat map of reporter transcription factors of deficient effects comparison.

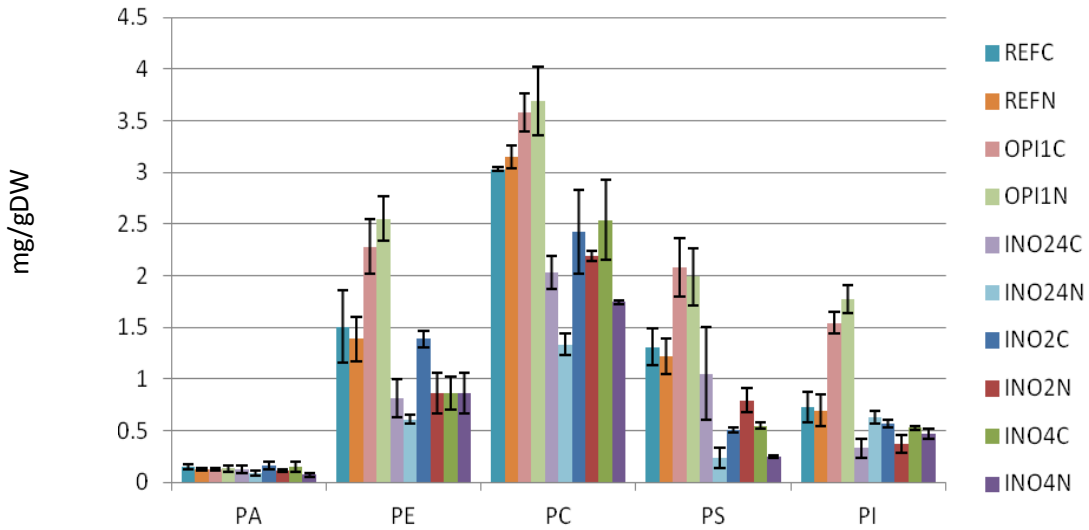


Figure S6. Abundance of different phospholipid species in units of mg/gDW

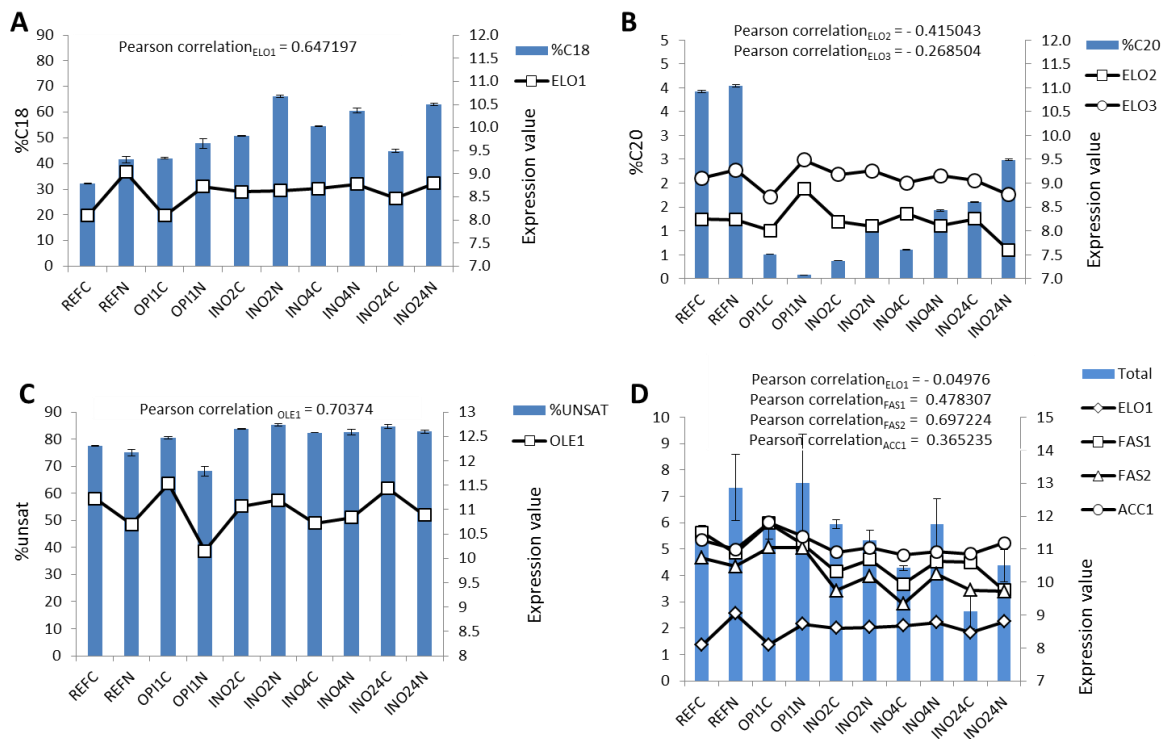


Figure S7. Correlations between the transcription level of fatty acid enzymes (synthase and elongases) and their products. **(A)** Correlation between expression value (\log_2) of *ELO1* and percentage of C18 fatty acids. **(B)** Correlation between expression value (\log_2) of *ELO2*, *ELO3* and percentage of C20 fatty acids. **(C)** Correlation between expression value (\log_2) of *OLE1* and percentage of unsaturated fatty acids. **(D)** Correlation between expression value (\log_2) of *ELO1*, *FASI*, *FAS2*, *ACCI* and total fatty acids in the unit of mmol/gDW.

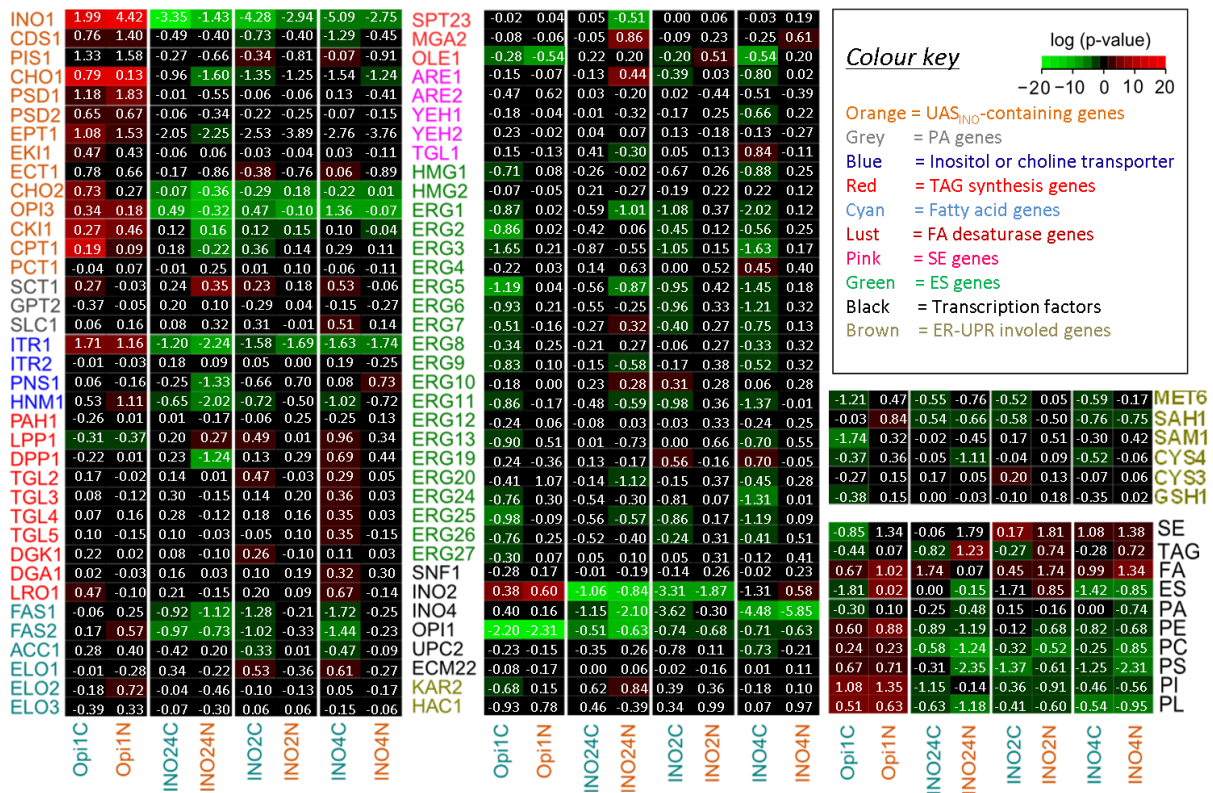


Table S1. The list of average molecular weights for phospholipid amount calculation.

Lipids	Average MW (g/mol)
PA	685.10
PE	706.19
PC	748.27
PS	772.18
PI	842.29

Table S2. Summary of over-representative biological process in of the significant genes which are positively correlated to *IN/O4* showing higher than 0.50 in Pearson correlation values.

Description	p-value	Gene in the test
cellular process	1.04E-13	APPL, ABC1, MDJ1, UBP10, SAP4, BNA5, CRH1, NSP1, EPT1, RET2, TRK2, GLT1, EMP47, PEX30, RTA1, RGT2, LCB5, SPOT71, PXR1, AAD15, SPO74, HIR3, MAM1, HFM1, DLD1, SRC1, ALR2, MGRI, PAN3, TOM70, VPS45, NRK1, PIM1, UBR2, SLN1, BEM4, FAR11, IMH1, RAD2, THI7, NUP42, MPE1, SRO77, YTA7, ACT1, PCL19, ECM18, CCC2, PYC1, GAT1, VBA2, GAT3, DUG3, RIC1, RPT6, JEM1, ARG4, COY1, AQR1, IZH1, HTD2, SMA1, RPS19A, SMP3, GDE1, ECM5, YIP3, RNT1, SSA2, HNM1, RPT4, ARF2, UBA1, SAM50, RT1, PHO5, ADD66, MSD1, PTC2, SPR28, MSR1, HEM2, MLH2, SAL1, MF(ALPHA)1, SKS1, KAR2, PBA1, FRE2, CUP1-2, CUP1-1, MPH1, GUP1, HST3, RNR3, MCDA2, VAM6, AD01, HSP60, TSA1, YRM1, UFD2, CDS1, SPO23, NOC2, RAD50, FAS1, FAS2, EEB1, MSB2, NOT3, CTM1, MOT2, SSC1, BO1, MOT3, HUG1, TH3, YME2, DAK1, MSP1, ATG11, FHL1, INO1, APC1, INO2, SPP382, AFG3, RPI1, BET3, NT1, SPO11, BET4, CK11, SPO13, CHO1, KTI11, AFG1, TYE7, MAS1, CHO2, THI21, PET112, PEX10, YRF1-5, CWC25, YRF1-6, YRF1-7, AAD3, YRF1-1, PMT3, YRF1-2, YRF1-3, YRF1-4, STV1, SAM3, SAM2, SRS2, GPI17, CBP2, MOGL, COG4, APS1, BCK1, HSP78, AAD4, ABZ1, INO80, VMR1, BSC6, OPI1, QDR1, OPI3, YDC1, TOP2, RPN9, ATG5, CLP1, HXT11, HXT12, PDI1, RPN6, FZO1, REC104, ITR1, PSD1, XDJ1, RGM1, ENT5, MMR1, URK1, SEC39, PMR1, RAD14, NPI4, BCH1, SMF1, CHS5, UBX2, SEC21, BDS1, TAT1, FKS3, SEC24, MET6, FAA1, SEC27, UBX6, MUC1, URA8, NS1, BPH1, SET2, DNA2, SAC6, SCL1, NNT1, AAH1, ZIP1, CPT1, RSF1, ERO1, ALG1, YTU2, PEX6, TPO4, BAP3, SIC1, RSC30, JLP1, AGA1, PCP1, RPS23A, SEY1, VPS16, RPS23B, UGO1, MGM1, NRG2, MSK1, CYS4, RSE1, REV1, SIT4, LHS1, IMD2, RPL31A, DRE2, GPBL, COQ1, SCJ1, LYS21, HSC82, BFR2, DSE4, DSE3, LYPL, SPT6, MNNS5, HAT2, SDA1, KRE5, SEC61, DSS1, RPA34, MATA1, PHA1, DNFL1, DIT2, MEP3, DIT1, ICT1, MS1, PDR1, NAM9, VPS35, ZWF1, NAM2, LPP1, PDR3, SCO1, MDL1, FOL1, SSM4, JIP5, ACC1, MSH5, SSK22, SAH1, EHT1, MON1, PHR1, PRM7, RPN11, YTA12, FIG2, CRN1, NEW1, RPB10, PHB2, TDPI, VPS27, HMLALPHA1, UTR2
phospholipid biosynthetic process	3.72E-08	URA8, CPT1, SMP3, MCD4, GAT1, INO1, INO2, PSD1, EPT1, CDS1, OPI3, CK11, OPI7, CHO1, ICI1, GUP1, CHO2
establishment of localization	8.45E-08	NSPL, VMR1, BSC6, OPI1, QDR1, TRK2, RET2, EMP47, PDR11, ATG5, RGT2, HXT11, HXT12, SRC1, ALR2, TOM70, VPS45, ITR1, IMH1, ENTS5, NUP42, THI7, SRO77, ACT1, SEC39, PMR1, NPL4, CCC2, BCH1, VBA2, SMF1, RIC1, CHS5, UBX2, COY1, AQR1, SEC24, FAAC1, TAT1, SEC21, FAP1, RPS19A, UBX6, SEC27, NIS1, BPH1, YIP3, SSA2, HNM1, ARF2, SAC6, SAM50, AUS1, ERO1, TPO4, PEK6, SAL1, BAP3, SKS1, KAR2, PCP1, FRE2, GUP1, VPS16, UGO1, MSK1, MCD4, VAM6, LHS1, YRM1, HSP60, NOC2, SCJ1, BFR2, SSS1, LYP1, AIG11, MSP1, AFG3, BEI3,

		BET4, SDA1, SEC61, DSS1, MEP3, DNF1, AFG1, MASI, SYG1, VPS35, PEX10, PDR5, SCO1, MDL1, ACC1, STV1, SAM3, MON1, MOG1, SFH5, COG4, APS1, YTA12, NEW1, HSP78, VPS27
transport	9.87E-08	NSP1, VMR1, BSC6, QDR1, TRK2, RET2, EMP47, PDR11, ATG5, RGT2, HXT11, HXT12, ALR2, TOM70, VPS45, ITR1, IMHI, ENT5, NUP42, TH17, SRO77, ACT1, SEC39, PMR1, NPL4, CCC2, BCH1, VBA2, SMF1, RIC1, CHS5, UBX2, COY1, AQR1, SEC21, TAT1, SEC24, FAAC1, RPS19A, SEC27, NIS1, BPH1, YIP3, SSA2, HNMI, ARF2, SAC6, SAM50, AUS1, ERO1, TPO4, PEX6, SAL1, BAP3, SKS1, KAR2, PCP1, FRE2, GUP1, VPS16, UBX6, SEC27, VAM6, LHS1, YRM1, HSF60, NOC2, SCJ1, BFR2, SSC1, LYPI, ATG11, MSPI, AFG3, BET3, BET4, SDA1, SEC61, DSS1, MEP3, DNF1, AFG1, MAS1, SYG1, VPS35, PEX10, PDR5, MDL1, SCO1, ACC1, STV1, SAM3, MON1, MOG1, SFH5, COG4, APS1, YTA12, NEW1, HSP78, VPS27
localization	1.34E-07	NSP1, VMR1, BSC6, OPI1, QDR1, TRK2, RET2, EMP47, PDR11, ATG5, RGT2, HXT11, HXT12, SRC1, ALR2, TOM70, VPS45, ITR1, IMHI, ENT5, NUP42, TH17, SRO77, YTA7, MMR1, ACT1, SEC39, PMR1, NPL4, CCC2, BCH1, VBA2, SMF1, RIC1, CHS5, UBX2, COY1, AQR1, SEC21, TAT1, SEC24, FAA1, RPS19A, UBX6, SEC27, NIS1, BPH1, YIP3, SSA2, HNMI, ARF2, SAC6, SAM50, AUS1, ERO1, TPO4, PEX6, SAL1, BAP3, SKS1, KAR2, PCP1, FRE2, GUP1, VPS16, UGO1, MSK1, MCD4, VAM6, LHS1, YRM1, HSP60, NOC2, SCJ1, BFR2, SSC1, LYPI, ATG11, MSPI, AFG3, BET3, BET4, SDA1, SEC61, SPO13, DSS1, DNF1, MEP3, AFG1, MAS1, SYG1, VPS35, PDR5, PEX10, SCO1, MDL1, ACC1, STV1, SAM3, MON1, MOG1, SFH5, COG4, APS1, YTA12, CRN1, NEW1, HSP78, PHB2, VPS27
cellular lipid metabolic process	2.55E-07	CPT1, ALG1, GAT1, INO1, INO2, EPT1, OPI1, CKI1, OPP3, YDC1, CHO1, ICT1, LCB5, IZH1, HTD2, GUPI, CHO2, FAA1, LPP1, URA8, HST3, SMP3, ACC1, GDE1, EHT1, PSD1, CDS1, GPI17, FAS1, FAS2, EEB1, COQ1
establishment of protein localization	3.39E-07	NSP1, PEX6, OPI1, RET2, ATG5, KAR2, PCP1, VPS16, SRC1, TOM70, VPS45, VAM6, LHS1, HSP60, IMHI, ENT5, NUP42, SCJ1, ACT1, SEC39, BFR2, NPL4, SSC1, BCH1, ATG11, MSPI, AFG3, BET4, SDA1, SEC61, RIC1, CHS5, UBX2, DNF1, AFG1, MASI, SEC21, VPS35, SEC24, PEX10, UBX6, SEC27, ACC1, STV1, BPH1, YIP3, MON1, SSA2, MOG1, COG4, APS1, YTA12, ARF2, HSP78, SAM50, VPS27
intracellular protein transport	7.93E-07	MSP1, NSP1, ATG11, PEX6, AFG3, BET4, SEC61, RIC1, RET2, DNF1, ATG5, PCP1, KAR2, AFG1, MAS1, SEC21, VPS35, VPS16, SEC24, PEX10, SEC27, ACC1, TOM70, VPS45, LHS1, BPH1, HSP60, MON1, SSA2, IMHI, MOG1, NUP42, APS1, YTA12, HSP78, SAM50, VPS27, SSC1
lipid biosynthetic process	1.28E-06	URA8, CPT1, SMP3, ACC1, MCD4, GAT1, INO1, INO2, PSD1, EPT1, OPI1, CDS1, CKI1, OPI3, GPI17, YDC1, FAS1, FAS2, COQ1, CHO1, ICT1, HTD2, CHO2, GUP1
glycerophospholipid biosynthetic process	1.57E-06	CPT1, SMP3, MCD4, PSD1, EPT1, CDS1, CKI1, GPI17, OPI3, CHO1, ICT1, GUP1, CHO2

macromolecule localization	1.66E-06	NSP1, PEX6, OPI1, RET2, PDR11, ATG5, PCP1, KAR2, VPS16, MSK1, SRC1, TOM70, VPS45, LHS1, VAM6, HSP60, IMH1, ENT5, NUP42, YTA7, SCJ1, ACT1, SEC39, BFR2, NPL4, SSC1, BCH1, ATG11, MSP1, AFG3, SDA1, BET4, SEC61, SPO13, RIC1, CHS5, DSS1, UBX2, DNF1, AFG1, MAS1, SEC21, VPS35, SEC24, PEX10, FAA1, RPS19A, UBX6, SEC27, ACC1, STV1, BPH1, YIP3, MON1, SSA2, MOG1, SFH5, COG4, APS1, ARF2, HSP78, SAM50, VPS27, AUS1
protein transport	1.99E-06	NSP1, PEX6, RET2, ATG5, KAR2, PCP1, VPS16, TOM70, VPS45, VAM6, LHS1, HSP60, IMH1, ENT5, NUP42, SCJ1, ACT1, SEC39, BFR2, NPL4, SSC1, BCH1, ATG11, MSP1, AFG3, BET4, SDA1, SEC61, RIC1, CHS5, UBX2, DNF1, AFG1, MAS1, SEC21, VPS35, SEC24, PEX10, SEC27, ACC1, BPH1, SSA2, MON1, MOG1, COG4, APS1, YTA12, ARF2, HSP78, SAM50, VPS27
phospholipid metabolic process	2.48E-06	URA8, CPT1, SMP3, GDE1, MCD4, GAT1, INO1, INO2, PSD1, EPT1, CDS1, CKI1, GPI17, CHO1, ICT1, GUP1, CHO2, LPP1
glycerolipid biosynthetic process	2.50E-06	CPT1, SMP3, MCD4, PSD1, EPT1, CDS1, CKI1, GPI17, OPI3, CHO1, ICT1, GUP1, CHO2
protein localization	3.16E-06	NSP1, PEX6, OPI1, RET2, ATG5, KAR2, PCP1, VPS16, SRC1, TOM70, VPS45, VAM6, LHS1, HSP60, IMH1, ENT5, NUP42, YTA7, SCJ1, ACT1, SEC39, BFR2, NPL4, SSC1, BCH1, ATG11, MSP1, AFG3, SDA1, BET4, SEC61, SPO13, RIC1, CHS5, UBX2, DNF1, AFG1, MAS1, SEC21, VPS35, SEC24, PEX10, UBX6, SEC27, ACC1, STV1, BPH1, YIP3, MON1, SSA2, MOG1, COG4, APS1, YTA12, ARF2, HSP78, SAM50, VPS27
phosphatidylcholine biosynthetic process	3.28E-06	CPT1, PSD1, CHO2, EPT1, CKI1, OPI3
telomere maintenance via recombination	3.52E-06	YRF1-5, YRF1-6, YRF1-7, YRF1-1, YRF1-2, YRF1-3, YRF1-4, RAD50
organophosphate metabolic process	4.22E-06	URA8, CPT1, SMP3, GDE1, MCD4, GAT1, INO1, INO2, PSD1, EPT1, OPI1, CDS1, CKI1, OPI3, GPI17, CHO1, ICT1, GUP1, CHO2, LPP1
intracellular transport	5.50E-06	NSP1, PEX6, SAL1, RET2, EMP47, ATG5, KAR2, PCP1, VPS16, MSK1, TOM70, VPS45, LHS1, HSP60, NOC2, IMH1, ENT5, NUP42, SRO77, ACT1, SEC39, SSC1, BCH1, ATG11, MSP1, AFG3, BET3, SDA1, SEC61, RIC1, CHS5, DSS1, DNF1, COY1, AFG1, MAS1, SEC21, VPS35, SEC24, PEX10, RPS19A, SEC27, ACC1, BPH1, YIP3, MON1, SSA2, MOG1, COG4, APS1, YTA12, NEW1, ARF2, HSP78, SAM50, VPS27
cellular protein localization	6.03E-06	NSP1, MSP1, ATG11, PEX6, AFG3, BET4, SEC61, SPO13, RIC1, RET2, DNF1, ATG5, PCP1, KAR2, AFG1, SEC21, MAS1, VPS35, VPS16, SEC24, PEX10, SEC27, ACC1, TOM70, VPS45, LHS1, BPH1, HSP60, MON1, SSA2, IMH1, MOG1, NUP42, APS1, YTA12, YTA7, HSP78, SAM50, VPS27, SSC1

intracellular protein transmembrane transport	8.00E-06	YTA12, TOM70, HSP78, PCP1, KAR2, LHS1, AFG3, HSP60, SEC61, SSA2, SSC1
lipid metabolic process	8.77E-06	CPT1, ALG1, GAT1, INO1, INO2, EPT1, OPI1, CKII, OPP3, YDC1, CHO1, ICT1, LCB5, IZH1, HTD2, GUP1, CHO2, FAA1, LPP1, URA8, HST3, SMP3, ACC1, GDE1, MCD4, EHT1, PSD1, CDS1, GPI17, FAS1, FAS2, FEB1, COQ1
transmembrane transport	1.08E-05	NSPL, VBA2, TPO4, AFG3, VMR1, BAP3, SALL1, BSC6, SEC61, QDR1, TRK2, MEP3, RGT2, PCP1, KAR2, AQR1, FRE2, TAT1, HXT11, HXT12, UGO1, MDL1, ALR2, TOM70, LHS1, STV1, ITT1, HSP60, YRM1, SAM3, SSA2, HNM1, NUP42, THI7, YTA12, HSP78, NPL4, CCC2, SSC1, LYP1
response to stimulus	1.12E-05	MDJ1, MLH2, INO80, OPI1, MF(ALPPHA)1, QDR1, SKS1, RSC30, ATG5, RTA1, AGA1, RGT2, KAR2, LCB5, FRE2, CUP1-2, CUP1-1, AAD15, MPH1, SEY1, SLH1, PAU1, REV1, PAN3, DAN4, SIT4, LHS1, HSP60, TSA1, YRM1, SLN1, UFD2, BEM4, FAR11, IMH1, RAD50, GPB1, RAD2, SC1, MSB2, HSC82, ACT1, RAD14, SSC1, HUG1, SPT6, DAK1, GAT1, HAT2, INO2, ARR2, ICT1, AQR1, AFG1, MSH1, IZH1, PDR1, BDS1, PDR5, ZWF1, PDR3, SCO1, AAD3, MSH5, SSK22, BPH1, SSA2, SRS2, PHR1, DNA2, FIG2, ARF2, HSP78, TDP1, SAC6, PHO5, AAD4, PTC2
phosphatidylcholine metabolic process	1.32E-05	CPT1, PSD1, CHO2, EPT1, CKII, OPI3
cellular macromolecule localization	1.39E-05	NSPL, MSP1, ATG11, PEX6, AFG3, BET4, SEC61, SPO13, RIC1, RET2, DNFI, ATG5, PCP1, KAR2, AFG1, SEC21, MAS1, VPS35, VPS16, SEC24, PEX10, SEC27, ACC1, TOM70, VPS45, LHS1, BPH1, HSP60, MON1, SSA2, IMH1, MOG1, NUP42, APS1, YTA12, YTA7, HSP78, SAM50, VPS27, SSC1
establishment of localization in cell	1.41E-05	NSPL, PEX6, SAL1, RET2, EMP47, ATG5, KAR2, PCP1, VPS16, MSK1, TOM70, VPS45, IHS1, HSP60, NOC2, IMH1, ENT5, NUP42, SRO77, ACT1, SEC39, PMR1, SSC1, BCH1, ATG11, MSP1, AFG3, BET3, SDA1, BET4, SEC61, RIC1, CHS5, DSS1, UBX2, DNFI, COY1, AFG1, MAS1, SEC21, VPS35, SEC24, PEX10, RPS19A, SEC27, ACC1, BPH1, YIP3, MON1, SSA2, MOG1, COG4, APS1, NEW1, ARF2, HSP78, SAM50, VPS27

Table S3. Summary of over-representative biological process in of the significant genes which are negatively correlated to *INO4* showing lower than -0.50 in Pearson correlation values.

Description	p-value	Gene in the test
mitochondrion organization	1.60E-68	MRPL40, YML6, MRPS35, MDJ1, MRS11, MRPL37, MRPL36, MRPL32, MGR2, FZO1, MRPL50, TOM70, MHRI, MSW1, PAM17, SLMS5, MRPL49, ATP12, ATP11, MSF1, MRPS18, MST1, TOM20, DIA4, MDM34, QR17, SHE9, MSE1, MDM35, SWS2, MRPS28, PNT1, TIM13, CCE1, SAM50, MSD1, MSR1, RPO41, MRPL13, RRF1, SAM37, PCP1, MRP17, UGO1, COX18, MGMI, MSK1, MRPL1, MSS2, COX23, MRPL6, ACO1, MRPL8, MRPL7, SHY1, MRPS5, HSP60, MRP4, MRPS9, RSM7, MRP7, MRPS8, PET123, BCS1, MRP2, SSC1, YME2, RSM18, RSM19, MSPI, MIA40, AFG3, TPM1, ISM1, MSY1, MRPL120, IMG1, MRPL11, IMG2, MRPL10, MRPL13, MRPL15, MRPL17, MRPL16, MASI, MGE1, MRPL19, NAM9, RSM10, MRF1, PET112, NAM2, ERV1, RSM26, TCM62, MRP20, MRP21, CBP4, MRPL31, IFM1, MRPL24, MRPL23, RPN11, MRPL22, YTA12, MRPL28, HSP78, MRPL27, PHB2, MRPL25, SLS1, RSM25, RSM23, DNMI, RSM22
mitochondrial translation	4.29E-59	YML6, MRPL40, MRPS35, MSR1, MRPL13, RRF1, MRPL51, MRPL36, MRPL37, MRPL38, MSK1, MRPL1, MRPL50, MRPL6, MRPL8, MRPL7, MRPS5, MSW1, MRP4, MRPS9, RSM7, MRP7, MRPS8, SLM5, MRP2, MRPS18, RSM18, RSM19, MST1, DIA4, ISM1, MSY1, MRPL20, IMG1, MRPL11, IMG2, MRPL10, MRPL13, MRPL15, MRPL17, MRPL16, MRPL19, NAM9, RSM10, MRF1, PET112, NAM2, MSE1, SWS2, RSM26, MRPS28, MRP20, MRP21, MRPL31, IFM1, MRPL22
organelle organization	2.23E-20	YML6, MRPL40, MRPS35, MDJ1, MRS11, PEX30, MSO1, TOP3, MRPL51, MRPL36, MRPL37, MRPL38, MRPL32, HFM1, MGR2, FZO1, SRC1, MRPL50, TOM70, VPS45, MHR1, MSW1, BEM4, MCM22, NUP42, MAD3, PAM17, SLMS5, MRPL49, ATP12, PEX27, ATP11, MSF1, MRPS18, MST1, TOM20, LST8, DIA4, MDM34, QR17, SHE9, MDM35, SRO7, MSE1, SWS2, MRPS28, PNT1, TIM13, CCE1, SAM50, GTS1, MSD1, ZIP1, MSR1, RPO41, MRPL13, RRF1, RDIL, PEX4, SAM37, LGE1, PCP1, KAR2, PAAL, MRPL17, UGO1, COX18, MGM1, MSS2, MRPL1, COX23, MRPL6, ACO1, MRPL8, MRPL7, VAM6, SHY1, MRPS5, HSP60, HIF1, SPO22, MRP4, MRPS9, RSM7, MRP27, MRPS8, APC9, PET123, BCS1, MRP2, SMC1, YME2, RSM18, RSM19, ATG12, MSP1, MIA40, HAT2, AFG3, TPM1, ISM1, MSY1, MRPL20, IMG1, MRPL11, IMG2, MRPL10, MRPL13, MRPL15, MRPL17, PEX17, MRPL16, AFG1, MGE1, MASI, MRPL19, NAM9, RSM10, MRF1, PEX12, PET112, PEX10, NAM2, ERV1, TCM62, RSM26, MRP20, MRP21, RXT3, TLG2, CBP4, MRPL31, IFM1, MRPL24, MRPL23, RPN11, MRPL22, YTA12, BCK1, MRPL28, MRPL27, HSP78, PHB2, MRPL25, SLS1, RSM25, RFA3, RFA2, DNMI, RSM23, RSM22
cellular component organization	4.25E-17	YML6, MRPL40, MRPS35, MDJ1, MRS11, PEX30, MSO1, TOP3, ATG5, MRP51, YTH1, MRPL36, SPO71, MRPL37, MRPL38, ATP23, MRPL32, HFM1, MGR2, FZO1, SRC1, MRPL50, TOM70, VPS45, MHR1, PIM1, MSW1, BEM4, MCM22, NUP42, MAD3, KTR3, PAM17, SLMS5, HBS1, MRPL49, ATP12, PEX27, ATP11, MSF1, MRPS18, MST1, TOM20, LST8, DIA4, HRD1, MDM34, FK53, QR17, SHE9, SMA1, MDM35, SRO7, MSE1, SWS2, MRPS28, OSH6, PNT1, TIM13, CCE1, SAM50, ADD66, GTS1, MSD1, SPR3,

		ZIP1, COX11, MSR1, RPO41, NAS6, MRP13, RDI1, RRF1, PEX4, SAM37, LGE1, CUP2, KAR2, PCP1, PAA1, PAA1, MRP17, SPS22, GUP1, COX18, UGO1, MGMI, MSK1, DAN2, COX23, MSS2, MRP11, MRP16, MCD4, ACO1, MRPL8, VAM6, MRPL7, SHY1, MRP55, HSP60, HIF1, SPO22, HPF1, MRP4, MRPS9, RSM7, MRP7, APC9, PET123, BCS1, MRP2, SSC1, YME2, RSM18, ATG12, RSM19, MSP1, VPH2, MIA40, HAT2, SPP382, AFG3, TPM1, DSS1, MRPL20, MSY1, ISM1, IMG1, MRPL11, IMG2, MRPL10, MRPL13, MRPL15, DIT1, PEX17, MRPL17, AFG1, MRPL16, MGE1, MRP1, RSM10, PEX12, PET112, NAM2, SCO1, ERV1, CDA1, PPM1, TCM62, CWC23, RSM26, MRP20, MRP21, HSV2, RXT3, TLG2, CBP4, RPB4, MRPL31, IFM1, MRPL24, MRPL23, RPN11, MRPL22, YTA12, BCK1, MRPL28, MRPL27, HSP78, PHB2, MRPL25, SLS1, CYT2, RSM25, RFA3, RFA2, DNM1, RSM23, RSM22	
tRNA aminoacylation for mitochondrial protein translation	3.03E-12	MSR1, SLM5, MST1, MSF1, MSD1, DIA4, MSW1, MSK1, MSE1, ISM1, MSY1	
cellular process	7.52E-12	MRPL40, UBP11, MDJ1, SAP4, ECM22, CAK1, UBP16, SLM3, MPD1, TBS1, TRK2, MSS18, EMP47, PEX30, RTA1, MRP51, MTG2, MRPL36, SPO71, MRPL37, AAD15, SPO74, MRPL38, MRP132, HFM1, OXR1, MGR2, DLD1, SRC1, MRP49, MGR1, MRPL50, TOM70, VPS45, PIM1, MSW1, BEM4, NUP42, SPO2, RRD2, KTR3, MTF2, ARH1, SLM5, HBS1, MRPL49, ATP12, PEX27, ATP11, MSF1, CCC2, PYC1, VBA2, MST1, EUG1, HRD1, ACPI, COY1, SNO3, SNO2, HAP5, MGA2, QRI7, SMA1, SRO7, QRI5, MSE1, SUV3, SGA1, GRX5, UBP5, ARF2, TIM13, CCE1, SAM50, ADD66, ISD11, GTS1, MSD1, COX11, MRS1, HEM2, COX10, NAS6, MLH2, RDH1, SAL1, SAM37, ISA2, HNT3, FRE6, CBT1, CUP2, CT2, KAR2, HNT1, PBA1, MSC6, PAA1, GUP1, MPH1, MSS1, SPS22, COX18, IAHL, MSS1, DAN2, COX23, MRPL1, MSS2, CDC8, MRPL6, MCD4, RNR3, ACO1, MRPL8, NMA2, VAM6, MRPL7, SHY1, MRPL9, HSP60, SPO22, HPP1, CBS2, NUS1, RSM7, MED8, APC9, PET123, CTM1, BO1, GYP7, SSC1, HUG1, YME2, DAK2, ATG12, CYM1, MSP1, SPP382, AFG3, BET3, NTA1, BET4, FPR2, MRPL20, MRPL11, MRPL10, MRPL13, MRPL15, PEX17, MRPL17, AFG1, MRPL16, MGE1, MASI, MRF1, MSS116, PEX12, PET112, PEX10, ERV1, CDA1, TCM62, AAD3, CWC23, PMT3, VTA1, ASK10, NAT2, HSV2, TLG2, EM12, CBP4, MRPL31, CBP2, IFM1, EM15, MRPL24, MRPL23, TEX1, MRPL22, BC1, MRPL28, MRPL27, HSP78, MRPL25, STE3, MHT1, PRE8, AAD4, RFA3, COG1, ABZ1, RFA2, DNMI, ABZ2, YML6, NBP35, MRPS35, DER1, ENBL, VMR1, PET8, QDR1, MRS11, MSO1, TOP3, HXT17, ATG5, CLP1, YTH1, TPT1, HXT13, YUH1, HXT11, HXT12, FZO1, REC104, MHR1, NCE103, XDJ1, MCM22, NFU1, MAD3, PAM17, MCH2, FAD1, PMR1, ADK2, NPL4, FET3, BCH1, MRPS18, MCI17, POL31, FMS1, CUS2, RML2, TOM20, LST8, DIA4, MDM34, SRX1, PYK2, MTQ1, SCS3, CPR6, MSM1, MNS1, BDS1, TAT1, FKS3, SHE9, MDM35, SWS2, MUC1, MRPS28, PET54, OSH6, ARN1, PNT1, CRC1, SCL1, PAD1, SPR3, ZIP1, ALG1, RPO41, MRPL13, MNP1, RRF1, RECI04, MNP1, RMD9, PCP1, REH1, SOL2, MRPL17, SOL1, NTG1, NTG2, UGO1, MGMI, MSK1, PRP46, LHS1, MRPS5, HIF1, IMD2, MAM33, ARL3, MRPs4, VID22, COQ3, COQ1, MRPS9, MRP7, MRPS8, APL3, PLM2, BCS1, MRP2, ADD37, RSM18, RSM19, HCS1, VPH2, HUA1, MIA40, ACB1, HAT2, TPM1, STL1, DSS1, MSY1, ISM1, IMG1, PDR8, MTM1, IMG2, LIP2, DIT1, NAM9, PDR1, RSM10, ZWF1, NAM2, MDL2, LPP1, SCO1, RSM28, PPM1, RSM26, MRP20, MRP21, RXT3, RPB4, RPN11, YTA12, BCK1, MRPL28, MRPL27, HSP78, PHB2, MRPL25, SLS1, CYT2, RSM23, RSM22	
protein targeting to	1.01E-09	TOM70, MSP1, MIA40, AFG3, HSP60, TOM20, SAM37, MRS11, YTA12, PAM17, HSP78, PCP1, TIM13, MAS1, MGE1, SAM50,	

mitochondrion		SSC1, ERV1
protein localization in mitochondrion	1.01E-09	TOM70, MSP1, MIA40, AFG3, HSP60, TOM20, SAM37, MRS11, YTA12, PAM17, HSP78, PCP1, TIM13, MAS1, MGE1, SAM50, SSC1, ERV1
cellular protein metabolic process	1.26E-09	YML6, MRPL40, MRPS35, UBP11, MDJ1, ECM22, DER1, CAK1, UBP16, MPD1, ATG5, RTA1, MRP51, MTG2, MRPL36, MRPL37, YUH1, MRPL38, MRPL32, MRP49, MGRL, MRPL50, PIM1, MSW1, XDJ1, NUP42, SIP2, RRI2, KTR3, MTF2, SLM5, HBS1, MRPL49, MSF1, NPL4, FET3, MRPS18, PYC1, MST1, RML2, EUG1, DIA4, HRD1, MTQ1, SCS3, CPR6, MSM1, MGA2, MSE1, SWS2, MRPS28, UBP5, SCL1, ADD66, PAD1, MSD1, MSR1, ALG1, MRPL13, MNPL, RRF1, PEX4, LGE1, RMD9, PCP1, KAR2, HNT1, MRPL17, NTGL, GUP1, UGO1, COX18, MSK1, MRPL1, COX23, MRPL6, MCD4, NMA2, MRPL8, MRPS5, HSP60, MRPL9, HIF1, HPFL, VID22, MRPS9, RSM7, NUS1, CBS2, MRPL7, MRPS8, APC9, PET123, CTM1, MRP2, SSC1, GYP7, ADD37, RSM18, RSM19, CYM1, ATG12, HUAI, ACB1, HAT2, AFG3, NTA1, FPR2, BET4, DSS1, MRPL20, MSY1, ISMI, IMG1, MRPL11, MTM1, IMG2, LIP2, MRPL10, MRPL13, MRPL15, MRPL17, AFG1, MRPL16, MRPL19, MGE1, MAS1, NAM9, MRFL, RSM10, PET112, PEX10, NAM2, RSM28, PPM1, TCM62, CWC23, RSM26, PMT13, MRPL20, RXT3, CBP4, MRPL31, IFM1, MRPL24, MRPL23, RPN11, MRPL22, YTA12, BCK1, MRPL28, MRPL27, HSP78, PHB2, SKM1, MRPL25, SLS1, CYT2, PRE8, RSM25, RFA3, ABZ1, RFA2, RSM23, RSM22
mitochondrial transport	2.10E-09	TOM70, MSP1, MIA40, AFG3, HSP60, TOM20, SAL1, SAM37, MRS11, YTA12, PAM17, HSP78, PCP1, TIM13, MAS1, MGE1, SAM50, MSK1, SSC1, ERV1
protein metabolic process	4.49E-09	YML6, MRPL40, NBP35, MRPS35, UBP11, MDJ1, ECM22, DER1, CAK1, UBP16, MPD1, ATG5, RTA1, MRP51, MTG2, MRPL36, MRPL37, YUH1, MRPL38, ATP23, MRPL32, MRP49, MGR1, MRPL50, PIM1, MSW1, XDJ1, NUP42, SIP2, RRI2, KTR3, MTF2, SLM5, HBS1, MRPL49, MSF1, NPL4, FET3, MRPS18, PYC1, MST1, RML2, EUG1, DIA4, HRD1, MTQ1, SCS3, CPR6, MSM1, MNS1, ORI7, MGA2, MSE1, SWS2, MRPS28, UBP5, SCL1, ADD66, PAD1, MSD1, MSR1, ALG1, NAS6, MRPL13, MNPL, RRF1, PEX4, ISA2, LGE1, RMD9, PCP1, KAR2, HNT1, MRPL17, NTGL, GUP1, UGO1, COX18, MSK1, MRPL1, COX23, MRPL6, MCD4, NMA2, MRPL8, MRPL7, MRPS5, HSP60, MRPL9, HIF1, HPFL, VID22, MRPS9, RSM7, NUS1, CBS2, MRPL7, MRPS8, APC9, PET123, CTM1, MRP2, SSC1, GYP7, ADD37, RSM18, ATG12, CYM1, RSM19, HUA1, ACB1, HAT2, AFG3, NTA1, BET4, FPR2, DSS1, MRPL20, MSY1, ISMI, IMG1, MRPL11, MTM1, IMG2, LIP2, MRPL10, MRPL13, MRPL15, MRPL17, AFG1, MRPL16, MRPL19, MGE1, MAS1, NAM9, MRFL, RSM10, PET112, PEX10, NAM2, RSM28, PPM1, TCM62, CWC23, RSM26, PMT3, MRPL20, MRP21, NAT2, RXT3, CBP4, MRPL31, IFM1, MRPL24, MRPL23, RPN11, MRPL22, YTA12, BCK1, MRPL28, MRPL27, HSP78, PHB2, SKM1, MRPL25, SLS1, CYT2, PRE8, RSM25, RFA3, ABZ1, RFA2, RSM23, RSM22
translation	9.20E-09	MRPL40, YML6, MRPS35, ECM22, MTG2, MRP51, MRPL37, MRPL36, MRPL38, MRPL32, MRP49, MRP50, MSW1, NUP42, MTF2, HBS1, SLM5, MRPL49, MSF1, FET3, MRPS18, MST1, RML2, DIA4, SCS3, MTQ1, MNPL, RMD9, HNT1, NTGL, MRP17, UGO1, COX18, MSK1, MRPL1, COX23, MRPL6, MSD1, PAD1, MSR1, MRPL13, RRF1, MNPL, PEX4, RMD9, HNT1, NTGL, MRP17, UGO1, COX18, MSK1, MRPL1, COX23, MRPL6, MRPL8, MRPL7, MRPL9, MRPS5, MRPS9, MRPS8, MRP7, PET123, MRP2, RSM18, RSM19, CYM1, ACB1, ISMI, MSY1, MRPL20, MRPL11, IMG1, MRPL10, IMG2, MTM1, MRPL13, MRPL15, MRPL17, MRPL16, MRPL19, NAM9,

		RSM10, MRF1, PET112, NAM2, RSM28, RSM26, MRP20, MRP21, CBP4, MRPL31, IFM1, MRPL24, MRPL23, MRPL22, MRPL28, MRPL27, MRPL25, SLS1, RSM25, RSM23, ABZ1, RSM22
intracellular protein transmembrane transport	1.70E-08	TOM70, LHS1, MIA40, AFG3, HSP60, TOM20, YTA12, HSP78, PAM17, KAR2, PCP1, SLS1, MGE1, SSC1, ERV1
tRNA aminoacylation	9.98E-08	MSR1, MST1, MSW1, DIA4, MSY1, ISM1, MSM1, SLM5, MSF1, PET112, MSD1, NAM2, MSE1, MSK1
amino acid activation	9.98E-08	MSR1, MST1, MSW1, DIA4, MSY1, ISM1, MSM1, SLM5, MSF1, PET112, MSD1, NAM2, MSE1, MSK1
tRNA aminoacylation for protein translation	2.89E-07	MSR1, MST1, MSW1, DIA4, MSY1, ISM1, MSM1, SLM5, MSF1, MSD1, MSE1, MSK1, NAM2
protein import into mitochondrial intermembrane space	3.55E-07	YTA12, PCP1, MIA40, AFG3, HSP60, ERV1
protein import	6.21E-07	TOM70, MSP1, MIA40, AFG3, HSP60, TOM20, PEX4, SAM37, MRS11, NUP42, YTA12, PAM17, HSP78, PEX17, PCP1, AFG1, TIM13, MASI, MGE1, SAM50, PEX12, PEX10, SSC1, ERV1
mitochondrial genome maintenance	2.21E-06	MGR2, YM2, MDJ1, RPO41, HSP78, ACO1, MRPL8, MHR1, CCE1, UGO1, QRI7, MGM1
Group I intron splicing	3.82E-06	SUV3, PET54, MSS116, NAM2, CBP2, MSS18
RNA splicing, via transesterification reactions with guanosine as nucleophile	3.82E-06	SUV3, PET54, MSS116, NAM2, CBP2, MSS18
mitochondrial membrane organization	4.68E-06	MSS2, TOM70, PNT1, TIM13, TOM20, SAM50, MSF1, COX18, SHE9, SAM37, MRS11
aerobic respiration	1.00E-05	MRPS35, DLID1, MRPL1, MIC17, COX11, ACO1, RPO41, MNP1, SHY1, MAM33, DIA4, EMIS, MRPL22, RMD9, CHT2, SLS1, MRF1, BCS1
cellular protein complex	1.37E-05	PPM1, COX23, TCM62, NAS6, VPH2, PIM1, SHY1, HSP60, TOM20, CBP4, SAM37, DSSI, CBT1, PEX17, PBA1, ATP12, CYT2,

assembly		ATP11, ADD66, BCS1, MDM35, SCO1
regulation of mitochondrion organization	1.89E-05	HSP78, MHHR1, PET54, NTG1, MSS51, PET494

Table S4. Summary of over-representative biological process in of the significant genes which are positively correlated to *INO2* showing higher than 0.50 in Pearson correlation values.

Description	p-value	Gene in the test
lipid biosynthetic process	4.56E-11	CPT1, ACC1, INO1, PSD1, INO4, EPT1, CDS1, CKI1, OPI3, FAS1, CHO2, HTD2, CHO2, FEN1
phosphatidylcholine biosynthetic process	2.33E-10	CPT1, CHO2, PSD1, EPT1, CKI1, OPI3
phosphatidylcholine metabolic process	1.01E-09	CPT1, CHO2, PSD1, EPT1, CKI1, OPI3
cellular lipid metabolic process	2.77E-09	CPT1, ACC1, INO1, EHT1, PSD1, INO4, EPT1, CDS1, CKI1, OPI3, FAS1, FAS2, CHO1, HTD2, CHO2, FEN1
ethanolamine and derivative metabolic process	3.22E-09	CPT1, CHO2, PSD1, EPT1, CKI1, OPI3
phospholipid biosynthetic process	5.02E-09	CPT1, CHO1, INO1, CHO2, INO4, PSD1, EPT1, CDS1, CKI1, OPI3
small molecule metabolic process	8.77E-09	SPE3, CPT1, INO1, ADH7, EPT1, CKI1, OPI3, SAP30, ARG4, CHO1, GLO2, HTD2, CHO2, URA10, FEN1, FOL1, URA5, ACC1, HIS3, ADO1, SAHI, EHT1, PSD1, SAM2, SET2, FAS1, XPT1, NNT1
lipid metabolic process	2.62E-08	CPT1, ACC1, INO1, EHT1, PSD1, INO4, EPT1, CDS1, CKI1, OPI3, FAS1, FAS2, CHO1, HTD2, CHO2, FEN1
glycerophospholipid biosynthetic process	5.50E-08	CPT1, CHO1, CHO2, PSD1, EPT1, CDS1, CKI1, OPI3
glycerolipid biosynthetic process	7.48E-08	CPT1, CHO1, CHO2, PSD1, EPT1, CDS1, CKI1, OPI3
cellular biogenic amine metabolic process	8.89E-08	SPE3, CPT1, CHO2, PSD1, EPT1, CKI1, OPI3
small molecule biosynthetic process	3.81E-07	SPE3, FOL1, ACC1, URAS5, HIS3, INO1, ADO1, EPT1, SAM2, CKI1, FAS1, XPT1, ARG4, HTD2, URA10, FEN1
phospholipid metabolic process	3.92E-07	CPT1, CHO1, INO1, CHO2, INO4, PSD1, EPT1, CDS1, CKI1, OPI3
organophosphate metabolic process	5.35E-07	CPT1, CHO1, INO1, CHO2, INO4, PSD1, EPT1, CDS1, CKI1, OPI3

cellular amino acid derivative metabolic process	6.63E-07	SPE3, CPT1, CHO2, PSD1, EPT1, SAM2, CKI1, OPI3
glycerophospholipid metabolic process	1.68E-06	CPT1, CHO1, CHO2, PSD1, EPT1, CDS1, CKI1, OPI3
fatty acid biosynthetic process	2.67E-06	FAS1, FAS2, ACC1, HTD2, FEN1
glycerolipid metabolic process	2.92E-06	CPT1, CHO1, CHO2, PSD1, EPT1, CDS1, CKI1, OPI3
cellular biosynthetic process	9.56E-06	SPE3, CPT1, RSF1, RPL22A, DPH5, INO1, INO4, EPT1, CKI1, OPI3, SAP30, ARG4, AGA1, CHO1, KAR4, HTD2, CHO2, NRG2, FEN1, URA10, FOL1, ACC1, URAS3, ADO1, SAM3, PSD1, CDS1, RPL31A, PRI1, SAM2, SET2, PRM7, FAS1, SSN3, FAS2, XPT1, FIG2, BSC1, TMA20, MOT2
amine metabolic process	1.36E-05	SPE3, FOL1, CPT1, HIS3, SAH1, PSD1, EPT1, CKI1, SAM2, OPI3, ARG4, CHO2, UTR2
biosynthetic process	1.45E-05	SPE3, CPT1, RSF1, RPL22A, DPH5, INO1, INO4, EPT1, CKI1, OPI3, SAP30, ARG4, AGA1, CHO1, KAR4, HTD2, CHO2, NRG2, FEN1, URA10, FOL1, ACC1, URAS3, ADO1, SAM3, PSD1, CDS1, RPL31A, PRI1, SAM2, SET2, PRM7, FAS1, SSN3, FAS2, XPT1, FIG2, BSC1, TMA20, MOT2
cellular amine metabolic process	2.16E-05	FOL1, SPE3, CPT1, ARG4, HIS3, SAH1, CHO2, PSD1, EPT1, SAM2, CKI1, OPI3
lipid biosynthetic process	4.56E-11	CPT1, ACC1, INO1, PSD1, INO4, EPT1, CDS1, CKI1, OPI3, FAS2, CHO1, HTD2, CHO2, FEN1
phosphatidylcholine biosynthetic process	2.33E-10	CPT1, CHO2, PSD1, EPT1, CKI1, OPI3
phosphatidylcholine metabolic process	1.01E-09	CPT1, CHO2, PSD1, EPT1, CKI1, OPI3
cellular lipid metabolic process	2.77E-09	CPT1, ACC1, INO1, EHT1, PSD1, INO4, EPT1, CDS1, CKI1, OPI3, FAS2, CHO1, HTD2, CHO2, FEN1
ethanolamine and derivative metabolic process	3.22E-09	CPT1, CHO2, PSD1, EPT1, CKI1, OPI3
phospholipid biosynthetic process	5.02E-09	CPT1, CHO1, INO1, CHO2, INO4, PSD1, EPT1, CDS1, CKI1, OPI3
small molecule metabolic process	8.77E-09	SPE3, CPT1, INO1, ADH7, EPT1, CKI1, OPI3, SAP30, ARG4, CHO1, GLO2, HTD2, CHO2, URA10, FEN1, FOL1, URAS5, ACC1, HIS3, ADO1, SAH1, EHT1, PSD1, SAM2, SET2, FAS1, XPT1, NNT1
lipid metabolic process	2.62E-08	CPT1, ACC1, INO1, EHT1, PSD1, INO4, EPT1, CDS1, CKI1, OPI3, FAS2, CHO2, HTD2, CHO2, FEN1

glycerophospholipid biosynthetic process	5.50E-08	CPT1, CHO1, CHO2, PSD1, EPT1, CDS1, CKI1, OPI3
glycerolipid biosynthetic process	7.48E-08	CPT1, CHO1, CHO2, PSD1, EPT1, CDS1, CKI1, OPI3
cellular biogenic amine metabolic process	8.89E-08	SPE3, CPT1, CHO2, PSD1, EPT1, CKI1, OPI3
small molecule biosynthetic process	3.81E-07	SPE3, FOL1, ACC1, URA5, HIS3, INO1, ADO1, EPT1, SAM2, CKI1, FAS1, FAS2, XPT1, ARG4, HTD2, URA10, FEN1
phospholipid metabolic process	3.92E-07	CPT1, CHO1, INO1, CHO2, INO4, PSD1, EPT1, CDS1, CKI1, OPI3
organophosphate metabolic process	5.35E-07	CPT1, CHO1, INO1, CHO2, INO4, PSD1, EPT1, CDS1, CKI1, OPI3
cellular amino acid derivative metabolic process	6.63E-07	SPE3, CPT1, CHO2, PSD1, EPT1, SAM2, CKI1, OPI3
glycerophospholipid metabolic process	1.68E-06	CPT1, CHO1, CHO2, PSD1, EPT1, CDS1, CKI1, OPI3
fatty acid biosynthetic process	2.67E-06	FAS1, FAS2, ACC1, HTD2, FEN1
glycerolipid metabolic process	2.92E-06	CPT1, CHO1, CHO2, PSD1, EPT1, CDS1, CKI1, OPI3
cellular biosynthetic process	9.56E-06	SPE3, CPT1, RSF1, RPL22A, DPH5, INO4, EPT1, CKI1, OPI3, SAP30, ARG4, AGA1, CHO1, KAR4, HTD2, CHO2, NRG2, FEN1, URA10, FOL1, ACC1, URA5, HIS3, ADO1, SAM3, PSD1, CDS1, RPL31A, PRI1, SAM2, SET2, PRM7, FAS1, SSN3, FAS2, XPT1, FIG2, BSC1, TMA20, MOT2
amine metabolic process	1.36E-05	SPE3, FOL1, CPT1, HIS3, SAH1, PSD1, EPT1, CKI1, SAM2, OPI3, ARG4, CHO2, UTR2
biosynthetic process	1.45E-05	SPE3, CPT1, RSF1, RPL22A, DPH5, INO4, EPT1, CKI1, OPI3, SAP30, ARG4, AGA1, CHO1, KAR4, HTD2, CHO2, NRG2, FEN1, URA10, FOL1, ACC1, URA5, HIS3, ADO1, SAM3, PSD1, CDS1, RPL31A, PRI1, SAM2, SET2, PRM7, FAS1, SSN3, FAS2, XPT1, FIG2, BSC1, TMA20, MOT2
cellular amine metabolic process	2.16E-05	FOL1, SPE3, CPT1, ARG4, HIS3, SAH1, CHO2, PSD1, EPT1, SAM2, CKI1, OPI3

Table S5. Summary of over-representative biological process in of the significant genes which are negatively correlated to *INO2* showing lower than -0.50 in Pearson correlation values.

Description	p-value	Gene in the test
intracellular protein transport	8.36E-10	MSP1, NSP1, ATG11, PEX6, AFG3, BET4, SEC61, RIC1, RET2, DNF1, ATG5, PCP1, KAR2, AFG1, MASI, SEC21, VPS35, VPS16, SEC24, PEX10, SEC27, TOM70, VPS45, LHS1, BPH1, HSP60, MON1, SSA2, IMH1, NUP42, APS1, YTA12, HSP78, SAM50, VPS27, SSC1
establishment of protein localization	2.10E-09	NSP1, PEX6, OPI1, RET2, ATG5, KAR2, PCP1, VPS16, SRC1, TOM70, VPS45, VAM6, LHS1, HSP60, IMH1, NUP42, SCJ1, ACT1, SEC39, NPL4, SSC1, BCH1, ATG11, MSP1, AFG3, BET4, SEC61, RIC1, CHS5, UBX2, DNF1, AFG1, MASI, SEC21, VPS35, SEC24, PEX10, SEC27, STV1, BPH1, SSA2, MON1, COG4, APS1, YTA12, ARF2, HSP78, SAM50, VPS27
protein transport	4.54E-09	BCH1, NSP1, MSP1, ATG11, PEX6, AFG3, BET4, SEC61, CHS5, RIC1, RET2, UBX2, DNF1, ATG5, PCP1, KAR2, AFG1, SEC21, MASI, VPS35, VPS16, SEC24, PEX10, SEC27, TOM70, VPS45, LHS1, VAM6, BPH1, HSP60, MON1, SSA2, IMH1, COG4, NUP42, APS1, YTA12, SCJ1, ARF2, HSP78, ACT1, SEC39, SAM50, VPS27, NPL4, SSC1
cellular protein localization	5.21E-09	NSP1, MSP1, ATG11, PEX6, AFG3, BET4, SEC61, SPO13, RIC1, RET2, DNF1, ATG5, PCP1, KAR2, AFG1, MASI, SEC21, VPS35, VPS16, SEC24, PEX10, SEC27, TOM70, VPS45, LHS1, BPH1, HSP60, MON1, SSA2, IMH1, NUP42, APS1, YTA12, YTA7, HSP78, SAM50, VPS27, SSC1
protein localization	1.34E-08	NSP1, PEX6, OPI1, RET2, ATG5, KAR2, PCP1, VPS16, SRC1, TOM70, VPS45, VAM6, LHS1, HSP60, IMH1, NUP42, YTA7, SCJ1, ACT1, SEC39, NPL4, SSC1, BCH1, ATG11, MSP1, AFG3, BET4, SEC61, SPO13, RIC1, CHS5, UBX2, DNF1, AFG1, MASI, SEC21, VPS35, SEC24, PEX10, SEC27, STV1, BPH1, SSA2, MON1, COG4, APS1, YTA12, ARF2, HSP78, SAM50, VPS27
cellular macromolecule localization	1.36E-08	NSP1, MSP1, ATG11, PEX6, AFG3, BET4, SEC61, SPO13, RIC1, RET2, DNF1, ATG5, PCP1, KAR2, AFG1, MASI, SEC21, VPS35, VPS16, SEC24, PEX10, SEC27, TOM70, VPS45, LHS1, BPH1, HSP60, MON1, SSA2, IMH1, NUP42, APS1, YTA12, YTA7, HSP78, SAM50, VPS27, SSC1
macromolecule localization	2.32E-08	NSP1, PEX6, OPI1, RET2, PDR11, ATG5, KAR2, PCP1, VPS16, MSK1, SRC1, TOM70, VPS45, VAM6, LHS1, HSP60, IMH1, NUP42, YTA7, SCJ1, ACT1, SEC39, NPL4, SSC1, DSS1, UBX2, DNF1, AFG1, MASI, SEC21, VPS35, SEC24, PEX10, SEC27, STV1, BPH1, SSA2, SFH5, COG4, APS1, YTA12, ARF2, HSP78, SAM50, VPS27, AUS1

cellular process	3.40E-08	APP1, ABC1, MDJ1, SAP4, BNA5, CRH1, NSP1, RET2, TRK2, EMP47, PEX30, RTA1, LCB5, SPO71, AAD15, SPO74, HIR3, MAMI, HFMI, SRC1, DLD1, PAN3, MGRI, TOM70, VPS45, PIM1, UBR2, SLN1, BEM4, FAR11, IMH1, RAD2, NUP42, MP1, YTA7, ACT1, PYC1, VBA2, RIC1, RPT6, JEM1, COY1, IZH1, SMA1, SMP3, GDE1, ECM5, SSA2, RPT4, ARF2, UBA1, SAM50, ADD66, MSD1, SPR28, MSL1, MLH2, SAL1, SKS1, KAR2, PBA1, FRE2, CUP1-2, CUP1-1, MPH1, GUP1, HST3, RNR3, MCD4, NM2, VAM6, YRM1, TAA1, HSP60, UFD2, SPO23, RAD50, MSB2, CTM1, BO1, SSC1, HUG1, YME2, ATG11, MSP1, DAK1, FHL1, APC1, AFG3, SPP382, NTA1, BET3, BET4, SPO13, AFG1, MAS1, THI21, PET112, PEX10, YRF1-5, CWC25, YRF1-6, YRF1-7, AAD3, YRF1-1, PMT3, YRF1-2, YRF1-3, YRF1-4, STV1, SRS2, GP117, CBP2, COG4, APS1, BCK1, HSP78, AAD4, ABZ1, INO80, VMR1, OPI1, QDR1, YDC1, TOP2, RPN9, ATG5, CLP1, HXT11, HXT12, PD11, RPN6, FZO1, REC104, XDI1, MMR1, SEC39, PMR1, NPL4, RAD14, BCH1, SMF1, CHS5, UBX2, SEC21, BDS1, TAT1, SEC24, FKS3, SEC27, MUC1, NIS1, BPH1, DNA2, SCL1, ZIP1, ERO1, ALG1, PEX6, BAP3, SIC1, RSC30, JLP1, PCP1, VPS16, SEY1, RPS23A, UGO1, RPS23B, MGR1, MSK1, RSE1, LHS1, IMD2, DRE2, GPB1, COQ1, SCJ1, HSC82, DSE4, DSE3, SPT6, HAT2, SEC61, KRE5, DSS1, DIT2, DNFI, DT1, ICT1, PDR1, NAM9, VPS35, ZWF1, NAM2, LPPI, PDR3, SCO1, MDL1, SSM4, MSH5, SSK22, MON1, PHR1, RPN11, YTA12, CRN1, PHB2, TDP1, VPS27	
localization	6.40E-08	ERO1, NSP1, PEX6, VMR1, BAP3, SAL1, OPI1, QDR1, RET2, TRK2, SKS1, EMP47, PDR11, ATG5, PCP1, KAR2, FRE2, GUP1, HXT11, VPS16, HXT12, UGO1, MSK1, SRC1, TOM70, MCD4, VPS45, LHS1, VAM6, HSP60, YRML, IMH1, NUP42, MMR1, YTA7, SCJ1, ACT1, SEC39, PMR1, NPL4, CCC2, SSC1, BCH1, MSPI, ATG11, VBA2, AFG3, SMF1, BET3, BET4, SEC24, FKS3, SEC61, SPO13, CHS5, RIC1, DSS1, UBX2, DNFI, COY1, AFG1, SEC21, MAS1, VPS35, TAT1, SEC24, PDR5, PEX10, SEC27, SCO1, MDL1, NIS1, STV1, BPH1, MON1, SSA2, SFH5, COG4, APS1, YTA12, CRN1, PHB2, VPS27, AUS1	
transport	1.25E-07	ERO1, NSP1, PEX6, VMR1, BAP3, SAL1, OPI1, QDR1, RET2, TRK2, SKS1, EMP47, PDR11, ATG5, PCP1, KAR2, FRE2, GUP1, HXT11, VPS16, HXT12, UGO1, MSK1, SRC1, TOM70, MCD4, VPS45, LHS1, VAM6, HSP60, YRML, NUP42, SCJ1, ACT1, SEC39, PMR1, NPL4, CCC2, SSC1, BCH1, MSPI, ATG11, VBA2, AFG3, SMF1, BET3, BET4, SEC61, CHS5, RIC1, DSS1, UBX2, DNFI, COY1, AFG1, SEC21, MAS1, VPS35, TAT1, SEC24, PDR5, PEX10, SEC27, SCO1, MDL1, NIS1, STV1, BPH1, MON1, SSA2, SFH5, COG4, APS1, YTA12, ARF2, HSP78, SAM50, VPS27, AUS1	
establishment of localization	1.27E-07	ERO1, NSP1, PEX6, VMR1, BAP3, SAL1, OPI1, QDR1, RET2, TRK2, SKS1, EMP47, PDR11, ATG5, PCP1, KAR2, FRE2, GUP1, HXT11, VPS16, HXT12, UGO1, MSK1, SRC1, TOM70, MCD4, VPS45, LHS1, VAM6, HSP60, YRML, IMH1, NUP42, SCJ1, ACT1, SEC39, PMR1, NPL4, CCC2, SSC1, BCH1, MSPI, ATG11, VBA2, AFG3, SMF1, BET3, BET4, SEC61, CHS5, RIC1, DSS1, UBX2, DNFI, COY1, AFG1, SEC21, MAS1, VPS35, TAT1, SEC24, PDR5, PEX10, SEC27, SCO1, MDL1, NIS1, STV1, BPH1, MON1, SSA2, SFH5, COG4, APS1, YTA12, ARF2, HSP78, SAM50, VPS27, AUS1	

response to stimulus	1.50E-07	MDJ1, MLH2, INO80, OPI1, QDR1, SKS1, RSC30, RTA1, ATG5, KAR2, LCB5, FRE2, CUP1-2, CUP1-1, MPH1, AAD15, SEY1, SLH1, PAU1, DAN4, PAN3, LHS1, TSA1, HSP60, YRM1, SLN1, UFD2, BEM4, FAR11, IMH1, RAD50, GPB1, RAD2, SCJ1, MSB2, HSC82, ACT1, RAD14, SSC1, HUG1, SPT6, DAK1, HAT2, ARR2, ICT1, AFG1, IZH1, PDR1, BDS1, PDR5, ZWF1, PDR3, SCO1, AAD3, MSH5, SSK22, BPH1, SSA2, SRS2, PHR1, DNA2, BCK1, ARF2, HSP78, TDPI, AAD4
intracellular transport	2.16E-07	BCH1, NSP1, MSP1, ATG11, PEX6, AFG3, BET3, SAL1, BET4, SEC61, CHS5, RIC1, RET2, DSS1, EMP47, DNFI, ATG5, COY1, PCP1, KAR2, AFG1, SEC21, MAS1, VPS35, VPS16, SEC24, PEX10, MSK1, SEC27, TOM70, VPS45, LHS1, BPH1, HSP60, MON1, SSA2, IMH1, COG4, APS1, NUP42, YTA12, HSP78, ARF2, ACT1, SEC39, SAM50, VPS27, SSC1
telomere maintenance via recombination	2.61E-07	YRF1-5, YRF1-6, YRF1-7, YRF1-1, YRF1-2, YRF1-3, YRF1-4, RAD50
intracellular protein transmembrane transport	2.75E-07	YTA12, TOM70, HSP78, PCP1, KAR2, LHS1, AFG3, HSP60, SEC61, SSA2, SSC1
cellular localization	3.33E-07	NSP1, PEX6, SAL1, RET2, EMP47, ATG5, KAR2, PCP1, VPS16, MSK1, TOM70, VPS45, LHS1, HSP60, IMH1, NUP42, YTA7, MMR1, ACT1, SEC39, PMR1, SSC1, BCH1, ATG11, MSP1, AFG3, BET3, BET4, SEC61, SPO13, RIC1, CHS5, DSSI, UBX2, DNFI, COY1, AFG1, MAS1, SEC21, VPS35, SEC24, PEX10, SEC27, BPH1, MON1, SSA2, COG4, APS1, YTA12, CRN1, ARF2, HSP78, PHB2, SAM50, VPS27
establishment of localization in cell	3.55E-07	NSP1, PEX6, SAL1, RET2, EMP47, ATG5, KAR2, PCP1, VPS16, MSK1, TOM70, VPS45, LHS1, HSP60, IMH1, NUP42, ACT1, SEC39, PMR1, SSC1, BCH1, ATG11, MSP1, AFG3, BET3, BET4, SEC61, RIC1, CHS5, DSSI, UBX2, DNFI, COY1, AFG1, MAS1, SEC21, VPS35, SEC24, PEX10, SEC27, BPH1, SSA2, MON1, COG4, APS1, YTA12, ARF2, HSP78, SAM50, VPS27
protein targeting	8.88E-07	ATG11, NSP1, AFG3, PEX6, BET4, SEC61, ATG5, KAR2, PCP1, AFG1, MAS1, VPS16, PEX10, TOM70, VPS45, LHS1, HSP60, SSA2, MON1, NUP42, YTA12, HSP78, SAM50, VPS27, SSC1
proteasome assembly	2.67E-06	RPN9, RPT4, HSC82, PBA1, ADD66, DSS1, RPN6, RPT16
cellular component organization	3.55E-06	APP1, MDJ1, CRH1, NSP1, INO80, RET2, TOP2, RPN9, PEX30, ATG5, SPO71, HIR3, MAM1, HFM1, RPN6, SRC1, FZO1, TOM70, VPS45, PIM1, BEM4, NUP42, MPE1, MMR1, ACT1, SEC39, RAD14, CHS5, RPT6, JEM1, SEC24, FKS3, SMA1, ECM5, BPH1, DNA2, RPT4, SAM50, ADD66, MSD1, SPR28, ZIP1, MSR1, PEX6, RSC30, KAR2, PCP1, PBA1, GUP1, VPS16, SEY1, UGO1, MGM1, RSE1, HST3, MCD4, VAM6, HSP60, DRE2, RAD50, MSB2, HSC82, SSC1, YME2, AFG3, SPP382, HAT2, KRE5, SPO13, DSSI, DIT2, DNFI, DIT1, AFG1, MAS1, NAM9, PET12, PEX10, NAM2, SCO1, YRF1-5, YRF1-6, YRF1-7, YRF1-1,

		YRF1-2, YRF1-3, YRF1-4, RPN11, YTA12, BCK1, HSP78, CRN1, PHB2
mitochondrial transport	5.57E-06	YTA12, TOM70, HSP78, MSP1, PCP1, MAS1, AFG3, HSP60, SAM50, SAL1, MSK1, SSC1
proteolysis	8.21E-06	MDI1, YPS5, APC1, AFG3, RPT6, DSS1, RPN9, JEM1, UBX2, KAR2, AFG1, MAS1, ECM29, RPN6, SSM4, MGRI, PIM1, UFD2, GPB1, RPN11, RPT4, YTA12, UBA1, SCJ1, PRD1, SCL1, ADD66, NPL4
proteolysis involved in cellular protein catabolic process	8.47E-06	SSM4, MDI1, MGRI, APC1, PIM1, UFD2, DSS1, RPT6, GPB1, RPN9, JEM1, UBX2, KAR2, AFG1, ECM29, RPN6, SSM4, AFG1, SCL1, ADD66, NPL4, RPN6
protein catabolic process	1.05E-05	MDI1, PYC1, APC1, AFG3, NTA1, RPT6, DSS1, YDC1, RPN9, JEM1, UBX2, KAR2, AFG1, ECM29, RPN6, SSM4, MGR1, NMA2, PIM1, UFD2, GPB1, RPN11, RPT4, YTA12, SCJ1, SCL1, ADD66, NPL4
response to stress	1.35E-05	MDI1, SPT6, DAK1, HAT2, MLH2, INO80, OPI1, RSC30, ATG5, RTA1, ICT1, KAR2, LCB5, CUP1-2, AFG1, CUP1-1, MPH1, SEY1, ZWFL1, PAU1, PAN3, DAN4, MSH5, LHS1, SSK22, HSP60, TSA1, SLN1, UFD2, SRS2, SSA2, PHR1, IMHI, RAD50, DNA2, RAD2, BCK1, SCJ1, HSP78, ARF2, MSB2, TDPI, HSC82, ACT1, AAD4, RAD14, SSC1, HUG1
protein localization in organelle	1.63E-05	TOM70, NSP1, MSP1, LHS1, AFG3, HSP60, SEC61, SSA2, NUP42, YTA12, HSP78, KAR2, PCP1, MAS1, VPS35, SAM50, VPS27, SSC1
protein targeting to mitochondrion	1.86E-05	YTA12, TOM70, HSP78, MSP1, PCP1, MAS1, AFG3, HSP60, SAM50, SSC1
protein localization in mitochondrion	1.86E-05	YTA12, TOM70, HSP78, MSP1, PCP1, MAS1, AFG3, HSP60, SAM50, SSC1
homeostatic process	2.34E-05	YRF1-5, YRF1-6, YRF1-7, YRF1-1, YRF1-2, YRF1-3, VPS45, STV1, YRF1-4, TSA1, SMF1, TRK2, RAD50, DNA2, EMP47, HSC82, IZH1, VPS35, VPS16, PMR1, PDI1, CCC2, SSSC1, SCO1

Paper III

Mapping the interaction of Snf1 with TORC1 in *Saccharomyces cerevisiae*

Zhang, J., S. Vaga, **P. Chumnanpuen**, R. Kumar, G. N. Vemuri, R. Aebersold, and J. Nielsen

Molecular Systems Biology 2011, 7.

Mapping the interaction of Snf1 with TORC1 in *Saccharomyces cerevisiae*

Jie Zhang¹, Stefania Vaga², Pramote Chumnanpuen¹, Rahul Kumar¹, Goutham N Vemuri¹, Ruedi Aebersold^{2,3} and Jens Nielsen^{1,*}

¹ Department of Chemical and Biological Engineering, Chalmers University of Technology, Göteborg, Sweden, ² Department of Biology, Institute of Molecular Systems Biology, ETH Zürich, Zürich, Switzerland and ³ Faculty of Science, University of Zürich, Zürich, Switzerland

* Corresponding author. Department of Chemical and Biological Engineering, Chalmers University of Technology, Kemivägen 10, Göteborg 412 96, Sweden.
Tel.: +46 31 772 3804; Fax: +46 31 772 3801; E-mail: nielsen@chalmers.se

Received 20.7.11; accepted 29.9.11

Nutrient sensing and coordination of metabolic pathways are crucial functions for all living cells, but details of the coordination under different environmental conditions remain elusive. We therefore undertook a systems biology approach to investigate the interactions between the Snf1 and the target of rapamycin complex 1 (TORC1) in *Saccharomyces cerevisiae*. We show that Snf1 regulates a much broader range of biological processes compared with TORC1 under both glucose- and ammonium-limited conditions. We also find that Snf1 has a role in upregulating the NADP⁺-dependent glutamate dehydrogenase (encoded by *GDH3*) under derepressing condition, and therefore may also have a role in ammonium assimilation and amino-acid biosynthesis, which can be considered as a convergence of Snf1 and TORC1 pathways. In addition to the accepted role of Snf1 in regulating fatty acid (FA) metabolism, we show that TORC1 also regulates FA metabolism, likely through modulating the peroxisome and β-oxidation. Finally, we conclude that direct interactions between Snf1 and TORC1 pathways are unlikely under nutrient-limited conditions and propose that TORC1 is repressed in a manner that is independent of Snf1.

Molecular Systems Biology 7: 545; published online 8 November 2011; doi:10.1038/msb.2011.80

Subject Categories: metabolic and regulatory networks; cellular metabolism

Keywords: carbon metabolism; nitrogen metabolism; nutrient sensing; Snf1; TORC1

Introduction

Cells commonly face environmental changes such as varying availability of nutrients. Therefore, it is of crucial importance for them to adjust the metabolism accordingly. In this context, the nutrient sensing and related regulatory pathways are particularly important. Since there is a high degree of conservation in the functionality of these regulatory pathways in all eukaryotes, the budding yeast *Saccharomyces cerevisiae* serves as an excellent model and has been used for many studies on nutrient sensing and regulation in eukaryotic cells (Petranovic and Nielsen, 2008). *S. cerevisiae* senses extracellular nutrients and controls its metabolism through a complex regulatory network (Zaman *et al.*, 2008). Key components in this regulatory network include the Snf1 kinase complex and the target of rapamycin complex 1 (TORC1). Snf1 complex belongs to a remarkably conserved serine/threonine kinase family called AMP-activated kinase (AMPK) that exists in all eukaryotes (Polge and Thomas, 2007). The Snf1 kinase was first identified as the key enzyme in releasing the glucose repression on glucose depletion (Celenza and Carlson, 1984), and later found to be involved in the regulation of transcription through post-translational modifications of histone H3 and Gcn5 (Lo *et al.*, 2001; Liu *et al.*, 2010) and interaction with RNA polymerase II holoenzyme (Kuchin *et al.*, 2000). Upon activation by phosphorylation, Snf1 induces genes involved in gluconeogenesis, glyoxylate cycle and β-oxidation of fatty

acids (FAs) by regulating a set of different transcription factors (TFs) (Soontorngun *et al.*, 2007; Ratnakumar and Young, 2010) and represses lipid biosynthesis by inhibiting Acetyl-CoA carboxylase (Acc1) (Woods *et al.*, 1994), the committed step of FA synthesis pathway. Besides the aforementioned processes, Snf1 is also involved in the general stress response, pseudo-hyphal growth, ageing and ion homeostasis (Alepuz *et al.*, 1997; Kuchin *et al.*, 2002; Lin *et al.*, 2003; Portillo *et al.*, 2005; Hong and Carlson, 2007; Ye *et al.*, 2008)

TORC1 was first identified in the screening of yeast mutants against the antifungal reagent rapamycin. Similarly to Snf1, TORC1 is also highly conserved in eukaryotes (Schmelzle and Hall, 2000). TORC1 in *S. cerevisiae* (and some other unicellular eukaryotes such as *Schizosaccharomyces pombe*) consists of either Tor1 or Tor2, two homologous proteins, as well as other components, while in metazoans like flies, worms and mammals only one Tor protein can form the TORC1 (Inoki *et al.*, 2005). However, unlike Tor1, Tor2 can also form the TOR complex 2 (TORC2), which is insensitive to rapamycin and has distinct structures and functions compared with TORC1 (Loewith *et al.*, 2002; Jacinto *et al.*, 2004; Wullschleger *et al.*, 2005). TORC1 senses the availability and quality of the nutrients and regulates cell growth by antagonizing a spectrum of TFs in the cytoplasm. For example, TORC1 induces ribosome biogenesis through the TFs Sfp1 and Fhl1, in coordination with the protein kinase A (PKA) pathway, thus promotes protein translation and cell growth

(Marion *et al*, 2004; Martin *et al*, 2004). TORC1 also negatively regulates those genes whose expression is induced by limitation of nitrogen sources through the transcription activators Gln3 and Gat1 (Beck and Hall, 1999), prevents amino-acid biosynthesis by modulating Gcn4 translation (Valenzuela *et al*, 2001) and represses stress responses through the TFs Msn2 and Msn4 (Monteiro and Netto, 2004; Petkova *et al*, 2010). It has been shown that TORC1 is also involved in many other processes such as autophagy, ageing and cell cycle (Kamada *et al*, 2000; Colomina *et al*, 2003; Medvedik *et al*, 2007).

Recent systematic approaches indicate some coordination between Snf1 and TORC1 signaling pathways under nutrient-excess conditions (Zaman *et al*, 2008; Smets *et al*, 2010). However, it is not clear if there is any interaction between them under nutrient limitation. Although AMPK was shown to directly inhibit mTORC1 (AMPK and mTORC1 are the orthologs of Snf1 and TORC1 in mammals, respectively), a similar interaction was not identified in yeast (Hardie, 2007). Instead, it was suggested that Snf1 may be involved in nitrogen metabolism through the regulation of the transcription activators Gln3 and Gcn4 (Bertram *et al*, 2002; Shirra *et al*, 2008), which are targets of TORC1 and positively regulates genes that are subject to nitrogen catabolic repression. It has also been shown that Snf1 is directly involved in nitrogen signaling and regulated by nitrogen availability (Orlova *et al*, 2006).

Thus far, our knowledge of nutrient sensing and related regulatory pathways is limited to studies conducted under nutrient-excess conditions (e.g., shake flask batch cultivation with excessive amount of carbon and nitrogen sources). The coordination of the signaling pathways under nutrient limitation remains largely obscure. To address this limitation, we took advantage of the chemostat cultivations, which permit correlating observations with the limiting nutrient (Daran-Lapujade *et al*, 2009). We focused on the cellular response to carbon (glucose) or nitrogen (ammonium) limitation in *S. cerevisiae* strains that lacked *SNF1*, *TOR1* or both. We also assessed the role of Snf1 and TORC1 as kinases under these conditions using the state of the art phosphoproteomics technology, and their impact on gene expression with transcriptomics. We used the levels of selected metabolites, such as free amino acids and total FAs, as read-outs of the net contribution of these kinases, as amino-acid and FA metabolisms are known to be regulated by Snf1 and TORC1, respectively. By integrating these comprehensive data sets, we obtained substantial new insights into how Snf1 and TORC1 coordinate nutrient sensing and metabolic regulation.

Results and discussion

Cell physiology under nutrient-rich and -limited conditions

To evaluate the effects of deleting Snf1 and TORC1 on cell growth, we characterized the basic physiology of mutant strains *snf1* Δ , *tor1* Δ and *snf1* Δ *tor1* Δ together with the reference strain CEN. PK113-7D (Supplementary Table S1) by growing them first in batch and then switched to chemostat, both using defined minimum medium with glucose as the sole

carbon source. Chemostat cultures were used for several reasons. First, it is possible to correlate the observations with the limiting nutrient. Second, since the mutants have different maximum specific growth rates, chemostats offer a platform for comparing different strains at the same growth rate, thereby eliminating any growth-related effects (Fazio *et al*, 2008). Finally, since the mutant strain *snf1* Δ is unable to grow on non-fermentable carbon sources (such as ethanol and glycerol), glucose-limited chemostat is the only option to ensure Snf1 activity under comparable growth conditions. There are several good nitrogen sources for yeast, such as glutamine and ammonium (Zaman *et al*, 2008); however, glutamine can also be used as a carbon source and is therefore unsuitable for nutrient-limited cultures.

All mutant strains grew slower (by 12–22%) using glucose as the sole carbon source and ammonium as the sole nitrogen source, compared with the reference strain, indicating the contribution of Snf1 and TORC1 during exponential growth and deletion of either protein reduces cell growth on defined minimum medium (Table I). However, the observation of an equivalent reduction (about 20% lower) in the maximum specific growth rate for the *snf1* Δ *tor1* Δ strain seems to contradict the hypothetic genetic interaction between Snf1 and TORC1 on these conditions, as one would expect a more severe phenotypic change in the double mutant strain if a genetic interaction was present (Boone *et al*, 2007). Deletion of Snf1 (*snf1* Δ and *snf1* Δ *tor1* Δ) resulted in a substantial reduction (~25%) in the biomass yield compared with the reference strain in glucose-limited chemostat cultures (Table I). On the contrary, we observed a small increase in biomass yield for *tor1* Δ under these conditions. The double mutant produced acetate and glycerol, even under completely respiratory conditions. Interestingly, we did not see any substantial difference in the biomass yield on N-limited condition.

The effects of deleting Tor1 were relatively moderate, given that the TORC1 is the main regulator in cell growth and proliferation (Schmelzle and Hall, 2000). This could be due to the compensatory role of Tor2, which can also form TORC1. To evaluate this hypothesis, we examined the sensitivity of the reference and *tor1* Δ strains in the presence of rapamycin. While the reference strain could tolerate up to 2 nM of

Table I Cell physiology of all strains in batch and chemostat cultivations

Medium	Strain	μ_{max}	Y_{SX}	Y_{SAC}
		h^{-1}	g g^{-1}	Cmol Cmol^{-1}
C-limited	Reference	0.37 ± 0.01	0.515 ± 0.007	< 0.002
	<i>snf1</i> Δ	0.29 ± 0.00	0.384 ± 0.003	0.007 ± 0.004
	<i>tor1</i> Δ	0.33 ± 0.01	0.534 ± 0.003	< 0.002
	<i>snf1</i> Δ <i>tor1</i> Δ	0.30 ± 0.00	0.382 ± 0.002	0.028 ± 0.003
N-limited	Reference		0.097 ± 0.002	0.006 ± 0.000
	<i>snf1</i> Δ		0.102 ± 0.000	0.008 ± 0.000
	<i>tor1</i> Δ		0.095 ± 0.000	0.008 ± 0.001
	<i>snf1</i> Δ <i>tor1</i> Δ		0.107 ± 0.001	0.009 ± 0.000

All values are average \pm s.e.m. from at least three biological replicates. μ_{max} , maximum specific growth rate on glucose in batch cultures; Y_{SX} , biomass yield on glucose in chemostat cultures; Y_{SAC} , acetate yield on glucose in chemostat cultures. μ_{max} for each strain was determined based on the CO₂ emission during the batch phase of the culture.

rapamycin in the growth media, there was no observable growth of the *tor1Δ* strain at any concentration of rapamycin (Supplementary Figure S1). The increased sensitivity to rapamycin caused by loss of Tor1, which was consistent with previous findings (Chan *et al*, 2000; Reinke *et al*, 2004; Xie *et al*, 2005), suggested that the deletion of *TOR1* gene caused a substantial reduction in TORC1 signaling or complex activity and Tor2 could hence not fully compensate for the loss of Tor1 function. Since rapamycin inhibits the TORC1 by physically binding to the complex, these results clearly show that Tor1 is responsible for a majority of the TORC1 activity and the *tor1Δ* strain, therefore, represents a knockdown, but not necessarily a complete loss of function, of TORC1.

Global transcriptome changes due to loss of *SNF1* but not *TOR1*

We used the Affymetrix DNA microarray platform to measure the expression level of all genes and evaluate the global effect caused by deletion of the *SNF1* and *TOR1* genes under nutrient-limited conditions. The transcriptome data were decomposed using principal component analysis (PCA). The first principal component (PC1), which accounted for about 40% of the total variation in the data (Supplementary Figure S2A), primarily distinguished the impact of nutrient limitation (Figure 1A), which was expected as the cells were respiring at C-limited condition while they were respiro-fermenting at N-limited condition. The second principal component (PC2) accounted for the impact of *SNF1* deletion. It is also evident that the variance between *snf1Δ* and reference (represented by the distance between reference and *snf1Δ* in Figure 1A) is much larger at C-limited condition compared with N-limited

condition, confirming that Snf1 has a bigger role on glucose-limited condition. Surprisingly, our data did not reveal any transcriptional role for the *TOR1* gene, indicated by the overlapping of *tor1Δ* and the reference strain at all nutrient limitations (Figure 1). Furthermore, *TOR1* deletion did not seem to have a large impact even in the *snf1Δ* background, as evident from the close proximity of the *snf1Δtor1Δ* with *snf1Δ* under all the conditions studied. This result suggests that Tor1 is dispensable under either of nutrient-limited conditions. It is not clear whether the dispensability arises due to its partial redundancy with Tor2 or due to the suppression of the Tor1 function under these conditions. To further examine the extent of the changes in each mutant strain, we performed pair-wise comparisons. On the C-limited condition, the expression of 519 and 603 genes was changed significantly (adjusted $p < 0.001$) in *snf1Δ* and *snf1Δtor1Δ*, respectively, relative to the reference strain. Gene ontology (GO) terms analysis revealed that transcription of genes involved in nitrogen metabolism, ethanol metabolism and pheromone-dependent signal transduction appears to be specifically controlled by Tor1, other processes such as stress response and biosynthesis of ergosterol and glutamate were governed by Snf1 (Figure 1B).

The measurement of global gene expression provided clear insight into the metabolic differences between the strains. Increased acetate production (Table I) was in line with the lower expression of *ACS1* (encoding acetyl-CoA synthetase) in the *snf1Δ* and *snf1Δtor1Δ* strains (Supplementary Figure S3). The expression of the other acetyl-CoA synthetase (encoded by *ACS2*) that is not subject to glucose repression increased slightly in the *snf1Δ* strain, which is consistent with previous findings (van den Berg *et al*, 1996). Two other genes in acetate metabolism, *ADY2* (encodes an acetate transporter) and *ALD4* (encodes a mitochondrial aldehyde dehydrogenase), showed

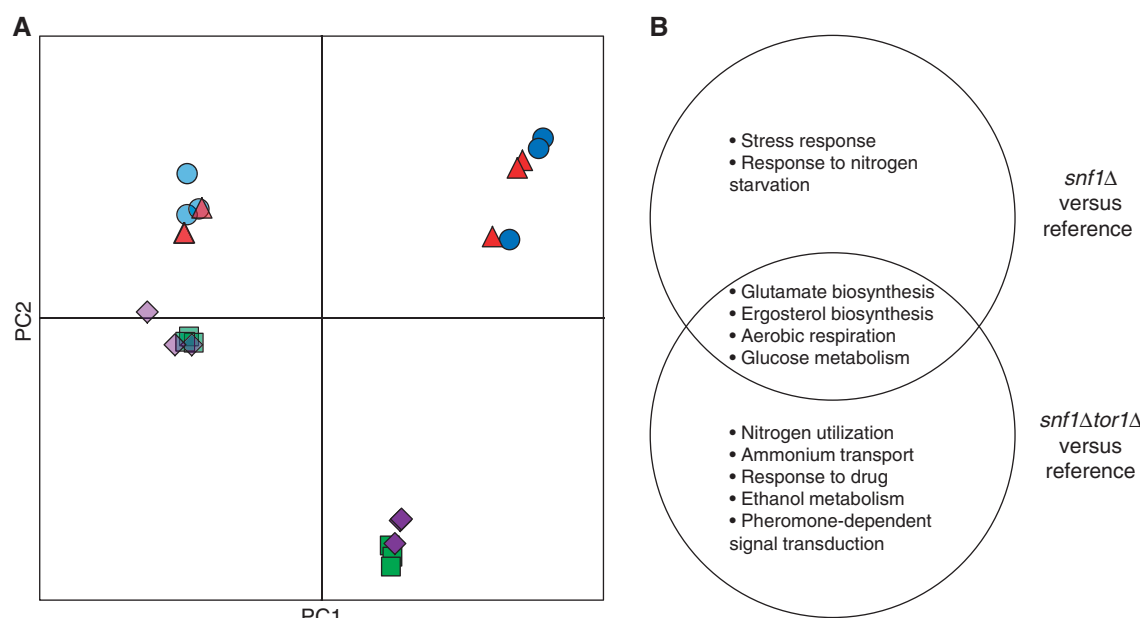


Figure 1 Deletion of *SNF1* but not *TOR1* caused global change in transcriptome. **(A)** Principal component analysis (PCA). Dark blue circles: reference on C-limited; dark green squares: *snf1Δ* on C-limited; dark red triangles: *tor1Δ* on C-limited; light blue circles: reference on N-limited; light green squares: *snf1Δ* on N-limited; light red triangles: *tor1Δ* on N-limited; light purple diamonds: *snf1Δtor1Δ* on N-limited. **(B)** The biological processes that were affected by deletion of *SNF1* (*snf1Δ* and *snf1Δtor1Δ*) on C-limited condition.

similar expression patterns (Supplementary Figure S3). The change in gene expression for both *ACS1* and *ADY2* was more prominent in the *snf1Δtor1Δ* strain compared with the *snf1Δ* strain. However, the expression of these genes being unchanged in the *tor1Δ* strain indicates that the role of TORC1 in acetate metabolism relies on Snf1 activity, or in other words it seems like TORC1 has a role in the metabolism of alternative carbon sources through an active Snf1 kinase.

To identify transcriptional regulation of metabolism in response to deletion of *SNF1* and/or *TOR1*, we overlaid the transcriptome onto a genome-scale metabolic model of *S. cerevisiae*. This method (Patil and Nielsen, 2005; Oliveira *et al*, 2008) allows identifying the so-called *reporter features* (metabolites, TFs, etc) around which significant transcriptional activity occurred and also subnetworks of coordinated transcriptional changes. On C-limited condition, deleting *SNF1* (*snf1Δ* and *snf1Δtor1Δ*) resulted in an extensive transcriptional reprogramming around redox cofactors (NAD(P)⁺/NAD(P)H), Coenzyme A, several amino acids and α-ketoglutarate (Z-score > 1.5) (Supplementary Table S2). These differences were identified primarily through global TFs such as Msn2/4, Cat8, Ino2/4, Oaf1/Pip2, and Hap1 that regulate stress response, aerobic respiration, as well as glucose and sterol metabolism (Supplementary Table S2). Although deleting *TOR1* alone did not have any significant transcriptional response, deleting *TOR1* in the *snf1Δ* background resulted in an altered expression for a small subset of genes (involved in several processes including stress response, tRNA methylation, protein targeting to vacuole, ammonium transport, intracellular protein transport), indicating that these processes might be co-regulated by Snf1 and TORC1. Overall transcriptome data from glucose limitation contradict the hypothesis that Snf1 inhibits TORC1.

***TOR1* deletion had no distinct phosphorylation response**

Since both Snf1 and TORC1 are kinase complexes and regulate several processes mainly through phosphorylation of their respective target proteins (Zaman *et al*, 2008; Smets *et al*, 2010), we measured the level of phosphorylation of various proteins for all strains under C- and N-limited conditions. As with the transcriptome data, the phosphoproteome data were also analyzed using PCA. The analysis revealed that the *TOR1* deletion did not lead to a distinct phosphoproteome profile compared with the reference strain, irrespective of the nutrient limitation. Under all conditions studied, the phosphoproteome profile of *tor1Δ* always clustered with that of the reference and the phosphoproteome profile of *snf1Δtor1Δ* always clustered with that of *snf1Δ* (Figure 2). The reference and *tor1Δ* strains on C-limited were separated farthest from the other strains/conditions (Figure 2), indicating that the deletion of Snf1 has a dominant response irrespective of the limiting nutrient. Out of the 1714 phosphopeptides that were detected and identified, 399 and 206 peptides had significantly changed phosphorylation level in at least one mutant compared with the reference strain, on C- and N-limited conditions, respectively.

We observed a clear Snf1-dependent pattern of phosphorylation (lower phosphorylation level in *snf1Δ* and *snf1Δtor1Δ*

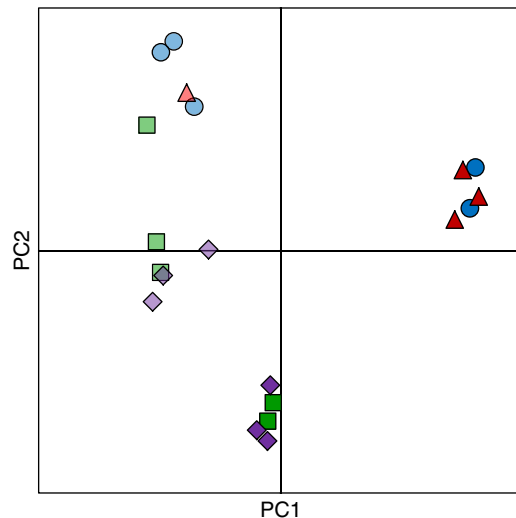


Figure 2 Principal component analysis of phosphoproteome data for all strains on C- and N-limited conditions. Dark blue circles: reference on C-limited; dark green squares: *snf1Δ* on C-limited; dark red triangles: *tor1Δ* on C-limited; dark purple diamonds: *snf1Δtor1Δ* on C-limited; light blue circles: reference on N-limited; light green squares: *snf1Δ* on N-limited; light red triangles: *tor1Δ* on N-limited; light purple diamonds: *snf1Δtor1Δ* on N-limited.

but not *tor1Δ*) for transcription repressor Cyc8 and its co-component Tup1 (Supplementary Figure S4). Since the Cyc8-Tup1 complex generally represses the transcription of many genes through different modes (Smith and Johnson, 2000), it may be responsible for upregulation of a subset of genes in the *snf1Δ* and *snf1Δtor1Δ* strains. This further supports that the transcriptome profile for *snf1Δ* and *snf1Δtor1Δ* was significantly changed directly due to the role of Snf1 in the regulation of transcription. This is supported by findings that several other proteins involved in regulation of transcription by histone modification (Bdf1, Eaf1, Leo1, Rph1 and Sin3) were also found to be differentially phosphorylated only in the *snf1Δ* and *snf1Δtor1Δ* strains. Significantly changed expression of *ACS1* in *snf1Δ* and *snf1Δtor1Δ* might also contribute to changes in histone acetylation and global changes in transcription observed in these mutants (Takahashi *et al*, 2006). These results are in complete consistency with the important role of Snf1 in the regulation of gene transcription (Usaite *et al*, 2009).

Mammalian TORC1 (mTORC1) is repressed by AMPK (Dennis *et al*, 2001; Bolster *et al*, 2002; Inoki *et al*, 2003), and several lines of evidence suggest direct or indirect interaction between Snf1 and TORC1 (Bertram *et al*, 2002; Orlova *et al*, 2006) in yeast. However, in our analysis, we did not find any change in the phosphorylation level of TORC1 due to loss of Snf1 kinase or *vice versa* (Supplementary Figure S5). Only Tco89 (a non-essential component of TORC1) was identified as differentially phosphorylated in a Tor1-dependent manner. Despite the state-of-art methods used in identifying phosphoproteins, it is likely that some phosphopeptides have not been identified due to low abundance, inefficient purification, poor ionization, etc. Considering this limitation, the absence of all components of the Snf1 and TORC1 pathways in

our phosphoproteome analyses compels us to conclude that Snf1 and TORC1 do not regulate the phosphorylation of each other under the conditions studied. It has been shown that phosphorylation of residual T210 on Snf1 is regulated by the nitrogen source or rapamycin through TORC1 (Orlova *et al*, 2006), which raised the possibility that TORC1 negatively regulates Snf1. However, both transcriptome and phosphoproteome data revealed a negligible role for Tor1 irrespective of Snf1 deletion, suggesting that TORC1 was mainly repressed at C-limited condition and this repression may be independent of Snf1. Based on these inferences, we propose that the Snf1 and TORC1 pathways only crosstalk via intermediate(s) under nutrient limitation. Such an intermediate would operate at the upstream of Snf1 and TORC1 and switches between the Snf1 and TORC1 activity (i.e., either Snf1 or TORC1, but not both, could be active under nutrient-limited conditions). One such intermediate could be the PKA/RAS pathway, which together with Snf1 can be perceived as a switch that senses the glucose concentration and regulates the cell metabolism accordingly (Zaman *et al*, 2009). The identification of significantly decreased phosphorylation of Bcy1, the regulatory subunit of PKA pathway, in the *snf1Δ* and *snf1Δtor1Δ* strains suggests a possible link between the Snf1 and PKA pathways (Supplementary Figure S5). PKA interacts with TORC1 in the regulation of protein translation and cell cycle (Martin *et al*, 2004; Wanke *et al*, 2005), and it may therefore bridge the Snf1 and TORC1 pathways. Since PKA and TORC1 are active in nutrient excess, while Snf1 is only fully active under glucose limitation or stress conditions, the media and growth conditions are essential for studying the regulatory pathways involved in nutrient sensing, because a shake flask cultivation using a rich medium (typically the YPD medium supplemented with 2% of glucose) is a completely different scenario from the chemostat culture fed with C- or N-limited medium.

Convergence of Snf1 and TORC1 onto amino-acid biosynthesis

Neither the transcriptome nor the phosphoproteome data supported a direct link between Snf1 and TORC1 or the pathways they regulate. However, integration of these data

using a metabolic model revealed extensive regulation around biosynthesis of amino acid and lipid (Supplementary Table S2). To investigate the regulation of amino-acid biosynthesis by Snf1 and TORC1, we quantified the intracellular level of 17 proteinogenic amino acids in all strains grown under both nutrient-limited conditions (Supplementary Table S3). Serine and arginine cannot be measured using the method applied and the cysteine level was below detection threshold. The free amino-acid pool under C-limited condition was 2- to 4.5-fold higher compared with that for N-limited condition for all the strains. During glucose limitation, the *tor1Δ* strain had about 17% higher level of free amino-acid pool, while the *snf1Δ* strain had a level about 29% lower compared with the reference strain (Figure 3A). During ammonium limitation, the strain *snf1Δ* had a similar level as the reference, while the *tor1Δ* and *snf1Δtor1Δ* strains had 170 and 93% higher total amino-acid level compared with the reference, respectively (Figure 3A). A substantial part of these differences was due to changes in glutamate and glutamine, which accounted for 60–75% of the total amino acid (Figure 3B and C).

To identify transcriptional regulation of amino-acid metabolism, we correlated the amino-acid levels with the expression of genes involved in their biosynthesis. Surprisingly, many genes responsible for the amino-acid biosynthesis were negatively correlated with the amino-acid levels (Figure 3; Supplementary Figure S6), indicating that the changes in the amino-acid abundance were not due to differential expression of corresponding amino-acid biosynthetic genes. We speculate that it may be due to that TORC1 senses a low level of glutamine (Figure 3B; Crespo *et al*, 2002) and consequently, the inhibition on Gcn4 is relieved (Valenzuela *et al*, 2001). Next, we studied the drain from the central carbon metabolism into the amino-acid biosynthesis. Since the expression of genes in TCA cycle is highly regulated by the nature and availability of carbon sources in an Snf1-dependent manner (Young *et al*, 2003), one may speculate if the lower level of Glx and other amino acids was due to the generally downregulated TCA cycle in the *snf1Δ* strain on C-limited and hence shortage of α -ketoglutarate, the direct precursor for amino acids of the glutamate family. However, a clear retrograde signaling response in the *snf1Δ* and *snf1Δtor1Δ* strains, reflected by both an induction of *CIT2* (about 4-fold) and genes responsible for

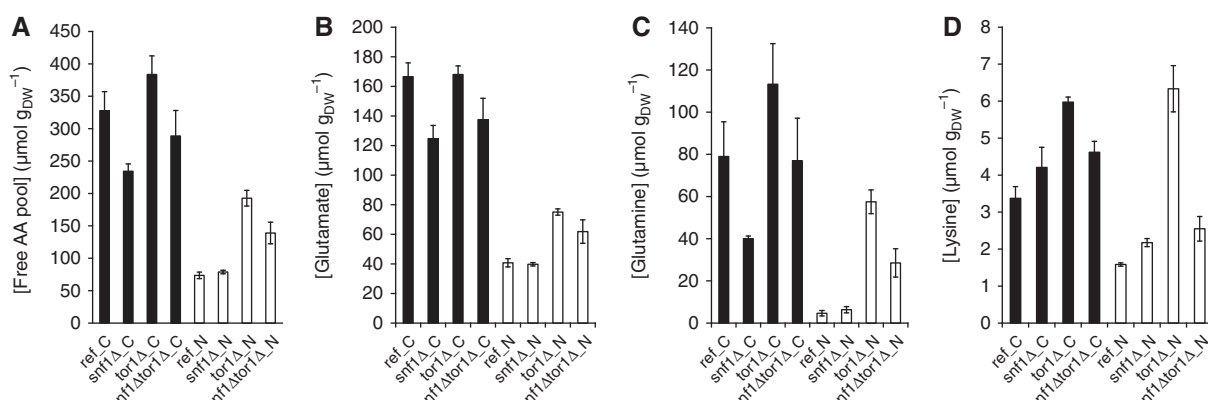


Figure 3 Intracellular levels of free amino acids. **(A)** Free amino-acid pool; **(B)** glutamate; **(C)** glutamine and **(D)** lysine. The error bars represent the s.e.m. from biological replicates from three chemostat cultures. Black—C-limited condition and white—N-limited condition.

the early steps in the TCA cycle (*CIT1*, *ACO1/ACO2*, *IDH1/IDH2*) (Liu and Butow, 2006), confirmed that the amino-acid biosynthesis was not limited by the supply of α -ketoglutarate. Instead, a plausible explanation for the lower level of amino-acid pool in the *snf1* Δ and *snf1* Δ *tor1* Δ strains would be that the expression of *GDH3*, which encodes one of the isoforms of glutamate dehydrogenase when cells are grown under derepressive conditions (DeLuna *et al.*, 2001), was transcriptionally downregulated by >4-fold in the *snf1* Δ and *snf1* Δ *tor1* Δ strains. The amino-acid biosynthesis was, therefore, likely limited by the inefficient conversion of α -ketoglutarate to glutamate, which is the main nitrogen source for cell growth. This phenomenon is similar to the one that was previously reported, where simply overexpression of *GDH2* in the mutant strain *gdh1* Δ grown on batch culture (where the *Gdh1* is the major isoform of glutamate dehydrogenase) changed the overall amino-acid pool significantly (Villas-Boas *et al.*, 2005). On the other hand, the increased level for amino acids in *tor1* Δ could be attributed to an impaired balance between protein synthesis and degradation as a consequence of *TOR1* deletion (Inoki *et al.*, 2005).

We also found that amino-acid biosynthesis is regulated at the post-translational level. For example, homocitrate synthase (encoded by *LYS20* and *LYS21*), which catalyzes the condensation of acetyl-CoA and α -ketoglutarate to form homocitrate, was found to be significantly more phosphorylated in the *snf1* Δ strain and to a lesser extent in the *snf1* Δ *tor1* Δ strain. However, the phosphorylation of only *LYS20* decreased in the *tor1* Δ strain (by ~2-fold; Supplementary Figure S7). Since the intracellular lysine level significantly increased in all mutant strains (being highest in *tor1* Δ) at C-limited condition (Figure 3C), we could conclude that the homocitrate synthase isoenzymes (Lys20 and Lys21) are not only regulated through feedback inhibition by lysine, but could also be regulated through phosphorylation of these enzymes in an Snf1/TORC1-dependent manner. Collectively, we propose that Snf1 and TORC1 regulate the amino-acid biosynthesis via two independent mechanisms.

TORC1 may have a role in the regulation of FAs

To unravel the role of Snf1 and TORC1 in the regulation of FA metabolism, we measured the relative abundance of FAs, including the free and ester form (e.g., in triacylglycerol), in the reference and mutant strains on both C- and N-limited conditions. Since Snf1 regulates FA biosynthesis by inhibiting acetyl-CoA carboxylase (Acc1) under derepressive conditions (Woods *et al.*, 1994), the significant increase of total FA in the *snf1* Δ and *snf1* Δ *tor1* Δ strains on C-limited condition was expectable (Figure 4). However, there was a significant variation in the FA species between different strains and the two growth conditions. The most abundant species was C18:1, where the largest differences between strains were observed (Figure 4E). The *snf1* Δ and *snf1* Δ *tor1* Δ strains had higher levels of C18 (i.e., both C18:0 and C18:1) and longer FAs, on both C- and N-limited conditions, compared with the reference strain (Figure 4D-F), except for C14 where the result was contrary (Figure 4A). The *snf1* Δ *tor1* Δ strain had higher amounts of C18 compared with the *snf1* Δ strain irrespective of the growth condition. The *tor1* Δ strain had higher C14 and

C16 on N-limited condition, but the levels were lower on C-limited condition, compared with the reference strain.

However, this was only observed for C18 and longer FAs in these two strains (Figure 4D and E), while the abundance of C14 was reduced in the mutant strains in which *SNF1* was deleted. There may be two mechanisms that can explain the different patterns between the FAs with different length. One possibility could be that while the inhibition of acetyl-CoA carboxylase by Snf1 was relieved, and the FA synthetase (encoded by *FAS1* and *FAS2*) is constitutively functional and steadily converting short chain FAs to synthesize up to C16. Consistently, the elongase I (encoded by *ELO1*) that convert C12-16 to C18 was also found to be transcriptionally upregulated in *snf1* Δ and *snf1* Δ *tor1* Δ ; therefore, C16 was not accumulated in the strain *snf1* Δ and *snf1* Δ *tor1* Δ (Figure 4B and C). It could also be that a lower peroxisome biogenesis due to the loss of Snf1 leads to a lower level of β -oxidation of the long chain FAs (Ratnakumar and Young, 2010), therefore not only the biosynthesis, but also the degradation of FAs is regulated by Snf1. We also observed that the deletion of *TOR1* had some effect on the abundance of FAs, although to a lesser extent compared with those for *SNF1* deletion (Figure 4D and E). The deletion of *TOR1* in the *snf1* Δ background strengthened the changes caused by the deletion of *SNF1* for C18:0, but rather damped the changes for C18:1 (the most abundant FA species). The FA data support the hypothesis that Tor1 has a role in the regulation of FAs. However, TORC1 is unlikely involved in the regulation of acetyl-CoA carboxylase, and we suspect that the TORC1 may have a role in the regulation of peroxisome and β -oxidation of FAs. It is also interesting to notice that although deletion of *TOR1* had not caused an evident change to the transcription and phosphorylation, many amino acids and FA species had changed significantly (Figures 3 and 4). This observation further supports the ideas that the intermediate metabolites are much more sensitive to mutations, while metabolic fluxes are rather robust (Cornish-Bowden and Cardenas, 2001; Raamsdonk *et al.*, 2001).

Regulation of translation and cell growth

Since TORC1 promotes biosynthesis of ribosome and protein (Wullschleger *et al.*, 2006), while Snf1 represses the energetically expensive processes such as biosynthesis of lipid and proteins (Hardie, 2007), we looked at the Snf1 and TORC1 regulation of protein translation, both at the transcriptome and at the phosphoproteome levels. Surprisingly, the deletion of *SNF1* led to a significantly (despite <2-fold) increased expression of many genes involved in translation initiation or elongation, while the deletion of *TOR1* alone did not cause any changes (Figure 5A). This held true even for the translation initiation or elongation factors (with only a few exceptions) that were found to be differentially phosphorylated in the mutant strains compared with the reference strain (Figure 5C). The observation that protein synthesis being primarily regulated by Snf1 instead of TORC1 seems to contradict the common knowledge that TORC1 is the main regulator for ribosomal translation (Inoki *et al.*, 2005). However, taken the growth conditions (i.e., glucose limitation) into account it is actually consistent with the role of Snf1 as a global regulator of energy homeostasis and a repressor of

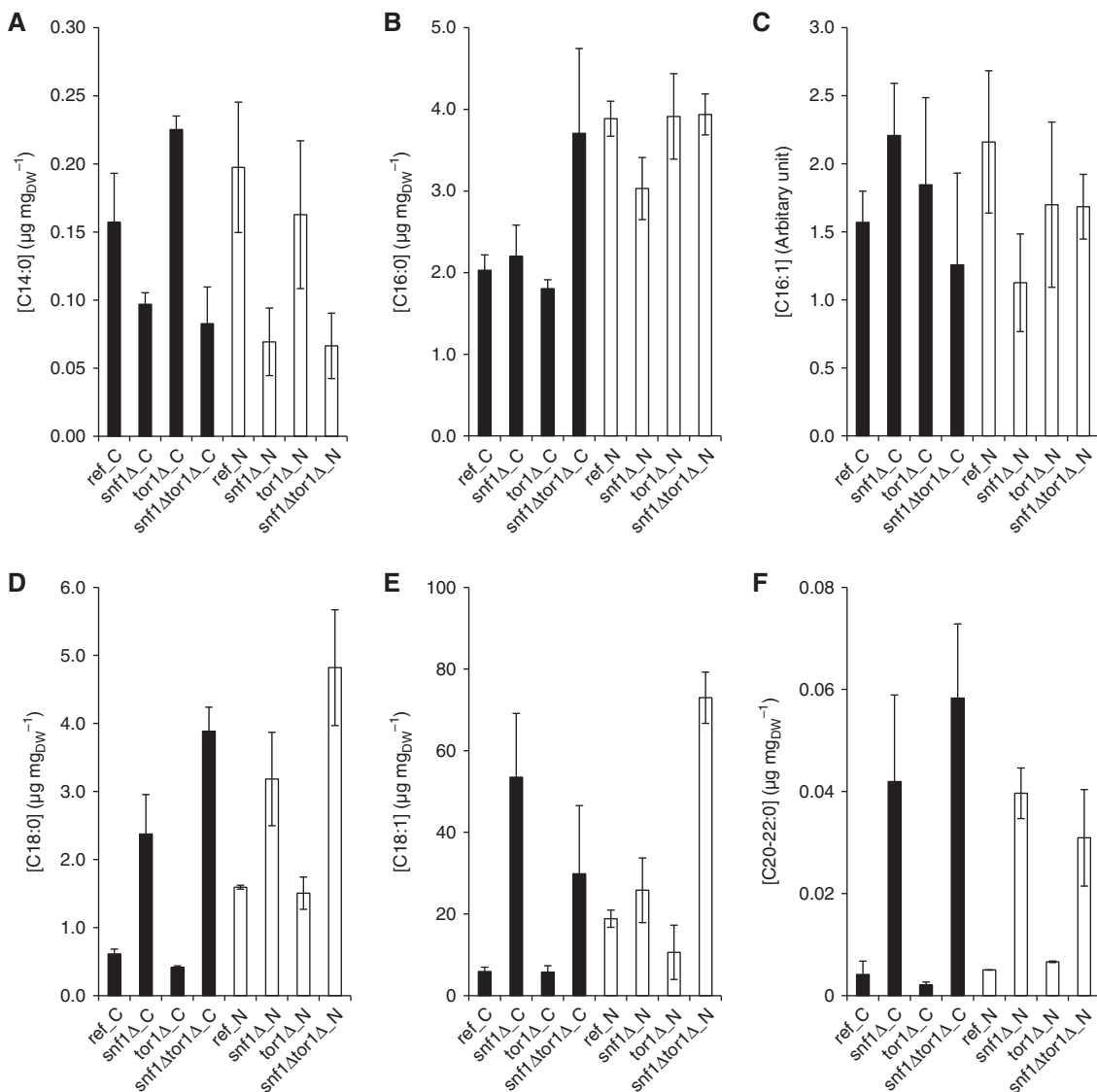


Figure 4 Abundance of fatty acids for all strains and two growth conditions. The abundance is based on the sum of FAs in the free as well as ester form. The error bars represent the s.e.m. from at least three replicates. (A) C14:0—myristic acid; (B) C16:0—palmitic acid; (C) C16:1—palmitoleic acid; (D) C18:0—stearic acid; (E) C18:1—oleic acid and (F) C20:0—arachidic acid and C22:0— behenic acid. Black—C-limited condition and white—N-limited condition.

anabolic processes (Hardie, 2007). The relative small changes in the *snf1Δtor1Δ* strain compared with the *snf1Δ* strain may advocate an inhibition of TORC1 under C-limited condition, as the TORC1 activity may require a high level of both ammonium and glucose (Figure 6). Interestingly, many genes involved in the mitochondrial ribosome and protein translation also had a similar pattern of expression where it was increased in the *snf1Δ* and *snf1Δtor1Δ* strains, and deletion of *TOR1* had either no effect or similar effect with a lower magnitude (Figure 5B). Collectively, we conclude that the Snf1 has a major role in cell the mitochondrial proteome under C-limited condition.

Conclusion

Through integration of different omics data sets with metabolite profiles and strain physiology, we address the question

of how Snf1 and TORC1, the two key regulators in the nutrient sensing pathways, coordinate metabolism with nutrient availability. The regulatory network is summarized in Figure 6. First, we showed that deletion of *SNF1* caused bigger phenotypic changes compared with deletion of *TOR1* grown on both nutrient-excess and -limited conditions and we demonstrate that it is likely due to that Snf1 kinase regulates a much broader range of biological processes such as global transcription, translation of protein, biogenesis of peroxisome and mitochondrion. The expression of NADP⁺-dependent glutamate dehydrogenase (Gdh3), which is upregulated under derepressing conditions (e.g., glucose limited), is regulated by Snf1, and the deletion of *SNF1* likely results in an inefficient condensation of α-ketoglutarate and ammonium to form glutamate. Consequently, the synthesis of glutamine as well as the other amino acids is limited, resulting in a moderate induction of amino-acid biosynthetic genes through the

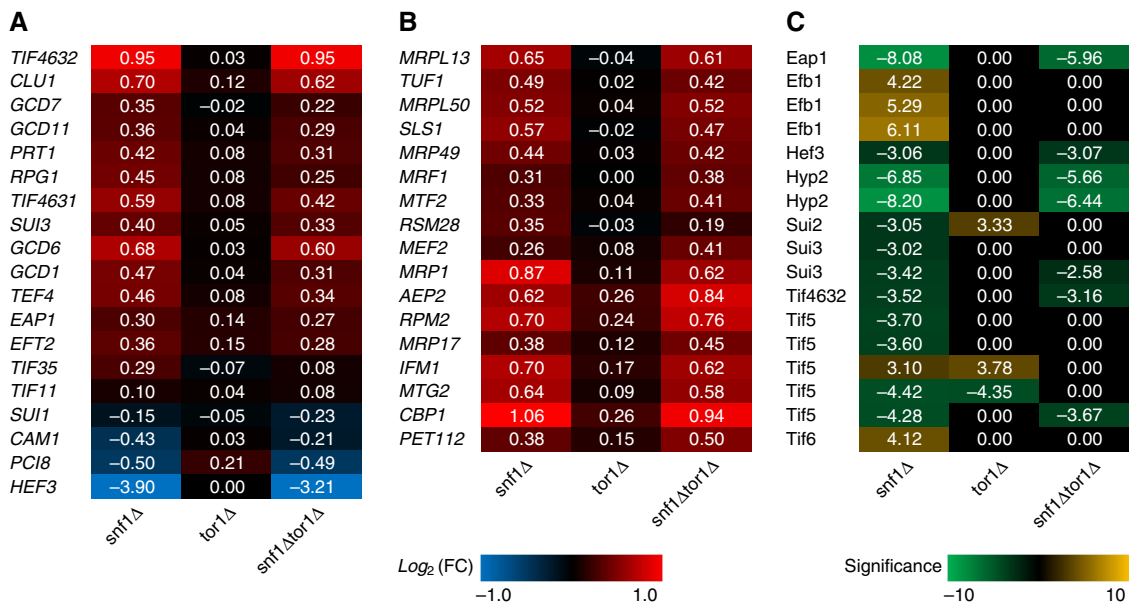


Figure 5 Regulation of genes and proteins involved in translation on C-limited condition. The red-blue heat map represents the relative changes of gene involved in (A) translation initiation and elongation and (B) mitochondrial ribosome and translation. (C) The yellow-green heat map represents the significance of phosphorylation changes of the proteins involved in translation. Positive numbers indicate higher while negative values indicate lower gene expression or protein phosphorylation in mutant strains compared with the reference on C-limited condition.

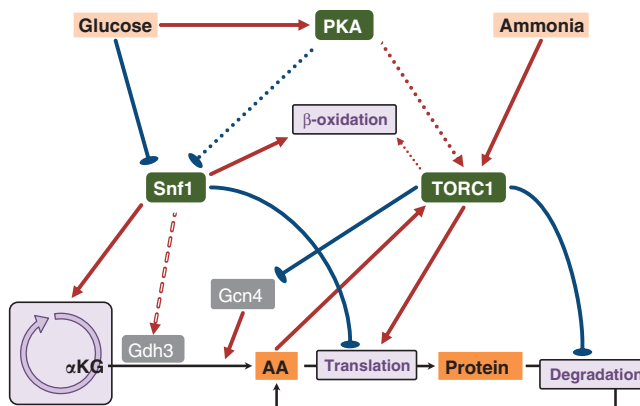


Figure 6 Summary of the main regulatory network of Snf1 and TORC1.

TORC1/Gcn4 regulatory circuit (Figure 6). However, to elucidate the molecular mechanism by which Snf1 upregulates *Gdh3* gene requires extensive targeted studies such as the protein–protein/protein–DNA interaction assays. We also showed that besides Snf1, TORC1 may also have a role in the regulation of FAs, probably through modulating the peroxisome biogenesis and β -oxidation of FA, but via an unidentified mechanism than that of Snf1 pathway. Finally, we conclude that Snf1 and TORC1 do not seem to interact with each other directly under nutrient-limited conditions, although they have functional overlaps. We propose that TORC1 might be repressed by another regulator (or a signal molecule), which is activated (or raised) under nutrient-limited conditions, and this repression may not depend on the Snf1 activity. Furthermore, this unknown upstream regulator (or signal molecule) might also toggle switch

between Snf1 and TORC1 activity to coordinate the cell growth and stress response under nutrient-rich and -limited conditions.

Materials and methods

Strains

The *S. cerevisiae* strains used in this study are the commonly used reference strain CEN.PK 113-7D (van Dijken *et al*, 2000) and its derivative strains (Supplementary Table S1). The *tor1* Δ strains (CEN.PK JZH-F1 and CEN.PK JZH-F2) were constructed by transforming the reference strains CEN.PK 113-7D and CEN.PK 113-1A (*Matα*) with a PCR amplified *KanMX* (from the strain BY4741) including ~400 bp upstream and downstream of the *TOR1* locus. The strain CEN.PK JZH-G1 *snf1* Δ ,*tor1* Δ was constructed by crossing the strain CEN.PK 506-1C and CEN.PK JZH-F2, followed by dissection and screening as described previously (Zhang *et al*, 2010). The gene

deletions were verified by PCR using primers outside the *SNF1* and *TOR1* loci and one primer inside the gene *KanMX*.

Chemostat cultivations

Chemostat cultures were grown at 30°C in 1.2 l bioreactors (DASGIP) with working volume of 0.5 l. The pH was controlled at 5.00 ± 0.05 with 2 M KOH and the dissolved oxygen was kept above 30%. The dilution rate was adjusted to 0.10 h⁻¹. For the C-limited cultures, one liter medium contained 10 g of glucose, 15 g of (NH₄)₂SO₄, 3 g of KH₂PO₄, 1.5 g of MgSO₄ · 7H₂O, 1 ml of vitamin solution (Usaite et al, 2008), 1 ml of trace metal solution (Usaite et al, 2008), and 50 µl of Antiform 204 (Sigma-Aldrich, USA). For N-limited cultivation, the medium was the same as the one used in C-limited cultures except that the concentrations for (NH₄)₂SO₄ and glucose were 1.0 and 60.0 g l⁻¹, respectively. The CO₂ emission (and residual O₂) was monitored from the exhaust gas using the gas analyzer (DASGIP, Germany) and was used to determine the maximum specific growth rate during the batch growth phase. Samples for cell dry weight, extracellular and intracellular metabolites, transcriptome and proteome were taken from the cultures after steady state was achieved for about 50 h.

Transcriptome

The samples for transcriptome were taken as described previously (Zhang et al, 2010). The cells were mechanically disrupted using FastPrep homogenizer (MP Biomedicals) and total RNA was isolated using the RNeasy Mini Kit (QIAGEN). The quality of total RNA was assessed using an Agilent 2100 Bioanalyzer (Agilent Technologies) with RNA 6000 Nano LabChip kit (Agilent Technologies). The labeled RNA was synthesized using the GeneChip® 3' IVT Express Kit (Affymetrix), which was then hybridized onto the GeneChip® Yeast Genome 2.0 Arrays (Affymetrix). Staining and washing of the hybridized arrays were carried out on the GeneChip® Fluidics Station 450 (Affymetrix) and scanned using the GeneChip® Scanner 3000 7G (Affymetrix). Affymetrix microarray data are available at GEO with the accession numbers GSE24421.

The transcriptome data were analyzed using Bioconductor in R. MAANOVA (MicroArray ANalysis Of Variance) was performed to determine the genes whose expression level have significantly changed due to their genetic differences. PCA was applied to reduce the number of dimensions of the data set and simplify the data structure. Selected significant genes were clustered using a consensus clustering methods (Grotkjaer et al, 2006), and the GO terms for the genes in each cluster were analyzed using the *Saccharomyces* Genome Database (SGD) (<http://www.yeastgenome.org/>) to find the significant biological processes in each cluster (*P*<0.01). The Reporter Metabolite and Reporter Effector algorithms were applied to the transcriptome data to identify the 'hot-spots' in the metabolic or regulatory network, around which the significant changes have occurred (Patil and Nielsen, 2005; Oliveira et al, 2008).

Phosphoproteome

The samples collected from the chemostat cultures were rapidly quenched by adding trichloroacetic acid to a final concentration of 6.25%, incubated on ice for 10 min and spun down by centrifuging (5000 r.p.m. at 4°C for 5 min). For each of the three replicates, 3 mg proteins were digested by trypsin (1:125 w/w) and cleaned by reverse phase chromatography. Phosphopeptides were enriched by titanium dioxide resin (1.25 mg GL Science resin for each sample) as previously described (Bodenmiller and Aebersold, 2010). The isolated phosphopeptides were analyzed by an LTQ-FT Ultra mass spectrometer (Thermo Scientific, Germany), interfaced with a nano-electrospray ion source. Chromatographic separation of peptides was performed on a Proxeon Easy-nLC II system (Odense, Denmark) using a 10.5 cm × 75 µm column packed with 3 µm Magic C18 material. Peptides were separated at a flow rate of 300 nL min⁻¹ with a gradient increasing from 5 to 40% acetone. The five most intense ions detected

in each MS1 scan were selected for fragmentation. The mass spectrometer data were searched against an SGD decoy database for yeast proteins using Sequest (Lundgren et al, 2009). OpenMS version 1.7 (Sturm et al, 2008) was used both to detect MS1 features and to align them between the different experimental conditions. By using a decoy database (Kall et al, 2008), a Peptide Prophet's probability threshold (0.9) was computed in order to achieve a false discovery rate <1%, and was used to filter OpenMS results. Phosphopeptides features with identical sequence and phosphorylation state but different charge were merged together. Only features which were detected at least twice in the three replicates were considered for statistical analysis by BAMarray version 3.0 (Ishwaran et al, 2006), which was used to compute the statistical significance of the regulated features. Two replicas for *tor1Δ* grown on N-limited condition were removed from statistical analysis due to their low data quality. The data can be downloaded from Tranche using the following link: <https://proteomecommons.org/dataset.jsp?id=5JoVUbWQTC1tQWzvMlovAN8GJNgGqoWwZsdmcLwhgAjp4xJvlrJipf8V%2BbiCh2VjatUQaDbyCd%2F51j7%2B%2B5vI1Ejfl9MAAAAAAAACUQ%3D%3D>.

Free amino acids

The extraction of free amino acids was performed as described with modifications (Smits et al, 1998). First, 20 mg of freeze-dried cell pellets was suspended in 2.5 ml of cold methanol and 1 ml of chloroform, followed by addition of 4 ml of chloroform (-20°C) and 2 ml of Pipes-EDTA (3 mM each, pH 7.0). After shaking horizontally at 300 r.p.m. and -20°C for 45 min, the mixture was centrifuged at 3000 g and -10°C for 20 min, and the upper (aqueous) phase was collected. The free amino acids were concentrated and derivatized using the EZ:faast™ kit (Phenomenex) and quantified using GC-MS (Thermo Scientific) as described in the kit manual. The measurements are listed in Supplementary Table S3.

Fatty acids

The total FA was extracted and esterified as described previously with modifications (Abdulkadir and Tsuchiya, 2008). First, about 15 mg of freeze-dried biomass was mixed with 5 µg of heptadecanoic acid (internal standard) in 625 µl of hexane and 250 µl of 14% BF₃ in methanol. The head space of the tube was flushed with nitrogen gas to avoid oxidation and capped tightly before heated in a water bath (Grant OLS200, Cambridge, UK) at 100°C for 90 min with shaking at 70 r.p.m. After cooling to room temperature, 125 µl of hexane was added followed by addition of 250 µl distilled water. The tube was then shaken vigorously for 1 min and centrifuged for 3 min at 2500 r.p.m. (650 g). Finally, 750 µl of the upper phase, that is, hexane containing the FA methyl ester (FAME), was transferred into a gas chromatography-mass spectrometry (GC-MS) vial using a Pasteur pipette. The FAMEs were separated and quantified using Trace GC DSQII single quadrupole GC-MS (Thermo Scientific). Separation was performed with an Omegawax 250 (Supelco, Bellefonte, PA) column (30 m × 0.25 mm internal diameter, 0.25 µm film thickness). Helium was used as a carrier gas and the program was as follows. After the injection at 50°C, the oven temperature was raised to 180°C (20°C min⁻¹), held for 1 min, raised to 210°C (3°C min⁻¹), held for 5 min, raised to 215°C (1°C min⁻¹), held for 3 min, raised to 221°C (1°C min⁻¹), held for 5 min, raised to 230°C (3°C min⁻¹), held for 5 min, raised to 250°C (3°C min⁻¹), held for 2 min, and finally raised to 270°C (4°C min⁻¹), held for 2 min. Mass transfer line and ion source were held at 250 and 200°C, respectively. FAME peaks were identified by searching their spectrum pattern against the NIST library. The FAME mixture (C14–22) standard (Sigma-Aldrich) and heptadecanoic acid (Sigma-Aldrich) serial diluted in hexane were injected in the same analysis to generate standard curves for the quantification. The measurements are listed in Supplementary Table S4.

Supplementary information

Supplementary information is available at the *Molecular Systems Biology* website (www.nature.com/msb).

Acknowledgements

This work was financially supported by the Chalmers Foundation, the Knut and Alice Wallenberg Foundation, the EU funded project UNICELLSYS and SystemsX.ch the Swiss Initiative in Systems Biology. We thank Dr Peter Kötter and Dr Matthias Rose (Frankfurt, Germany) for providing the strain BY4741.

Author contributions: JN conceived the study. RA and JN directed the research. JZ, SV, PC and RK performed the experiments. JZ, SV, PC, RK and GV analyzed the data. JZ wrote the manuscript. SV, PC, RK, GV, RA and JN edited and approved the manuscript.

Conflict of interest

The authors declare that they have no conflict of interest.

References

- Abdulkadir S, Tsuchiya M (2008) One-step method for quantitative and qualitative analysis of fatty acids in marine animal samples. *J Exp Mar Biol Ecol* **354**: 1–8
- Alepuz PM, Cunningham KW, Estruch F (1997) Glucose repression affects ion homeostasis in yeast through the regulation of the stress-activated ENA1 gene. *Mol Microbiol* **26**: 91–98
- Beck T, Hall MN (1999) The TOR signalling pathway controls nuclear localization of nutrient-regulated transcription factors. *Nature* **402**: 689
- Bertram PG, Choi JH, Carvalho J, Chan TF, Ai W, Zheng XF (2002) Convergence of TOR-nitrogen and Snf1-glucose signaling pathways onto Gln3. *Mol Cell Biol* **22**: 1246–1252
- Bodenmiller B, Aebersold R (2010) Quantitative analysis of protein phosphorylation on a system-wide scale by mass spectrometry-based proteomics. *Methods Enzymol* **470**: 317–334
- Bolster DR, Crozier SJ, Kimball SR, Jefferson LS (2002) AMP-activated protein kinase suppresses protein synthesis in rat skeletal muscle through down-regulated mammalian target of rapamycin (mTOR) signaling. *J Biol Chem* **277**: 23977–23980
- Boone C, Bussey H, Andrews BJ (2007) Exploring genetic interactions and networks with yeast. *Nat Rev Genet* **8**: 437–449
- Celenza JL, Carlson M (1984) Cloning and genetic mapping of SNF1, a gene required for expression of glucose-repressible genes in *Saccharomyces cerevisiae*. *Mol Cell Biol* **4**: 49–53
- Chan TF, Carvalho J, Riles L, Zheng XF (2000) A chemical genomics approach toward understanding the global functions of the target of rapamycin protein (TOR). *Proc Natl Acad Sci USA* **97**: 13227–13232
- Colomina N, Liu Y, Aldea M, Gari E (2003) TOR regulates the subcellular localization of Ime1, a transcriptional activator of meiotic development in budding yeast. *Mol Cell Biol* **23**: 7415–7424
- Cornish-Bowden A, Cardenas ML (2001) Functional genomics. Silent genes given voice. *Nature* **409**: 571–572
- Crespo JL, Powers T, Fowler B, Hall MN (2002) The TOR-controlled transcription activators GLN3, RTG1, and RTG3 are regulated in response to intracellular levels of glutamine. *Proc Natl Acad Sci USA* **99**: 6784
- Daran-Lapujade P, Daran JM, van Maris AJ, de Winde JH, Pronk JT (2009) Chemostat-based micro-array analysis in baker's yeast. *Adv Microb Physiol* **54**: 257–311
- DeLuna A, Avendano A, Riego L, Gonzalez A (2001) NADP-glutamate dehydrogenase isoenzymes of *Saccharomyces cerevisiae*. Purification, kinetic properties, and physiological roles. *J Biol Chem* **276**: 43775–43783
- Dennis PB, Jaeschke A, Saitoh M, Fowler B, Kozma SC, Thomas G (2001) Mammalian TOR: a homeostatic ATP sensor. *Science* **294**: 1102–1105
- Fazio A, Jewett MC, Daran-Lapujade P, Mustacchi R, Usaite R, Pronk JT, Workman CT, Nielsen J (2008) Transcription factor control of growth rate dependent genes in *Saccharomyces cerevisiae*: a three factor design. *BMC Genomics* **9**: 341
- Grotkjaer T, Winther O, Regenberg B, Nielsen J, Hansen LK (2006) Robust multi-scale clustering of large DNA microarray datasets with the consensus algorithm. *Bioinformatics* **22**: 58–67
- Hardie DG (2007) AMP-activated/SNF1 protein kinases: conserved guardians of cellular energy. *Nat Rev Mol Cell Biol* **8**: 774–785
- Hong SP, Carlson M (2007) Regulation of snf1 protein kinase in response to environmental stress. *J Biol Chem* **282**: 16838–16845
- Inoki K, Ouyang H, Li Y, Guan KL (2005) Signaling by target of rapamycin proteins in cell growth control. *Microbiol Mol Biol Rev* **69**: 79–100
- Inoki K, Zhu T, Guan KL (2003) TSC2 mediates cellular energy response to control cell growth and survival. *Cell* **115**: 577–590
- Ishwaran H, Rao JS, Kogalur UB (2006) BAMarraytrade mark: Java software for Bayesian analysis of variance for microarray data. *BMC Bioinformatics* **7**: 59
- Jacinto E, Loewith R, Schmidt A, Lin S, Ruegg MA, Hall A, Hall MN (2004) Mammalian TOR complex 2 controls the actin cytoskeleton and is rapamycin insensitive. *Nat Cell Biol* **6**: 1122–1128
- Kall L, Storey JD, MacCoss MJ, Noble WS (2008) Assigning significance to peptides identified by tandem mass spectrometry using decoy databases. *J Proteome Res* **7**: 29–34
- Kamada Y, Funakoshi T, Shintani T, Nagano K, Ohsumi M, Ohsumi Y (2000) Tor-mediated induction of autophagy via an Apg1 protein kinase complex. *J Cell Biol* **150**: 1507
- Kuchin S, Treich I, Carlson M (2000) A regulatory shortcut between the Snf1 protein kinase and RNA polymerase II holoenzyme. *Proc Natl Acad Sci USA* **97**: 7916–7920
- Kuchin S, Vyas VK, Carlson M (2002) Snf1 protein kinase and the repressors Nrg1 and Nrg2 regulate FLO11, haploid invasive growth, and diploid pseudohyphal differentiation. *Mol Cell Biol* **22**: 3994–4000
- Lin SS, Manchester JK, Gordon JI (2003) Sip2, an N-myristoylated beta subunit of Snf1 kinase, regulates aging in *Saccharomyces cerevisiae* by affecting cellular histone kinase activity, recombination at rDNA loci, and silencing. *J Biol Chem* **278**: 13390–13397
- Liu Y, Xu X, Kuo M-H (2010) Snf1p regulates Gcn5p transcriptional activity by antagonizing Spt3p. *Genetics* **184**: 91–105
- Liu Z, Butow RA (2006) Mitochondrial retrograde signaling. *Annu Rev Genet* **40**: 159
- Lo WS, Duggan L, Emre NC, Belotserkovskya R, Lane WS, Shiekhattar R, Berger SL (2001) Snf1—a histone kinase that works in concert with the histone acetyltransferase Gcn5 to regulate transcription. *Science* **293**: 1142–1146
- Loewith R, Jacinto E, Wullschleger S, Lorberg A, Crespo JL, Bonenfant D, Oppiger W, Jenoe P, Hall MN (2002) Two TOR complexes, only one of which is rapamycin sensitive, have distinct roles in cell growth control. *Mol Cell* **10**: 457–468
- Lundgren DH, Martinez H, Wright ME, Han DK (2009) Protein identification using Sorcerer 2 and SEQUEST. *Curr Protoc Bioinformatics* Chapter 13: Unit 13.3
- Marion RM, Regev A, Segal E, Barash Y, Koller D (2004) Sfp1 is a stress- and nutrient-sensitive regulator of ribosomal protein gene expression. *Proc Natl Acad Sci USA* **101**: 14315
- Martin DE, Soulard A, Hall MN (2004) TOR regulates ribosomal protein gene expression via PKA and the Forkhead transcription factor FHL1. *Cell* **119**: 969
- Medvedik O, Lamming DW, Kim KD, Sinclair DA (2007) MSN2 and MSN4 link calorie restriction and TOR to sirtuin-mediated lifespan extension in *Saccharomyces cerevisiae*. *PLoS Biol* **5**: e261
- Monteiro G, Netto LE (2004) Glucose repression of PRX1 expression is mediated by Tor1p and Ras2p through inhibition of Msn2/4p in *Saccharomyces cerevisiae*. *FEMS Microbiol Lett* **241**: 221–228
- Oliveira AP, Patil KR, Nielsen J (2008) Architecture of transcriptional regulatory circuits is knitted over the topology of bio-molecular interaction networks. *BMC Syst Biol* **2**: 17

- Orlova M, Kanter E, Krakovich D, Kuchin S (2006) Nitrogen availability and TOR regulate the Snf1 protein kinase in *Saccharomyces cerevisiae*. *Eukaryot Cell* **5**: 1831–1837
- Patil KR, Nielsen J (2005) Uncovering transcriptional regulation of metabolism by using metabolic network topology. *Proc Natl Acad Sci USA* **102**: 2685–2689
- Petkova MI, Pujol-Carrión N, Arroyo J, García-Cantalejo J, Angeles de la Torre-Ruiz M (2010) Mtl1 is required to activate general stress response through Tor1 and Ras2 inhibition under conditions of glucose starvation and oxidative stress. *J Biol Chem* **285**: 19521–19531
- Petranovic D, Nielsen J (2008) Can yeast systems biology contribute to the understanding of human disease? *Trends Biotechnol* **26**: 584–590
- Polge C, Thomas M (2007) SNF1/AMPK/SnRK1 kinases, global regulators at the heart of energy control? *Trends Plant Sci* **12**: 20–28
- Portillo F, Mulet JM, Serrano R (2005) A role for the non-phosphorylated form of yeast Snf1: tolerance to toxic cations and activation of potassium transport. *FEBS Lett* **579**: 512–516
- Raamsdonk LM, Teusink B, Broadhurst D, Zhang N, Hayes A, Walsh MC, Berden JA, Brindle KM, Kell DB, Rowland JJ, Westerhoff HV, van Dam K, Oliver SG (2001) A functional genomics strategy that uses metabolome data to reveal the phenotype of silent mutations. *Nat Biotechnol* **19**: 45–50
- Ratnakumar S, Young ET (2010) Snf1 dependence of peroxisomal gene expression is mediated by Adr1. *J Biol Chem* **285**: 10703–10714
- Reinke A, Anderson S, McCaffery JM, Yates 3rd J, Aronova S, Chu S, Fairclough S, Iverson C, Wedaman KP, Powers T (2004) TOR complex 1 includes a novel component, Tco89p (YPL180w), and cooperates with Ssd1p to maintain cellular integrity in *Saccharomyces cerevisiae*. *J Biol Chem* **279**: 14752–14762
- Schmelzle T, Hall MN (2000) TOR, a central controller of cell growth. *Cell* **103**: 253–262
- Shirra MK, McCartney RR, Zhang C, Shokat KM, Schmidt MC, Arndt KM (2008) A chemical genomics study identifies Snf1 as a repressor of GCN4 translation. *J Biol Chem* **283**: 35889–35898
- Smets B, Ghillebert R, De Snijder P, Binda M, Swinnen E, De Virgilio C, Winderickx J (2010) Life in the midst of scarcity: adaptations to nutrient availability in *Saccharomyces cerevisiae*. *Curr Genet* **56**: 1–32
- Smith RL, Johnson AD (2000) Turning genes off by Ssn6-Tup1: a conserved system of transcriptional repression in eukaryotes. *Trends Biochem Sci* **25**: 325–330
- Smits HP, Cohen A, Buttler T, Nielsen J, Olsson L (1998) Cleanup and analysis of sugar phosphates in biological extracts by using solid-phase extraction and anion-exchange chromatography with pulsed amperometric detection. *Anal Biochem* **261**: 36–42
- Soontorngun N, Larochelle M, Drouin S, Robert F, Turcotte B (2007) Regulation of gluconeogenesis in *Saccharomyces cerevisiae* is mediated by activator and repressor functions of Rds2. *Mol Cell Biol* **27**: 7895–7905
- Sturm M, Bertsch A, Gropl C, Hildebrandt A, Hussong R, Lange E, Pfeifer N, Schulz-Trieglaff O, Zerck A, Reinert K, Kohlbacher O (2008) OpenMS - an open-source software framework for mass spectrometry. *BMC Bioinformatics* **9**: 163
- Takahashi H, McCaffery JM, Irizarry RA, Boeke JD (2006) Nucleocytosolic acetyl-coenzyme A synthetase is required for histone acetylation and global transcription. *Mol Cell* **23**: 207–217
- Usaite R, Jewett MC, Oliveira AP, Yates 3rd JR, Olsson L, Nielsen J (2009) Reconstruction of the yeast Snf1 kinase regulatory network reveals its role as a global energy regulator. *Mol Syst Biol* **5**: 319
- Usaite R, Nielsen J, Olsson L (2008) Physiological characterization of glucose repression in the strains with SNF1 and SNF4 genes deleted. *J Biotechnol* **133**: 73–81
- Valenzuela L, Aranda C, Gonzalez A (2001) TOR modulates GCN4-dependent expression of genes turned on by nitrogen limitation. *J Bacteriol* **183**: 2331
- van den Berg MA, de Jong-Gubbels P, Kortland CJ, van Dijken JP, Pronk JT, Steensma HY (1996) The two acetyl-coenzyme A synthetases of *Saccharomyces cerevisiae* differ with respect to kinetic properties and transcriptional regulation. *J Biol Chem* **271**: 28953–28959
- van Dijken JP, Bauer J, Brambilla L, Duboc P, Francois JM, Gancedo C, Giuseppin ML, Heijnen JJ, Hoare M, Lange HC, Madden EA, Niederberger P, Nielsen J, Parrou JL, Petit T, Porro D, Reuss M, van Riel N, Rizzi M, Steensma HY et al (2000) An interlaboratory comparison of physiological and genetic properties of four *Saccharomyces cerevisiae* strains. *Enzyme Microb Technol* **26**: 706–714
- Villas-Boas SG, Moxley JF, Akesson M, Stephanopoulos G, Nielsen J (2005) High-throughput metabolic state analysis: the missing link in integrated functional genomics of yeasts. *Biochem J* **388**: 669–677
- Wanke V, Pedruzzi I, Cameroni E, Dubouloz F, De Virgilio C (2005) Regulation of G0 entry by the Pho80-Pho85 cyclin-CDK complex. *EMBO J* **24**: 4271
- Woods A, Munday MR, Scott J, Yang X, Carlson M, Carling D (1994) Yeast SNF1 is functionally related to mammalian AMP-activated protein kinase and regulates acetyl-CoA carboxylase *in vivo*. *J Biol Chem* **269**: 19509–19515
- Wullschleger S, Loewith R, Hall MN (2006) TOR signaling in growth and metabolism. *Cell* **124**: 471–484
- Wullschleger S, Loewith R, Oppiger W, Hall MN (2005) Molecular organization of target of rapamycin complex 2. *J Biol Chem* **280**: 30697–30704
- Xie MW, Jin F, Hwang H, Hwang S, Anand V, Duncan MC, Huang J (2005) Insights into TOR function and rapamycin response: chemical genomic profiling by using a high-density cell array method. *Proc Natl Acad Sci USA* **102**: 7215–7220
- Ye T, Elbing K, Hohmann S (2008) The pathway by which the yeast protein kinase Snf1p controls acquisition of sodium tolerance is different from that mediating glucose regulation. *Microbiology* **154**: 2814–2826
- Young ET, Dombek KM, Tachibana C, Ideker T (2003) Multiple pathways are coregulated by the protein kinase Snf1 and the transcription factors Adr1 and Cat8. *J Biol Chem* **278**: 26146
- Zaman S, Lippman SI, Schneper L, Slonim N, Broach JR (2009) Glucose regulates transcription in yeast through a network of signaling pathways. *Mol Syst Biol* **5**: 245
- Zaman S, Lippman SI, Zhao X, Broach JR (2008) How *Saccharomyces* responds to nutrients. *Annu Rev Genet* **42**: 27–81
- Zhang J, Olsson L, Nielsen J (2010) The beta-subunits of the Snf1 kinase in *Saccharomyces cerevisiae*, Gal83 and Sip2, but not Sip1, are redundant in glucose derepression and regulation of sterol biosynthesis. *Mol Microbiol* **77**: 371–383



Molecular Systems Biology is an open-access journal published by European Molecular Biology Organization and Nature Publishing Group. This work is licensed under a Creative Commons Attribution-Noncommercial-No Derivative Works 3.0 Unported License.

Paper IV

Lipid biosynthesis monitored at the single-cell level in *Saccharomyces cerevisiae*

Chumnanpuen, P., C. Brackmann, S. K. Nandy, S. Chatzipapadopoulos, J. Nielsen, and A. Enejder.

Biotechnology Journal 2012, DOI: 10.1002/biot.201000386

Technical Report

Lipid biosynthesis monitored at the single-cell level in *Saccharomyces cerevisiae*

Pramote Chumnanpuen¹, Christian Brackmann², Subir K. Nandy¹, Susana Chatzipapadopoulos², Jens Nielsen¹ and Annika Enejder²

¹ Systems and Synthetic Biology, Department of Chemical and Biological Engineering, Chalmers University of Technology, Gothenburg, Sweden

² Molecular Microscopy, Department of Chemical and Biological Engineering, Chalmers University of Technology, Gothenburg, Sweden

There is increasing interest in bioengineering of lipids for use in functional foods, pharmaceuticals, and biofuels. *Saccharomyces cerevisiae* is a widely utilized cell factory for biotechnological production, thus a tempting alternative. Herein, we show how its neutral lipid accumulation varies throughout metabolic phases under nutritional conditions relevant for large-scale fermentation. Population-averaged metabolic data were correlated with lipid storage at the single-cell level monitored at submicron resolution by label-free coherent anti-Stokes Raman scattering (CARS) microscopy. While lipid droplet sizes are fairly constant, the number of droplets is a dynamic parameter determined by glucose and ethanol levels. The lowest number of lipid droplets is observed in the transition phase between glucose and ethanol fermentation. It is followed by a buildup during the ethanol phase. The surplus of accumulated lipids is then mobilized at concurrent glucose and ethanol starvation in the subsequent stationary phase. Thus, the highest amount of lipids is found in the ethanol phase, which is about 0.3 fL/cell. Our results indicate that the budding yeast, *S. cerevisiae*, can be used for the biosynthesis of lipids and demonstrate the strength of CARS microscopy for monitoring the dynamics of lipid metabolism at the single-cell level of importance for optimized lipid production.

Received 4 November 2010
Revised 17 June 2011
Accepted 11 August 2011
Article online 17 August 2011

Supporting information available online



Keywords: CARS microscopy · Lipid droplet quantification · Lipid storage · Nutrient Stress · *Saccharomyces cerevisiae*

1 Introduction

Baker's yeast, *Saccharomyces cerevisiae*, is an important cell factory used for the biotechnological production of a range of fuels, chemicals, and food ingredients. However, its ability to produce lipid species as alternatives to vegetable oils for human

consumption, petroleum-based fuels, or as components in pharmaceuticals has not been explored, to date, because it accumulates only minor amounts of lipids; estimated at less than 15% of its biomass [1]. Instead, the focus has been on the use of oleaginous yeasts, such as *Yarrowia lipolytica*, which have a capability to accumulate lipids at levels corresponding to more than 36% of their biomass [1]. Unfortunately, to achieve these high lipid levels, special cultivation conditions must be ensured and are presently restricted to laboratory-scale growth [2]. The thought of using *S. cerevisiae* instead as a study organism for lipid biosynthesis is therefore tempting because this organism is tolerant to harsh industrial conditions, is very well characterized, and is already used for large-scale production of different products.

Correspondence: Prof. Annika Enejder, Molecular Microscopy, Department of Chemical and Biological Engineering, Chalmers University of Technology, Kemivägen 10, SE-412 96 Gothenburg, Sweden
E-mail: enejder@chalmers.se

Abbreviations: Bodipy, boron dipyrromethene; CARS, coherent anti-Stokes Raman scattering; gDW, gram dry weight; HGLN, high glucose, low nitrogen; LGHN, low glucose, high nitrogen; TAG, triacylglyceride

All eukaryotic cells have a pool of neutral lipids stored as cytoplasmic droplets, which serve as reservoirs of cellular energy and building blocks for membrane lipids, consisting of triacylglyceride (TAG) and sterol esters [3, 4] surrounded by a monolayer of phospholipids and associated proteins [5–7]. In yeast, the lipid droplets consist of about 50% each of TAG and sterol esters [6, 8, 9]; the total amount of which is, in general, considered to be low relative to the dry cell mass (<15%). However, we hypothesize that the amount of neutral lipid storage in yeast is a highly dynamic variable because a unicellular organism, such as yeast, is able to quickly and easily adjust the internal metabolism to new conditions. Indeed, environmental stress and starvation induce increased synthesis and accumulation of neutral lipids [6, 10]. Clearly, fundamental insights into lipid droplet cell biology are of utmost importance for efficient utilization of the yeast lipid metabolism for the biosynthesis of valuable lipid species using *S. cerevisiae* as a cell factory.

To support this development, we have quantified the accumulation of TAG throughout different metabolic stages (i.e., glucose, ethanol, and stationary phases in batch cultivation) characteristic for industrially grown yeast and carried out unique single-cell monitoring of the three-dimensional distribution and amounts of lipids stored in living, unlabeled cells by coherent anti-Stokes Raman scattering (CARS) microscopy. This emerging technique has several advantages over present technology based on fluorescence microscopy, the main disadvantage of which is necessary labeling with fluorescent markers, resulting in a strong dependence on labeling efficiency or expression of fluorescent protein in the structure of interest. Together with dependence on fluorescence yield, which is determined by the local chemical environment, this introduces variations and uncertainties in quantitative analysis, for example, reported for the commonly used lipid stains Nile red and boron dipyrromethene (Bodipy) [11]. Furthermore, by using labeling, the cells are studied in a modified state with possible effects on their properties and for lipids it was shown that the use of alcohols in staining protocols influenced lipid droplet morphology [12]. It is often also of interest to co-localize visualized lipid droplets with other organelles by means of double labeling protocols. However, this possibility is often limited due to the broad fluorescence emission of Nile red or the combined green and red fluorescence identified for Bodipy and recently addressed by Ohsaki et al. [13]. Fluorescence microscopy is also, in many situations, limited by sample photo-bleaching, in particular, when using pro-

tein tagging. Nevertheless, intracellular lipid droplets in *S. cerevisiae* have been visualized by fluorescence tagging the protein Erg6 with green fluorescent protein (GFP) [7]. Thus, the drawbacks of established technology make a label-free method for lipid visualization and quantification without these limitations of high interest. CARS microscopy probes intrinsic molecular vibrations, making it a label-free technique that allows live-cell studies under native conditions. In addition, it offers the advantages of three-dimensional imaging with high spatial resolution, good sample penetration, and low risk for photo-induced effects and damage. CARS is a laser-induced nonlinear optical four-wave mixing process in which combined excitation and scattering generates blueshifted anti-Stokes scattered photons in a sample. An enhanced CARS signal is achieved as the applied laser fields are tuned into resonance with a Raman-active molecular vibration, and thereby target specific species or molecular groups. Compared with spontaneous Raman scattering, which also allows specific imaging probing molecular vibrations, CARS is induced by resonant vibrational excitation and results in coherent, directed signal emission that allows efficient collection. Thus, CARS signals are orders of magnitude higher than those of spontaneous Raman scattering, effectively reducing image acquisition times, clearly favorable for studies in living cells. CARS probing the symmetric stretching vibration of CH₂ groups in lipid acyl chains has become an established method for chemically specific imaging of lipids [14, 15] and applied in studies on single cells [16], multi-cellular organisms [17], and tissues [18, 19]. Specific imaging of intracellular lipid droplets in *S. cerevisiae* by CARS microscopy has also been presented [20].

In this study, the levels of lipid accumulation in yeast were investigated for two nutrient stress conditions: (i) high carbon and low nitrogen access and (ii) low carbon and high nitrogen access [21]. The overall yeast metabolism was monitored by biomass measurements and analysis of all key extracellular metabolites, temporal profiles of OD₆₀₀, dry cell weight, CO₂, and chromatography (HPLC) measurements. In addition, TAG analysis was carried out to obtain a population-based average of triacylglyceride contents for comparison with single-cell data obtained from CARS microscopy. This experimental outline allowed us to monitor and quantify lipid accumulation under conditions typical for large-scale industrial growth at both population-averaged and single-cell levels and to identify phases for optimal lipid yield using the conventional and robust yeast strain *S. cerevisiae*.

2 Materials and Methods

2.1 Yeast strain and cultivation conditions

Batch cultivations of yeast strain CEN.PK 113-7D MAT α SUC2 MAL2-8C (Scientific Research and Development GmbH, Germany) were set up in duplicate under two different conditions, corresponding to nitrogen and carbon starvation. Aerobic batch cultivations were carried out in well-controlled 1-L bioreactors (DASGIP) with a working volume of 700 mL. The growth medium employed in the cultivations was that specified by Verduyn et al. [22], but the initial concentrations of nitrogen ($(\text{NH}_4)_2\text{SO}_4$) and carbon (glucose) sources were adjusted, according to the stoichiometry for cell growth as described by Stephanopoulos et al. [23] and the “calorie restriction condition” defined by Lin and Sinclair [24]. A glucose concentration of at least 20 g/L and an ammonium sulfate concentration of 3.5 g/L are required in the medium to reach a biomass concentration of 12 gram dry weight (gDW)/L for the CEN.PK 113-7D yeast strain. Therefore, glucose and $(\text{NH}_4)_2\text{SO}_4$ concentrations of 20 g/L and 2 g/L, respectively, were used in the medium to achieve a condition of nitrogen starvation, the high glucose, low nitrogen (HGLN) condition. To instead induce a glucose starvation condition (low glucose, high nitrogen (LGHN)), a glucose concentration of 5 g/L and a $(\text{NH}_4)_2\text{SO}_4$ concentration of 3.5 g/L were used.

Cells were transferred from the pre-culture to obtain initial cell concentrations corresponding to an OD_{600} of around 0.01. The fermentations were carried out with aeration using atmospheric air set to 30 L/h (1 atm., 30°C) and agitation at 800 rpm. The temperature was kept constant at 30°C and the pH was maintained at 5.0 by the addition of 2M KOH. The concentrations of carbon dioxide and oxygen in the exhaust gas were monitored by an off-gas analyzer (DASGIP).

Samples were harvested from the cultivation media every second hour and immediately filtered through a 0.45 μm pore-size cellulose acetate filter (VWR) and stored at -20°C before analysis. Biomass production was evaluated by measurements of OD_{600} and dry cell weight. Glucose, glycerol, ethanol, and acetate concentrations were determined by HPLC analysis using an Aminex HPX-87H column (Biorad, Hercules, CA) [25].

2.2 CARS microscopy

CARS microscopy measurements were carried out using a laser system consisting of a Nd:Vanadate pump laser (Picotrain, HighQ Lasers GmbH) combined with a ring-cavity optical parametric oscilla-

tor (OPO; Levante, APE GmbH). The system provided two laser beams of picosecond pulse trains required to induce the CARS process: one from the Nd:Vanadate laser at 1064 nm and one from the OPO at 817 nm. The frequency shift between the beams corresponds to the symmetric stretching vibration of acyl-chain CH_2 groups, at 2845 cm^{-1} , and therefore, gives rise to a resonantly enhanced CARS signal from CH_2 bonds in the sample. The co-propagating beams were directed into an inverted laser-scanning microscope (Eclipse TE-2000-E, Nikon) equipped with a beam scanner (Nikon C1) and focused on the sample (objective 40 \times Nikon Plan Fluor, N.A. 1.3). Typical average laser powers at the sample were 20 mW per beam. The forward-propagating CARS signal, generated at 663 nm, was collected to a photomultiplier tube (Hamamatsu R6357) equipped with bandpass filters. Three-dimensional image data, z stacks, were acquired by scanning different horizontal planes in the sample. A further description of the CARS microscopy setup can be found in reference [15].

The yeast-cell samples for CARS microscopy were prepared by taking cell culture suspension from the fermentation vessel after 12, 21, and 38 h of growth. A small volume, 3 μL , was transferred to a chamber consisting of two cover-glass slides and a gasket (Invitrogen, Secure Seal Spacer $d = 9 \text{ mm}$ $h = 0.12 \text{ mm}$) mounted in a sandwich construction. The cells were immobilized during measurements by coating the lower cover slide with poly-L-lysine to attach the cells to the glass surface.

For each condition and time point studied, z stacks of CARS images were measured, covering an area of $20 \times 20 \mu\text{m}^2$ (256 \times 256 pixels) and a depth of 10 μm (vertical step size 0.5 μm). The spatial resolution of the CARS microscopy setup was estimated to 0.4 μm laterally and 1 μm axially, corresponding to a probe volume of 0.13 μm^3 (fL). Numbers and sizes of lipid droplets in 232 and 197 yeast cells were evaluated for the HGLN and LGHN conditions, respectively.

Image analysis consisted of two major steps: a local intensity thresholding procedure [26] was employed to identify lipid droplets, which were then automatically counted and measured using a plug-in tool (3D Object Counter) for the ImageJ image analysis software [27]. Although the lipid droplets were monitored in three dimensions through the cells, evaluation of droplet size was based on two-dimensional information due to the lower spatial resolution of the microscope in the axial (z) direction. Hence, lipid droplet sizes were determined using the built-in ImageJ particle analyzer routine for analysis of the image plane corresponding to the central position of the imaged cells.

2.3 Lipid extraction and TAG measurement

The freeze-dried samples from each time point were extracted and analyzed in technical replicates. The lipid extraction method was adapted from Bligh and Dyer [28]. 20 mg of freeze-dried yeast cells were incubated with 7 mL chloroform/methanol (2:1, v/v) for 3 h at 4°C on a rotary shaker with a speed of 200 rpm and supplemented with 1.7 mL of 0.73% sodium chloride, vigorously shaken. Following centrifugation at 3000 rpm at 4°C for 4 min, the organic phase was collected for later analysis, whereas the remaining aqueous phase was vigorously mixed and centrifuged with 5 mL chloroform/methanol (85:15, v/v). The total procedure was repeated three times. The collected organic material was combined and evaporated under a nitrogen stream at 40°C. Total lipids were dissolved in 0.5 mL chloroform/methanol (2:1, v/v) and kept at -30°C. The resulting lipid extract was further fractionated using TLC, in which the lipid solution was applied to a TLC plate (Silica gel 60, 20 × 20 cm, 0.5 mm layer, Merck, Darmstadt, Germany) using a solvent system of heptane/2-propanol/acetic acid (95:5:1, v/v/v). Individual lipids were visualized by spraying the sample with 0.2% 2',7'-dichlorofluoresceine in ethanol and identified by comparison of their R_f values with known standards. The bands corresponding to triacylglycerides were manually scraped off for TAG measurement, using the commercial kit "Triglycerides Liquid Stable Reagent" (Thermo Scientific). Results were given in mmol/gDW, which was converted into % (w/w) using an approximate molar mass for TAG in yeast of 819 g/mol, assuming a composition of 33% 16-carbon chains (three chains; 769.2 g/mol) and 61% 18-carbon chains (three chains; 846 g/mol) [29].

2.4 Statistical analysis

To ensure that the biological duplicates in each condition and also the technical replicates were not significantly different, the student paired *t* test was performed. SPSS software version 17.0 (SPSS Inc, Chicago, IL) was used for all analyses and *P* values of ≤ 0.05 were considered to differ significantly.

3 Results and discussion

The population-averaged data show general trends for the impact of starvation on the cell metabolism. Under HGLN conditions, the cells took approximately 21 h to finish their exponential phase with a glucose consumption rate of 0.019 g/(gDW h)

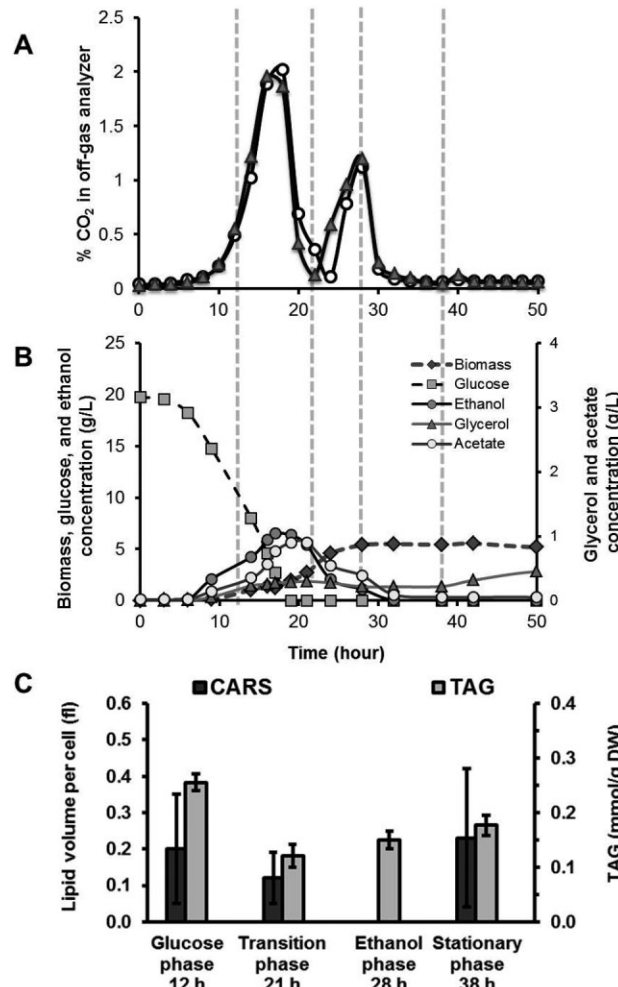


Figure 1. Fermentation profiles for the HGLN condition. (A) CO_2 profiles measured on duplicate fermenters and showing two peaks, representing growth on glucose and ethanol, respectively. The vertical dashed lines represent the time points for lipid analysis (12, 21, 28, and 38 h). (B) Profiles of biomass and metabolite concentrations (glucose, glycerol, acetate, and ethanol) measured during fermentation. (C) Cellular lipid content during fermentation presented as average lipid volume per cell with standard deviation (for details, see the Results and discussion), evaluated from CARS microscopy images ($n = 232$) and amount of TAG ($n = 6$). Data are presented as means \pm SD. The evaluated lipid volumes correspond to 4.5, 3.5, and 3.8 lipid droplets per cell for the time points 12, 21, and 38 h, respectively.

(Figs. 1A and B and Table 1). In contrast, the condition with glucose starvation and excess nitrogen (LGHN) made the cells finish their exponential phase faster; the shift from glucose to ethanol phase occurred within 15 h with a glucose consumption rate of 0.012 g/(gDW h) (Figs. 2A and B, and Table 1). This resulted in 2.5 times less biomass production and a lower maximum specific growth rate than that of the HGLN condition. In addition, the total yields of ethanol, glycerol, and acetate

Table 1. Specific rates and yields for the two sets of fermentations

Condition	μ_{\max} ^{a)}	Y_{sx} ^{b)}	Y_{se} ^{c)}	Y_{sg} ^{d)}	Y_{sa} ^{e)}	$r_s^f)$
HGLN	0.21	0.089	0.42	0.078	0.093	0.019
LGHN	0.17	0.070	0.35	0.035	0.046	0.012

a) The specific growth rate of biomass (unit: h^{-1}).
b) Biomass yield on glucose (unit: g biomass formed/g glucose consumed).
c) Ethanol yield on glucose (unit: g ethanol formed/g glucose consumed).
d) Glycerol yield on glucose (unit: g glycerol formed/g glucose consumed).
e) Acetate yield on glucose (unit: g acetate formed/g glucose consumed).
f) Specific glucose uptake rate (unit: g glucose/g biomass/h).

were lower (Table 1) due to a lack of the primary nutrient source, glucose.

Both nutritional conditions (Figs. 1 and 2) showed fermentative metabolism in which consumption of glucose resulted in production of biomass, ethanol, glycerol, and acetate. In parallel, high glucose concentrations lead to a higher production of fatty acids, resulting in an accumulation of lipid droplets, probably by the integration of signals through the protein kinase Snf1 [30]. After 12 h of growth in the glucose phase, the amount of TAG, about 0.25 mmol/gDW (20.5% w/w), was similar for both excess and limited access to glucose. The corresponding data obtained from the single-cell CARS microscopy studies were 4.5 and 3.8 lipid droplets per cell on average and evaluated lipid droplet diameters of 0.4 and 0.5 μm for the HGLN and LGHN conditions, respectively. Sizes of intracellular lipid droplets in *S. cerevisiae* were determined, using electron microscopy by Czabany et al. [31], resulting in diameters in the range of 0.3–0.5 μm . Typical lipid droplet sizes are thus similar to the spatial resolution of optical microscopy and imaging results in a size overestimation due to convolution with the microscope point-spread function [32]. For CARS microscopy, the nonlinear dependence on excitation intensity and density of probed molecular bonds reduces such an effect to some extent [26]. Nevertheless, an overestimation can still be expected for the diameters evaluated from CARS microscopy, which also seems probable in relation to the electron microscopy results. Assuming spherical lipid droplets, average lipid volumes per cell of 0.2 fL (Figs. 1C and 2C) can be estimated for both conditions and, in relation to the spatial resolution, apparent differences in diameters and calculated volumes must be considered of low significance. Nevertheless, the evaluated averages provide volume estimations as presented in Figs. 1C and 2C. Thus, both methods for lipid quantification indicated that lipid accumulation could not be significantly enhanced by loading the medium with excess amounts of glucose. After 21 h, corresponding to the glucose-ethanol transitional

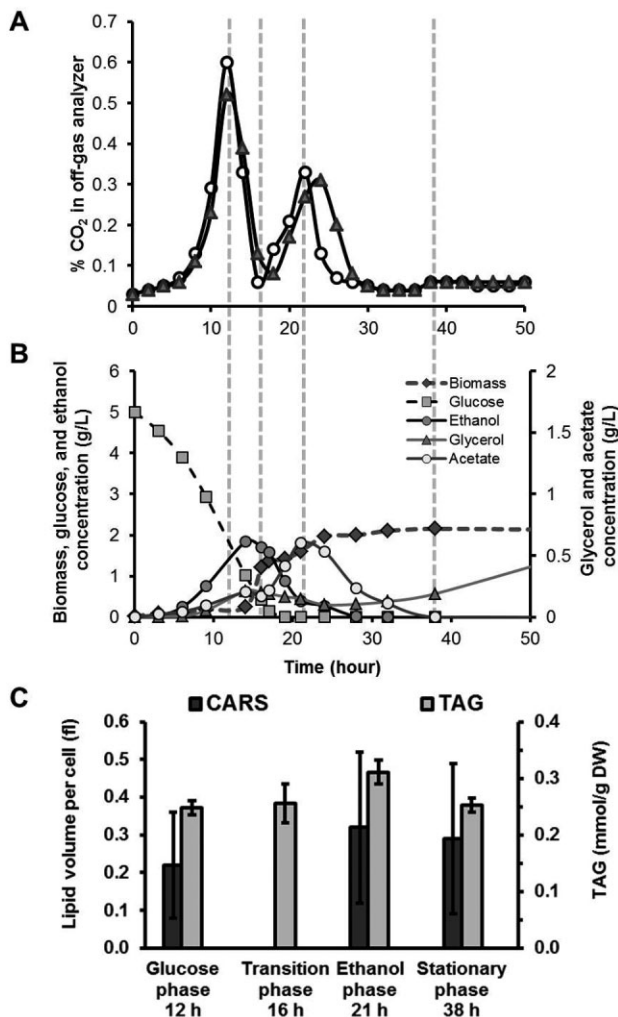


Figure 2. Fermentation profiles for the LGHN condition (A) CO_2 profiles measured on duplicate fermenters and showing two peaks representing growth on glucose and ethanol, respectively. The vertical dashed lines represent the time points for lipid analysis (12, 16, 21, and 38 h). (B) Profiles of biomass and metabolite concentrations (glucose, glycerol, acetate, and ethanol) measured during fermentation. (C) Cellular lipid content during fermentation presented as average lipid volume per cell with standard deviation (for details, see the Results and discussion), evaluated from CARS microscopy images ($n = 197$) and amount of TAG ($n = 6$). Data are presented as means \pm SD. The evaluated lipid volumes correspond to 3.8, 6.2, and 3.6 lipid droplets per cell for the time points 12, 21, and 38 h, respectively.

phase for HGLN fermentation, the TAG amount decreased to around 0.12 mmol/gDW (9.8% w/w), also found by CARS measurements, corresponding to 3.5 lipid droplets per cell on average. With an evaluated droplet diameter of 0.4 μm , this amounts to a lipid volume of 0.1 fL per cell for this condition and time point. The observed decrease is reasonable, considering that the cells need to mobilize TAG when glucose is depleted before ethanol metabolism increases and becomes effective. In con-

trast, the amount of TAG remained constant for LGHN conditions during the glucose–ethanol transition phase at 16 h (Fig. 2C). For the ethanol phase, an increase in TAG to about 0.31 mmol/gDW (25.4% w/w) and an increase in the number of lipid droplets to 6.2 per cell (diameter 0.5 µm, volume per cell 0.3 fL) is observed (Fig. 2C). A slight increase in TAG level (~ 20%) was found after 28 h when the cells shifted to the ethanol phase in HGLN cultivation (Fig. 1C). Under the LGHN fermentation conditions, lipid accumulation is stimu-

lated by conversion of ethanol into lipid precursors in *S. cerevisiae* [33], exhibiting TAG densities also reported for the oleaginous yeast strain *Yarrowia lipolytica* [1]. The quantitative single-cell analysis made by CARS microscopy indicates that by harvesting the population in the ethanol phase, when many cells show a high number of lipid droplets, the maximal lipid yield can be achieved, estimated to be 0.3 fL per cell. In the subsequent stationary phase, sampled at 38 h, both conditions show similar numbers of lipid droplets per cell: 3.8 and 3.6 for

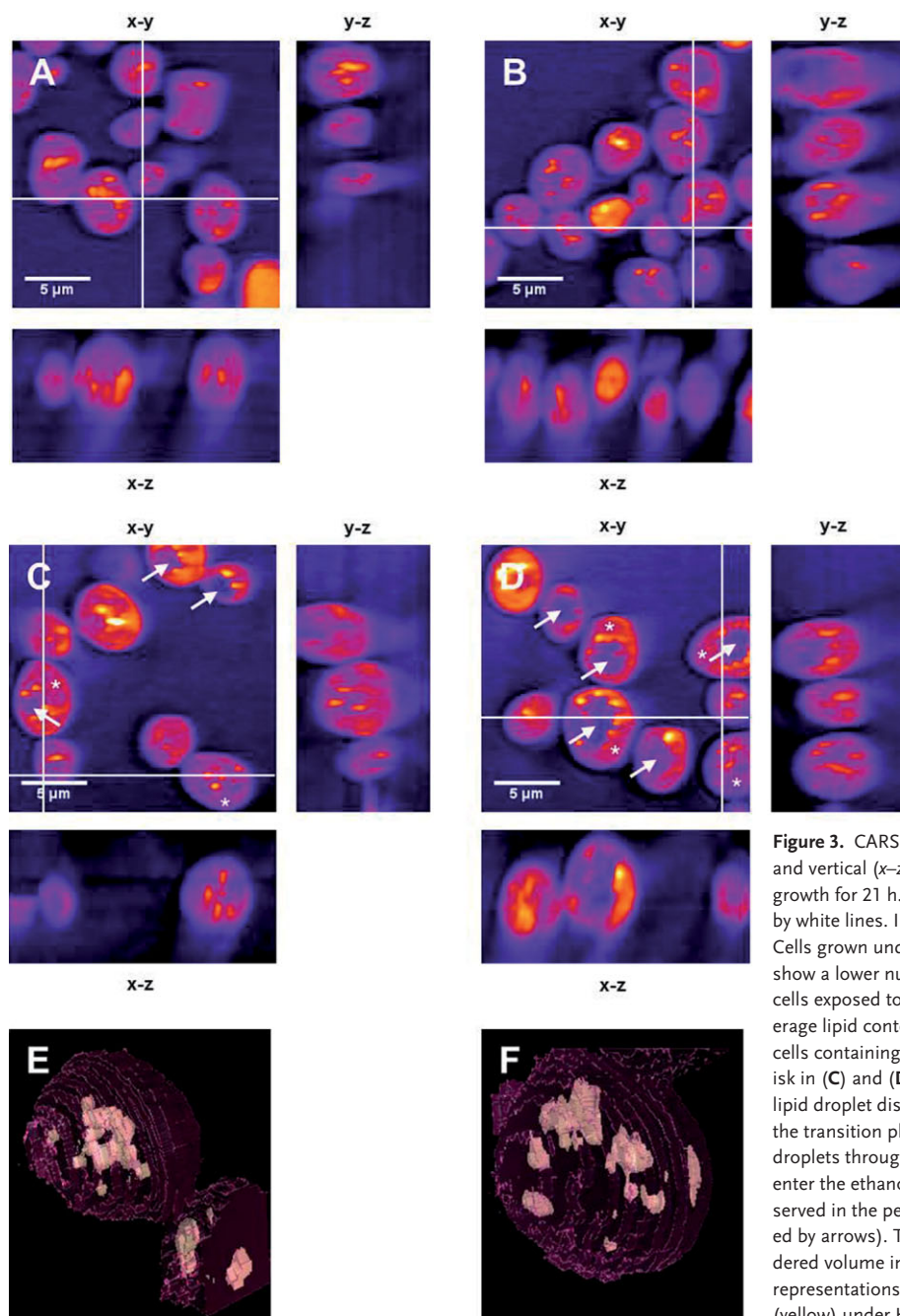


Figure 3. CARS microscopy images showing horizontal (x-y) and vertical (x-z, y-z) views of yeast cells measured after growth for 21 h. Positions of the vertical views are indicated by white lines. Image sizes, $20 \times 20 \mu\text{m}$ and $20 \times 10 \mu\text{m}$. Cells grown under HGLN conditions (**A** and **B**), on average show a lower number of lipid droplets per cell compared with cells exposed to LGHN conditions (**C** and **D**). The higher average lipid content for the LGHN condition is represented by cells containing multiple lipid droplets indicated by an asterisk in (**C**) and (**D**). The two conditions also show different lipid droplet distribution patterns. Whereas HGLN cells in the transition phase exhibit an even distribution of lipid droplets throughout the intracellular volume, LGHN cells enter the ethanol phase and lipid droplets can often be observed in the periphery surrounding larger vacuoles (indicated by arrows). This arrangement can also be seen in the rendered volume images, showing complete three-dimensional representations of yeast cells (magenta) and lipid droplets (yellow) under HGLN (**E**) and LGHN (**F**) conditions.

HGLN and LGHN, respectively. The evaluated average lipid droplet diameters were 0.5 µm for both HGLN and LGHN conditions at this time point and calculated volumes per cell were 0.2 and 0.3 fL, respectively. A difference could be observed in the corresponding TAG levels, 0.18 mmol/gDW (13.86% w/w) for HGLN conditions and 0.25 mmol/gDW (19.25% w/w) for LGHN condition. Thus, in the stationary phase, TAG production increased following the ethanol phase for HGLN, whereas TAG was mobilized for LGHN. CARS microscopy measurements signify that the mechanisms of droplet formation appear to be a fundamental, standardized process in which average sizes and lipid densities are more or less constant, irrespective of nutritional conditions or fermentative phases. Note that the normalized CARS signal varied by merely 15% throughout the different metabolic conditions investigated, indicating similar lipid droplet densities.

The error bars for the evaluated volumes per cell (Figs. 1C and 2C) indicate cell-to-cell variations also observed in the CARS microscopy images shown in Figs. 3A–D. Images were measured after growth for 21 h for the HGLN (Figs. 3A and B) and LGHN (Figs. 3C and 3D) conditions. In addition to horizontal x - y plane views, vertical x - z and y - z plane views measured at the positions of the white lines are shown. Even though individual HGLN cells in Figs. 3A and B show up to 5 droplets per cell, most cells show less, resulting in the reported average value of 3.5 droplets per cell for this condition and time point. In contrast, a higher number of lipid droplets per cell was more common for LGHN (Figs. 3C and 3D, cells indicated by asterisks). CARS data show a larger spread than the TAG levels, based on measurements of much larger cell populations. However, it should be noted that the data spread does not represent the precision of the CARS technique, but rather cell-to-cell variations encountered with any microscopy technique based on single-cell measurements. Nevertheless, it is interesting to see that the average trends of the CARS measurements are consistent with those of the TAG levels. More in-depth comparison between data evaluated from CARS microscopy images and TAG values needs to take lipid droplet sizes more into account and is dependent on the previously discussed size accuracy. In addition, effects such as cell shrinking, resulting in a reduction in cell size without a decrease in cell mass, may need to be considered for a comparison of CARS and TAG results of the stationary phase.

In addition to quantitative measurements of lipid content at the single-cell level, CARS microscopy z stacks provide unique three-dimension-

al information on the lipid droplet distribution represented by the planar horizontal and vertical views shown in Figs. 3A–D and the volume images in Figs. 3E and F. This allows us to evaluate the intracellular arrangement of the lipid droplets and a significant difference was observed for the two nutritional conditions after 21 h. Whereas the lipid droplets were evenly distributed in cells under HGLN conditions (still in the transition phase at 21 h), they were located in the periphery of cells exposed to LGHN conditions (early ethanol phase at 21 h). This was most likely due to the formation of vacuoles in many LGHN cells, of which 89% exhibited a vacuole, in contrast to the HGLN cells (18%). This trend can be seen in Fig. 3, where several of the LGHN cells in Figs. 3C and D have a vacuole, as indicated by arrows. This difference in lipid droplet arrangement is also shown in the single-cell volume images in Figs. 3E and F (see the Supporting information for 360° rendering movies).

Together, the results clearly show that there is dynamic regulation of the lipid metabolism in the widely utilized yeast strain *S. cerevisiae* and these dynamic changes can be captured at the single-cell level using CARS microscopy. The accumulation of TAG involves both nutrient sensing of nitrogen, carbon, and energy sources [6], probably by the integration of signals through the protein kinase Snf1 [30].

4 Concluding remarks

We have demonstrated the strength of combining population-averaged metabolic analysis with single-cell imaging using CARS microscopy. *S. cerevisiae*, which is widely used in the biotechnical industry, had a highly dynamic ability to accumulate lipids, depending on nutritional conditions and fermentative phase. By controlling parameters such as nitrogen, carbon, and energy sources, lipid biosynthesis can be influenced. Interestingly, the amount of accumulated lipids during the glucose phase was not significantly influenced by the initial glucose concentration, indicating that it could not be used to enhance lipid synthesis. The highest amounts of accumulated neutral lipids, about 0.3 fL/cell and 0.31 mmol TAG/gDW (25.4% w/w), were found in the ethanol phase and exceeded the amount of lipids synthesized during glucose fermentation.

Part of this work was financed by the Chalmers Foundation and the Knut and Alice Wallenberg Foundation. We also acknowledge financial support from

the EU-funded project UNICELLSYS, the Swedish Scientific Research Council, and the European Cooperation in Science and Technology (COST). P.C. would also like to thank the Office of the Higher Education Commission, Thailand for support by grant under the Strategic Scholarships for Frontier Research Network for Ph.D. program.

The authors have declared no conflict of interest.

5 References

- [1] Beopoulos, A., Cescut, J., Haddouche, R., Uribelarrea, J. L. et al., *Yarrowia lipolytica* as a model for bio-oil production. *Prog. Lipid Res.* 2009, **48**, 375–387.
- [2] Bankar, A. V., Kumar, A. R., Zinjarde, S. S., Environmental and industrial applications of *Yarrowia lipolytica*. *Appl. Microbiol. Biotechnol.* 2009, **84**, 847–865.
- [3] Goodman, J. M., Demonstrated and inferred metabolism associated with cytosolic lipid droplets. *J. Lipid Res.* 2009, **50**, 2148–2156.
- [4] Zweytick, D., Athenstaedt, K., Daum, G., Intracellular lipid particles of eukaryotic cells. *Biochim. Biophys. Acta* 2000, **1469**, 101–120.
- [5] Brown, D. A., Lipid droplets: Proteins floating on a pool of fat. *Curr. Biol.* 2001, **11**, R446–449.
- [6] Mullner, H., Daum, G., Dynamics of neutral lipid storage in yeast. *Acta Biochim. Pol.* 2004, **51**, 323–347.
- [7] Natter, K., Leitner, P., Faschinger, A., Wolinski, H. et al., The spatial organization of lipid synthesis in the yeast *Saccharomyces cerevisiae* derived from large scale green fluorescent protein tagging and high resolution microscopy. *Mol. Cell. Proteomics* 2005, **4**, 662–672.
- [8] Leber, R., Zinser, E., Zellnig, G., Paltauf, F., Daum, G., Characterization of lipid particles of the yeast, *Saccharomyces cerevisiae*. *Yeast* 1994, **10**, 1421–1428.
- [9] Schaffner, G., Matile, P., Structure and composition of bakers-yeast lipid globules. *Biochem. Physiol. Pflanz.* 1981, **176**, 659–666.
- [10] Gasch, A. P., Werner-Washburne, M., The genomics of yeast responses to environmental stress and starvation. *Funct. Integr. Genomics* 2002, **2**, 181–192.
- [11] Gocze, P. M., Freeman, D. A., Factors underlying the variability of lipid droplet fluorescence in MA-10 Leydig tumor cells. *Cytometry* 1994, **17**, 151–158.
- [12] Fukumoto, S., Fujimoto, T., Deformation of lipid droplets in fixed samples. *Histochem. Cell Biol.* 2002, **118**, 423–428.
- [13] Ohsaki, Y., Shinohara, Y., Suzuki, M., Fujimoto, T., A pitfall in using BODIPY dyes to label lipid droplets for fluorescence microscopy. *Histochem. Cell Biol.* 2010, **133**, 477–480.
- [14] Le, T. T., Yue, S., Cheng, J. X., Shedding new light on lipid biology with coherent anti-Stokes Raman scattering microscopy. *J. Lipid Res.* 2010, **51**, 3091–3102.
- [15] Enejder, A., Brackmann, C., Svedberg, F., Coherent anti-Stokes Raman scattering microscopy of cellular lipid storage. *IEEE J. Sel. Top. Quantum Electron.* 2010, **16**, 506–515.
- [16] Nan, X., Cheng, J. X., Xie, X. S., Vibrational imaging of lipid droplets in live fibroblast cells with coherent anti-Stokes Raman scattering microscopy. *J. Lipid Res.* 2003, **44**, 2202–2208.
- [17] Hellerer, T., Axang, C., Brackmann, C., Hillertz, P. et al., Monitoring of lipid storage in *Caenorhabditis elegans* using coherent anti-Stokes Raman scattering (CARS) microscopy. *Proc. Natl. Acad. Sci. USA* 2007, **104**, 14 658–14 663.
- [18] Huff, T. B., Shi, Y., Fu, Y., Wang, H., Cheng, J. X., Multimodal nonlinear optical microscopy and applications to central nervous system imaging. *IEEE J. Sel. Top. Quantum Electron.* 2008, **14**, 4–9.
- [19] Le, T. T., Langohr, I. M., Locker, M. J., Sturek, M., Cheng, J. X., Label-free molecular imaging of atherosclerotic lesions using multimodal nonlinear optical microscopy. *J. Biomed. Opt.* 2007, **12**, 054007.
- [20] Brackmann, C., Norbeck, J., Åkeson, M., Bosch, D. et al., CARS microscopy of lipid stores in yeast: the impact of nutritional state and genetic background. *J. Raman Spectro.* 2009, **40**, 748–756.
- [21] Nandy, S. K., Venkatesh, K. V., Effect of carbon and nitrogen on the cannibalistic behavior of *Bacillus subtilis*. *Appl. Biochem. Biotechnol.* 2008, **151**, 424–432.
- [22] Verduyn, C., Postma, E., Scheffers, W. A., Vandijken, J. P., Effect of benzoic acid on metabolic fluxes in yeasts – a continuous-culture study on the regulation of respiration and alcoholic fermentation. *Yeast* 1992, **8**, 501–517.
- [23] Stephanopoulos, G. N., Aristidou, A. A., Nielsen, J., *Metabolic Engineering: Principles and Methodologies*, Academic Press, San Diego, 1998, pp. 119–121.
- [24] Lin, S. J., Sinclair, D., Molecular mechanisms of aging: Insights from budding yeast, in: Guarente, L. P., Partridge, L., Wallace, D. C. (Eds.), *Molecular Biology of Aging*, Cold Spring Harbor Laboratory Press, Cold Spring Harbor, 2008, pp. 483–516.
- [25] Zaldivar, J., Borges, A., Johansson, B., Smits, H. P. et al., Fermentation performance and intracellular metabolite patterns in laboratory and industrial xylose-fermenting *Saccharomyces cerevisiae*. *Appl. Microbiol. Biotechnol.* 2002, **59**, 436–442.
- [26] Hagmar, J., Brackmann, C., Gustavsson, T., Enejder, A., Image analysis in nonlinear microscopy. *J. Opt. Soc. Am. A* 2008, **25**, 2195–2206.
- [27] Abramoff, M. D., Magelhaes, P. J., Ram, S. J., Image processing with ImageJ. *Biophotonics International* 2004, **11**, 36–42.
- [28] Bligh, E. G., Dyer, W. J., A rapid method of total lipid extraction and purification. *Can. J. Biochem. Physiol.* 1959, **37**, 911–917.
- [29] Clausen, M. K., Christiansen, K., Jensen, P. K., Behnke, O., Isolation of lipid particles from baker's yeast. *FEBS Lett.* 1974, **43**, 176–179.
- [30] Usaite, R., Jewett, M. C., Oliveira, A. P., Yates, J. R., 3rd et al., Reconstruction of the yeast Snf1 kinase regulatory network reveals its role as a global energy regulator. *Mol. Syst. Biol.* 2009, **5**, 319, 319–330.
- [31] Czabany, T., Wagner, A., Zweytick, D., Lohner, K. et al., Structural and biochemical properties of lipid particles from the yeast *Saccharomyces cerevisiae*. *J. Biol. Chem.* 2008, **283**, 17 065–17 074.
- [32] Pawley, J. B. (Ed.), *Handbook of Biological Confocal Microscopy*, Springer, New York, 2006.
- [33] Modig, T., Liden, G., Taherzadeh, M. J., Inhibition effects of furfural on alcohol dehydrogenase, aldehyde dehydrogenase and pyruvate dehydrogenase. *Biochem. J.* 2002, **363**, 769–776.

Paper V

Rapid quantification of yeast lipid using microwave-assisted total lipid extraction and HPLC-CAD

Chumnanpuen, P.*, S. Khoomrung*, I. Nookaew, J. Nielsen. 2012.

**Equal contribution*

Submitted for publication

Rapid Quantification of Yeast Lipid using Microwave-assisted Total Lipid Extraction and HPLC-CAD

*Pramote Chumnanpuen[#], Sakda Khoomrung[#], Intawat Nookaew, and Jens Nielsen**

Systems and Synthetic Biology,
Department of Chemical and Biological Engineering,
Chalmers University of Technology,
Kemivägen 10, SE-412 96 Gothenburg, Sweden

#Authers contributed equally

*Corresponding Author:

Jens Nielsen

Systems and Synthetic Biology, Department of Chemical and Biological Engineering,
Chalmers University of Technology, Kemivägen 10, SE-412 96 Gothenburg, Sweden.

Email: nielsenj@chalmers.se

Abstract

We present a rapid quantification of yeast lipids using microwave-assisted total lipid extraction followed by HPLC-CAD. The microwave extraction was completed within 10 min at 60°C and the quantification of all lipid classes can be done in 45 min per sample at 35°C by HPLC-CAD analysis, which is significantly faster than with conventional lipid extraction methods. The developed method was validated in two ways; (I) through comparison with a conventional method (by Schneiter & Daum, 2006) and (II) through validation with spiked lipid standards (CH, TAG, FA) into the extraction solvent. There were no significant differences ($P>0.01$) in yields of lipid classes with both validations. By performing a simple modification of closed-vessel microwave extraction it was possible to carry out the cell disruption and extraction in Pyrex glass tubes kept inside the closed vessel. Hereby we are able to increase the number of sample preparations to several hundred samples per day. Pre-treated cell disruption steps are not required since the microwave extraction method provides equally quantitative results. The new microwave-assisted extraction method facilitates the preparation of extracted total lipid directly from yeast cells, but the method is likely to also be applicable for other biological samples.

List of Abbreviations

CL = cardiolipin, ES = ergosterol, FA = fatty acid, HILIC = hydrophilic interaction liquid chromatography, PA = phosphatidic acids, PC = phosphatidylcholine, PE = phosphatidylethanolamine, PI = phosphatidylinositol, PL = phospholipids, PS = phosphatidylserine, SE = sterolester, SM = sphingomyelin, TAG = triacylglycerol

Key Words

Yeast, total lipid extraction, lipid quantification, Microwave, HPLC-CAD

1. Introductions

Lipids are energy storage molecules and important structural components of all eukaryotic cell membranes. Yeast cell membranes are composed of three main components: phospholipids, sterols, and intramembrane proteins(1-3). The principal sterol in *Saccharomyces cerevisiae* is ergosterol (3). The principal phospholipids in this organism have been shown to be phosphatidic acid, phosphatidylethanolamine, phosphatidyl-inositol, phosphatidylserine, and phosphatidylcholine with fatty acid chains that are predominantly oleic acid (C18:1) and palmitoleic acid (C16:1), with smaller amounts of palmitic acid (16:0) and stearic acid (18:0), and very low amount of myristic acids (C14:0) (4, 5). Like other eukaryotes, yeast cells also have a pool of neutral lipids stored as cytoplasmic droplets (which serve as reservoirs of cellular energy and building blocks for membrane lipids) consisting of triacylglycerides (TAG) and sterol esters (SE) (6, 7) surrounded by a monolayer of phospholipids and associated proteins (2, 8, 9). In yeast, lipid droplets consist of TAG and SE in a ratio of about 1:1 (9-11). The total amount of lipids stored in lipid droplets is in general considered to be low relative to the dry cell mass (<15%), but we hypothesize that the amount of neutral lipid storage in yeast is a highly dynamic variable as a unicellular organism, like yeast, is able to fast and easily adjust its internal metabolism to new environmental conditions. Indeed, environmental stress and starvation have been shown to induce increased synthesis and accumulation of neutral lipids (9, 12).

For analysis of lipid compositions in yeast cells lipid extraction is a key process and the efficiency of extraction depends of the method applied. Lipid is most efficiently extracted from freeze-dried or freeze-thawed yeast cells(13) and these are the most commonly applied methods. Mechanical disintegration of the cells (sonication and bead mills), cell wall digestion (using zymolyase) or drying yeast at moderate temperatures can, however, enhance lipid extraction (3, 14, 15). The addition of steps for sample preparation and extraction do, however, cause problems about increasing

labor time but also imposes requirements for advanced skills to perform each specific step as well as it increases the possibility of errors because of sample loss during the multiple steps.

Recently, microwave technology has been introduced for lipid extraction in terms of performing fatty acid methyl ester (FAME) derivatization of fatty acids derived from several eukaryotic cells such as plant, animal, and fungal cells (16-20). To improve the sampling time we recently developed a modified closed-vessel method with microwave-assisted derivatization and demonstrated its application yeast fatty acid analysis (21). However, the application of microwave technology for total lipid extraction followed by analysis of all the lipid has not been studied before.

For lipid class separation and quantification, numerous high performance liquid chromatography (HPLC) methods have been used and developed for plant, animal, and microbial lipids (22, 23). Hydrophilic interaction chromatography (HILIC) is one of the most useful columns not only in metabolomic profiling but also for lipid profiling (24). This column is a relatively recent development, also termed reverse normal phase chromatography, which uses a polar stationary phase and its associated layer of water to promote chromatographic retention with partitioning against a mobile phase which has a high content of organic solvent.(25, 26) In this mode polar compounds are retained strongly and their elution is promoted by gradually increasing the aqueous content of the mobile phase.

Like ELSD, CAD allows HPLC detection of non-volatile or semi-volatile compounds and it has been used for lipid analysis (27). However, conventional UV detection is often not adequate and limited to chromophores (28) while other methods such as flame ionization detection (FID) or evaporative light-scattering detection (ELSD) have limitations in terms of precision, sensitivity and dynamic range (29, 30). For detection purposes, the usual optical methods (UV and fluorescence) are not well adapted to the direct analyses of lipids. Currently, ELSD and CAD detection methods

are used for the direct analyses of lipid classes. Both detection methods share the same principle of operation: (1) the mobile phase leaving the column is sprayed using a pneumatic nebulizer, (2) the droplets enter the heated tube where the solvent (partially) evaporates, (3) the solute particles enter into the detection chamber. However, the principal difference between the two detection methods is the technology used for solute particles detection: light diffusion for ELSD and aerosol charging for CAD(30). The CAD as a detector for lipid analysis has advantages over ELSD by higher sensitivity and better precision judged by both lowest limits of detection (LOD) and repeatability (RSD) values (30, 31). Comparing to another popular detector for lipid analysis mass spectrometry (MS) detector, CAD is cheaper and easier to use.

Here we present a new method for rapid quantification of yeast lipids using microwave-assisted total lipid extraction followed by HPLC-CAD. The method is validated and demonstrated for use in analysis of yeast lipids.

2. Material and Methods

2.1 Chemicals and Standards

All solvents and reagents in our study are analytical grade. Hexane and BF_3 (14% in MeOH), GC grade were purchased from Sigma-Aldrich, Germany. Milli-Q water (Gradient A10) was used throughout this study. All lipid standards and FAMEs standards were analytical grade, purchased from Sigma-Aldrich, Germany.

2.2 Yeast Strain and Cultivation Conditions

The yeast strain CEN.PK 113-7D MAT α SUC2 MAL2-8C (Scientific Research and Development GmbH, Germany) were grown aerobically in 50 mL Yeast Extract Peptone Dextrose (YPD) medium in 500-mL baffled shake flasks at 30 °C and 230 rpm. The initial glucose was 20 g/L concentration and the initial cell concentrations corresponding to an OD_{600} around 0.01 were inoculated.

Samples were harvested from the cultivation media during the stationary phase at 36 hours and transferred into 50 mL-falcon tubes

(VWR, Sweden) and centrifuged at a speed of 3,000 rpm for 5 min at 4°C to collect the biomass. The samples were then immediately frozen in liquid nitrogen and placed in freeze-dryer (instrument info) at -40 °C overnight.

2.3 Microwave-assisted lipid extraction

The lipid extraction method was performed based on the total lipid extraction protocol by Bligh and Dyer (1959) (32) with several modifications and the modified closed-vessel microwave system was adopted from Khoomrung et al (2012) (21). First, 10 mg of freeze-dried cell were weighed into the extraction tube and 10 µg of the internal standard (cholesterol) was added. After the addition of 7 ml of chloroform-methanol (2:1, v/v), the tubes were flushed with N_2 gas into the tube to get rid of air and closed tightly with a Teflon screw cap. All the extraction tubes were vortexed vigorously before placed in the microwave extraction capsule that contained 30 ml water inside. The extraction method was performed by reaching 60 °C in 6 min with 800 watt and stay at 60 °C for 10 min. After the samples cooled down to room temperature, 1.7 ml of 0.73% NaCl was added and the sample was vortexed vigorously. Thereafter the sample was centrifuged at 3000 rpm for 5 min for phase separation and the organic phase (at the bottom) was transferred into a new clean extraction tube. After the sample had been dried under vacuum and re-suspended with 200 µl of chloroform-methanol (2:1, v/v) the total lipid sample was transferred into the amber HPLC vials.

2.4 Lipid analysis via HPLC-CAD

Lipid separation and quantification were performed using the method modified from Silversand and Haux (33). Lipid separation was accomplished by HPLC (Dionex) equipped with a charge aerosol detector; CAD (Corona) supplied with nitrogen gas at 35 psi gas pressure. All the separated fractions were collected by an automated fraction collector; AFC-3000 (Dionex). A 5 µl volume of sample was injected in to the Luna 5 µm HILIC 200 Å 100 x 3.0 mm LC Column (Phenomenex). The

flow-rate was fixed at 0.8 ml/min during all runs. In this study, the proper column temperature was optimized by scanning the range 20 - 55°C. The chromatogram was record at 10 Hz frequency and gain for 100 pA. The polar and neutral lipid classes were separated by three solvent mixtures and gradient systems as follow: (A) hexane-acetic acid (99:1, v/v); (B) acetone-isopropanol-acetic acid (29:70:1, v/v/v); (C) water-acetone-isopropanol-acetic acid (9:20:70:1, v/v/v/v). Triethylamine (0.08%, v/v) was added to the solvent C to adjust pH. The samples were injected at time 0 and the gradient profile started at 100% of Solvent A and the solvent B was gradually increased to 5% in 14 min and it was always kept at 5% along the process. At the 15 min time point, solvent C was added to the system in a gradient where it was increasing to 40 % in 5 min, followed by a slower increase to 45% in 20 min. Finally, the gradient was reduced from 5% to 0% of solvent B and from 45% to 0% of solvent C in 5 min and then maintained at 100% of solvent A for 5 min. In total, the solvent program for the separation of all lipid classes took 45 min. Pure lipid standards were analyzed individually using chromatography to confirm their retention times and purity. Lipid standards were also co-eluted together with samples to identify peaks in unknown samples. Solutions of known concentrations of different lipid classes were mixed and lipid standard curves were generated to study the linearity of the detection method and to quantify lipid classes in unknown samples. Calibration curves were prepared for 5-1000 µg ml⁻¹ of PA, PE, PC, PS, PI, ES, TAG, FA, and ES. Each concentration of the standard solutions was injected twice and the average log₁₀ peak area for each lipid was plotted against the absolute amount of lipid. Correlation (r^2) was determined for all curves by linear regression.

2.5 FAMEs analysis

We used a standard procedure developed in our laboratory (21). Briefly, 10 mg of freeze-dried samples was mixed with 4 mL of hexane, 2 mL of 14 % BF₃ (in Methanol) and 5 µg of internal standard (17:0 fatty acid

standard was added. The sample was then flushed into the tube's head space with nitrogen gas for 30s and closed tightly with a Teflon screw cap. The tube was placed in to vessel containing 30 mL of milliQ water and then sealed with TFM screw cap. The tube was heated using a microwave digestion system (milestone start D, Sorisole Bergamo, Italy) equipped with rotor PRO-24. The temperature programming of microwave digestion was ramped (from room temperature) to 120 °C within 6 min and thereafter maintained at this temperature for 10 min. After cooling the sample to room temperature, 2 mL of milliQ water was added and the sample was shaken vigorously for 1 min followed by centrifugation at 2500 rpm for 5 min. The upper phase (hexane phase which contained the FAMEs) was analysed by GC-MS.

The FAMEs were separated and quantified using Focus GC ISQ single quadrupole GC-MS (Thermo Fisher scientific, USA). The separation of FAMEs was performed on Zebron (ZB-WAX) GC column (30 m x 0.25 mm I. D., 0.25 µm film thickness) from Phenomenex, Macclesfield, UK. The sample was injected in splitless injection mode (1µL at 240 °C) and Helium was used a carrier gas (1 mL/min). The column temperature was initially set at 50 °C (1.5 min), where after the temperature was ramped to 180 °C (25°C/min) for 1 min, followed by a further increased to 220 °C (10°C/min) where it was held for 1 min. Finally, the temperature was increased to 250 °C (15°C/min) and held for 3 min. The mass transfer line and ion source were set at 250 °C and 200 °C, respectively. The FAMEs were detected with electron ionization (70 eV) in scan mode (50-650 m/z) and selected ion monitoring mode at m/z 55, 67, 74 and 79 (for quantitative analysis). The identification of unknown FAMEs from yeast cells was achieved by comparing their retention times and mass spectrum profiles with known standards (Fig. 1). The quantification of FAMEs was performed using QuanBrowser function in the Xcalibur software version 2.0 (Thermo Fisher Scientific).

2.5 Data analysis

Result were expressed as mean \pm standard deviation from three independent replicates. The statistic program for social science (SPSS) software version 19.0 (SPSS Inc.) was used for statistical analysis. P values <0.01 were considered as statistically significant.

3. Results and Discussions

3.1 Chromatographic separation and lipid quantification using HPLC-CAD

The optimized separation and quantification method is to be used further in the validation part of the microwave-assisted extraction procedure and to obtain a solid protocol for lipid classes separation by the HILIC column, the column temperature, memory effect and quantification method were evaluated.

3.1.1 Effect of column temperature on the separation of lipid classes

One of the most investigated parameter for lipid separation using HPLC is the column temperature. To select a moderate temperature for lipid separation, we performed the lipid analysis using the HILIC column operated in a range of 20 – 55 °C. The chromatographic results in Fig. 1A show the effects of column temperature to the separation of all lipid classes. For neutral lipids, the two yeast storage lipids such as steryl ester (SE) and triacylglycerol (TAG) seem to separate well only at $\geq 25^\circ\text{C}$, since a low column temperature effects the eluting time of TAG resulting in a broad peak at 20 °C. However, this evidence was not found to affect the SE peak at all. The free fatty acid (FA) peak was sharper at higher column temperature and had peak tail problems at low column temperature.

We used cholesterol (CH), which yeast cannot produce, as the spiked internal standard. It is therefore important to have a good separation between CH and ergosterol (ES), which is the main sterol in yeast. Focusing on the two sterol standards, CH and ES, just like TAG, were separated well only at $\geq 25^\circ\text{C}$ and a higher column temperature speed up the eluting time. Therefore, the sterol peaks

were sharper, came out faster, and separated better at higher column temperatures.

Phospholipids (PL) separation, on the other hand, could be separate well only at 30-35 °C. The lower column temperature affects separation of all PLs, i.e. PA had peak tailed effect and there were co-elution problems for PE-PC and PS-PI. The higher column temperature, in contrast, results in increasing eluting time. Thus, the PI peak was broad and low at high column temperatures ($\geq 40^\circ\text{C}$).

To investigate the specific effect of column temperature on the PI peak, we perform the exact same optimization but using only PI instead of mixed standards as shown in Fig. S1. We found the same pattern as found for mixed standards which proves that when PI is delayed in elution it is detected as a broad and low peak at high column temperature.

Considering all the effects of column temperature for each lipid peak, we selected 35 °C as the optimal for lipid class separation for both neutral lipids and phospholipids. At this selected column temperature, all the peaks are well separated without peak tails effect.

3.1.2 Sample carryover

Sample carryover is a significant problem when dealing with HPLC separation(34), the % column recovery normally can be used to evaluate sample carryover. However, it was not possible to determine the column recovery when the analysis was performed on gradient HPLC-CAD. Because the analyte intensity obtained from CAD detector depends on the composition of the mobile phase and increases with organic solvent. To evaluate sample carryover, we run a modified gradient-HPLC program that similar to the program we used for lipid classes separation with increasing solvent C up to 65% (held for 5 min) instated of the 45% in normal run time (data not shown). The increasing solvent C in system is intended to increase polarity to the system to elute polar lipids that may remain from the previous run. There were no peak in those test run was detected and this was an evidence for no sample carryover.

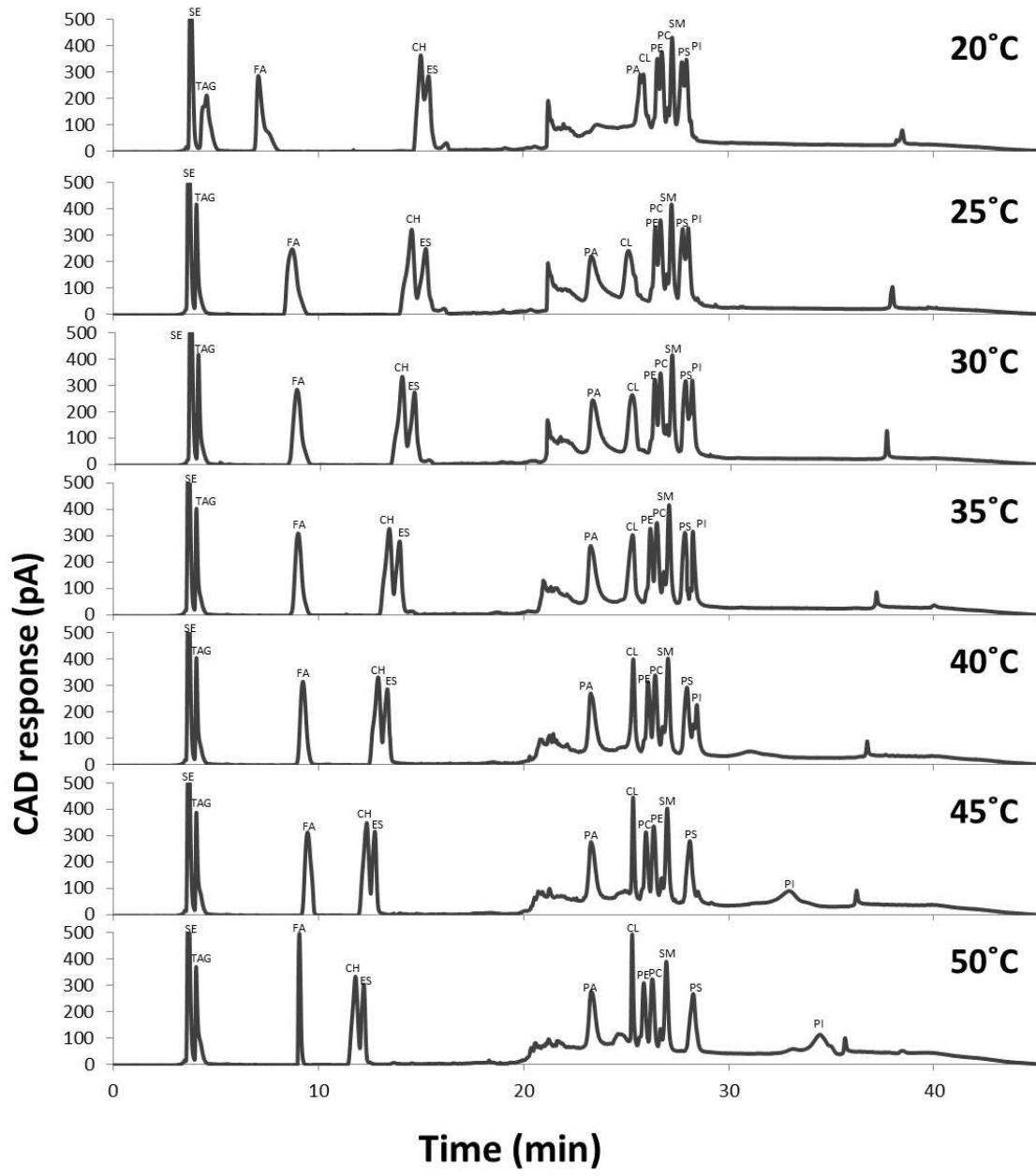


Figure 1. Effect of column temperature on the separation of all lipid classes, separated on a HILIC column (Luna 5 μ m 200 \AA 100 x 3.0 mm, 0.8 mL/min solvent flow rate) with triple gradient mobile phase.

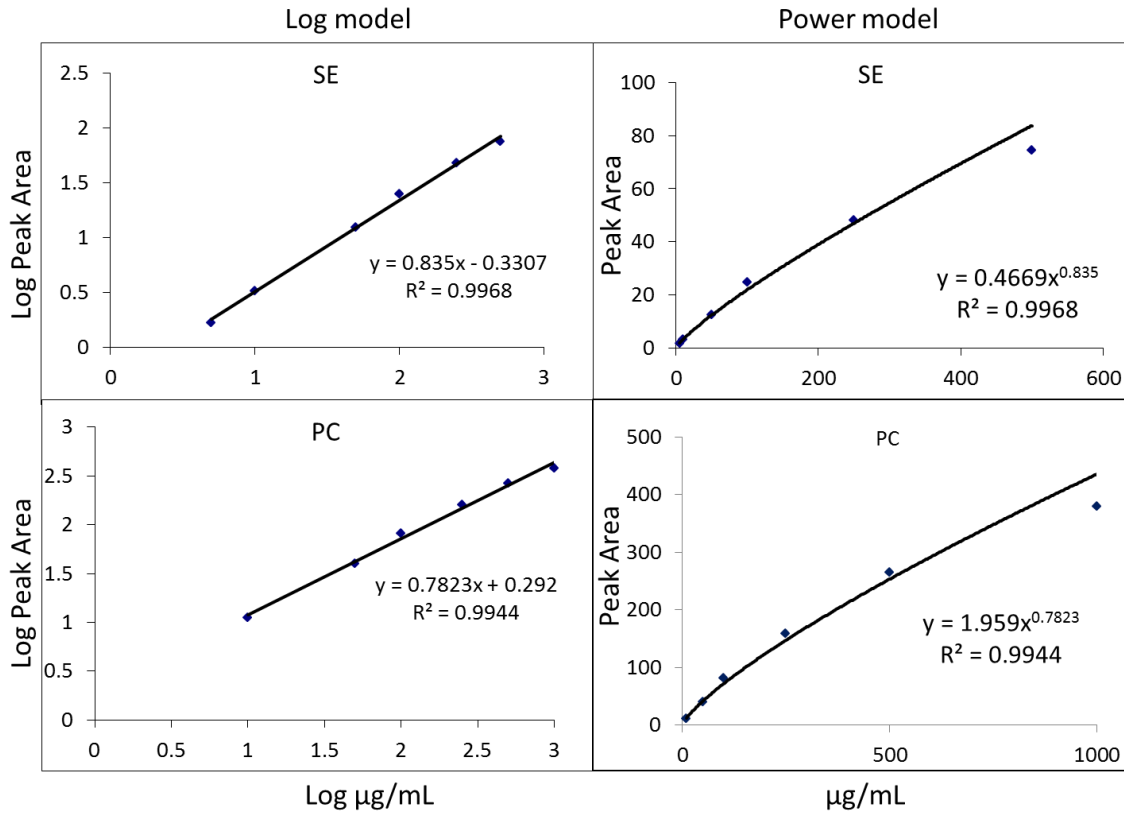


Figure 2. Example calibration curves and response model for lipid analysis by HPLC-CAD analysis.

3.1.3 Response model for calibration curve

The Calibration standards were diluted with chloroform-methanol (2:1, v/v), which was also used as blank and extraction solution throughout this lipid analysis study. Triplicate 5 μ L injections of each solution with variable amount of lipid compounds in the range of 5–1000 μ g/mL were investigated.

The relationship between the lipid concentration and CAD response (peak area) has been reported as having a non-linear pattern, but a Log model or a power-law model can describes the detector response more accurately(30, 31). To select the appropriate model to generate calibration curves for lipid class quantification, we evaluated both models in our mixed standard concentration range.

Examples of calibration curves for SE (neutral lipid) and PC (phospholipids) are shown in Fig. 2 and it is seen that non-linear regression was preferred using a classical log-log transformation of both lipid concentration

(on X-axis) and peak area (on Y-axis). Plotting $\log y = \log A + b \log x$ is also often used to linearize the ELSD response function (30), and we therefore selected the log model to generate our calibration curve for quantification.

3.1.4 Validation of the lipid quantification method

The accuracy expresses the closeness of agreement between the reference value and the value determined by the analytical method. Typically, accuracy is represented and determined by recovery studies, but there are three ways to determine accuracy: (1) by comparison to a reference standard, (2) recovery of the analyte spiked into blank matrix, or (3) standard addition of the analyte (35). In this study, evaluation of accuracy was carried out by spiking at three levels of the expected concentration for individual lipid class into the blank matrix

(extracting solvent). Accuracy values were reported as RSD value calculated from our quantification method based on the calibration curve (Table 1).

At low concentrations (low injection mass about 5-50 µg/mL), the repeatability is about 15% (SRD) whereas a 5% repeatability can be reached at higher injected amounts (100-500

µg/mL). A repeatability of less than 5% is encountered for CH, PE, PC, and PS. The intermediate precision (RSD values) of all lipid classes were varying between 7.3 and 19.2 which are consistent with the precision range for the CAD detector as earlier reported by Ramos et al (30).

Table 1 Repeatability and intermediate precision study of CAD detection based on the calibration curve generated from log transformation.

Lipids	Levels N° (µg/mL)			Repeatability			Intermediate
	1	2	3	1	2	3	(%RSD at level 2)
SE	50	100	250	15.6	8.9	5.2	8.7
TAG	50	100	250	13.2	9.2	5.1	9.4
FA	5	10	50	17.5	11.7	8.3	11.4
CH	100	250	500	9.4	7.4	3.2	7.3
ES	50	100	250	12.6	8.1	6.3	8.5
PA	10	50	100	19.3	14.1	9.7	13.8
CL	10	50	100	20.1	13.5	9.3	13.7
PE	50	100	250	14.7	7.3	4.4	7.5
PC	50	100	250	11.5	5.9	2.8	11.1
PS	10	50	100	22.3	15.8	3.5	15.6
PI	10	50	100	19.1	15.5	5.4	19.2

3.2 Sample preparation for total lipid extraction using microwave

The closed-vessel system for microwave-assisted lipid extraction is illustrated in Fig.3 and was modified from Khoomrung et al (2012) (21). The ideal method used for sample preparation in biological research should be simple, rapid, precise and accurate. Besides these essential factors, sample preparation rate (number of samples that can be performed per hour or per day) is also important.

Normally, the conventional lipid extraction procedure by Schneiter and Daum (36) contains 4 key steps; (1) cell disruption, (2) extraction of the lipids with

chloroform/ methanol (2:1, v/v), (3) removal of nonlipid contaminants by washing the extraction with aqueous salt solutions, and (4) Drying of the extraction by removal of the organic solvent.

In order to perform fast sample preparation, we replaced the conventional extraction with microwave-assisted extraction that can extract the total lipid without the requirement of a cell disruption step, which dramatically reduces the extraction time. Moreover, we increased the speed of sample preparation by using a modified closed-vessel systems to be able to carry out the whole extraction process within one Pyrex glass tubes. With this approach, we eliminated most of the time consuming steps

for transferring of mixture solution from one extraction tube to new glass tubes or flasks several times (at the glass beads removal, washing, and phase separation steps). Hereby we are able to reach a sample preparation rate of up to several hundred samples per day.

From, microscopic analysis we found that microwave-assisted extraction at low extraction temperature (room temperature and 40 °C) was not able to break the freeze-dried yeast cells as we can still see subcellular compartments (Fig.4). At medium temperature 60 °C, yeast cells seem to be disintegrated and the sub

cellular structure were not found inside the yeast cells, which indicate leakage and infusion of extraction solvent into the cells. At high temperature (80°C), however, we started to see formation of some cell debris caused by over heating, and even more damaged cell debris was found at higher temperatures (100-120 °C). Based on these findings, we strongly believe that the extraction temperature of the microwave must have some effect on the total lipid yield that can be detected by subsequent HPLC-CAD analysis. We therefore evaluated lipid yields from extraction at different temperatures in the following section.

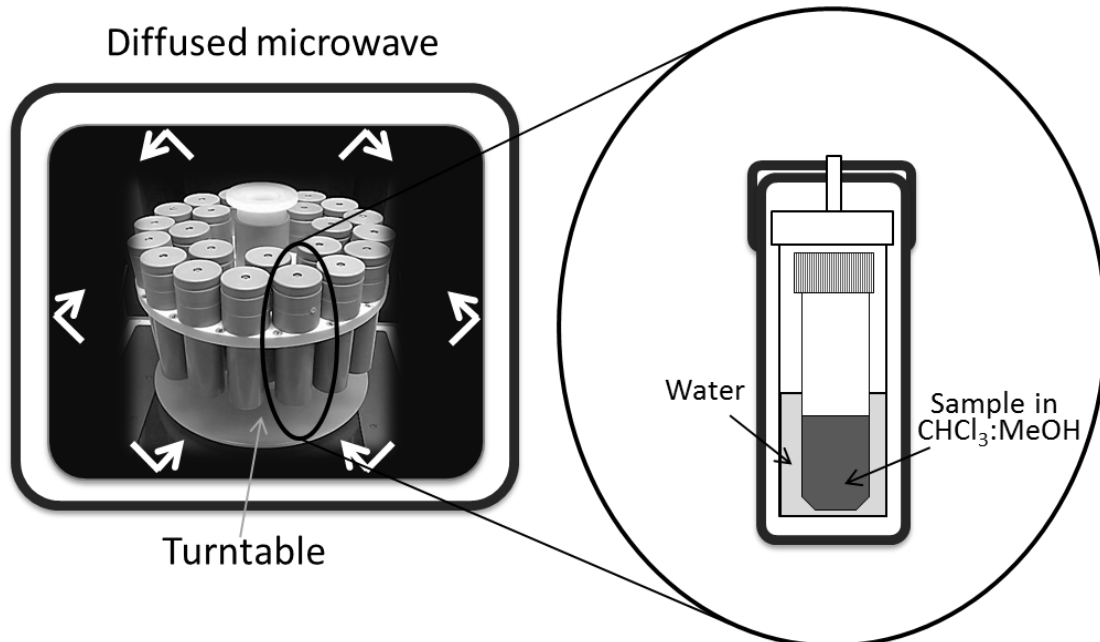


Figure 3. The modified closed-vessel system for total lipid extraction using microwave.

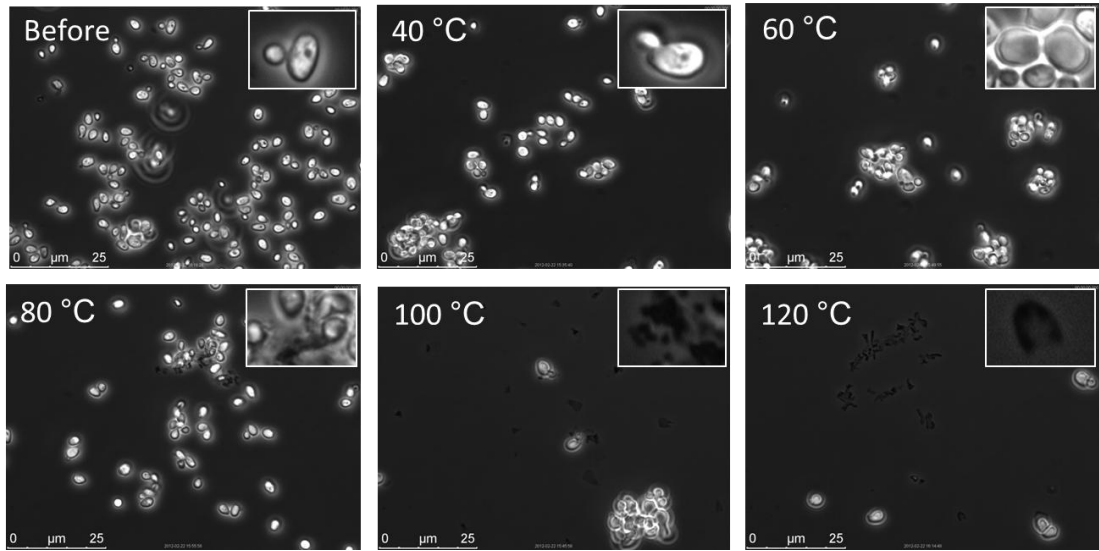


Figure 4. Microscopic results showing the effect of different extraction temperatures on cell disintegration.

3.3 Optimization of extraction temperature

The extraction temperature and duration are the most important factors contributing to the yield of microwave extraction. To select the suitable temperature for microwave extraction, we performed lipid extraction by the microwave-assisted method at different temperatures (from 40-120 °C) with 10 minutes as fixed extraction time.

3.3.1 Yields of total lipid extraction at different temperatures.

Due to the rigid cell wall of yeast, which can stand a high pressure of more than 300 Mpa (37), yeast samples are more difficult to handle in term of obtaining complete extraction compared to many other biological samples. Although the microscopic results showed the ability to disintegrate yeast cells by the microwave extraction method, this analysis method do not provide quantitative data on the extraction yield. The accuracy of the extraction method was therefore further investigated by measurement of the total lipid yield obtained from different extraction conditions with the microwave method.

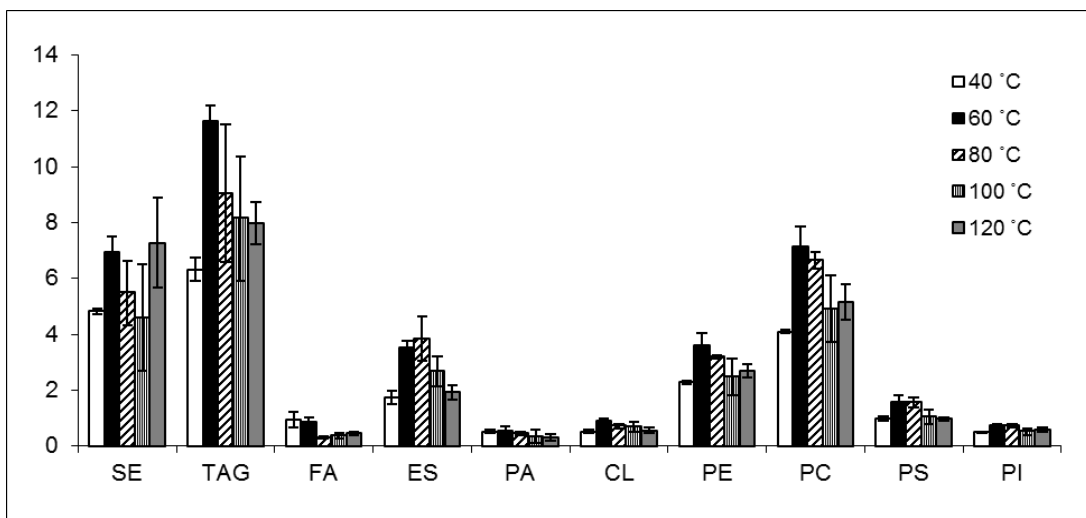


Figure 5. Optimizing extraction temperature. All reactions were performed in 10 min. Cholesterol was used as internal standard. Error bars correspond to standard deviation ($n = 3$).

The yields of different lipid classes extracted by different temperatures in a 10 min period are shown in Fig. 5. Based on these results, 60 °C was found to be the most moderate temperature for microwave extraction since it provided the highest yields for all lipid classes and gave the best reproducibility (judged by the error bar). At 40 °C there was only extracted 50-70% of each lipid class compared with the lipid yields obtained at 60 °C. At higher temperatures (80-120°C) the lipid yields were also significantly reduced ($P < 0.05$) especially the ES seems to have a 35-50% reduction. This drop can be explained by enhanced lipid degradation at high temperatures. In particular, ES has been known as a lipid compound that is sensitive to light and heat, and temperatures $\geq 70^\circ\text{C}$ can damage its structure(38). The yield results were also consistent with the microscopic results (Fig. 4) which indicated that the cell could be disrupted at $\geq 60^\circ\text{C}$ and that this effected the extraction efficiency and that high temperatures (80-120°C) can cause overheating of the cells and hereby reduce the extraction yields. We therefore selected 60 °C as the operational temperature.

3.3.2 Effect of the extraction temperature on bound and free FA

In the presence of methanol in the extraction solvent, esterification of bound or free fatty acids can happen and this might affect the yield and structure of all extracted lipid classes. Even though it has been known that high temperature and a catalyst (such as BF_3) are needed for the esterification reaction, we still wanted to make certain that there was no esterification happening during our extraction method.

To ensure that the microwave extraction method did not enhance the esterification of yeast lipid samples, we decided to perform an experiment where we spiked TAG (bound FA) and FA (free FA) into a blank sample and measured the remaining concentrations and also the FAME (esterified FA) levels which might have been generated after both conventional and microwave extraction at different extraction temperatures.

The results of this analysis are collected in Fig. 6, and based on the results we found that when 100 µg of TAG (19:0) and 100 µg of FA (19:0) were spiked into the extraction solvent, the detected results of TAG and FA by HPLC-CAD and FAME (19:0) by GC-MS were comparable ($P < 0.01$) at low temperature (40-60°C) with our microwave method as well as with the conventional

method. There was no significantly changed in %recovery of the spiked standards. In general, bound fatty acids require longer time to complete the conversion as compared to free fatty acids (39). Comparing the bound FA (TAG) and free FA, the results showed a higher sensitivity to free FA that is a better substrate for esterification as it results in about 10-15% reduction at 80-120°C while TAG were esterified about 10-15% only at higher temperatures, i.e. 100-120°C. This experiment confirms that the selected extraction temperature (60°C) is the most reasonable candidate for our microwave extraction method as there is hardly any esterification or trans-esterification happening.

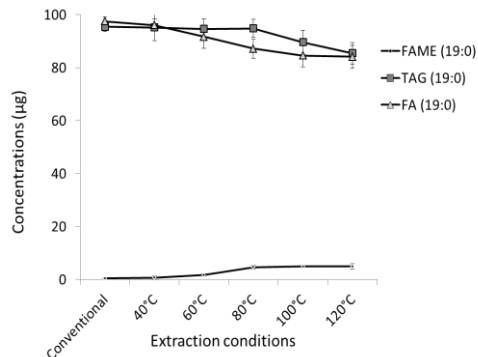


Figure 6. Heat-induced esterification effect by extraction temperature. The bound fatty acid standard (TAG, 19:0) and Free fatty acid (FA) were spiked into the blank extraction solvent. The %recovery of TAG and FA were detected by HPLC-CAD and the *de novo* esterified fatty acids (FAME, 19:0) were quantified by GC-MS. All reactions were performed in 10 min. Error bars correspond to standard deviation ($n = 3$).

3.4 Optimization of the extraction time

The optimum reaction time for lipid extraction depends on type and size of the sample. A sample in complex matrices may require longer time for complete conversion compared with a sample in a simple matrix. To identify the optimal reaction time, we performed microwave-assisted lipid extraction between 5 and 30 min (Fig. 7), and this showed that a reaction time of 10 min was sufficient to complete the lipid extraction using the microwave-assisted

method for yeast. In general, extraction duration using microwave is very short compared to conventional extraction because the low temperature and closed-vessel microwave can disintegrate yeast cells and enhance the extraction efficiency. Although a reaction time shorter than 10 min may also provide complete extraction, it would not make a significant difference in practice, and we therefore selected 10 min reaction time as the optimal condition.

3.5 Validation of microwave-assisted extraction method

To validate the efficiency of our microwave extraction method, we compared the extracted lipid yields of each lipid class by our optimized method (60°C, 10 min) with the conventional method (Fig. 8). The results indicated that microwave-assisted extraction method for total lipids was equally effective as compared to the conventional method. This could be due to the fact that the extraction occurred in closed-vessel microwave operated under higher temperature and pressure (60 °C, 30 bars), and the yeast cell wall could simply be disrupted by this treatment. Clearly it is advantageous with lipid extraction using the microwave method as this is simple, rapid and involves fewer costs.

Moreover, based on the recovery of the spiked CH standard, the efficiencies of total lipid obtained from both methods were found to be the same, i.e. there was an insignificant difference ($P > 0.01$) in %recovery of CH (conventional closed-vessel: $92 \pm 6\%$ and modified closed-vessel: $93 \pm 8\%$). The high %recovery of CH and also TAG&FA (in the *Effect of the extraction temperature on bound and free FA* section) obtained from both methods indicates that these two methods are equally efficient for lipid extraction, as shown by low amounts of spiked lipid standards lost during the entire process of sample preparation. In contrast, the reproducibility (judged by the standard deviations shown as error bars in Fig. 8) were significant better with our new method compared to the conventional method ($P > 0.01$). Presumably, this is due to the non-homogenously disruption of using glass

beads in the conventional method, probably resulting in varying efficiency of cell disruption in each extraction tubes.

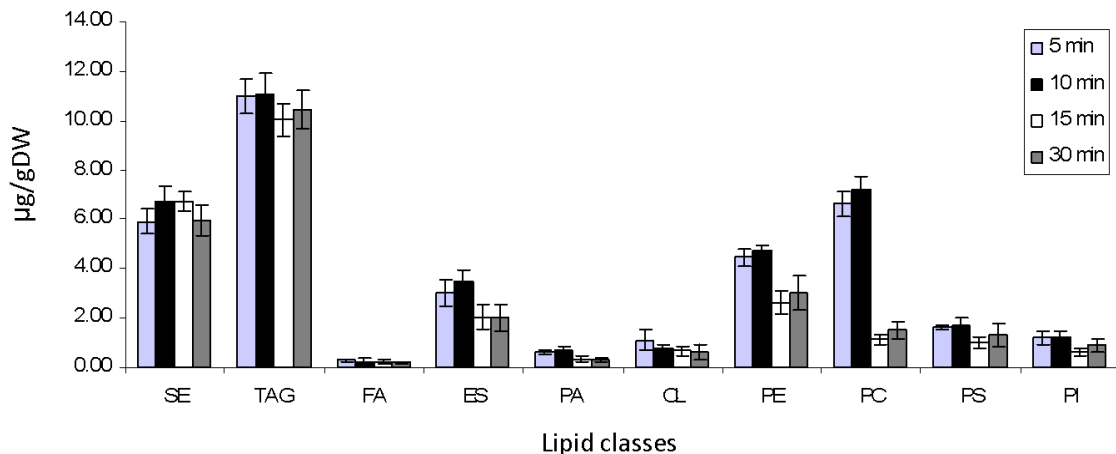


Figure 7. Optimizing extraction duration. All reactions were performed at 60 °C. Cholesterol was used as internal standard. Error bars correspond to standard deviation ($n = 3$).

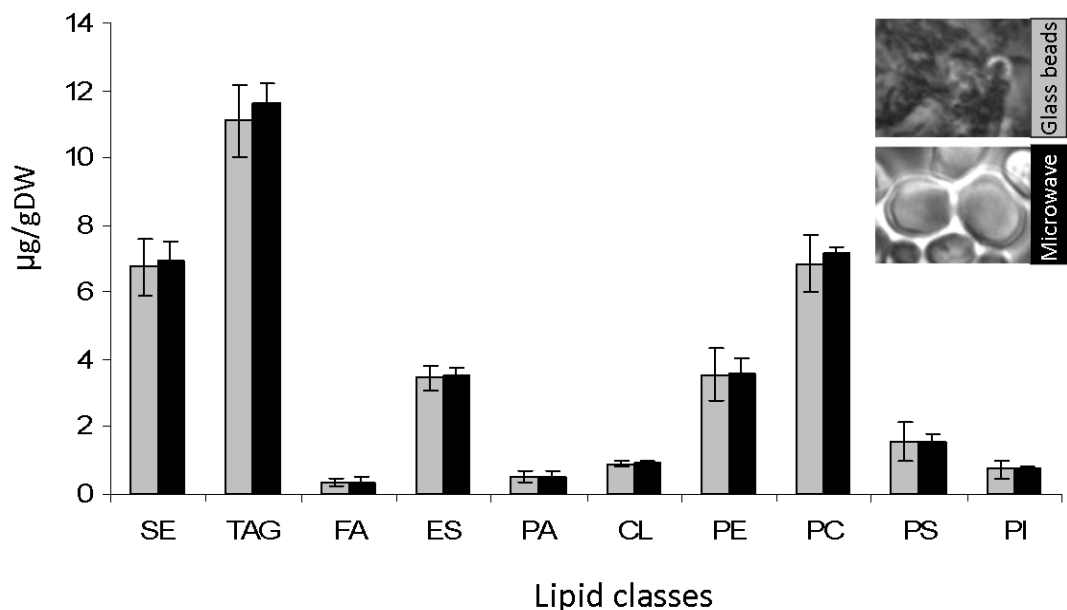


Figure 8. Comparison of microwave (10 min at 60 °C) and conventional method (3 hr at room temperature). Cholesterol was used as internal standard. Error bars correspond to standard deviation ($n = 3$).

4. Conclusions

There were no significant differences ($P > 0.01$) in yields of lipid classes with both

validations. By performing a simple modification of closed-vessel microwave extraction it was possible to carry out the cell

disruption and extraction in Pyrex glass tubes kept inside the closed vessel at 60°C for 10 min. Hereby the sample preparations rate can reach several hundred samples per day. The new microwave-assisted extraction method facilitates the preparation of extracted total lipid directly from yeast cells, but the method is likely to also be applicable for other biological samples.

The optimized condition for lipid class quantification is with the HILIC column at 35 °C for 45 min at a flow rate 0.8 mL/min and detection using CAD. To obtain an acceptable accuracy value, log transformation is needed for generating calibration curves for quantifications of each lipid class.

Acknowledgements

Part of this work was financed by Chalmers Foundation, the Knut and Alice Wallenberg Foundation and the Swedish Research Council (Vetenskapsrådet). We also acknowledge funding from the EU-funded project UNICELLSYS. Pramote Chumnanpuen also would like to thank the Office of the Higher Education Commission, Thailand for supporting by a stipend for his Ph.D. program under the program Strategic Scholarships for Frontier Research Network for his Ph.D. program. We also thank Suwanee Jansa-ard for assistance with HPLC-CAD analysis.

References

1. Nurminen, T., E. Oura, and H. Suomalainen. 1970. The enzymic composition of the isolated cell wall and plasma membrane of baker's yeast. *Biochem J* **116**: 61-69.
2. Natter, K., P. Leitner, A. Faschinger, H. Wolinski, S. McCraith, S. Fields, and S. D. Kohlwein. 2005. The spatial organization of lipid synthesis in the yeast *Saccharomyces cerevisiae* derived from large scale green fluorescent protein tagging and high resolution microscopy. *Mol Cell Proteomics* **4**: 662-672.
3. Rattray, J. B., A. Schibeci, and D. K. Kidby. 1975. Lipids of yeasts. *Bacteriol Rev* **39**: 197-231.
4. Tuller, G., T. Nemec, C. Hrastnik, and G. Daum. 1999. Lipid composition of subcellular membranes of an FY1679-derived haploid yeast wild-type strain grown on different carbon sources. *Yeast* **15**: 1555-1564.
5. Swan, T. M., and K. Watson. 1997. Membrane fatty acid composition and membrane fluidity as parameters of stress tolerance in yeast. *Can J Microbiol* **43**: 70-77.
6. Goodman, J. M. 2009. Demonstrated and inferred metabolism associated with cytosolic lipid droplets. *J Lipid Res* **50**: 2148-2156.
7. Zweytick, D., K. Athenstaedt, and G. Daum. 2000. Intracellular lipid particles of eukaryotic cells. *Biochim Biophys Acta* **1469**: 101-120.
8. Brown, D. A. 2001. Lipid droplets: proteins floating on a pool of fat. *Curr Biol* **11**: R446-449.
9. Mullner, H., and G. Daum. 2004. Dynamics of neutral lipid storage in yeast. *Acta Biochim Pol* **51**: 323-347.
10. Leber, R., E. Zinser, G. Zellnig, F. Paltauf, and G. Daum. 1994. Characterization of lipid particles of the yeast, *Saccharomyces cerevisiae*. *Yeast* **10**: 1421-1428.
11. Schaffner, G., and P. Matile. 1981. Structure and Composition of Bakers-Yeast Lipid Globules. *Biochemie Und Physiologie Der Pflanzen* **176**: 659-666.
12. Gasch, A. P., and M. Werner-Washburne. 2002. The genomics of yeast responses to environmental stress and starvation. *Funct Integr Genomics* **2**: 181-192.
13. Souzu, H. 1973. Proceedings: The phospholipid degradation and cellular death caused by freeze-thawing or freeze-drying of yeast. *Cryobiology* **10**: 427-431.

14. Letters, R. 1966. Phospholipids of yeast. II. Extraction, isolation and characterisation of yeast phospholipids. *Biochim Biophys Acta* **116**: 489-499.
15. Engler, C. R., and C. W. Robinson. 1979. Disruption of *Candida-Utilis* Cell-Walls. *Abstr Pap Am Chem S*: 47-&.
16. Dodds, W. K. 1989. Microscale vertical profiles of n(2) fixation, photosynthesis, o(2), chlorophyll a, and light in a cyanobacterial assemblage. *Appl Environ Microbiol* **55**: 882-886.
17. Boldor, D., A. Kanitkar, B. G. Terigar, C. Leonardi, M. Lima, and G. A. Breitenbeck. 2010. Microwave assisted extraction of biodiesel feedstock from the seeds of invasive chinese tallow tree. *Environ Sci Technol* **44**: 4019-4025.
18. Lee, J. Y., C. Yoo, S. Y. Jun, C. Y. Ahn, and H. M. Oh. 2010. Comparison of several methods for effective lipid extraction from microalgae. *Bioresour Technol* **101 Suppl 1**: S75-77.
19. Virot, M., V. Tomao, C. Ginies, F. Visinoni, and F. Chemat. 2008. Microwave-integrated extraction of total fats and oils. *J Chromatogr A* **1196-1197**: 57-64.
20. Young, D. D., J. Torres-Kolbus, and A. Deiters. 2008. Microwave-assisted synthesis of unnatural amino acids. *Bioorg Med Chem Lett* **18**: 5478-5480.
21. Khoomrung, S., P. Chumnanpuen, S. Jansa-ard, I. Nookaew, and J. Nielsen. 2012. Fast and accurate preparation fatty acid methyl esters by microwave-assisted derivatization in yeast *Saccharomyces cerevisiae* *Submitted to Analytical Biochemistry: Methods in the Biological Sciences*
22. Moreau, R. A. 1990. Plant Lipid Class Analysis by Hplc. *Plant Lipid Biochemistry, Structure and Utilization*: 20-22.
23. Moreau, R. A., and P. T. Asmann. 1989. Quantitative-Analysis of Lipids in Plastids by Hplc-Fid. *Cur Top Pl* **2**: 274-276.
24. Zheng, L., R. T'Kind, S. Decuyper, S. J. von Freyend, G. H. Coombs, and D. G. Watson. 2010. Profiling of lipids in *Leishmania donovani* using hydrophilic interaction chromatography in combination with Fourier transform mass spectrometry. *Rapid Commun Mass Spectrom* **24**: 2074-2082.
25. Nesterenko, E. P., P. N. Nesterenko, and B. Paull. 2009. Zwitterionic ion-exchangers in ion chromatography: A review of recent developments. *Anal Chim Acta* **652**: 3-21.
26. Jandera, P. 2008. Stationary phases for hydrophilic interaction chromatography, their characterization and implementation into multidimensional chromatography concepts. *J Sep Sci* **31**: 1421-1437.
27. Moreau, R. A. 2006. The analysis of lipids via HPLC with a charged aerosol detector. *Lipids* **41**: 727-734.
28. Schonherr, C., S. Touchene, G. Wilser, R. Peschka-Suss, and G. Francese. 2009. Simple and precise detection of lipid compounds present within liposomal formulations using a charged aerosol detector. *J Chromatogr A* **1216**: 781-786.
29. Loughlin, J., H. Phan, M. Wan, S. Guo, K. May, and B. W. Lin. 2007. Evaluation of charged aerosol detection (CAD) as a complementary technique for high-throughput LC-MS-UV-ELSD analysis of drug discovery screening libraries. *Am Lab* **39**: 24-+.
30. Ramos, R. G., D. Libong, M. Rakotomanga, K. Gaudin, P. M. Loiseau, and P. Chaminade. 2008. Comparison between charged aerosol detection and light scattering detection for the analysis of *Leishmania* membrane phospholipids. *J Chromatogr A* **1209**: 88-94.

31. Moreau, R. A. 2009. Lipid analysis via HPLC with a charged aerosol detector. *Lipid Technology* **21**: 191-194.
32. Bligh, E. G., and W. J. Dyer. 1959. A rapid method of total lipid extraction and purification. *Can J Biochem Physiol* **37**: 911-917.
33. Silversand, C., and C. Haux. 1997. Improved high-performance liquid chromatographic method for the separation and quantification of lipid classes: application to fish lipids. *J Chromatogr B Biomed Sci Appl* **703**: 7-14.
34. Mitulović, G., C. Stingl, I. Steinmacher, O. Hudecz, J. R. A. Hutchins, J.-M. Peters, and K. Mechtler. 2009. Preventing Carryover of Peptides and Proteins in Nano LC-MS Separations. *Anal Chem* **81**: 5955-5960.
35. Snyder, L. R., J. J. Kirkland, and J. L. Glajch. 1997. Practical HPLC method development. 2nd ed. Wiley, New York.
36. Schneiter, R., and G. Daum. 2006. Extraction of yeast lipids. *Methods Mol Biol* **313**: 41-45.
37. Hartmann, C., and A. Delgado. 2004. Numerical simulation of the mechanics of a yeast cell under high hydrostatic pressure. *J. Biomech.* **37**: 977-987.
38. Kadakal, C., and N. Artik. 2008. Degradation kinetics of ergosterol in tomato paste serum. *Eur Food Res Technol* **227**: 683-688.
39. Ichihara, K., and Y. Fukubayashi. 2010. Preparation of fatty acid methyl esters for gas-liquid chromatography. *J.Lipid Res.* **51**: 635-640.

Paper VI

Fast and accurate preparation fatty acid methyl esters by microwave-assisted derivatization in yeast *Saccharomyces cerevisiae*

Khoomrung, S.*, **P. Chumnanpuen***, S. Jansa-ard, I. Nookaew, J. Nielsen

*Equal contribution

Under minor revision in Applied Microbiology and Biotechnology.

Fast and accurate preparation fatty acid methyl esters by microwave-assisted derivatization in yeast *Saccharomyces cerevisiae*

Sakda Khoomrung[†], Pramote Chumnanpuen[†], Suwanee Jansa-ard, Intawat Nookaew, and Jens Nielsen*

Department of Chemical and Biological Engineering
Chalmers University of Technology
SE-412 96 Göteborg, Sweden

[†]These authors contributed equally to this work

*Corresponding author:
Department of Chemical and Biological Engineering
Chalmers University of Technology
Kemivägen 10
SE-412 96 Göteborg, Sweden
Telephone: +46 31 772 3804
Fax: +46 31 772 3801
email: nielsenj@chalmers.se

Abstract

We present a fast and accurate method for preparation of fatty acid methyl esters (FAMEs) using microwave-assisted derivatization of fatty acids present in yeast samples. The esterification of free/bound fatty acids to FAMEs was completed within 5 min, which is 24 times faster than with conventional heating methods. The developed method was validated in two ways; (I) through comparison with a conventional method (hot plate) and (II) through validation with the standard reference material 3275-2 omega-3 and omega-6 fatty acids in fish oil (from the Nation Institute of Standards & Technology, USA). There were no significant differences ($P>0.01$) in yields of FAMEs with both validations. By performing a simple modification of closed-vessel microwave heating it was possible to carry out the esterification in Pyrex glass tubes kept inside the closed vessel. Hereby we are able to increase number of sample preparations to several hundred samples per day as the time for preparation of re-used vessels was eliminated. Pre-treated cell disruption steps are not required since the direct FAMEs preparation provides equally quantitative results. The new microwave-assisted derivatization method facilitates the preparation of FAMEs directly from yeast cells, but the method is likely to also be applicable for other biological samples.

Key words

Fatty acid methyl esters, fatty acid analysis, microwave-assisted derivatization, *Saccharomyces cerevisiae*.

Introduction

Baker's yeast, *Saccharomyces cerevisiae* is an important and widely utilized cell factory for a number of biotechnological applications. There is an increasing interest in metabolic engineering of lipid metabolism in different cell factories as these can be used for biotechnological production of a range of fuels, chemicals and food ingredients. *S. cerevisiae* is the key biofuel cell factory as it is used to produce bioethanol, and the industry is therefore keen to further exploit this cell factory as a platform for production of more advanced biofuels (de Jong et al. 2011; Shi et al. 2011). Not only because there is much knowledge available for this organism due to its use as a eukaryotic model organism, but also because it is tolerant to harsh industrial conditions and already used for large-scale production of different products. The total cell lipids and fatty acid composition (which is the key precursor for biofuel production) is quite diverse among various yeast strains, and a fast and accurate method for quantification of fatty acids is needed for high through-put screening for the best producing strains.

The procedure for the quantification of fatty acids by GC-MS consists of several steps, i.e. esterification of fatty acids (sample preparation), sample injection, separation, identification and quantification (Eder 1995). The accuracy of total fatty acids quantification is generally influenced by a number of experimental factors, and the esterification of lipids is the most critical step among these. Acid-catalyzed transesterification is the most common used method for preparation of fatty acid methyl esters (FAMEs) and it is found in various applications (Abdulkadir and Tsuchiya 2008; Khoomrung et al. 2008; Ichihara and Fukubayashi 2010; Glaser et al. 2010). Although, preparation of FAMEs with this method delivers precise and accurate results, the reaction time to complete the conversion of lipids to FAMEs (from one to four hours) is time consuming when using conventional heating method (Ulberth and Henninger 1992b; Shimasaki et al. 1977; Masood et al. 2005). Recently, there has been growing interest to speed up reaction of chemical synthesis by microwave irradiation in

different applications (Söderholm et al. 2010). The applications of microwave-assisted derivatization to prepare FAMEs from fatty acids (free & bound fatty acids) can be found in various types of biological samples i.e. edible oil, bacterial cells, animal tissue, and plasma samples (Zhang et al. 2000; Tomas et al. 2009; Itonori et al. 2004; Jeyashoke et al. 1998; Liebeke et al. 2010). However, there has been no attempt to establish a proper method for FAMEs preparation in yeast samples.

Yeast differs from other biological samples because of their rigid cell wall structure, leading to difficulties to isolate and analyze lipids and other intracellular metabolites. This could be confirmed by a recent study (Canelas et al. 2010) showing that accurate quantitative analysis of metabolite levels in yeast samples is difficult to obtain whereas the relative metabolite levels can be measured consistently in different laboratories. Several methods used for FAMEs preparation in yeast originate from Moss et al. (1974), which was originally developed for bacterial fatty acids analysis (Moss et al. 1974). This FAMEs preparation method has been applied to yeast samples in several studies (Sancho et al. 2000; Noronha-da-Costa et al. 1996; Wei et al. 2006). Briefly, bound fatty acids have to be split from lipids by saponification and then converted into methyl esters by esterification. Although this method delivers accurately quantitative results, having several steps of sample preparation (saponification, esterification, extraction, and base wash) is time consuming and increases the possibility of errors because of sample loss during the multi steps in the sample preparation processes. To overcome those problems, a one-step method combining saponification and esterification in one step (Abdulkadir and Tsuchiya 2008), was recently introduced for analysis of yeast FAMEs (Zhang et al. 2011). Although the one-step method provides quantitative data and simplifies sample handling, the long reaction time (at least 1.5 hour) of FAME preparation remains an issue when dealing with a large number of samples. Furthermore, conventional heating by a hot plate cannot provide homogeneously

radiated heat to the whole chamber leading to reduced precision of the measurement.

Here, we present a fast, accurate, reliable and simple method for preparation of FAMEs by microwave-assisted derivatization specified to yeast samples. The developed method was further applied with and without different cell disruption. We believe that this novel approach can be applied for lipid analysis in other fungi and microbial cells which have similar matrices to yeast cells.

Materials and Methods

Chemicals and Standards

Reagents

Hexane and BF_3 (14% in MeOH), GC grade were purchased from Sigma-Aldrich, Germany. Milli-Q water (Gradient A10) was used throughout this study.

Standards and standard reference material

Standard FAMEs and heptadecanoic acid (17:0) were analytical grade, purchased from Sigma-Aldrich, Germany. The standard reference material (SRM) 3275-2 omega-3 and omega-6 fatty acids in fish oil was purchased from the National Institute of Standards & Technology, Gaithersburg, Maryland, USA.

Yeast Strain and Cultivation Conditions

The yeast strain CEN.PK113-7D MAT α SUC2 MAL2-8C (Scientific Research and Development GmbH, Germany) were grown aerobically in 50 mL Yeast Extract Peptone Dextrose (YPD) medium in 500-mL baffled shake flasks at 30 °C and 230 rpm. The initial glucose concentration was 20 g/L concentration and the inoculum cell concentration was corresponding to an OD_{600} of about 0.01.

Samples were harvested from the cultivation media during the early stationary phase at 20 hours and transfer into 50 mL falcon tubes (VWR, Sweden) and centrifuged at 3,000 rpm for 5 min at 4°C to collect the biomass. The samples were then immediately frozen in liquid nitrogen and placed in freeze-dryer (alpha 1-4 LSC, CHRIST, GmbH, Germany) at -40 °C at 1.03 atm overnight.

Preparation of FAMEs

The procedure developed was modified from the method of Abdulkadir and Tsuchiya (Abdulkadir and Tsuchiya 2008). The biomass sample (~ 10 mg) was mixed with 4 mL of hexane, 2 mL of 14 % BF_3 in MeOH and 25 μL of internal standard (17:0; 4000 $\mu\text{g/mL}$). The sample was flushed into the tube with nitrogen gas for 30s and closed tightly with a Teflon screw cap. The tube was placed in a vessel (12 cm X 3 cm I. D., 0.5 cm thickness; Milestone Start D, Sorisole Bergamo, Italy) containing 30 mL of Milli-Q water and then sealed with a TFM screw cap. The vessel was heated using a microwave digestion system equipped with PRO-24 medium pressure high throughput rotor (Milestone Start D, Sorisole Bergamo, Italy). The temperature programming of the microwave derivatization was ramped to 120 °C (from room temperature) within 6 min and maintained at 120 °C for 5 min. After cooling down the sample to room temperature, 2 mL of Milli-Q water was added and shaken vigorously for 1 min and centrifuged at 2500 rpm (1328 g) for 5 min. The upper phase (hexane phase which contained the FAMEs) was analyzed by GC-MS.

Determination of FAMEs by GC-MS

The FAMEs were separated and quantified using Focus GC ISQ single quadrupole GC-MS (Thermo Fisher scientific, USA). The separation of FAMEs was performed on Zebron (ZB-WAX) GC column (30 m x 0.25 mm I. D., 0.25 μm film thickness) from Phenomenex, Macclesfield, UK. The sample was injected in splitless injection mode (1 μL at 240 °C) and Helium was used a carrier gas (1 mL/min). The column temperature was initially set at 50 °C (1.5 min), where after the temperature was ramped to 180 °C (25°C/min) for 1 min, followed by a further increased to 220 °C (10°C/min) where it was held for 1 min. Finally, the temperature was increased to 250 °C (15°C/min) and held for 3 min. The mass transfer line and ion source were set at 250 °C and 200 °C, respectively. The FAMEs were detected with electron ionization (70 eV) in scan mode (50-650 m/z) and selected ion monitoring mode at m/z 55, 67, 74 and 79

(for quantitative analysis). The identification of unknown FAMEs from yeast cells was achieved by comparing their retention times and mass spectrum profiles with known standards (Fig. 1). The quantification of FAMEs was performed based on the five

points external calibration curve in the range of 0.1 - 25 µg/mL. The FAMEs data analysis was performed by QuanBrowser function in the Xcalibur software version 2.0 (Thermo Fisher Scientific).

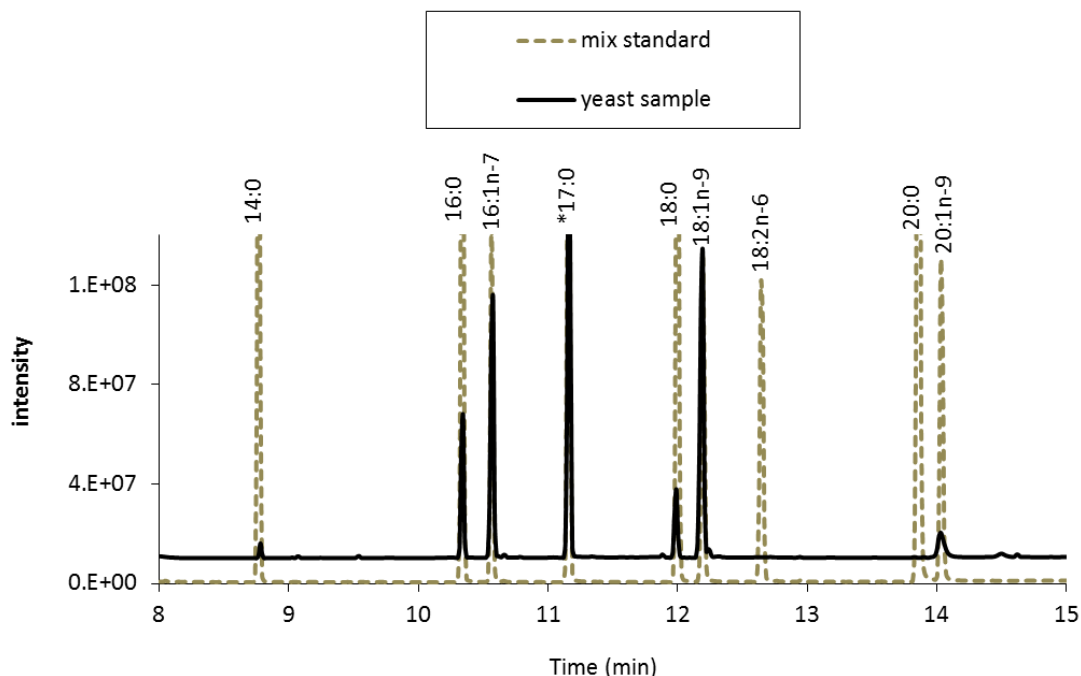


Figure 1. Identification of FAMEs from yeast sample with known standards.

Cell disruptions

All yeast samples were disrupted using three different methods. After the disruption procedure, all samples were freeze-dried overnight to eliminate digesting buffers and were further prepared using the method described in 2.3. The disruption protocols used are given as follows:

Cell wall digestion using zymolyase: Cell wall digestion with zymolyase was slightly modified from Gu *et al.* (2004) (Gu *et al.* 2004). Freeze-dried cell pellets (~10 mg) were treated with 5 unit of zymolyase in 0.5 mL of digesting buffer (1.2 M glycerol, 100 mM sodium thioglycolate, 50 mM Tris-sulfate, pH 7.5) at 30°C for 45 min.

Cell disruption by bead mills: 0.5 mL of digesting buffer was added to ~10 mg of freeze-dried cell pellets in Pyrex tubes. Thereafter 20-30 acid washed glass beads (425-600 µm) were added and vigorously vortex for 45 min.

Cell disruption by sonication: 0.5 mL of digesting buffer was added to ~10 mg of freeze-dried cell pellets in Pyrex tubes. Thereafter sonication was performed using Elma S180H (Elmasonic) at 30°C for 45 min.

Data analysis

Results were expressed as mean ± standard deviation from three independent replicates. The statistic program for social science (SPSS) software version 19.0 (SPSS Inc.) was used for statistical analysis. *P* values <0.01 were considered as statistically significant.

Results

Comparison of the modified closed-vessel method and the conventional microwave method

To compare the esterification yields from conventional closed-vessel method and from our modified closed-vessel system as illustrated in Fig. 2, we performed the

FAME synthesis experiment of yeast samples using both methods. We then evaluated the efficiency of FAME formation of our modified method and the

conventional microwave operating procedure which involves direct heating of the sample inside the closed vessel at high pressure (30 bars).

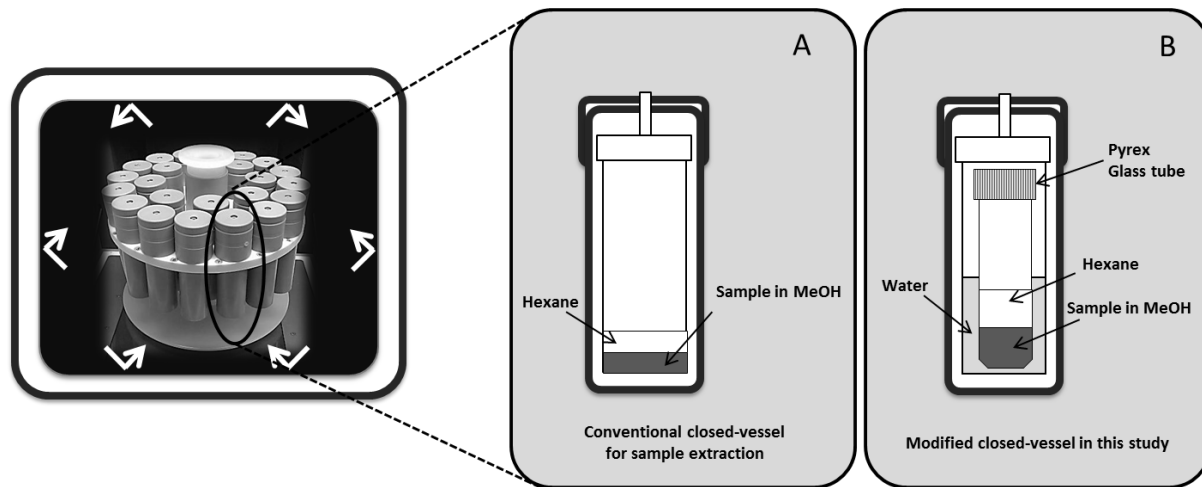


Figure 2. Experimental designed. Conventional closed-vessel (A) and Modified closed vessel (B).

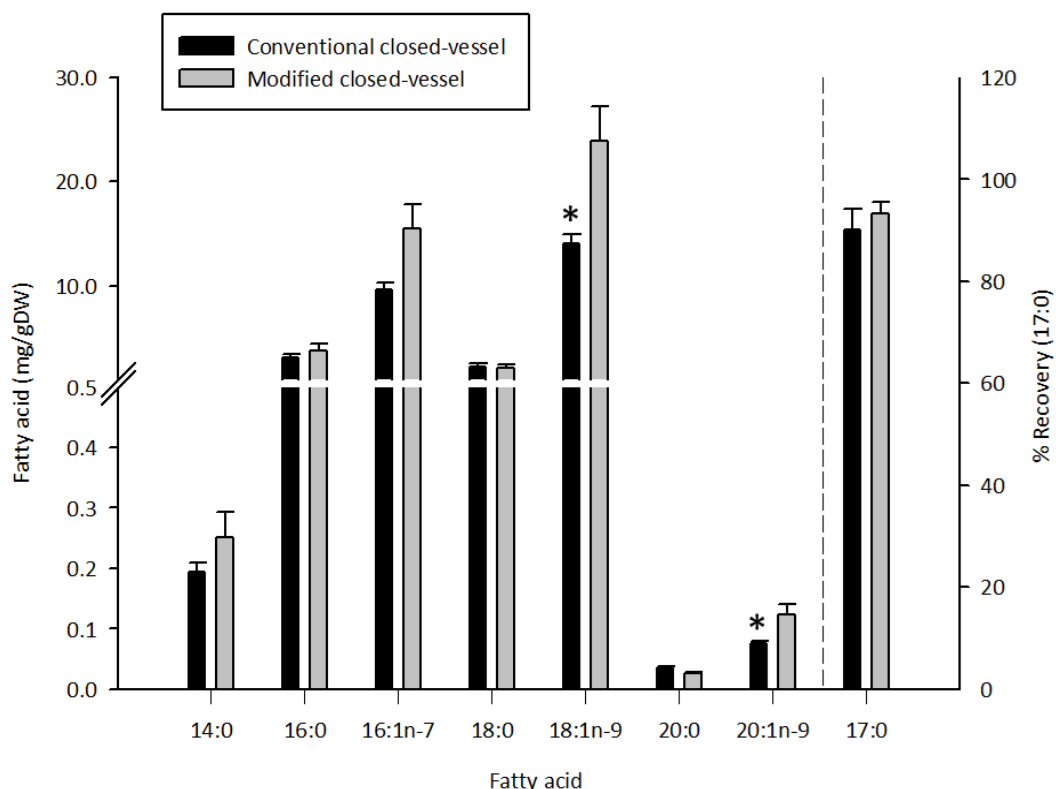


Figure 3. Comparison of conventional vessel and modified vessel. The reaction containing a mixture of yeast sample ~10 mg, BF_3 in MeOH (2 mL) and hexane (4 mL) was heated at 120 °C for 5 min. Heptadecanoic acid (17:0) was used as internal standard. *significantly different ($P < 0.01$). Error bars correspond to standard deviation ($n = 3$).

S. cerevisiae was used as a model in the study, the esterification was carried out in the microwave at 120 °C for 5 min and 17:0 fatty

acid was added as an internal fatty acid standard. Based on the recovery of 17:0 (Fig.3), the efficiencies of esterification

obtained from both methods were found to be the same, i.e. there was an insignificant difference ($P>0.01$) in %recovery of 17:0 (conventional closed-vessel: $90 \pm 4\%$ and modified closed-vessel: $93 \pm 3\%$). The high %recovery of 17:0 obtained from both methods indicates that these two methods are equally efficient for the preparation of FAMEs, as shown by low amounts of 17:0 lost during the entire process of sample preparation. In contrast, the yields of 18:1n-9 and 20:1n-9 fatty acids from yeast samples which are mostly bound fatty acids (Leber et al. 1994) were significant higher with the modified method compared with the conventional method ($P>0.01$). Presumably, this is due to incomplete conversion of bound fatty acids to FAMEs with the conventional method, probably because the heat used for esterification in the conventional vessel only comes from absorption of energy by 2 mL MeOH (hexane does not absorb microwave energy). Since the efficiency of the

preparation of FAMEs by microwave derivatization is influenced by several parameters, we further investigated different operational parameters. Based on the better efficiency in generating FAMEs from yeast, being simpler and less time consuming, the modified closed-vessel was selected for further studies.

Optimizing parameters for esterification

Extraction temperature and extraction time

The extraction temperature and duration are the most important factors contributing to the yield of FAMEs. To select the suitable temperature for the derivatization method, we performed the FAME reaction at different temperatures (from 80- 120 °C) with 10 minutes as fixed reaction time. The results of using three different temperatures (Fig. 4) showed that the optimum temperature was 100-120°C, with an insignificant difference in yield of all FAMEs ($P>0.01$) for these two temperatures.

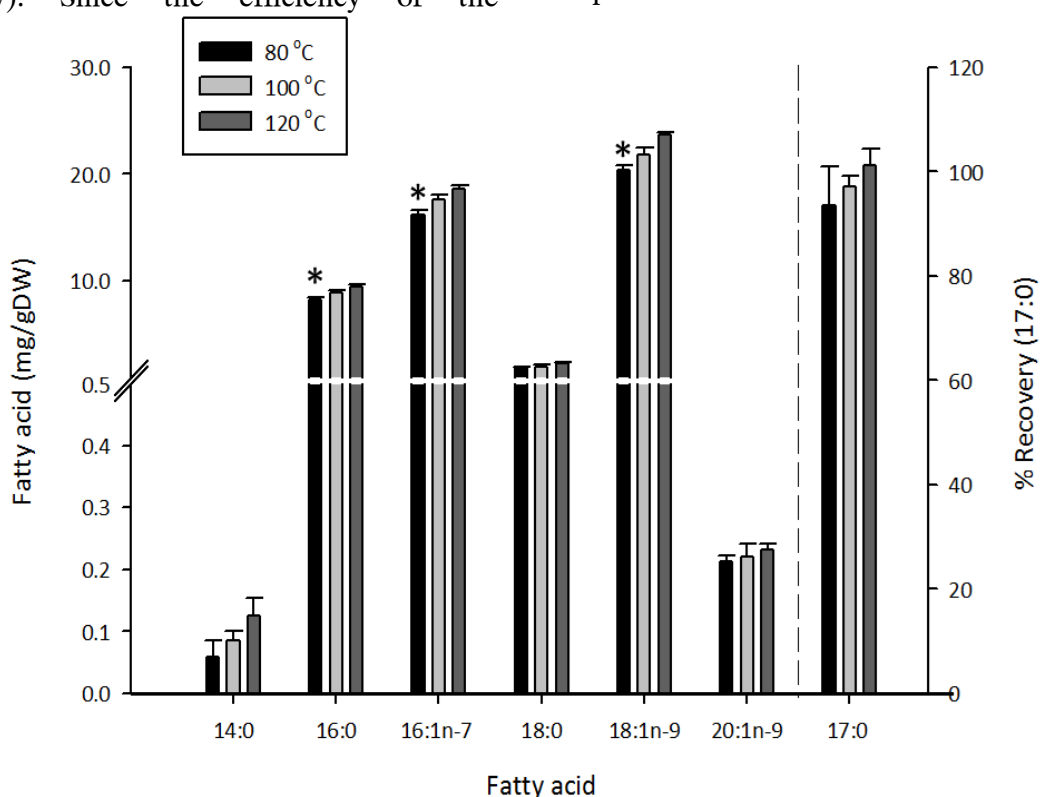


Figure 4. Optimizing derivatization temperature. All reactions were performed in 10 min. Heptadecanoic acid (17:0) was used as internal standard. *indicates that the fatty acids performed at 80°C were significantly lower ($P <0.01$) than 100 and 120°C. Error bars correspond to standard deviation ($n = 3$).

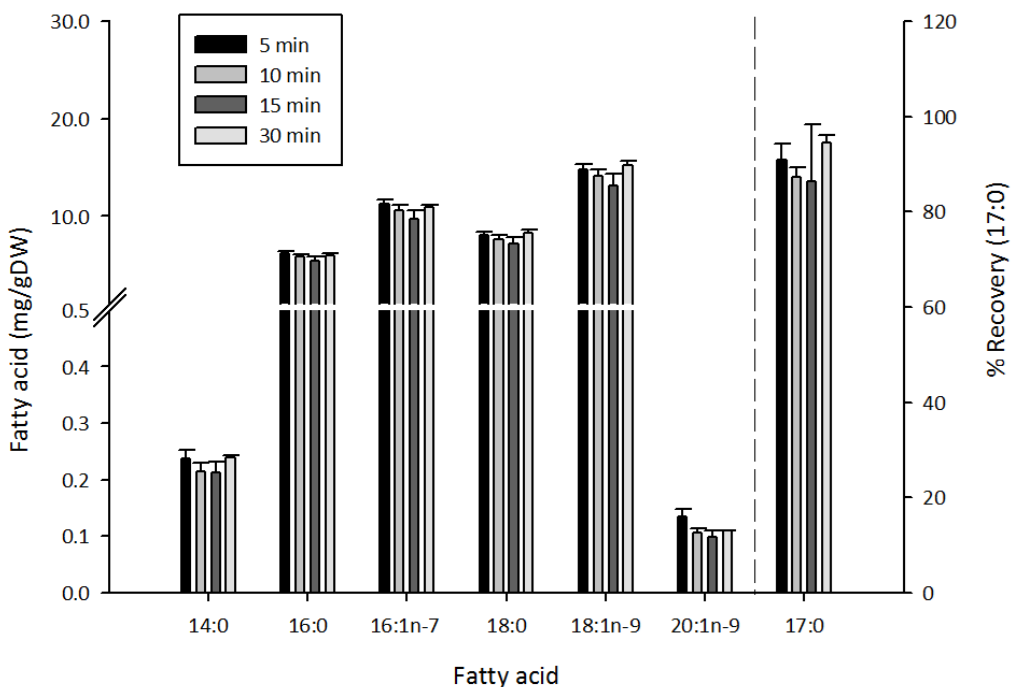


Figure 5. Optimizing the reaction time. All reactions were performed at 120 °C. Heptadecanoic acid (17:0) was used as internal standard. Error bars correspond to standard deviation (n = 3).

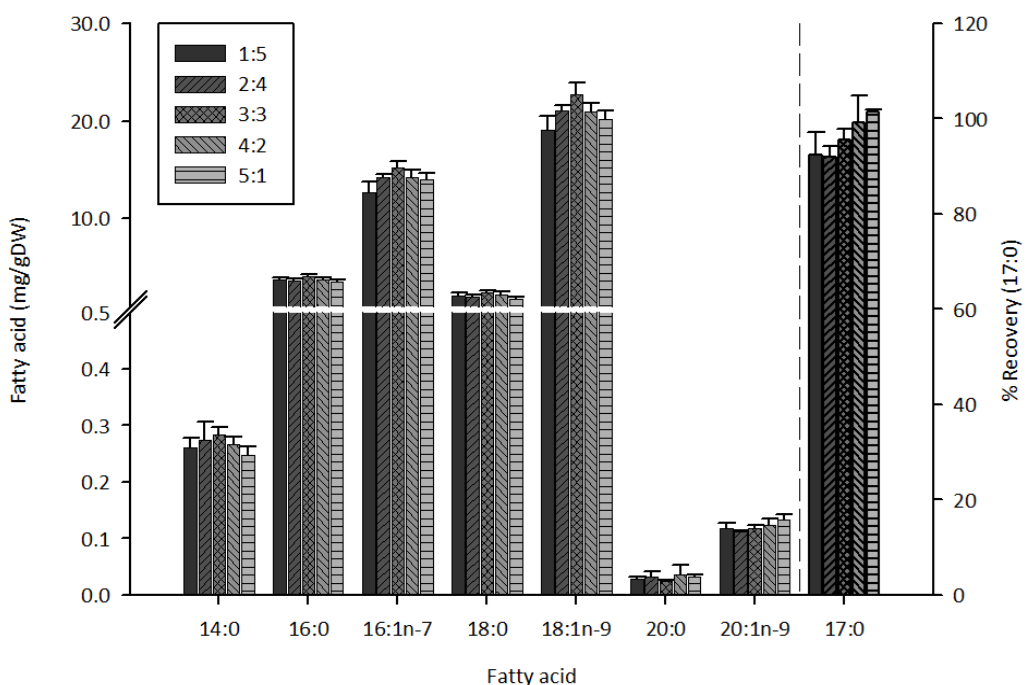


Figure 6. Optimizing solvent (Hexane : MeOH) ratio. The volume of MeOH was varied from 1-5 mL. All reactions were performed at 120 °C for 5 min. Heptadecanoic acid (17:0) was used as internal standard. Error bars correspond to standard deviation (n = 3).

To identify the optimal reaction time, we performed microwave-assisted derivatization between 5 and 30 min (Fig. 5), and this showed that a reaction time of 5 min was sufficient to complete the conversion of all fatty acids in *S. cerevisiae*.

Methanol volume

Here we evaluated variation of the MeOH volume between 1 and 5 mL with the amount of sample kept constant of approximately 10 mg. Based on this we found that a volume of at 1 mL MeOH was sufficient to complete the conversion of FAMEs (Fig. 6), increasing the volume of MeOH to 5 mL did not increase the yield (insignificant difference $P>0.01$), and this indicated that 1 mL of MeOH was sufficient to complete the trans-esterification for a ~10 mg yeast sample. As the lipid content of yeast may vary we though recommend to use 2 mL of MeOH. Using higher amounts of MeOH will result in increasing costs of BF_3 , and 2 mL represents a compromise between keeping costs low and ensuring efficient extraction also in yeast samples where the lipid content may be high.

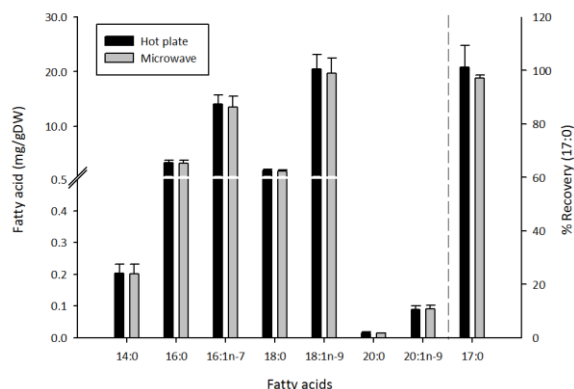


Figure 7. Comparison of microwave (5 min at 120 °C) and hot plate heating methods (120 min at 120 °C). Heptadecanoic acid (17:0) was used as internal standard. Error bars correspond to standard deviation ($n = 3$).

Method validation

Comparison microwave method with conventional method (hot plate)

In order to compare our microwave method with the conventional method using a hot plate, we first optimized the necessary conditions for preparation of FAMEs by the conventional method. The optimum conditions were found to be 120 °C and 120

min reaction time (see Fig. S1 and S2). There was no significant difference ($P>0.01$) between results (Fig. 7) obtained with the conventional method and the method developed here, which indicated that they are equally effective, but reducing the FAME preparation time (from 120 min to 5 min) represents a clear advantage of the microwave-assisted derivatization method compared with the conventional method.

Method validation with standard reference material (SRM)

Validation of the new method using SRM was intended for quality assurance for the entire measurement process (May et al. 1992). Accurate and quantitative analysis of fatty acids in biological samples requires complete esterification of lipids to FAMEs independently of changes in the fatty acid composition and that there are no changes in the fatty acid structures during the esterification process.

To evaluate whether our new method do not have any problems of this sort we analyzed a, SRM. We could not identify a SRM that contains an identical matrix to *S. cerevisiae* (Sander et al. 2009), and we therefore used SRM 3275-2 (omega-3 and omega-6 fatty acid) from National Institute of Standards & Technology, USA, to validate the accuracy of our method.

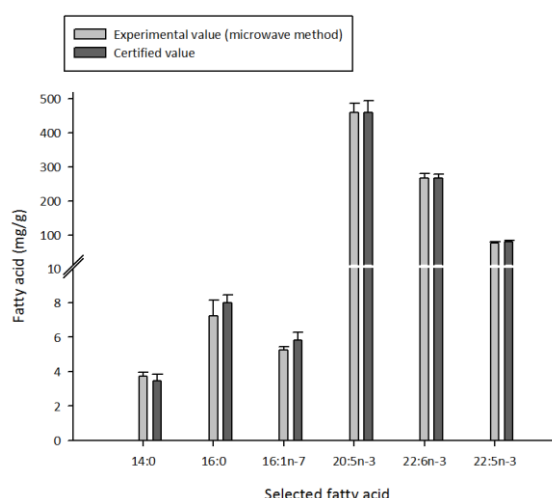


Figure 8. Results from validation method with SRM 3275-2 (omega-3 and omega-6 fatty acid). All reactions were performed at 120 °C for 5 min. Heptadecanoic acid (17:0) was used as internal standard. Error bars correspond to standard deviation ($n = 3$).

The results in Fig. 8 show that there is no significant difference ($P>0.01$) between the experimental results obtained here and certified values for each of the selected fatty acids. This strongly indicates a high accuracy of our developed method, as well as that heating by microwave irradiation do not cause any change in either the structure of the fatty acids.

Determination of total fatty acids in yeast samples (*S. cerevisiae*)

Although the method was validated with SRM (at stated above), it is scientifically difficult to conclude that yields of FAMEs obtained from microwave method was absolutely correct because of their large differences in matrices. The possibility to improve the accuracy of the method was therefore further investigated. Four different ways of sample pre-treatment (cell

disruption to break down cell wall) before preparation of FAMEs was evaluated. All the conditions used for sample pre-treatment were optimized (Fig. S3).

The yields of FAMEs (Fig. 9) from yeast samples prepared by three different ways of cell disruption (zymolyase digestion, bead mills mechanical disruption, and sonication) were comparable ($P>0.01$) to the non-disrupted cells. The results indicated that direct preparation of FAMEs by the microwave method was equally effective as compared to other ways of FAME preparation. This could be due to the fact that the esterification occurred in closed-vessel microwave operated under high temperature and pressure (120 °C, 30 bars), and the yeast cell wall could simply be disrupted by this treatment.

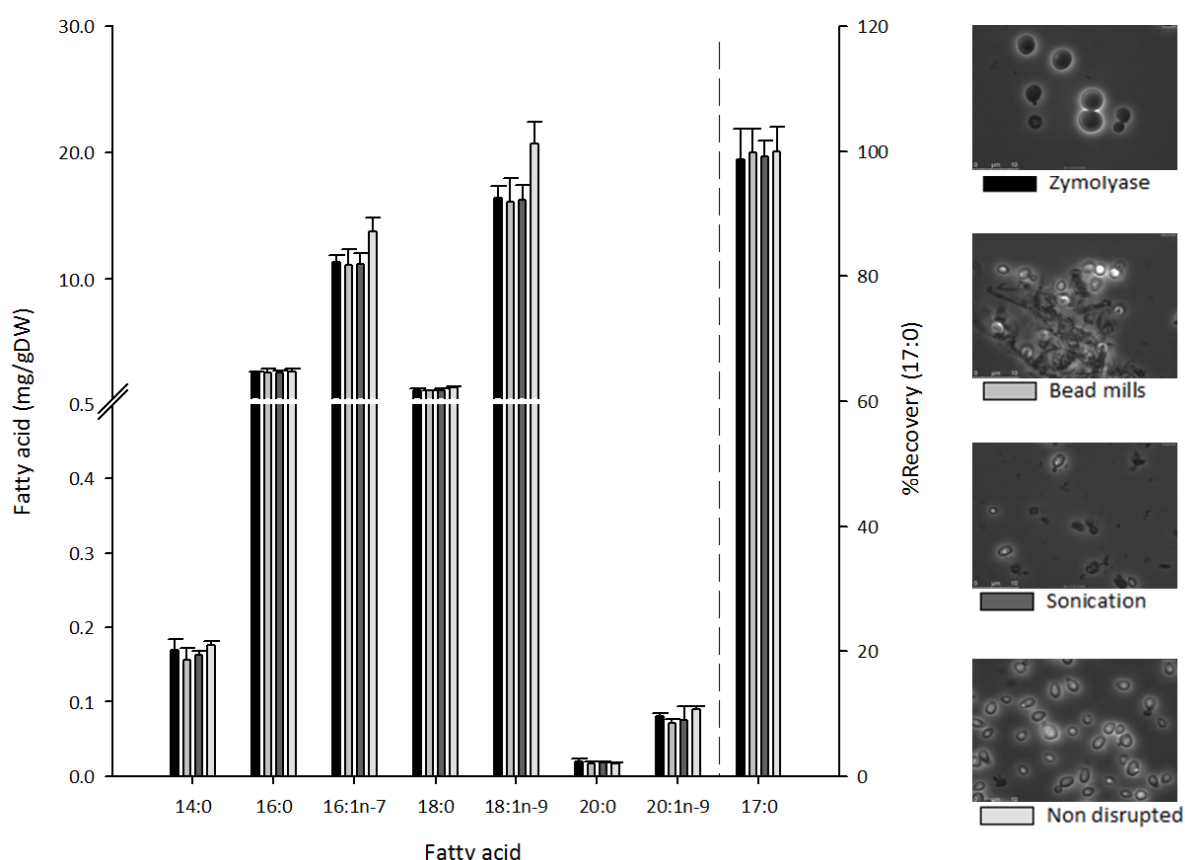


Figure 9. Comparison yields of FAMEs between non-disrupted cells and three different ways of sample pre-treatment (zymolyase digestion, bead mills, and sonication). All reactions were performed at 120 °C for 5 min. Heptadecanoic acid (17:0) was used as internal standard. Error bars correspond to standard deviation ($n = 3$).

Discussions

The ideal method used for sample preparation in biological research should be simple, rapid, precise and accurate. Besides these essential factors, sample preparation rate (number of samples that can be performed per hour or per day) is also important. In order to perform fast sample preparation, we replaced the conventional heating (using hot plate or water bath) with microwave heating, which dramatically reduces the FAME reaction time. Moreover, we increased the speed of sample preparation by modifying the conventional closed-vessel to be able to use with Pyrex glass tubes (Fig. 2). With this approach, we eliminated most of the time consuming steps for vessel preparation, such as cleaning or drying (vessel can be immediately re-used for the next reaction) including the transferring of mixture solution from the vessel to the glass tube (at the separation state). Hereby we are able to reach a sample preparation rate of up to several hundred samples per day.

The choosing of solvents is also important for FAME synthesis. Although water has been known as the best solvent for microwave extraction when compared with other solvents because of the high efficiency in energy transfer (Sanchez-Prado et al. 2010), the presence of water (>2% in reaction mixture) in esterification reactions could significantly affect the FAME yields (Ulberth and Henninger 1992a; Lepage and Roy 1986). Here we designed the procedure such that we can use water as the solvent to absorb the microwave energy outside the Pyrex glass tube. This enables a high efficiency of heat transfer through the Pyrex glass tube containing the sample, BF_3 in MeOH, and hexane. Methanol is considered as a key solvent for FAME reactions as the yields of FAMEs from lipids are directly influenced by the ratio between MeOH and lipids in the sample (Liu 1994). Hexane is used in the reaction to maintain the solubility of lipids and fatty acids and also trapping FAMEs after the conversion process. Normally, the amount of hexane used in the trans-esterification reaction is larger than that of MeOH in order to simplify sample collection and minimize sample loss. Even

though MeOH is able to absorb microwave energy it has much less capacity than water (Eskilsson and Bjorklund 2000). It could be possible to increase yields of those FAMEs in the conventional method by increasing the volume of MeOH (which we used 2 mL for our experiment) or increasing the reaction time (longer than 5 min), but this will increase cost or time for the sample preparation.

In general, bound fatty acids require longer time to complete the conversion as compared to free fatty acids (Ichihara and Fukubayashi 2010), and as mentioned above this could explain the similar results of 17:0 recovery obtained with the two methods and the different yields of 18:1n-9 and 20:1n-9 FAMEs from yeast samples.

The optimum derivatization temperature found from this study was in good agreement with what has been reported earlier using conventional heating (Masood et al. 2005; Ichihara and Fukubayashi 2010; Abdulkadir and Tsuchiya 2008; Eder 1995). Although the higher temperature may provide equal or higher yields of FAMEs, the operation of derivatization above 120 °C was not possible due to the damaging of the sample. The temperature at 120 °C was therefore selected as an optimum point and used for further investigation. The optimum reaction time for preparation of FAMEs depends on type and size of the sample. A sample in complex matrices may require longer time for complete conversion compared with a sample in a simple matrix. In general, derivatization time using microwave is very short compared to conventional heating because the solvents (water and MeOH) are directly absorbing the microwave energy and release it to the surrounding solution efficiently. Although a reaction time shorter than 5 min may also provide complete conversion, it would not make a significant difference in practice, and we therefore selected 5 min reaction time as the optimal condition.

Due to the rigid cell wall of yeast, which can withstand a pressure of >300 Mpa (Hartmann and Delgado 2004), yeast samples are more difficult to handle in term of completeness of extraction compared to many other biological samples. However, we have already proved by our results that the

modified closed-vessel system can also obtain the same yield of FAME even the yeast cell are disrupted or not. Clearly it is advantageous with direct preparation of FAME using the microwave method as this is simple, rapid and involves little costs.

In summary, the preparation of FAMEs from *S. cerevisiae* can be done rapidly by microwave-assisted derivatization and complete esterification can be obtained within 5 min. The preparation of FAMEs using the method developed here is not only a rapid method for sample preparation but also simple, provides high accuracy and precision, and the method is likely to be applicable to other biological samples besides yeast.

Acknowledgments

Part of this work was financed by Chalmers Foundation, the Knut and Alice Wallenberg Foundation and the Swedish Research Council (Vetenskapsrådet). We also acknowledge funding from the EU-funded project UNICELLSYS. We would like to thank Dr. Verena Siewers for valuable assistance with microscopic results. Pramote Chumnanpuen also would like to thank the Office of the Higher Education Commission, Thailand for supporting by a stipend for his Ph.D. program under the program Strategic Scholarships for Frontier Research Network.

References

- Abdulkadir S, Tsuchiya M (2008) One-step method for quantitative and qualitative analysis of fatty acids in marine animal samples. *J Exp Mar Biol Ecol* 354 (1):1-8. doi:10.1016/j.jembe.2007.08.024
- Canelas AB, Harrison N, Fazio A, Zhang J, Pitkanen JP, van den Brink J, Bakker BM, Bogner L, Bouwman J, Castrillo JI, Cankorur A, Chumnanpuen P, Daran-Lapujade P, Dikicioglu D, van Eunen K, Ewald JC, Heijnen JJ, Kirdar B, Mattila I, Menonides FI, Niebel A, Penttila M, Pronk JT, Reuss M, Salusjarvi L, Sauer U, Sherman D, Siemann-Herzberg M, Westerhoff H, de Winde J, Petranovic D, Oliver SG, Workman CT, Zamboni N, Nielsen J (2010) Integrated multilaboratory systems biology reveals differences in protein metabolism between two reference yeast strains. *Nat Commun* 1:1-8. doi:10.1038/ncomms1150
- de Jong B, Siewers V, Nielsen J (2011) Systems biology of yeast: enabling technology for development of cell factories for production of advanced biofuels. *Curr Opin Biotechnol* 23:1-7. doi:10.1016/j.copbio.2011.11.021
- Eder K (1995) Gas chromatographic analysis of fatty acid methyl esters. *J Chromatogr B Biomed Appl* 671 (1-2):113-131
- Eskilsson CS, Bjorklund E (2000) Analytical-scale microwave-assisted extraction. *J Chromatogr A* 902 (1):227-250
- Glaser C, Demmelmair H, Koletzko B (2010) High-throughput analysis of total plasma fatty acid composition with direct *in situ* transesterification. *Plos One* 5 (8):e12045. doi:10.1371/journal.pone.0012045
- Gu ZM, Valianpour F, Chen SL, Vaz FM, Hakkaart GA, Wanders RJA, Greenberg ML (2004) Aberrant cardiolipin metabolism in the yeast *taz1* mutant: a model for Barth syndrome. *Mol Microbiol* 51 (1):149-158. doi:DOI 10.1046/j.1365-2958.2003.03802.x
- Hartmann C, Delgado A (2004) Numerical simulation of the mechanics of a yeast cell under high hydrostatic pressure. *J Biomech* 37 (7):977-987. doi:10.1016/j.jbiomech.2003.11.028
- Ichihara K, Fukubayashi Y (2010) Preparation of fatty acid methyl esters for gas-liquid chromatography. *JLipid Res* 51 (3):635-640. doi:10.1194/jlr.D001065
- Itonori S, Takahashi M, Kitamura T, Aoki K, Dulaney JT, Sugita M (2004) Microwave-mediated analysis for sugar, fatty acid, and sphingoid compositions of glycosphingolipids. *J Lipid Res* 45 (3):574-581. doi:10.1194/jlr.D300030-JLR200
- Jeyashoke N, Krisnangkura K, Chen ST (1998) Microwave induced rapid

- transmethylation of fatty acids for analysis of food oil. *J Chromatogr A* 818 (1):133-137
- Khoomrung S, Laoteng K, Jitsue S, Cheevadhanarak S (2008) Significance of fatty acid supplementation on profiles of cell growth, fatty acid, and gene expression of three desaturases in *Mucor rouxii*. *Appl Microbiol Biotechnol* 80 (3):499-506. doi:10.1007/s00253-008-1569-0
- Leber R, Zinser E, Paltauf F, Daum G, Zellnig G (1994) Characterization of lipid particles of the yeast, *Saccharomyces cerevisiae*. *Yeast* 10 (11):1421-1428. doi:10.1002/yea.320101105
- Lepage G, Roy CC (1986) Direct transesterification of all classes of lipids in a one-step reaction. *J Lipid Res* 27 (1):114-120
- Liebeke M, Wunder A, Lalk M (2010) A rapid microwave-assisted derivatization of bacterial metabolome samples for gas chromatography/mass spectrometry analysis. *Anal Biochem* 401 (2):312-314. doi:S0003-2697(09)00278-4 [pii] 10.1016/j.ab.2009.04.030
- Liu KS (1994) Preparation of Fatty-Acid Methyl Esters for Gas-Chromatographic Analysis of Lipids in Biological-Materials. *J Am Oil Chem Soc* 71 (11):1179-1187
- Masood A, Stark KD, Salem N, Jr. (2005) A simplified and efficient method for the analysis of fatty acid methyl esters suitable for large clinical studies. *J Lipid Res* 46 (10):2299-2305. doi:10.1194/jlr.D500022-JLR200
- May WE, Benner BA, Jr., Wise SA, Schuetzle D, Lewtas J (1992) Standard reference materials for chemical and biological studies of complex environmental samples. *Mutat Res* 276 (1-2):11-22
- Moss CW, Lambert MA, Merwin WH (1974) Comparison of rapid methods for analysis of bacterial fatty-acids. *Appl Microbiol* 28 (1):80-85
- Noronha-da-Costa P, Rodrigues C, Spencer-Martins I, Loureiro V (1996) Fatty acid patterns of film-forming yeasts and new evidence for the heterogeneity of *Pichia membranaefaciens*. *Lett Appl Microbiol* 23 (2):79-84
- Sanchez-Prado L, Garcia-Jares C, Llompart M (2010) Microwave-assisted extraction: Application to the determination of emerging pollutants in solid samples. *J Chromatogr A* 1217 (16):2390-2414. doi:10.1016/j.chroma.2009.11.080
- Sancho T, Gimenez-Jurado G, Malfeito-Ferreira M, Loureiro V (2000) Zymological indicators: a new concept applied to the detection of potential spoilage yeast species associated with fruit pulps and concentrates. *Food Microbiol* 17 (6):613-624. doi:DOI 10.1006/fmic.2000.0360
- Sander L, Schantz M, Sharpless K, Wise S (2009) Standard Reference Materials to support measurement of fatty acids. *Lipid Technol* 21 (1):7-12. doi:10.1002/lite.200800080
- Shi S, Valle-Rodriguez JO, Siewers V, Nielsen J (2011) Prospects for microbial biodiesel production. *Biotechnol J* 6 (3):277-285. doi:10.1002/biot.201000117
- Shimasaki H, Phillips FC, Privett OS (1977) Direct transesterification of lipids in mammalian tissue for fatty acid analysis via dehydration with 2,2'-dimethoxypropane. *J Lipid Res* 18 (4):540-543
- Söderholm S, Damm M, Kappe C (2010) Microwave-assisted derivatization procedures for gas chromatography/mass spectrometry analysis. *Mol Diversity* 14 (4):869-888. doi:10.1007/s11030-010-9242-9
- Tomas A, Tor M, Villorbina G, Canela R, Balcells M, Eras J (2009) A rapid and reliable direct method for quantifying meat acylglycerides with monomode microwave irradiation. *J Chromatogr A* 1216 (15):3290-3295. doi:DOI 10.1016/j.chroma.2009.01.055
- Ulberth F, Henninger M (1992a) One-Step Extraction Methylation Method for Determining the Fatty-Acid

- Composition of Processed Foods. J Am Oil Chem Soc 69 (2):174-177
- Ulberth F, Henninger M (1992b) One-step extraction/methylation method for determining the fatty acid composition of processed foods. J Am Oil Chem Soc 69 (2):174-177. doi:10.1007/bf02540571
- Wei DS, Li MC, Zhang XX, Zhou H, Xing LJ (2006) A novel Delta(12)-fatty acid desaturase gene from methylotrophic yeast *Pichia pastoris* GS115. Acta Biochim Pol 53 (4):753-759
- Zhang J, Vaga S, Chumnanpuen P, Kumar R, Vemuri GN, Aebersold R, Nielsen J (2011) Mapping the interaction of Snf1 with TORC1 in *Saccharomyces cerevisiae*. Mol Syst Biol 7. doi:Artn 545
- Doi 10.1038/Msb.2011.80
- Zhang ZX, Xiong GH, Lie GK, He XQ (2000) Sample pretreatment with microwave-assisted techniques. Anal Sci 16 (2):221-224

Supplementary for the manuscript:

Title: Fast and accurate preparation fatty acid methyl esters by microwave-assisted derivatization in yeast *Saccharomyces cerevisiae*

Sakda Khoomrung[†], Pramote Chumnanpuen[†], Suwanee Jansa-ard, Intawat Nookaew, Jens Nielsen*

Department of Chemical and Biological Engineering
Chalmers University of Technology

SE-412 96 Göteborg, Sweden

[†]These authors contributed equally to this work

*Corresponding author:

Department of Chemical and Biological Engineering
Chalmers University of Technology
Kemivägen 10
SE-412 96 Göteborg, Sweden
Telephone: +46 31 772 3804
Fax: +46 31 772 3801
email: nielsenj@chalmers.se

Figure S1. Optimizing derivatization temperature. All reactions were performed in 120 min. Error bars correspond to standard deviation (n=3).

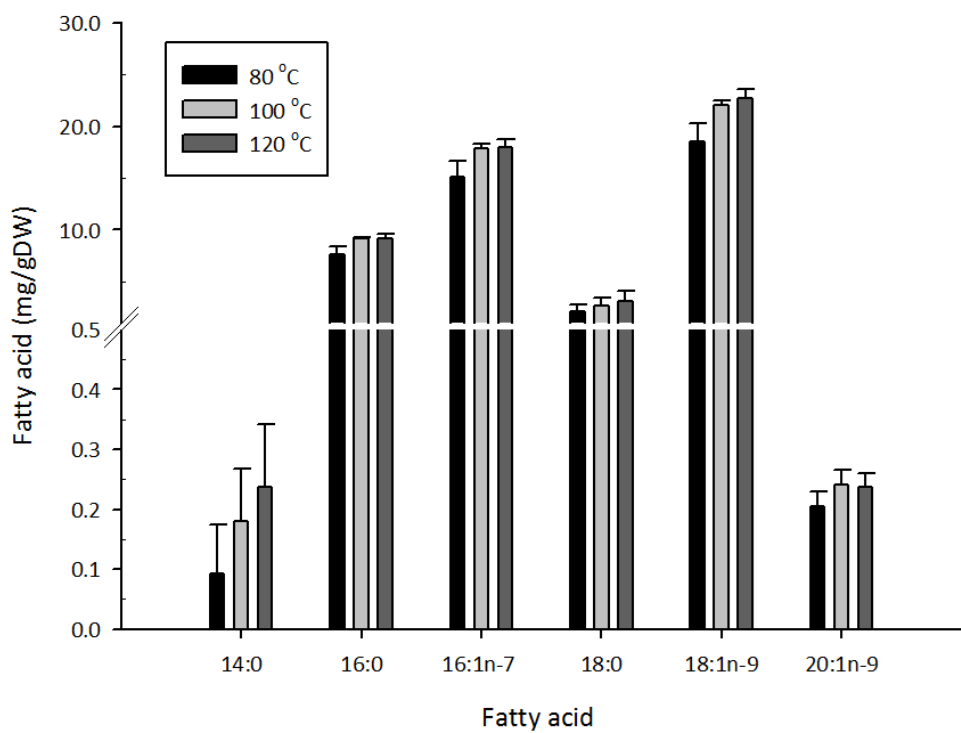


Figure S2. Optimizing the reaction time. All reactions were performed at 120 °C. Error bars correspond to standard deviation (n=3)

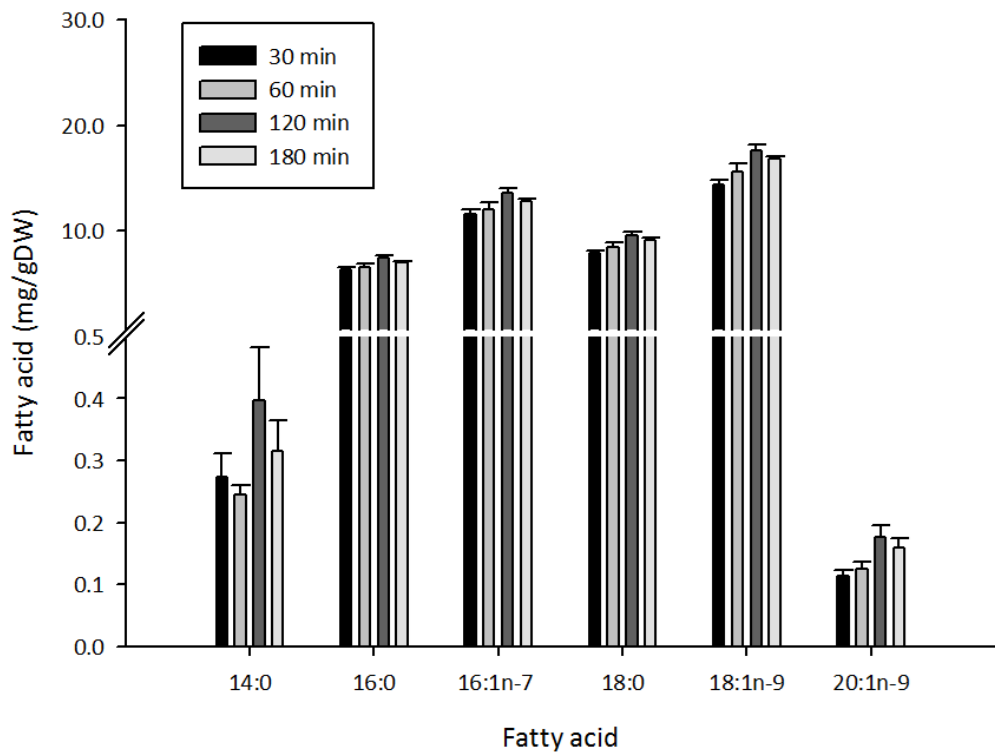


Figure S3. Optimizing the disruption method for yeast cell using zymolyase, sonication, and bead mills from 15 to 45 min. The white scale bar is equal to 10 μ m for all frames.

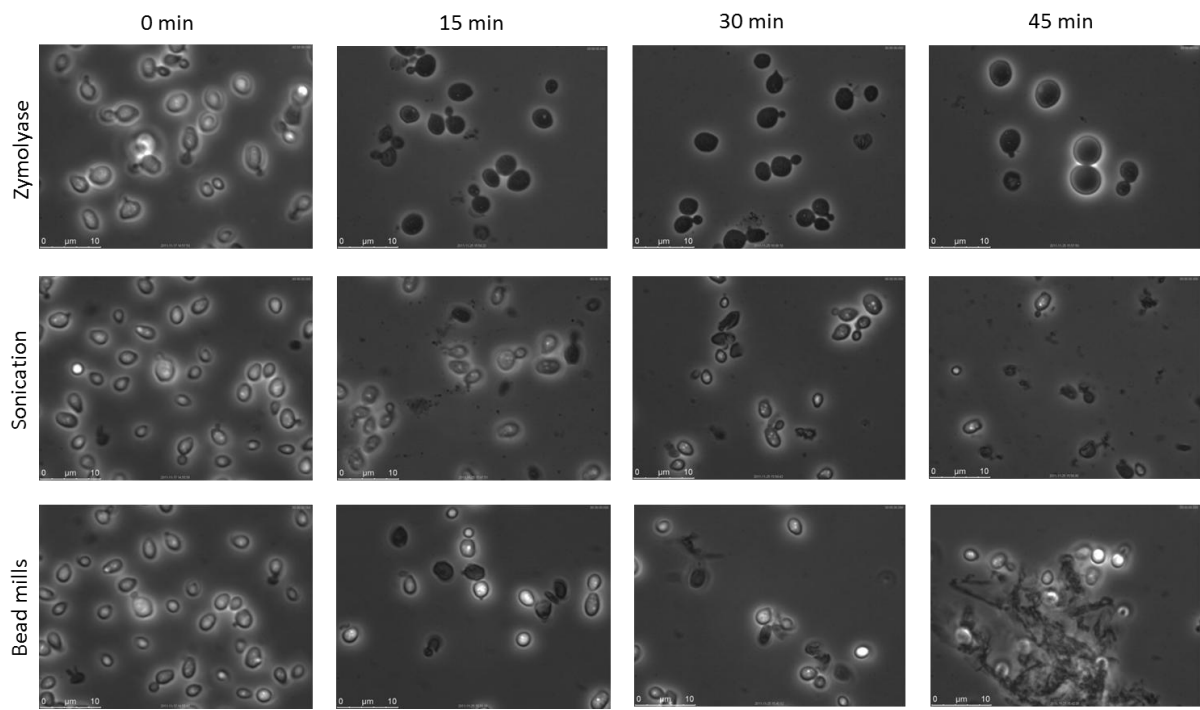


Figure S4. The microscopic result of yeast cells after microwaved at 120 °C for 5 min.

